



THE
Water
Research
FOUNDATION



PROJECT NO.
4752



Effect of Major Stress Events on Buried Pipe Service Life



Los Angeles
Department of
Water & Power

Effect of Major Stress Events on Buried Pipe Service Life

Prepared by:

Charles Scawthorn and Keith Porter
SPA Risk LLC

Co-sponsored by:

Los Angeles Department of Water and Power

2022



The Water Research Foundation (WRF) is a nonprofit (501c3) organization which provides a unified source for One Water research and a strong presence in relationships with partner organizations, government and regulatory agencies, and Congress. The foundation conducts research in all areas of drinking water, wastewater, stormwater, and water reuse. The Water Research Foundation's research portfolio is valued at over \$700 million.

The Foundation plays an important role in the translation and dissemination of applied research, technology demonstration, and education, through creation of research-based educational tools and technology exchange opportunities. WRF serves as a leader and model for collaboration across the water industry and its materials are used to inform policymakers and the public on the science, economic value, and environmental benefits of using and recovering resources found in water, as well as the feasibility of implementing new technologies.

For more information, contact:

The Water Research Foundation

1199 North Fairfax Street, Suite 900
Alexandria, VA 22314-1445
P 571.384.2100

6666 West Quincy Avenue
Denver, Colorado 80235-3098
P 303.347.6100

www.waterrf.org
info@waterrf.org

©Copyright 2022 by The Water Research Foundation. All rights reserved. Permission to copy must be obtained from The Water Research Foundation.

WRF ISBN: 978-1-60573-578-8

WRF Project Number: 4752

This report was prepared by the organization(s) named below as an account of work sponsored by The Water Research Foundation. Neither The Water Research Foundation, members of The Water Research Foundation, the organization(s) named below, nor any person acting on their behalf: (a) makes any warranty, express or implied, with respect to the use of any information, apparatus, method, or process disclosed in this report or that such use may not infringe on privately owned rights; or (b) assumes any liabilities with respect to the use of, or for damages resulting from the use of, any information, apparatus, method, or process disclosed in this report.

Prepared by SPA Risk LLC

This document was reviewed by a panel of independent experts selected by The Water Research Foundation. Mention of trade names or commercial products or services does not constitute endorsement or recommendations for use. Similarly, omission of products or trade names indicates nothing concerning The Water Research Foundation's position regarding product effectiveness or applicability.

Acknowledgments

Staff of the Los Angeles Department of Water and Power, particularly Dr. Craig Davis, G.E. (now retired but previously Water System Resilience Program Manager for LADWP) are warmly thanked. LADWP sponsored this research with WRF and its generosity is gratefully acknowledged. The assistance of many other persons at LADWP, including Albert Gastelum, Manager of Water Quality; Patrick J. Horton, Emergency Preparedness Coordinator; Martin L. Adams, General Manager; Ray Hardjadinata; Enrique Polanco, Civil Engineering Associate; Ofelia Rubio, Manager of Water Distribution Resiliency & Technology; Salman Sufi ; Maral J. Sarkissian, Asset Manager; Sabrina Y. Tsui, Water Master Planning Manager; Greg Ammon; John Nguyen; Dean Terada; and Baldiwala Shabbir, is sincerely appreciated.

Staff of the San Francisco Public Utilities Commission generously furnished data for this project. Katie Miller, David Myerson, Sam Young and Steve Ritchie are all warmly thanked, for this study and many previous projects. The East Bay Municipal Utility District also generously provided data for this study, and Xavier Irias, Serge Terentieff, Carlton Chan, Roberts McMullin, Elena Dudek, Dave Katzev, Max Fefer and Bill Maggiore are all warmly thanked. Bill Heubach and Catherine Wendland of Seattle Public Utilities are gratefully thanked for making SPU data available. Portland Water Bureau also generously provided data for this study, and the assistance of Mike Saling, Jeff Leighton and Ryan Nelson is gratefully acknowledged. Other persons who assisted in discussions and various other ways to this study include Lisa Nelson and Robert Wurgler of the California Geological Survey.

Research Team

Principal Investigator:

Charles Scawthorn, SE, DEng
SPA Risk LLC

Co-principal Investigator:

Keith A. Porter, PE, PhD
SPA Risk LLC

Image Processing:

Joseph McGlinchy
University of Colorado, Boulder

WRF Project Subcommittee or Other Contributors

Greg de Lamare,
Metropolitan Water District of Southern California

William F. Heubach,
Seattle Public Utilities

Xavier J. Irias,
Woodard & Curran

WRF Staff

John Albert, MPA
Chief Research Officer

Jian Zhang, PhD, PE
Research Program Manager

Abstract and Benefits

Do major stress events such as strong earthquake ground shaking significantly reduce remaining service life of buried water distribution pipe? This issue emerged following the 2014 Mw 6.0 Napa earthquake, where FEMA compensation to the affected water utility depended on whether pipe remaining service life had been shortened by the earthquake.

This study employs a statistical approach informed by mechanics of materials, using data from five major west coast cities (Los Angeles, San Francisco, Portland OR, Seattle and the East Bay region of the San Francisco Bay Area). The data ranged from scanned paper maps to GIS databases. Data processing included an innovative method for extracting repair locations from the paper map images which in itself should be of interest for utilities interested in broadening the basis for their asset management programs. The resulting dataset was for 16,000 miles of buried water distribution pipe composed of more than 600,000 GIS segments that required more than 64,000 repairs over varying periods (depending on utility) from 1975 to 2017.

Multi-variate statistical analysis was then applied to this dataset to develop measures of buried pipe service life as a function of covariates of pipe diameter, material, age, soil and slope, and earthquake. Survival functions using Kaplan Meier (KM) plots were created, which **found that pipes subjected to higher ground motions have a lower probability of survival than those not subjected to high ground motions, for example reducing affected pipe value by as much as one-third. The implications of this finding are profound, in that they show that earthquakes cause substantial long-term losses to water utility buried pipe networks, reducing the useful life of these pipes by a significant amount.** This is the first time this effect has been quantified. The implications of these findings for disaster aid policy are important in that substantially larger claims for disaster assistance are warranted.

Benefits: The benefits of this project may be summarized as:

- Confirmation of the hypothesis that major stress events cause a long-term significant decrease in buried water distribution pipe service life.
- Quantification of this decrease.
- Translation of this decrease into meaningful financial terms.
- Discussion of the implications of these findings for current post-disaster aid policies.
- Development of statistical measures of the effects of various parameters (pipe diameter, material, age, slope) on repair frequency.
- Development of an innovative image processing methodology allowing extraction of repair locations from older repair record maps.

We believe these findings are important for the water industry, in terms of identifying and quantifying a hitherto largely unrecognized effect of major stress events and understanding the financial and disaster aid implications of this effect. More broadly, the data and methods employed in this study should help to improve the basis for utility asset management programs.

Keywords: pipe, water distribution network, repairs, leaks, corrosion, fatigue, deterioration, aging, earthquakes, stress events, natural hazards, asset management, disaster aid, Stafford Act, Disaster Recovery Reform Act of 2018, infrastructure, survival analysis, Kaplan Meier, Miner's Rule.

Contents

Acknowledgments.....	ii
Abstract and Benefits.....	v
Tables.....	vii
Figures.....	viii
Acronyms and Abbreviations.....	xiv
Executive Summary.....	xv
Chapter 1: Introduction.....	1
1.1 Purpose and Research Direction.....	1
1.2 Background.....	1
1.3 Previous Research.....	2
1.4 Approach.....	5
1.5 Organization of the Report.....	6
Chapter 2: Physically Based Modeling of Buried Pipe.....	7
2.1 Closely Related Physical Models.....	7
2.1.1 Pipe Failure Models.....	7
2.1.2 Material Fatigue Models.....	8
2.2 Variables Available from Utilities.....	9
2.3 Traffic, Thermal, and Seismic Fatigue Proxies for Hidden Variables.....	9
2.3.1 Uncertain S-N Curves for Some Pipe Materials.....	10
2.3.2 Vehicle Loading.....	11
2.3.3 Thermal Loading.....	12
2.3.4 Seismic Loading.....	14
2.4 Conclusions.....	15
Chapter 3: Data.....	17
3.1 Data Collection Methodology.....	17
3.2 Data Received.....	17
3.2.1 LADWP Data Format.....	17
3.2.2 SFPUC Data Format.....	30
3.2.3 EBMUD Data Format.....	31
3.2.4 PWB Data Format.....	34
3.2.5 SPU Data Format.....	36
3.2.6 Summary of Data.....	37
3.3 Data Processing and Covariate Data.....	37
3.3.1 LADWP.....	37
3.3.2 SFPUC.....	54
3.3.3 EBMUD.....	56
3.3.4 PWB.....	58
3.3.5 SPU.....	60
3.3.6 Geophysical Covariates.....	64
3.4 Datasets for Analysis.....	84
3.4.1 LADWP.....	84
3.4.2 SPU.....	86
3.4.3 SFPUC.....	88

3.4.4	EBMUD.....	89
3.4.5	PWB.....	90
3.4.6	Summary of Datasets.....	91
3.5	Completeness	95
Chapter 4: Analysis		99
4.1	Introduction	99
4.2	Regression Analysis of Repair Rates as a Whole.....	100
4.2.1	LADWP: Analysis of 1997-2017.....	100
4.2.2	SPU Data as a Whole.....	112
4.3	Regression Analysis of Repair Rate Annual Frequencies	121
4.3.1	LADWP: Analysis of 1975-2017 Dataset	121
4.3.2	EBMUD.....	136
4.3.3	SFPUC.....	144
4.3.4	PWB.....	152
4.3.5	SPU.....	160
4.3.6	Merged Dataset	168
4.4	Application	176
4.5	Survival Analysis.....	176
4.5.1	Basic Case.....	177
4.5.2	Effect of Earthquake	179
Chapter 5: Findings and Concluding Remarks		187
5.1	Findings.....	187
5.2	Implications.....	187
5.3	Future Research and Recommendations.....	187
Appendix A: Literature Review		191
Appendix B: Glossary of Terms		199
References		201

Tables

2-1	Parameters of Probabilistic S-N Curves for Cast Iron, Ductile Iron, and A36 Steel	11
2-2	Stresses Due to 1,000 Lb. of Wheel Loading.....	11
2-3	Sensitivity of Traffic-Load Fatigue Life to Hidden Variables X_2 and X_3	12
2-4	Average Seasonal Temperature Flux	13
2-5	Tensile Stress in Restrained Pipe Subject to 20F Temperature Drop	13
2-6	Sensitivity of Thermal-Load Fatigue Life to Hidden Variables X_4 and X_5	14
2-7	Seismic Cycle Ratio r_e Associated with a M_w 7.5 Earthquake Causing PGV = 25 cm/Sec	15
3-1	LADWP Data Received	23
3-2	Number of Repairs by Pipe Diameter, 1994 Northridge Earthquake	26
3-3	SPUC Data Received.....	30
3-4	EBMUD Data Received.....	31
3-5	PWB Data Received.....	34
3-6	SPU Data Received.....	36
3-7	Summary of Data	37
3-8	Minimum and Maximum Red, Green, and Blue Pixel Intensities Specified to Threshold Scanned Maps from Each Lustrum. Note the Difference between Pre- and Post-1975 Data, Which Reflects the Difference in Tone between the Data.....	42
3-9	Number of Repair Locations Identified from Scanned Maps for Period 1975-2000	46
3-10	LADWP Dataset Covariates.....	51
3-11	Summary of Slope Ranges for Subdivided NEHRP Vs30 Categories	76
3-12	SFPUC Pipe Segments and Length by Material	88
3-13	EBMUD Pipe Segments and Length by Material.....	89
3-14	PWB Pipe Segments and Length by Material	90
3-15	Repair Record Data Fields	92
3-16	Summary of Repair Record Data.....	92
3-17	No. Repairs per Year per Agency	93
3-18	LADWP No. Repairs per Year, 1988-2017	96
4-1	Analysis Dataset Structure	100
4-2	LADWP Regression Coefficients for Seven Models.....	135
4-3	EBMUD Regression Coefficients for Seven Models	136
4-4	SFPUC Regression Coefficients for Seven Models	144
4-5	PWB Regression Coefficients for Seven Models	152
4-6	SPU Regression Coefficients for Seven Models	160
4-7	Merged Regression Coefficients for Seven Models	168

Figures

1-1	U.S. Urban Growth 1790-2010.....	2
1-2	Survival Curves for Asbestos Cement Pipes as Function of the Number of Previous Breaks (NOPB).....	5
2-1	S-N Curve for Ductile Iron	10
3-1	LADWP Water Distribution Pipe Network	18
3-2	LADWP Data Map for Grid Cell 133-168 for Years 1990-1995	19
3-3	LADWP Data Map Showing Annotations (Highlighted Yellow) with Map Legend Below.....	20
3-4	LADWP 1960-2000: Repair Data Grid Cells, Cell 133-168 Highlighted Red	20
3-5	LADWP 1960-2000: Example Maps for Eight Lustra.....	21
3-6	LADWP 1960-2000: Example Maps for Several Grid Cells, Maps from Different Lustra	22
3-7	LADWP 1960-2000: Example Map Alignment across Cell Boundaries	22
3-8	LADWP Pipe and Repair Data.....	25
3-9	1994 M_w 6.7 Northridge Earthquake Ioseismal Distribution	27
3-10	Water Distribution Line Repairs.....	28
3-11	1994 M_w 6.7 Northridge Earthquake and LADWP Water Distribution Pipe Repairs	29
3-12	Comparison of Scanned Map Repair Locations (Blue) with 1994 Northridge Earthquake Repairs (Red), Showing No Correlation	30
3-13	San Francisco Pipe Data	31
3-14	EBMUD Pipe and Repair Data	33
3-15	Portland, OR Pipe and Repair Data.....	35
3-16	Seattle SPU Pipe Network with Detail Showing Break Locations	36
3-17	Entire Mosaic of 600 Scanned Maps for the 1975-80 Lustrum: (Top) Entire Mosaic with LA City Boundaries, in Manifold 9 GIS; (Bottom) Ditto, in QGIS 3.14.....	38
3-18	Clipped Mosaic of Two Repair Maps	39
3-19	Mis-Alignment of Scanned Map with Pipe GIS Layer – the Blue Lines Are the Pipe Network from the GIS SHP Files, and Align Very Well with Google Street Maps (Underlying Image – Note This Image Is Centered on LADWP’s John Ferraro Building) While Pipelines in the Scanned Images (Dashed Lines) Are Here Displaced Several Tens of Feet to the West.....	39
3-20	Detail of a Scanned Map on Left, with Background Thresholded Out, Revealing Only Annotations.....	40
3-21	Detail of a Scanned Map on Annotations Geo-located as “Nuggets” (Red). Detail Confirms Lower Annotation Is “95” and Not “85”	41
3-22	Example of ‘Select by Location’ to Determine Pipe Features within a Distance from the Annotation Features. Pipe Features Meeting This Criteria Are Highlighted in Cyan.....	43
3-23	Google Vision AI Result on an Image Chip Containing One of the Annotations from an Image in the 1996-2000 Lustrum.....	44
3-24	Detail of Stitched Mosaic, Port of Los Angeles, with Grid Boundaries (Black Lines) Overlaid.....	45
3-25	False Positives for Leak Annotations	46
3-26	Repair Locations 1975-2000 Derived from Annotations on Scanned Maps.....	47
3-27	Example “Nuggets” Highlighted Yellow for Each of Five Lustra	48
3-28	LADWP Pipe Repair Timeline: Blue Line Is Number of Repairs per Year (Right Axis) and Red Line Is Cumulative Repairs per Year (Right Axis)	50
3-29	LADWP Pipe Repair Heatmap Showing Areas of Concentration of Repairs	52
3-30	LADWP Pipe Network by Year of Installation	53
3-31	SFPUC Pipe Repair Timeline: Blue Line Is Number of Repairs per Year (Right Axis) and Red Line Is Cumulative Repairs per Year (Right Axis)	54

3-32	SFPUC Pipe Repair Heatmap Showing Areas of Concentration of Repairs.....	55
3-33	EBMUD Pipe Repair Timeline: Blue Line Is Number of Repairs per Year (Right Axis) and Red Line Is Cumulative Repairs per Year (Right Axis)	56
3-34	EBMUD Pipe Repair Heatmap Showing Areas of Concentration of Repairs.....	57
3-35	PWB Pipe Repair Timeline: Blue Line Is Number of Repairs per Year (Right Axis) and Red Line Is Cumulative Repairs per Year (Right Axis)	58
3-36	PWB Pipe Repair Heatmap Showing Areas of Concentration of Repairs	59
3-37	SPU Pipe Repair Timeline: Blue Line Is Number of Repairs per Year (Right Axis) and Red Line Is Cumulative Repairs per Year (Right Axis)	60
3-38	SPU Pipe Repair Heatmap Showing Areas of Concentration of Repairs.....	61
3-39	SPU Service Area within Which Is Displayed 10m Slope Data	62
3-40	2001 Nisqually Earthquake Intensity Distribution	63
3-41	2001 Nisqually Earthquake PGV Recorded in Central Seattle	64
3-42	Geologic Compilation of Quaternary Surficial Deposits in Southern California	65
3-43	Simplified Surficial Deposits in Southern California This Study, After	66
3-44	Pipe Axis Relative to Ground Surface Gradient	67
3-45	SRTM Digital Elevation Data	68
3-46	Slope as Derived SRTM Digital Elevation Data.....	68
3-47	USGS 3DEP 1/3 rd Arc-Second DEM Data Website.....	69
3-48	USGS 3DEP 1/3 rd Arc-Second DEM Data for Los Angeles.....	69
3-49	Slope Data Derived for Downtown Los Angeles: (Top) Map of Location; (Middle) Slope Data from 3DEP; (Bottom) Slope Data Derived from SRTM	70
3-50	Aspect Data Derived for (Top) Los Angeles; (Bottom) Aerial Image and Aspect Detail Vicinity of Will Rogers State Historic Park	71
3-51	Distribution of Slope at Pipe Centroid for LADWP Dataset – CDF Axis Is on Left	72
3-52	Slope Data for the SFPUC Service Area Derived from 3DEP Data.....	73
3-53	Slope Data for the EBMUD Service Area Derived from 3DEP Data	73
3-54	Slope Data for the PWB Service Area Derived from 3DEP Data	74
3-55	Slope Data for the SPU Service Area Derived from 3DEP Data.....	74
3-56	USGS Vs30 Map Viewer	75
3-57	Los Angeles Vs30 (Upper 30m Shear Wave Velocity) Is a Measure of Soil Stiffness and a Reasonable Proxy for Several Other Soil Proxies, Such as Corrosivity	76
3-58	Correlation of Vs30 with Slope Back-Calculated from Data in Table 3-11. Note Slope Here Is Measured in Terms of Rise over Run (i.e., Tangent) Rather Than in Degrees	77
3-59	Los Angeles Pipe Centroid Vs30 (Upper 30m Shear Wave Velocity) versus Slope (Degrees of Inclination).....	77
3-60	NOAA NCEI Data Website	79
3-61	Los Angeles Daily Rainfall Data 1950-2019.....	79
3-62	Los Angeles High-Low Temperature Data 1950-2019	80
3-63	LADWP Minimum Temperature Distribution on Day of Repairs (1997-2017)	80
3-64	Los Angeles Daily Minimum Temperature Distribution 1950-2020	81
3-65	1994 Northridge Earthquake Peak Ground Velocity (PGV) Distribution	82
3-66	1989 Loma Prieta Earthquake Peak Ground Velocity (PGV) Distribution.....	83
3-67	Histogram of LADWP GIS Pipe Segments by Material Type, LADWP Data.....	84
3-68	Histogram of LADWP GIS Total Pipe Length by Material Type, LADWP Data.....	85
3-69	Histogram of LADWP GIS Repairs (“Leaks”) by Year of Occurrence	85
3-70	Histogram of Total Length of LADWP Repaired GIS Pipe Segments Normalized by Length of GIS Pipe Segments by Material Type	86

3-71	Plot of Number of SPU Repairs by Year – the Data Clearly Are Non-homogenous.....	87
3-72	Histogram of Number of SPU Repairs by Pipe Material. Note Y Axis Is Logarithmic. Plot Shows That about 81% of the SPU System by Length Is Cast Iron, SPU Data.....	87
3-73	SFPUC Pipe Length by Material.....	88
3-74	EBMUD Pipe Length by Material	89
3-75	PWB Pipe Length by Material	90
3-76	Timeline and Cumulative Repairs per Year, Five Agencies	94
3-77	Normal Distribution Given (Top) Mean = 848 Repairs and Standard Deviation = 281 Repairs Corresponding to Years 1996-2016 and (Bottom) Mean = 1133 and St. Dev. = 125 Corresponding to Years 2010-2016	97
3-78	Examination of Data Completeness, Showing Relative Completeness for Period 2-8 Years before 2014 (i.e., 2013-2006) and Drop Off in Repairs Prior to Then.....	98
4-1	Raw Leak Frequency per GIS Pipe Segment, by Material and Diameter, LADWP Data.....	102
4-2	Leak Frequency per Thousand Foot of Pipe as a Function of Pipe Diameter and Material, LADWP Data	104
4-3	Histogram of LADWP Pipe GIS Segments by Year of Installation	105
4-4	Repair Frequency per Thousand Feet of Pipe Considering Material, Age, and Diameter, Based on a Linear Model. Plot Is an Example for Pipe Age Equal to 100 Years, LADWP Data	107
4-5	Repair Frequency per Thousand Feet of Pipe Considering Material, Age, and Diameter, Based on a Log-Log Model. Plot Is an Example for Pipe Age Equal to 100 Years, LADWP Data	109
4-6	Scattergram of Vs30 vs. Slope (Degrees).....	110
4-7	Correlations of Measured Vs30 (M/S) versus Topographic Slope (M/M) for Active Tectonic Regions	110
4-8	Repair Frequency per Thousand Feet of Pipe Considering Material, Age, Diameter, Vs30, and Slope, Based on a Log-Log Model. Plot Is an Example for Pipe Age Equal to 100 Years Vs30 = 400 Mps and Slope of 2 Degrees, LADWP Data	112
4-9	Raw SPU Leak Frequency per GIS Pipe Segment, by Material and Diameter, SPU Data.....	114
4-10	Raw SPU Leak Frequency per 1000 Ft. of GIS Pipe Segment, by Material and Diameter, SPU Data	116
4-11	Histogram of SPU GIS Pipe Segments by Material and Diameter.....	116
4-12	Histogram of SPU Pipe GIS Segments by year of Installation	117
4-13	Repair Frequency per Thousand Feet of Pipe Considering Material, Age, and Diameter, Based on a Linear Model. Plot is an Example for Pipe Age Equal to 100 Years, SPU Data	119
4-14	Repair Frequency per Thousand Feet of Pipe Considering Material, Age, and Diameter, Based on a Log-Log Model. Plot is an Example for Pipe Age Equal to 100 Years, SPU Data	121
4-15	Raw Leak Frequency per GIS Pipe Segment, by Material and Diameter, LADWP Data.....	123
4-16	Leak Frequency per GIS Pipe Segment as a Function of Pipe Diameter, Material, and Slope, LADWP Data	124
4-17	Leak Frequency per GIS Pipe Segment as a Function of Pipe Diameter, Material, and Slope, LADWP Data	126
4-18	Repair Frequency per Thousand Feet of Pipe Considering Material, Age, and Diameter, Based on a Linear Model. Plot Is an Example for Pipe Age Equal to 100 Years, LADWP Data.....	128
4-19	Repair Frequency per Thousand Feet of Pipe Considering Material, Age, and Diameter, Based on a Log-Log Model. Plot Is an Example for Pipe Age Equal to 100 Years, LADWP Data.....	130

4-20	Repair Frequency per Thousand Feet of Pipe Considering Material, Age, Diameter, and Slope Parallel and Perpendicular to the Pipe’s Longitudinal Axis, Based on a Log-Log Model. Plot Is an Example for Pipe Age Equal to 100 Years, LADWP Data.....	132
4-21	Repair Frequency per Thousand Feet of Pipe Considering Material, Age, Diameter, and Slope Parallel and Perpendicular to the Pipe’s Longitudinal Axis, Based on a Log-Log Model. Plot Is an Example for Pipe Age Equal to 100 Years, LADWP Data.....	134
4-22	Raw Leak Frequency per GIS Pipe Segment, by Material and Diameter, EBMUD Data	137
4-23	Leak Frequency per GIS Pipe Segment as a Function of Pipe Diameter, Material, and Slope, EBMUD Data.....	138
4-24	Leak Frequency per GIS Pipe Segment as a Function of Pipe Diameter, Material, and Slope, EBMUD data.....	139
4-25	Repair Frequency per Thousand Feet of Pipe Considering Material, Age, and Diameter, Based on a Linear Model. Plot Is an Example for Pipe Age Equal to 100 Years, EBMUD Data	140
4-26	Repair Frequency per Thousand Feet of Pipe Considering Material, Age, and Diameter, Based on a Log-Log Model. Plot Is an Example for Pipe Age Equal to 100 Years, EBMUD Data	141
4-27	Repair Frequency per Thousand Feet of Pipe Considering Material, Age, Diameter, and Slope Parallel and Perpendicular to the Pipe’s Longitudinal Axis, Based on a Log-Log Model. Plot Is an Example for Pipe Age Equal to 100 Years, EBMUD Data	142
4-28	Repair Frequency per Thousand Feet of Pipe Considering Material, Age, Diameter, and Slope Parallel and Perpendicular to the Pipe’s Longitudinal Axis, Based on a Log-Log Model. Plot Is an Example for Pipe Age Equal to 100 Years, EBMUD Data	143
4-29	Raw Leak Frequency per GIS Pipe Segment, by Material and Diameter, SFPUC Data	145
4-30	Leak Frequency per GIS Pipe Segment as a Function of Pipe Diameter, Material, and Slope, SFPUC Data.....	146
4-31	Leak Frequency per GIS Pipe Segment as a Function of Pipe Diameter, Material, and Slope, SFPUC Data.....	147
4-32	Repair Frequency per Thousand Feet of Pipe Considering Material, Age, and Diameter, Based on a Linear Model. Plot Is an Example for Pipe Age Equal to 100 Years, SFPUC Data	148
4-33	Repair Frequency per Thousand Feet of Pipe Considering Material, Age, and Diameter, Based on a Log-Log Model. Plot Is an Example for Pipe Age Equal to 100 Years, SFPUC Data	149
4-34	Repair Frequency per Thousand Feet of Pipe Considering Material, Age, Diameter, and Slope Parallel and Perpendicular to the Pipe’s Longitudinal Axis, Based on a Log-Log Model. Plot Is an Example for Pipe Age Equal to 100 Years, SFPUC Data	150
4-35	Repair Frequency per Thousand Feet of Pipe Considering Material, Age, Diameter, and Slope Parallel and Perpendicular to the Pipe’s Longitudinal Axis, Based on a Log-Log Model. Plot Is an Example for Pipe Age Equal to 100 Years, SFPUC Data	151
4-36	Raw Leak Frequency per GIS Pipe Segment, by Material and Diameter, PWB Data.....	153
4-37	Leak Frequency per GIS Pipe Segment as a Function of Pipe Diameter, Material, and Slope, PWB Data	154
4-38	Leak Frequency per GIS Pipe Segment as a Function of Pipe Diameter, Material, and Slope, PWB Data	155
4-39	Repair Frequency per Thousand Feet of Pipe Considering Material, Age, and Diameter, Based on a Linear Model. Plot Is an Example for Pipe Age Equal to 100 Years, PWB Data.....	156

4-40	Repair Frequency per Thousand Feet of Pipe Considering Material, Age, and Diameter, Based on a Log-Log Model. Plot Is an Example for Pipe Age Equal to 100 Years, PWB Data	157
4-41	Repair Frequency per Thousand Feet of Pipe Considering Material, Age, Diameter, and Slope Parallel and Perpendicular to the Pipe’s Longitudinal Axis, Based on a Log-Log Model. Plot Is an Example for Pipe Age Equal to 100 Years, PWB Data	158
4-42	Repair Frequency per Thousand Feet of Pipe Considering Material, Age, Diameter, and Slope Parallel and Perpendicular to the Pipe’s Longitudinal Axis, Based on a Log-Log Model. Plot Is an Example for Pipe Age Equal to 100 Years, PWB Data	159
4-43	Raw Leak Frequency per GIS Pipe Segment, by Material and Diameter, SPU Data	161
4-44	Leak Frequency per GIS Pipe Segment as a Function of Pipe Diameter, Material, and Slope, SPU Data	162
4-45	Leak Frequency per GIS Pipe Segment as a Function of Pipe Diameter, Material, and Slope, SPU Data	163
4-46	Repair Frequency per Thousand Feet of Pipe Considering Material, Age, and Diameter, Based on a Linear Model. Plot Is an Example for Pipe Age Equal to 100 Years, SPU Data	164
4-47	Repair Frequency per Thousand Feet of Pipe Considering Material, Age, and Diameter, Based on a Log-Log Model. Plot Is an Example for Pipe Age Equal to 100 Years, SPU Data	165
4-48	Repair Frequency per Thousand Feet of Pipe Considering Material, Age, Diameter, and Slope Parallel and Perpendicular to the Pipe’s Longitudinal Axis, Based on a Log-Log Model. Plot Is an Example for Pipe Age Equal to 100 Years, SPU Data	166
4-49	Repair Frequency per Thousand Feet of Pipe Considering Material, Age, Diameter, and Slope Parallel and Perpendicular to the Pipe’s Longitudinal Axis, Based on a Log-Log Model. Plot Is an Example for Pipe Age Equal to 100 Years, SPU Data	167
4-50	Raw Leak Frequency per GIS Pipe Segment, by Material and Diameter, Merged Data	169
4-51	Leak Frequency per GIS Pipe Segment as a Function of Pipe Diameter, Material, and Slope, Merged Data	170
4-52	Leak Frequency per GIS Pipe Segment as a Function of Pipe Diameter, Material, and Slope, Merged Data	171
4-53	Repair Frequency per Thousand Feet of Pipe Considering Material, Age, and Diameter, Based on a Linear Model. Plot Is an Example for Pipe Age Equal to 100 Years, Merged Data	172
4-54	Repair Frequency per Thousand Feet of Pipe Considering Material, Age, and Diameter, Based on a Log-Log Model. Plot Is an Example for Pipe Age Equal to 100 Years, Merged Data	173
4-55	Repair Frequency per Thousand Feet of Pipe Considering Material, Age, Diameter, and Slope Parallel and Perpendicular to the Pipe’s Longitudinal Axis, Based on a Log-Log Model. Plot Is an Example for Pipe Age Equal to 100 Years, Merged Data	174
4-56	Repair Frequency per Thousand Feet of Pipe Considering Material, Age, Diameter, and Slope Parallel and Perpendicular to the Pipe’s Longitudinal Axis, Based on a Log-Log Model. Plot Is an Example for Pipe Age Equal to 100 Years, Merged Data	175
4-57	Repair Frequency Pa per Thousand Ft of 8” CI Pipe as a Function of Age, Showing That Pipe has Increasing Repair Rates as It Gets Older	176
4-58	Empirical Cumulative Distribution Function (ECDF) for All GIS Pipe Segments, LADWP Data	178
4-59	Survival Function for All GIS Pipe Segments, LADWP Data	179
4-60	Instrumental Intensity vs. Other Intensity Measures including PGV. Note that Instrumental Intensity Is Essentially Synonymous with Modified Mercalli Intensity (MMI)	180
4-61	LADWP Pipe Network Overlaid on Northridge Earthquake ShakeMap PGV	180

4-62	Histogram of Pipe by Installation Date, Where “Loyr” (Low Year) Is the Subset of the Dataset with PGV \leq 20 Kine, While “Hiyr” Is the Subset with PGV $>$ 20 Kine, LADWP Data.....	181
4-63	ECDF for LADWP Dataset Segmented by PGV Less than 20 Kine (PGVlo, Red Line) and More than 20 Kine (PGVhi, Blue Line)	182
4-64	Similar to above except Only for CI, LADWP Data	183
4-65	Similar to above except Only for DI, LADWP Data.....	184
4-66	Similar to Figure 4-64 but Includes SPU (CI Only) as Well as LADWP (CI Only) Data.....	185
5-1	Possible Events for Future Research.....	188

Acronyms and Abbreviations

AC	Asbestos cement
CGS	California Geological Survey
CI	Cast iron
DEM	Digital elevation model
DI	Ductile iron
ECDF	Empirical cumulative distribution function
EDMUD	East Bay Municipal Utility District
GIS	Geographic Information System
KM	Kaplan-Meier (method)
LADWP	Los Angeles Department of Water and Power
MMI	Modified mercalli intensity
PGV	Peak ground velocity
PWB	Portland Water Bureau
SFPUC	San Francisco Public Utility Commission
SPU	Seattle Public Utility
SRTM	Shuttle radar topography mission (i.e., satellite DEM data)
STL	Steel
USGS	US Geological Survey
Vs30	Shear wave velocity, top 30 meters
WDN	Water distribution networks

Executive Summary

The key issue addressed in this research is the effect of major stress history on remaining service life of buried water distribution pipe. The focus is on the effects of major stress events, such as an earthquake. This issue emerged following the 2014 Mw 6.0 Napa earthquake, where FEMA compensation to the affected water utility depended on whether pipe remaining service life had been shortened by the earthquake. In larger earthquakes, which are anticipated in the near future in southern and northern California as well as in the Pacific Northwest, this may prove to be a challenging and contentious issue.

The method employed to investigate this question is statistical but informed by mechanics of materials. The statistics are water distribution system data and repair history, both ongoing and following major earthquakes. Data was collected from five major west coast utilities: Los Angeles Department of Water and Power (impacted by the 1994 Mw 6.7 Northridge earthquake); San Francisco Public Utilities Commission and East Bay Municipal Utilities District (1989 Mw 7.1 Loma Prieta earthquake); and the Portland Water Bureau and Seattle Public Utilities (negligible and minimal effects, respectively, from the 2001 Ms 6.8 Nisqually earthquake).

The data provided by these utilities varied in format, ranging from scanned paper maps to lists of repairs by address or distance from a street corner, or GIS databases, reflecting the introduction of GIS into the water industry in recent decades. Processing of this data was challenging, so the project developed an innovative method to extract repair locations from the paper map images. This extraction of older data from map images more than doubled the amount of repair data, both in period of observation (20 to 40 years) and in number of repairs, and significantly improved the basis for statistical analysis. The resulting dataset was for 16,000 miles of buried water distribution pipe composed of more than 600,000 GIS segments that required more than 64,000 repairs over varying periods (depending on utility) from 1975 to 2017. For many utilities who are currently basing their asset management programs on a short historical record, this methodology would allow a much broader empirical basis for their asset management programs.

The data was then segregated into earthquake and non-earthquake affected data sets and subjected to multi-variate statistical analysis to develop measures of buried pipe service life as a function of covariates of pipe diameter, material, age, soil, and slope. Survival functions using Kaplan Meier (KM) plots were created, which found that pipes subjected to higher ground motions have a lower probability of survival than those not subjected to high ground motions. For example, everything else being equal, a one-hundred-year-old pipe (i.e., installed in 1917, 100 years after the termination of the LADWP repair record available for this study) has about 25% probability of failure if it was subjected to PGV > 20 kine (cm/s) in the 1994 Northridge earthquake (termed the “hi” population), while if it was not shaken or subjected to non-damaging ground motion (“lo” population), the probability of failure is about half (12%), Figure ES-1.

This is a significant finding. If a utility determines 25% probability of failure as the criteria for replacement, the “hi” population has now reached the end of its useful life, while if the earthquake had not occurred, those pipes would still have a remaining useful life of about 40 years. At a real interest rate of 3%, \$1 of replacement expenditure postponed for 40 years has a value of \$3.26 at the end of that period. **In other words, the earthquake portion of the LADWP pipe network has had its useful life shortened by about 40 years, equivalent to a financial loss of 31% of its replacement value.**

At this project’s publication time, the 1994 event was 26 years ago. The City of Los Angeles will be burdened with a much larger pipe replacement task in the next two decades than if the earthquake had not occurred.

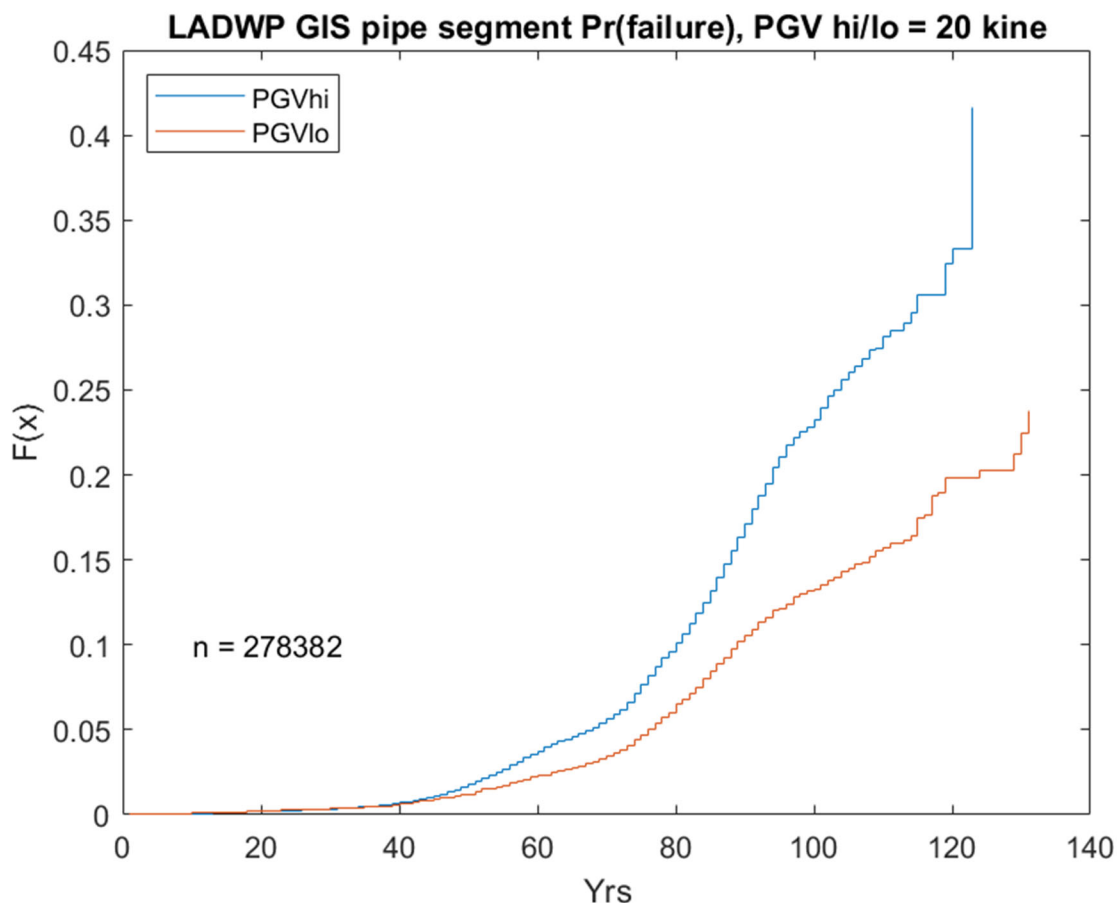


Figure ES-1. Kaplan Meier Plot for LADWP 1997-2017 Dataset Segmented by PGV Less than 20 Kine (PGVlo, Red Line) and More than 20 Kine (PGVhi, Blue Line).

The plot can be read that pipes that for example experienced a peak ground velocity (PGV) of less than 20 cm. per sec. (i.e., 20 kine) have about 25% probability of no repairs in 100 years, while pipes that experience more than 20 kine (i.e., were strongly shaken) have only about half that probability (12%).

The implications of this finding are profound, in that they show that earthquakes cause substantial long-term losses to water utility buried pipe networks, reducing the useful life of these pipes by a significant amount. This has been qualitatively understood by utility engineers of systems affected by major earthquakes but has not been previously quantified. **On this basis, substantially greater disaster assistance is warranted.**

These findings are important for the water industry, in terms of identifying and quantifying a hitherto largely unrecognized effect of major stress events and understanding the financial and disaster aid implications of this effect. More broadly, the data and methods employed in this study should help to improve the basis for utility asset management programs.

Related WRF Research:

- Recent Earthquakes: Implications for U.S. Water Utilities (4408)
- Seismic and Multi-Hazard Conference (5026)
- Seismic Fragility and Restoration of Pump Stations for Potable Water Supply (4709)

CHAPTER 1

Introduction

This section introduces the project and its research topic, discusses previous research on the topic, outlines the approach employed to investigate the topic, and summarizes the organization of this report.

1.1 Purpose and Research Direction

This is the final report on a research project funded by the Water Research Foundation to investigate the effect of stress history on remaining service life of buried water distribution network (WDN) pipe, particularly the effects of major stress events such as an earthquake¹.

The purpose of this research was to address the question: *after the prompt damage and repairs following an earthquake, is there a long-term effect of the earthquake, and does this effect reduce the useful service life of buried pipe?*

The key issue to be addressed in this research is the effect of stress history on remaining service life, particularly the effects of major stress events, such as an earthquake. This issue emerged following the 2014 Napa earthquake, where FEMA compensation to the affected water utility depended on whether pipe remaining service life had been shortened by the earthquake. In future larger earthquakes, which are anticipated in the near future in southern and northern California and the Pacific Northwest, this will prove to be a very challenging and contentious issue. This research is intended to address this issue by developing an analytical framework, data and methods that will permit estimation of remaining service life given the effects of both on-going factors ('normal' stresses, corrosion, etc.) as well as major stress events.

1.2 Background

Cities across the US have aging infrastructure, particularly water distribution networks (WDN). Most US cities were largely built-out by WW1, Figure 1-1, including their WDNs so that as of this writing in 2020 large parts of the nation's WDNs are approaching the end of their useful life:

"Most water systems and distribution pipes will be reaching the end of their expected life spans in the next 30 years (although actual life spans may be longer depending on utility practices and local conditions)." (NRC 2007)

Buried pipe has a relatively long but ill-defined service life. As US water infrastructure ages, the need to quantify remaining service life is becoming increasingly important as a key criterion in utility replacement programs. Service life of buried pipe depends on materials and methods of construction, the pipe's stress environment and the broader environment (particularly its soil but also including pressure and temperature fluctuations and other factors). Another factor is also operator policy – different utilities replace pipe differently, some on a regular schedule, some on a more opportunistic basis and some only when mandated by deteriorating service.

¹ Throughout the report, the emphasis is on earthquake as the major stress event, and the terms "stress event" and "earthquake" will be used synonymously.

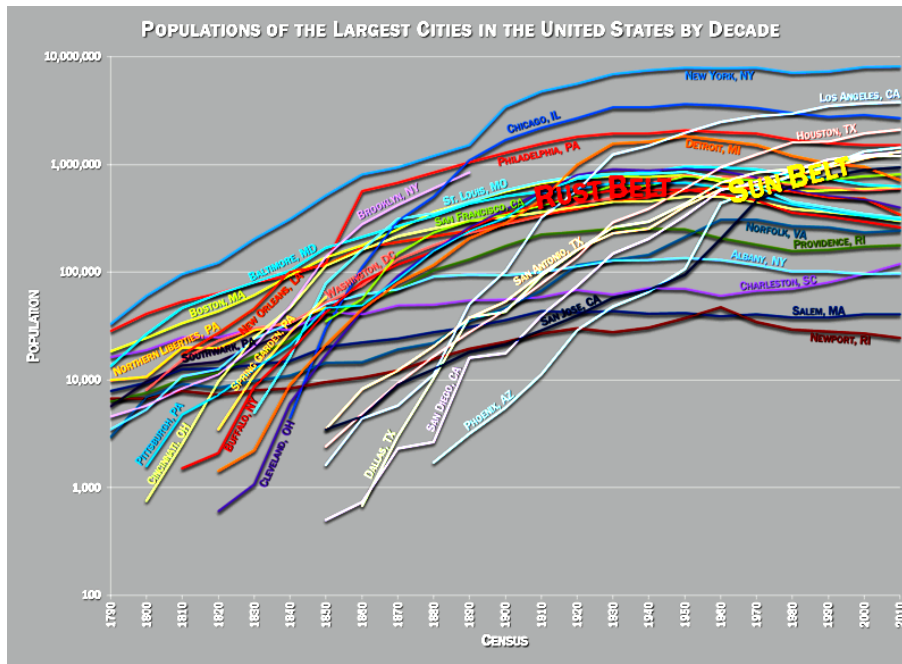


Figure 1-1. U.S. Urban Growth 1790-2010.

Replacement of WDN pipe before failure rates begin to significantly rise is prudent and cost-effective, since failures are very expensive (Water World 1999) and many times the cost of replacement.

Related to this situation is that some cities occasionally experience natural hazards such as earthquakes, that significantly stress their WDNs. These events can result in common cause failures of many pipes, with abrupt loss of service over large parts of the service area. This loss of service deprives firefighters of their primary water supply just as large numbers of fires occur (TCLEE 2005) as well as depriving customers of a vital lifeline for an extended period. This loss of water service for an extended period greatly reduces the ability of the region to recover quickly – that is, the region’s *resilience* is greatly reduced. To improve resilience, an approach of selected WDN replacement is emerging (Davis 2018) in which a *resilient network* is created.

An example of this is the City of Los Angeles and its Los Angeles Department of Water and Power (LADWP), who are initiating a major effort to improve the resilience of Los Angeles (Mayoral Seismic Safety Task Force 2014). A major part of this initiative will address the City’s aging water distribution network. A key issue for this initiative will be the remaining service life of distribution pipes, including how those pipes were affected by the 1994 Northridge earthquake and will be affected by future earthquakes.

These same questions exist for many other utilities, such as the San Francisco Public Utilities Commission. The same questions also confronted the City of Napa in the August 2014 Napa earthquake, for which preliminary analysis indicated that the Napa earthquake significantly shortened the life of portions of that water system (Scawthorn 2015; SPA Risk LLC. 2014). These questions are not confined to the seismic western US but may also confront virtually all major water utilities in the US when other kinds of major stress events (hurricanes, floods) are considered.

1.3 Previous Research

This section summarizes a review of previous research related to this study’s research question. More detailed review of selected papers is provided in Appendix A.

In summary, while there is a vast engineering literature on the topic of WDNs in general, their useful service life, pipe break rates, and earthquake effects on them, an extensive review of the literature found no publication or research addressing the specific topic of this study.

That is, while the issue of estimating the remaining useful life of buried water pipe has been previously addressed, surprisingly the effects of earthquakes or other low-cycle high stress events on the useful life of buried water pipe does not appear to have been previously addressed.

The remainder of this section discusses a few of the most relevant papers found during the literature review, and the reader is referred to Appendix A for more details.

A survey of US and European water utilities (Deb et al. 2002) found that the average break rate for US water utilities was in the range of 0.21 to 0.25 breaks per year per mile of pipe. Based on this data they developed a mechanistic model to account for pipe stress and degraded pipe condition. They also found four methods in use by water utilities for determining point of pipe renewal:

- Scoring systems to assign points based on characteristics of the pipe and its environment
- Economics to compare the costs of repair versus replacement
- Failure probability and regression methods: predict the probability of future failures
- Mechanistic models which attempt to simulate the deterioration of a pipe over time and the loads to which a pipe is subjected.

A broader study on the assessment and renewal of water distribution systems (Grigg 2004) found that “In general, repair, rehabilitation, and replacement practices among utilities vary greatly” (between utilities) and the “lines between repair, rehabilitation, and replacement can be blurred”.

An extensive survey of customer acceptance of water main structural reliability (Damodaran et al. 2005) found the following criteria for water pipe renewal:

- Based on internal costs alone, repair was favored over renewal when the break rate was two per year in the case of trenchless technologies and three per year in the case of open-trench technologies.
- When the external costs resulting from service disruption to 20 households were also factored in, all renewal technologies were favored over repair with two breaks per year.
- When external costs associated with traffic disruption are included with the scenario of service disruption, the decision to renew instead of repair occurs with fewer breaks. In the project scenario, when 150 cars are affected on a daily basis with 20 households affected by service disruption, at least one of the renewal options under consideration is justified over repair with one break per year. When the number of households increases to 50, all renewal technologies are justified with one break per year. When 300 cars and 50 households are affected, any one of the trenchless technologies under consideration is desirable even when there is only one break every other year.

An interesting study (Le Gat, Kropp and Poulton 2013) examined the question “Is the service life of water distribution pipelines linked to their failure rate? as part of developing an infrastructure management plan. From the perspective of the present study, the primary contribution of this work was its examination of WDN pipe survival rates using non-parametric methods.

Highly relevant has been the work of Rajani and co-workers at the National Research Council of Canada, who engaged in a long-term examination of the topic of WDN pipe in general (Rajani and Kleiner 2001;

Rajani, Kleiner and Sink 2012; Rajani and Tesfamariam 2007; Sadiq, Rajani and Kleiner 2004; Tesfamariam, Balvant Rajani and Sadiq. 2006)

In one of many interesting papers, they estimated that a number of factors contributing to the time to failure of cast iron (CI) water mains include: operational conditions; design parameters; external loads (traffic, frost, etc.); internal loads (operating and surge pressures); temperature changes; loss of bedding support, pipe properties and condition; and corrosion pit geometry. As noted by many authors, data on these effects are recorded rarely, if at all, and it is therefore difficult to ascertain the precise causes of failure. Even if all this information were available, any attempt to estimate the pipe condition state would involve considerable uncertainty owing to large spatial and temporal variability that is inherent in this information. Estimation of time to failure is further exacerbated by the uncertainties in determining future corrosion rates, which was handled by the investigators using possibility theory and fuzzy arithmetic.

In order to improve the data situation, several investigators have attempted to compile multi-agency databases of WDN pipe performance, (Folkman 2018) for example performing a survey of 281 water agencies (98 responded in detail). However, this compilation was not of actual data but rather respondent's experiences and opinions.

A critical review of statistical water main break forecasting prediction models (Nishiyama and Filion 2013) based on data for 2002–2012 found that the statistical characterization of the break rate of water mains by means of historical failure data were the key similarity between the models, which were categorized into deterministic, probabilistic, and soft computing methods.

A particularly relevant study (Fragiadakis and Christodoulou 2014) however examined the reliability of WDNs under normal and seismic loading, and found the most significant factor affecting reliability to be the number of previous breaks (NOPB). Figure 1-2 from (Christodoulou and Fragiadakis 2014) shows the very major impacts previous breaks have on the survival of pipes, and the reliability of a WDN.

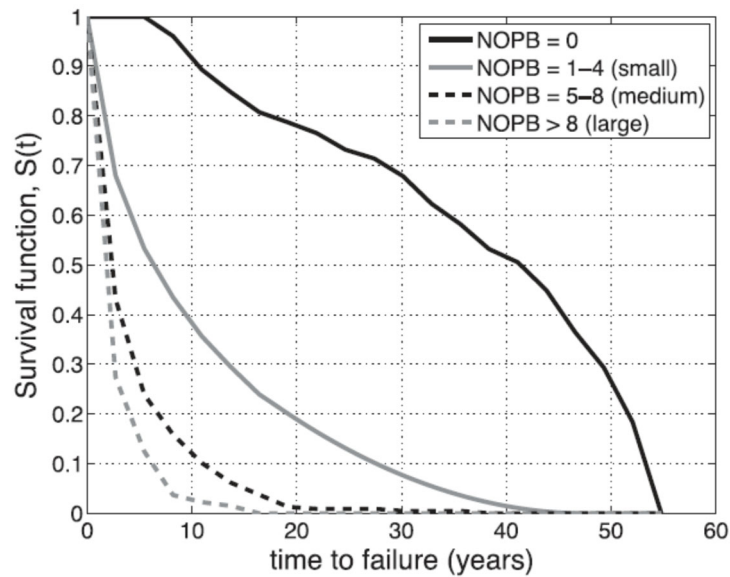


Figure 1-2. Survival Curves for Asbestos Cement Pipes as Function of the Number of Previous Breaks (NOPB).

Source: Christodoulou and Fragiadakis 2014

Lastly, in a work perhaps closest to the focus and methods employed here, (Bardet and Little 2014) found that clustered pipe breaks share many characteristics with human mortality observed during extreme climatological events such as heat waves or air pollution, so that a framework was introduced to analyze the time variations of disruptive pipe break. It was posited that at any time, a cohort of the pipes comprising the water distribution system will be in a weakened state due to fatigue and corrosion. This frail cohort becomes vulnerable during normal operations and ultimately breaks due to rapid increase in crack lengths induced by abnormal stressors. The epidemiological harvesting model so developed was found to have explanatory and predictive power. Major stress events such as earthquakes were however not included in the model.

In conclusion, many investigators have examined various aspects of WDN pipe and/or seismic performance, but not precisely the focal issue of this study. All investigators agree (a) there is poor collection of data on pipe performance (although this situation has improved recently), and (b) even with good data, the complexity of the problem results in large uncertainty. This has been noted by many authors and plagues the questions surrounding WDNs. A few investigators (Bardet and Little 2014; Fragiadakis and Christodoulou 2014; Park et al. 2008) employed survival analysis techniques, although only examining chronic effects such as corrosion and not acute effects such as earthquake. The reader is referred to Appendix A for more details.

1.4 Approach

The research approach employed in this study has been the collection of WDN pipe and performance data from five major west coast water agencies (“five agencies”):

- Los Angeles Department of Water and Power (LADWP)
- East Bay Municipal Utility District (EDMUD)
- Portland Water Bureau (PWB)
- San Francisco Public Utility Commission (SFPUC)
- Seattle Public Utility (SPU)

This data will be employed in a statistical manner using survival analysis to examine WDN pipe survivability. Several of the data sets contain pipe that has experienced to varying degrees either the 1989 Mw 7.1 Loma Prieta (EBMUD, SFPUC) or 1994 Mw 6.7 Northridge (LADWP) earthquakes, while two of the data sets (PWB, SPU) have not experienced major earthquakes and thus can serve as “control” sets. Regarding the latter statement, it should be noted that these latter two data sets are in regions with significant seismic hazard, and the Seattle (SPU) dataset has been subjected to the 1965 Mw 6.7 Puget Sound and 2001 Mw 6.8 Nisqually earthquakes. Relative to the Northridge and Loma Prieta events however, the Puget Sound and Nisqually events caused significantly less, almost negligible, damage, perhaps due to their greater hypocentral depths (greater than 50 km).

1.5 Organization of the Report

Following this Introduction, the next chapter discusses physically based modeling of buried pipe. The discussion of physically based modeling is not intended to develop a mechanics of materials solution to the question this study addresses. This is because there is an enormous literature on mechanics of materials approaches to buried pipe behavior, some of which has or will be cited (see also the literature review in Appendix A), the crux of which is that mechanics of materials approaches are useful when detailed data on pipe history, its materials, the surrounding soils and loading history are available. Such data is not typically available in detail for the many pipes in a WDN, so consequently there is also an enormous literature on statistical approaches to buried pipe behavior. Rather, the discussion of physically based models is intended to inform the statistical approach which is the fundamental method employed in this study. Chapter 3 discusses in detail the statistical data that are the foundation of this study. The data is summarized, and its treatment and cleaning are briefly reviewed, concluding with a summary of the final datasets to be employed for analysis. Analysis is presented in Chapter 4, following by a summary of findings in Chapter 5, and a discussion of conclusions and future research in Chapter 5. References and Appendix A complete the report.

CHAPTER 2

Physically Based Modeling of Buried Pipe

This chapter discusses physically based modeling of buried pipe with the goal less of developing a full mechanics of materials solution to the question this study addresses but more to inform the statistical approach subsequently employed.

2.1 Closely Related Physical Models

2.1.1 Pipe Failure Models

An extensive review of physically based models of water main structural deterioration is offered by (Rajani and Kleiner 2001). Their review considers several sources of environmental excitation to water mains, mostly corrosion, thermal forces, pressure surges, and geotechnical effects (frost loads, swelling clays, soil shrinkage, and poor compaction of backfill). Seismic forces are not specifically considered. The models they review estimate the resulting axial and hoop stresses in pipes as intermediate variables. By “intermediate variable,” we mean variables that matter to the observable outcomes we care about: water main failure through circular or longitudinal pipe fracture. They briefly touch on a few dozen models, and provide equations for about 10 models. The superset of inputs, intermediate variables, and outputs of these ten models are listed below.

Input data

- Frost depth
- Frost heave
- Trench width
- Soil material properties and pH
- Earth and surface loads
- Pipe material properties, dimensions, and age
- Internal pressure
- Temperature changes
- Pipe corrosion pit dimensions on inner and outer pipe surfaces

Intermediate variables

- Axial and hoop stresses

Output

- Occurrence of pipe fracture
- Remaining useful life

The present project is primarily interested in remaining useful life. Of all the models reviewed by Rajani and Kleiner, only one—(Randall-Smith 1992) – produces that output. (Conceivably one might create a new stochastic model of remaining useful life that relates occurrence of pipe failure to time-varying inputs, but this is not that project.) The (Randall-Smith 1992) model proposes the remaining useful life of water mains as

$$\rho = \left(\frac{t}{P_e + P_i} \delta \right) - t \quad \text{Equation 2-1}$$

where ρ is remaining life, t is the age of the water main, δ is the thickness of the original pipe wall, P_e is the external pit depth and P_i is the internal pit depth. There is no obvious method to account for thermal forces, pressure surges, or geotechnical effects, especially earthquake excitation.

2.1.2 Material Fatigue Models

Fatemi and Yang (1998) offer a similar review of cumulative fatigue damage and life prediction theories for homogeneous materials—not pipelines per se, but conceivably pipe made of cast iron, ductile iron, steel, and plastics in which polymers are not preferentially oriented. They review approximately 50 fatigue damage models and provide detail for about 25. Inputs, intermediate variables, and outputs each model generally include a subset of the following.

Input data

- Number of applied cycles
- Total cycles to failure
- Stress history, total or plastic strain history, or loading evolution
- Material properties (elastic modulus, original failure stress, plastic strain energy at failure, ductility capacity, etc.)
- Initial, intermediate, and final crack lengths
- Fatigue limit strain
- Critical crack length associated with crack propagation
- Frequency of cycles

Output

- The occurrence of material failure

None of the models resemble the input data of the pipe-failure models. Their input data resemble the intermediate variables of the pipe-failure models. All the models require some estimate of stress or strain history. They generally reflect variations or enhancements to Miner's rule:

$$D = \sum_i r_i = \sum_i \frac{n_i}{N_i} \quad \text{Equation 2-2}$$

Where:

D = damage, an index that ranges from 0 to 1.0 and 1.0 causes failure

i = an index to stress amplitude

σ_i = stress amplitude at level i

r_i = cycle ratio for load at stress amplitude σ_i

n_i = number of cycles at stress amplitude σ_i

N_i = fatigue life, in cycles, meaning the number of cycles associated with failure when loaded at σ_i

However, (Fatemi and Yang 1998) point out that Miner's rule is often unsatisfactory, for example because failure can occur at $D > 1$ when loading increases in intensity over time and at $D < 1$ when loading decreases. However, since we seek a simple model that does not depend on whether loading increases or decreases over time, we rely on

Equation 2-2. Furthermore, let us consider the subscript i to index sources of loading: traffic, thermal, and seismic loads, and let us account for corrosion and local stress concentrations as modifiers to local stress. Let us model traffic, thermal, and seismic loads as having characteristic stationary intensities, and replace

Equation 2-2 with

Equation 2-3 in which subscripts v, t, and e denote traffic, thermal, and earthquake, respectively. If all pipe failed through fatigue, then r_i would measure the fraction of the pipe life used up by loading condition i . We therefore seek r_e , the fraction of pipe that does not break in earthquakes but that is used up by fatigue caused by seismic loads below that required to cause a leak or a break during the earthquake.

$$D = r_v + r_t + r_e$$

$$= \left(\frac{n_v}{N_v} \right) + \left(\frac{n_t}{N_t} \right) + \left(\frac{n_e}{N_e} \right) \quad \text{Equation 2-3}$$

Each loading condition will be assigned a potentially uncertain stress level σ that can be aggravated by corrosion and by local constraints and other conditions causing stress concentrations that increase local cycle stresses and decrease fatigue life.

2.2 Variables Available from Utilities

Relevant to this study, pipe network and damage data available from utilities generally include the following:

- Pipe diameter and material
- Year of installation
- Occurrence and year of leak
- Geographic location
- Slope
- Outdoor temperature history, though not temperature at pipe burial depth
- Occurrence and degree of strong motion in terms of peak ground velocity

Traffic load, temperature, corrosion and fatigue data are rarely available, and usually only at very few locations within a WDN, and often only for short periods.

2.3 Traffic, Thermal, and Seismic Fatigue Proxies for Hidden Variables

Notice the lack of commonalities among the physical pipe-failure models, material-fatigue models, and pipe network and damage data. We have no information about the presence or extent of corrosion at the time of failure. We do not know whether thermal forces were significant at burial depth. We have no information about pressure surges at the time of failure, whether pressure variations caused significant cyclic stress loading, much less the degree or frequency of cyclic stress from pressure variations. We have no information about backfill, the presence of swelling clays, soil shrinkage, and poor compaction of backfill. We do not know which leaks were associated with axial forces (round cracks) or hoop stresses (longitudinal split).

We know that in the Loma Prieta earthquake, some utilities recorded water main damage modes (Lund and Schiff 1992). Those data reveal that approximately 7% of pipe repairs appeared to involve corrosion (33 instances out of 476 pipe breaks and leaks), but an engineer from the City of Napa reported that

corrosion damage was commonly observed at pipe breaks in the August 2014 South Napa earthquake (J. Eldredge, City of Napa, verbal commun., 22 Sep 2020).

The data necessary to model fatigue seems lacking from utilities; one might call them *hidden variables*. But can one at least estimate the effects of vehicle loading, thermal loading, seismic loading, and corrosion on an order-of-magnitude basis, and compare with parameters of common fatigue models?

2.3.1 Uncertain S-N Curves for Some Pipe Materials

Figure 2-1 shows an S-N curves for ductile iron in which it can be seen that N is uncertain given the applied stress amplitude σ and that N is lognormally distributed conditioned on σ . It will be useful to quantify the effect of that uncertainty.

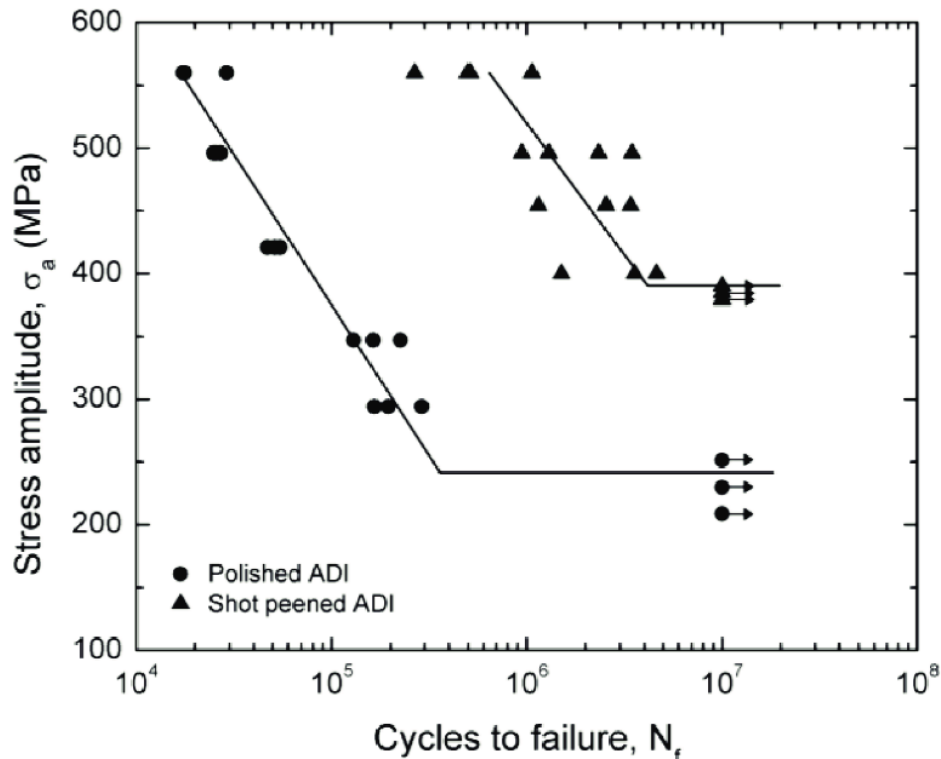


Figure 2-1. S-N Curve for Ductile Iron.

Source: Zammit 2018

One can approximate θ_N , the median value of fatigue life N , as log-log with applied stress amplitude σ :

$$\theta_N = \exp\left(m \cdot \ln\left(\frac{\sigma}{MPa}\right) + b\right): \quad \theta_N < N_\infty, \sigma < \sigma_u \quad \text{Equation 2-4}$$

where m and b are the slope and y-intercept of the line in log-log space, N_∞ denotes the value of N at which lower values of σ no longer cause fatigue damage and $\theta_N \rightarrow \infty$, and σ_u denotes rupture stress. One can also estimate the variability in the cast iron S-N relationships. At a constant level of stress, N appears to be approximately lognormally distributed.

In the case of cast iron, the 10th and 90th percentile bounds differ by a factor of $10^{1.15} = e^{2.65} = 14$, suggesting a standard deviation of $\ln(N)$ (denoted here by β) = $2.65/2.56 \approx 1.0$. Ductile iron and steel seem to have $\beta \approx 0.4$. One can thus approximate the probability distribution of N as in equation

$$P[N < v] = \Phi\left(\frac{\ln(v/\theta_N)}{\beta}\right); \quad v < N_\infty, \sigma < \sigma_u \quad \text{Equation 2-5}$$

In the equation, N is the uncertain fatigue life, in cycles, v is a particular value that N might take on, σ is the applied stress amplitude, θ_N is the median value of N from

Equation 2-4 and β is the standard deviation of the natural logarithm of N . Table 2-1 provides values of m , b , β , and N_∞ for each of the three materials. It also provides the elastic modulus E and rupture stress σ_u , the former from various sources and latter from Figure 2-1.

Table 2-1. Parameters of Probabilistic S-N Curves for Cast Iron, Ductile Iron, and A36 Steel.

Material	m	b	β	N_∞	E (GPa)	σ_u (MPa)
Cast iron	-6.29	37.8	1.0	200,000	125 ± 45	120
Polished austempered ductile iron	-0.78	14.8	0.4	300,000	165 ± 5	550
A36 steel	-8.23	57.4	0.4	1,000,000	200 ± 10	420

Since N is uncertain, especially for cast iron, ignoring X_4 , one can integrate over the range of N_e :

$$E[r_i] = \int_{v=0}^{\infty} \frac{n_i}{v} \cdot f_{N_i}(v) dv \quad \text{Equation 2-6}$$

$$= \int_{v=0}^{\infty} \frac{n_i}{v} \cdot \phi\left(\frac{\ln(v/\theta_{N_i})}{\beta_i}\right) dv$$

For each loading condition, vehicle loading, thermal loading, and seismic loading, it will be necessary to evaluate the number of cycles n_i , some characteristic stress level σ_i , and fatigue life N_i at stress level σ_i .

2.3.2 Vehicle Loading

Buried pipe under streets experience traffic loads on the order of 100 to 1000 cycles per day, or perhaps 10 million cycles in 100 years, equivalent to 100,000 cycles per year of age. Let

$$n_v = 100,000 \cdot \text{age} \quad \text{Equation 2-7}$$

We know that vehicle loads on buried can cause loading strains on the order of 10 microstrain (denoted here by $\mu\epsilon$) per 1,000 lb. of wheel loading (Page 1966). See Table 2-2 for the implied cyclic stress from vehicle loading (denoted here by σ_v): on the order of 1 to 2 MPa, or 0.4% to 1.1% of ultimate tensile strength.

Table 2-2. Stresses Due to 1,000 Lb. of Wheel Loading.

Material	Strain ($\mu\epsilon$)	Cyclic stress σ_v (MPa)	σ_v/σ_u
Cast iron	10	1.2	1%
Ductile iron	10	1.7	0.3%
Mild steel	10	2.0	0.5%

Stresses from 1,000-lb vehicle loads are all 2 orders of magnitude below the lower threshold for high cycle fatigue. Absent stress concentrations resulting from corrosion and hard points, traffic loads should be too small to lead to fatigue failure. Ring stress from vehicle loads increases approximately with the square of the reduction in wall thickness, meaning that a pit that measures half the wall thickness

increases maximum ring stress by a factor of 4. A pit would have to be on the order of 90% of the wall thickness to increase σ to the point where $N'_v < \infty$.

Local hard points might cause traffic-induced pipe stresses to be locally much higher, but it is hard to see how one could create a physical model for any kind of common local hard point without statistics of the dimensions of such hard points and other unknown support conditions. Let us therefore speculate with a simple uncertain parameter X_2 that increases ring stress due to local hard points, and another parameter X_3 that denotes the increase in ring stress associated with pit depth c in a pipe with wall thickness h :

$$X_3 = \left(\frac{h}{h-c} \right)^2 \quad \text{Equation 2-8}$$

Pit depth almost certainly increases with time, but the soil corrosivity parameters to model c as a time series seem to be all hidden.

What would the product of X_2 and X_3 have to be for vehicle loads to induce high-cycle fatigue in buried pipe? How sensitive to the product is fatigue life? Let N_∞ , σ_∞ denote the values of N and σ at which the S-N curve transitions from loglinear to flat. Let σ_v denote the cyclic stress from Table 2-2. Let $(\min X_2 \cdot X_3)$ denote the minimum value of the product for $X_2 \cdot X_3 \cdot \sigma_v \geq \sigma_\infty$. Let N_{v2} denote fatigue life N when $X_2 \cdot X_3 = 2 \cdot (\min X_2 \cdot X_3)$, that is, when one doubles the product from its threshold value. Table 2-3 shows the results, using the 50th percentile cast iron S-N curve, the polished DI S-N curve, and the A36 steel S-N curve.

Table 2-3. Sensitivity of Traffic-Load Fatigue Life to Hidden Variables X_2 and X_3 .

Material	N_∞	σ_∞	σ_v	$\min X_2 \cdot X_3 = \sigma_\infty / \sigma_v$	N_{v2}
Cast iron	200,000	70 MPa	1.2 MPa	60	4,000
Ductile iron	300,000	250 MPa	1.7 MPa	150	30,000
A36 steel	1,000,000	200 MPa	2.0 MPa	100	1,000

The table shows that N_v is enormously sensitive to the product $X_2 \cdot X_3$. For cast iron to experience damage from vehicle loading, the product would have to be on the order of 60 to produce cyclic stresses necessary for fatigue to matter. The product would have to be on the order of 100 to 150 to activate cyclic fatigue for ductile iron or steel. But merely doubling that product would reduce the fatigue life up to three orders of magnitude: from 200,000 to 4,000 cycles in cast iron, from 300,000 to 30,000 cycles in ductile iron, and from 1,000,000 to 1,000 cycles in A36 steel.

2.3.3 Thermal Loading

Rajani et al. (2012) seem to show that thermal loads do affect pipe life, and that the change in air temperature over 30 days correlates most strongly with damage. But since thermal stresses under ideal support conditions are too small to cause fracture, it seems reasonable to infer that local support constraints such as laterals cause stress concentrations that increase thermal stresses to the point where fatigue matters. The 30-day timestep does not seem to mean that the number of cycles for purposes of fatigue analysis is the pipe age in months; rather that the applied stress amplitude relates to the maximum temperature change in a 30-day period. Outside air temperature in many places can drop dramatically over the space of a month. It still seems reasonable to take the *number* of thermal fatigue cycles as the number of years the pipe has been in the ground,

$$n_t = \text{age} \quad \text{Equation 2-9}$$

The applied stress amplitude is probably related to the difference between daily-average summer temperatures and daily-average winter temperatures, transmitted to pipe through warmer or cooler water in reservoirs.

$$\Delta T = \bar{T}_{\text{summer}} - \bar{T}_{\text{winter}} \quad \text{Equation 2-10}$$

Table 2-4 shows average seasonal temperature variations in various west-coast locations. The figures use the median of daily high and daily low summer as the average daily summer temperature, and the average of the daily high and low winter temperature as the average daily winter temperature for use in Equation 2-10.

Table 2-4. Average Seasonal Temperature Flux.

Location	Δ T (deg F)
Los Angeles	17
Sacramento	27
San Diego	20
San Francisco	14
Seattle	24

Thermal stresses in a long uniform run of pipe with a coefficient of thermal expansion denoted by α subject to temperature change ΔT change is given by:

$$\sigma_t = E \cdot \alpha \cdot \Delta T \quad \text{Equation 2-11}$$

Table 2-4 suggests that pipe in the western United States might experience temperature changes of 15 to 30 deg F in a year. Restrained pipe subject to a 20 deg F temperature drop would experience strains on the order of 100 $\mu\epsilon$, 10 times greater than under vehicle loading, with stresses on the order of 10 to 30 MPa, but still only 5% to 10% of their ultimate tensile strength, as shown in Table 2-5. Where ranges are shown, the table uses the midpoint of the range for Equation 2-11.

Table 2-5. Tensile Stress in Restrained Pipe Subject to 20F Temperature Drop.

Material	α $\mu\epsilon/F$	Strain (-20F) ($\mu\epsilon$)	σ_t (-20 F) (MPa)	σ_t/σ_u
Cast iron	5.8	120	15	12%
Ductile iron	6.0	120	20	4%
Mild steel	7.0	140	28	7%

At these levels of stress, S-N curves again suggest that these materials ought to be able to experience an essentially infinite number of cycles without experiencing fatigue failure due to thermal stresses.

As with traffic loads, let us imagine that local support conditions and corrosion greatly amplify thermal stresses. Let X_4 denote a hidden variable that increases local thermal stresses because of local support conditions and let X_5 denote the increase in thermal stress due to reduction in cross sectional area from corrosion.

$$X_5 \approx \frac{h}{h - c_a} \quad \text{Equation 2-12}$$

Here, c_a denotes the average pit depth around the circumference of the pipe at an arbitrary cross section. Let us define $\min X_4 \cdot X_5$ as with traffic loads: the minimum value of the product required to make thermal forces play a role in fatigue, at last as modeled with Miner's rule. There is also an upper bound to $X_4 \cdot X_5$, above which the material ruptures without fatigue. Let us denote

$$\max(X_4 \cdot X_5) = \frac{\sigma_u}{\sigma_t} \quad \text{Equation 2-13}$$

Table 2-6 depicts the range of this amplifying factor $X_4 \cdot X_5$ over which fatigue can matter: a factor of about 2. The values shown in the table assume a 20 deg F temperature change over the space of about 30 days; other values of ΔT would produce a different range, but the high value would always be about 2 times the low value for these materials.

Furthermore, there is a minimum value of fatigue life associated with cyclic stresses near rupture. Let us denote this minimum by N_{\min} . It can be seen at the left end of the curves in Figure 2-1. The table shows the values for the most susceptible cast iron plot denoted $P = 10\%$, polished ADI, and A36 steel. Given n_t around 100, the maximum cycle ratio (denoted here by r_{\max}) is thus about $100/N_{\min}$, also shown in the table. The table shows that if thermal stresses contribute to cyclic fatigue, they can only reduce the life of the pipe on the order of 10%. At least according to the somewhat simple Miner's rule.

Table 2-6. Sensitivity of Thermal-Load Fatigue Life to Hidden Variables X_4 and X_5 .

Material	N_{∞}	σ_{∞} (MPa)	$\sigma_t(20F)$ (MPa)	$\min X_4 \cdot X_5 = \sigma_{\infty}/\sigma_t$	$\max X_4 \cdot X_5 = \sigma_u/\sigma_t$	N_{\min}	r_{\max}
Cast iron	200,000	70	15	5	8	4,000	0.025
Ductile iron	300,000	250	20	12	28	20,000	0.005
A36 steel	1,000,000	200	28	7	15	1,000	0.10

But since Rajani et al. (2012) do seem to show that thermal fatigue may be real, it also seems reasonable to hypothesize that local support conditions and corrosion, separately, together, or in concert with other causes, can amplify local stress on the order of 10 times that implied by thermal stress alone with ideal support conditions. Such amplification can cause fatigue under two conditions:

1. In the most susceptible pipe (e.g., cast iron) and
2. At high, but not-too-high, stress: i.e., between $0.5\sigma_u < (X_4 \cdot X_5 \cdot E \cdot \alpha \cdot \Delta T) < \sigma_u$

However, Rajani et al. (2012) suggest that such conditions may exist, implying that $X_4 \cdot X_5$ can reach 10. We also know that corrosion may be absent or not believed to be a factor in pipe failure, as in Lund and Schiff's (1992) observation that 93% of pipe failures in Loma Prieta exhibited no corrosion. That is, often $X_5 = 1$, which implies that support restraints and other causes of local stress concentrations can make X_4 reach 10.

2.3.4 Seismic Loading

O'Rourke (O'Rourke and Liu 2012) show that wave passage can cause ground strain of 500 to 1,000 $\mu\epsilon$ at peak ground velocity around 30 cm/sec. Taking pipe strain as equal to ground strain implies the equation for pipe stress σ_e in Equation 2-14. Note that earthquake wave passage can impose strains 10 times that from thermal loading and 100 times greater than vehicle loads.

$$\sigma_e = 25 \cdot 10^{-6} \cdot \frac{PGV}{\text{cm/sec}} \cdot E \quad \text{Equation 2-14}$$

What about number of cycles, n_e ? A review of available literature (Hancock and Bommer 2005) on the subject and find estimates ranging from $5 \leq n_e \leq 50$ for earthquakes with $6 \leq M_w \leq 8$. A reasonable approximation through the cloud of the relationships they show is given in Equation 2-15.

$$n_e = 4 + 4 \cdot (M_w - 5)^2$$

$$\geq 4$$

Equation 2-15

How much fatigue damage might an Mw 7 earthquake causing PGV = 30 cm/sec cause? Table 2-7 provides the answer: little. The seismic cycle ratio is enough to reduce the life of the cast-iron pipe by 0.03% but the ductile iron and A36 steel essentially none.

Table 2-7. Seismic Cycle Ratio r_e Associated with a M_w 7.5 Earthquake Causing PGV = 25 cm/Sec.

Material	n_e	σ_e (MPa)	N_e	$r_e = n_e/N_e$
Cast iron	20	95	64,000	0.0003
Ductile iron	20	125	infinite	0
A36 steel	20	150	infinite	0

But recall that there may be local support conditions and other causes of stress concentrations that increases seismic stress by a factor of $X_4 > 2$, sufficient to bring stress levels in the ductile iron and steel to the range of $0.5 \sigma_u < \sigma_e < \sigma_u$.

For cast iron, $\theta_N = 64,000$ and $\beta = 1$. Numerically integrating Equation 2-7 yields $E[r_e] = 0.0005$.

2.4 Conclusions

An attempt was made to derive a physically based model of earthquake fatigue on buried pipe based on a linear version of Miner's rule, considering vehicle loading, thermal stress, earthquake loading, with hidden variables to infer the effects of corrosion and other causes of local stress concentrations.

Water utilities lack much of the necessary information, especially regarding frost depth, frost heave, trench width, soil material properties and pH, earth and surface loads, internal pressure, water temperature changes, pipe corrosion pit dimensions on inner and outer pipe surfaces, and support conditions that might locally aggravate stress. However, enough experimental evidence exists to lead to several conclusions:

- Vehicle loading appears to be two orders of magnitude too small to cause fatigue
- Thermal loading does appear to cause fatigue failure, but mostly when aggravated by some combination of corrosion, local support conditions, and other causes of stress concentration that aggravate local stress by a factor up to 10 times what one might estimate from simple, ideal conditions of a continuous pipe
- Fatigue due to earthquake loading appears to be large enough to cause a decrease in pipe life under Miner's rule, even without local stress concentrations, but the decrease is modest. Even accounting for the wide variability in the S-N relationship for cast iron, a physically based fatigue estimate for cast iron pipe suggests that earthquake loading 20% below the rupture strength of cast iron should decrease its useful life by less than 0.1%. That estimate appears to be at odds with empirical observations.

A more sophisticated fatigue model might lead to different conclusions. A model that accounted for loading sequence (lower to higher stresses over time) might show more damage from earthquake loads. One might consider theories using micro fatigue crack growth. But with each step toward greater and

greater sophistication, one steps farther and farther from the data we seem to have from water utilities. It does not appear practical to derive a purely physically based estimate of earthquake-induced pipe aging with available data.

CHAPTER 3

Data

This section summarizes the data collected for this project, its treatment and cleaning and the resulting datasets to be employed for analysis.

3.1 Data Collection Methodology

Data was obtained by contacting key persons at each of the five agencies and receiving GIS and other data on the current water distribution pipe networks and repair data. Both sets of data but especially repair data varied greatly, the latter not only varying between agencies but also varying in time within each agency.

3.2 Data Received

This section summarizes the data received from the five agencies.

3.2.1 LADWP Data Format

The Los Angeles Department of Water and Power (LADWP) was founded in 1902 to supply water to residents and businesses in Los Angeles and surrounding communities and is the largest municipal utility in the United States, serving over four million residents 160 billion gallons of water (maximum flow). LADWP provides water to the City of Los Angeles through a water distribution pipe network serving an area measuring at maximum 44 miles N-S and 32 miles E-W. The network is comprised of 7,500 miles of pipe in 280,000 GIS pipe segments, Figure 3-1.

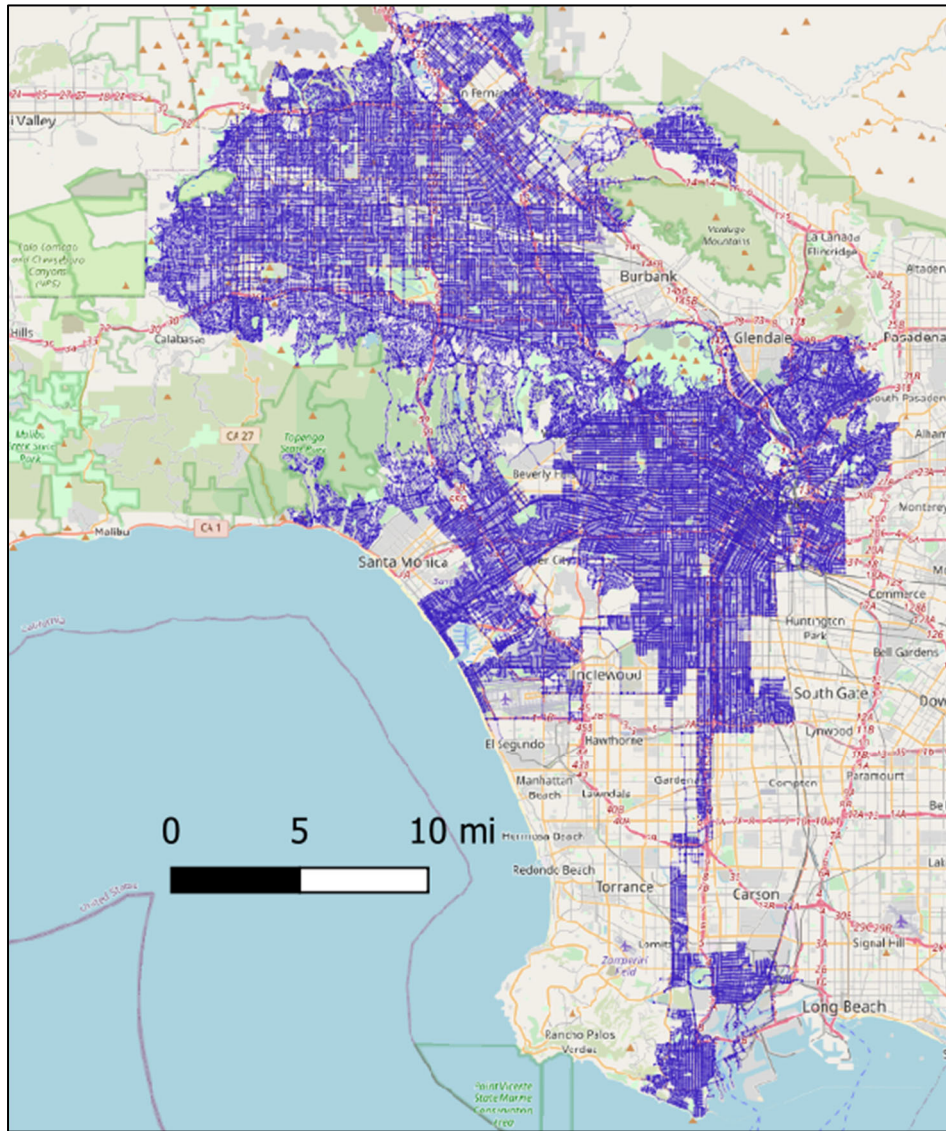


Figure 3-1. LADWP Water Distribution Pipe Network.

Data received from LADWP consisted of two types of data: (1) scanned paper maps for repair data for 1960-2000, and (b) digital datasets for 2000-2017. Some records exist for repairs prior to 1960 but were not employed for this project.

3.2.1.1 LADWP 1960-2000 Data

For the period 1960-2000 LADWP maintained its repair records largely in paper format on maps compiled for each half decade or lustrum, an example of which is shown in Figure 3-2. The maps were detailed drawings of the distribution system on which annotations consisting of a black ink line drawn through the pipe at the location of repair together with a two-digit number indicating the year of the repair were made for each repair, highlighted in Figure 3-3. The black ink annotations are darker than the underlying maps, but only barely and are difficult to discern. Since the forty years from 1960-2000 consist of eight lustra, there are eight maps for each grid cell. In total there are 604 grid cells, Figure 3-4 so that there exist approximately 4,800 maps. The map images vary in color and quality, with earlier maps having a sepia tone, Figure 3-5. The maps are geo-referenced, so that they may be geo-located in

the grid cells using GIS software, Figure 3-6. Although the images overlap, cropped alignment is reasonably good, Figure 3-7.

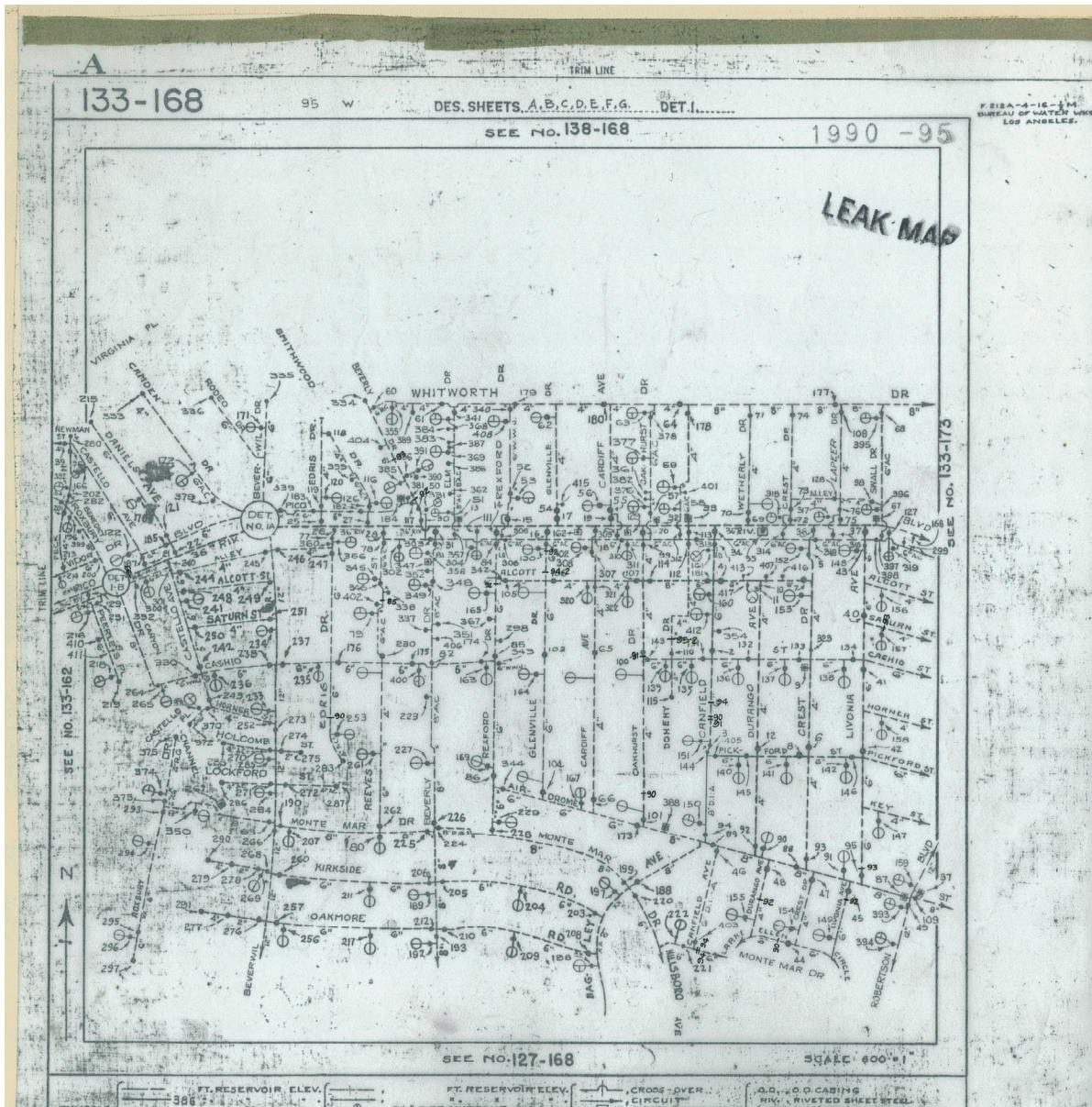


Figure 3-2. LADWP Data Map for Grid Cell 133-168 for Years 1990-1995.

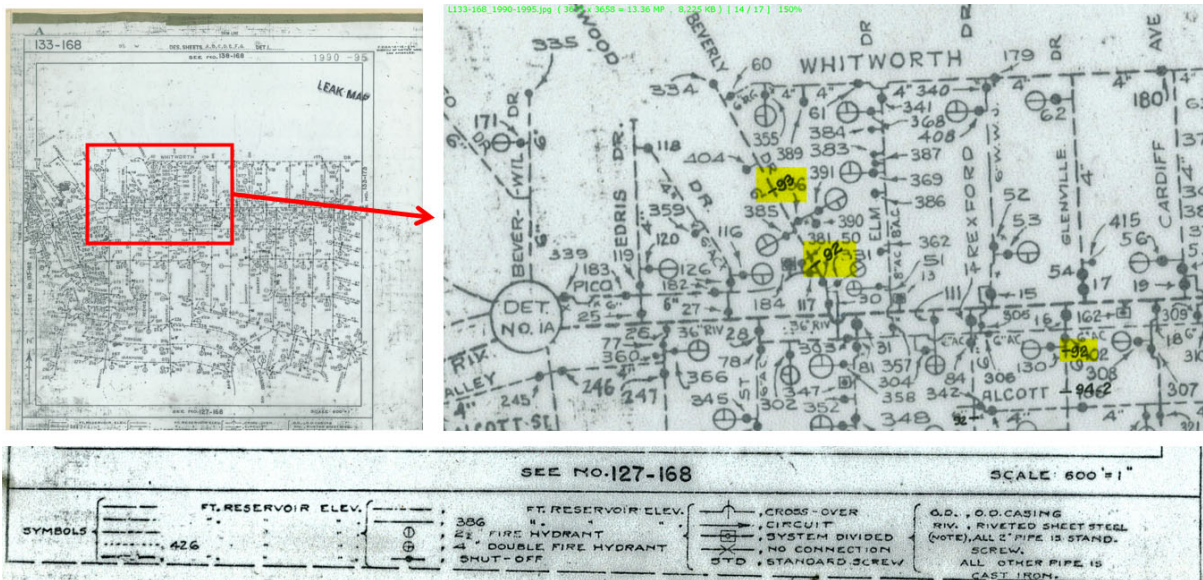


Figure 3-3. LADWP Data Map Showing Annotations (Highlighted Yellow) with Map Legend Below.

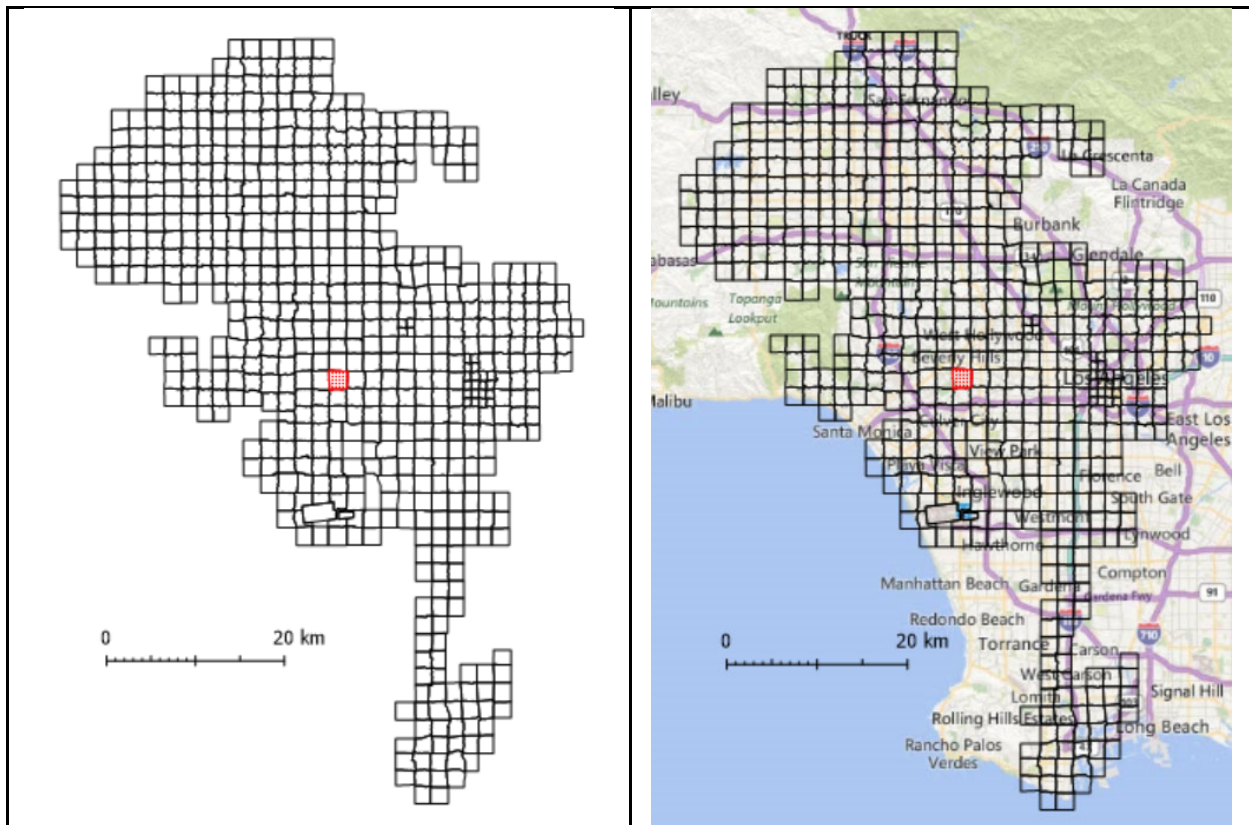
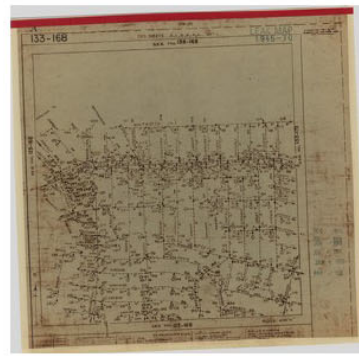


Figure 3-4. LADWP 1960-2000: Repair Data Grid Cells, Cell 133-168 Highlighted Red.



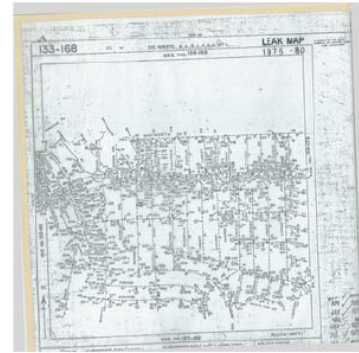
L133-168_1960-1965



L133-168_1965-1970



L133-168_1970-1975



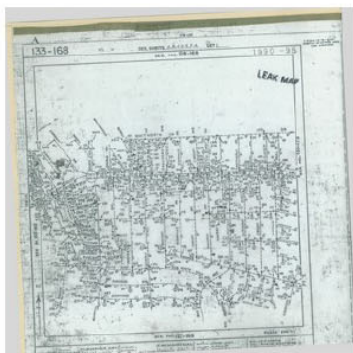
L133-168_1975-1980



L133-168_1980-1985



L133-168_1985-1990



L133-168_1990-1995



L133-168_1996-2000

Figure 3-5. LADWP 1960-2000: Example Maps for Eight Lustra.

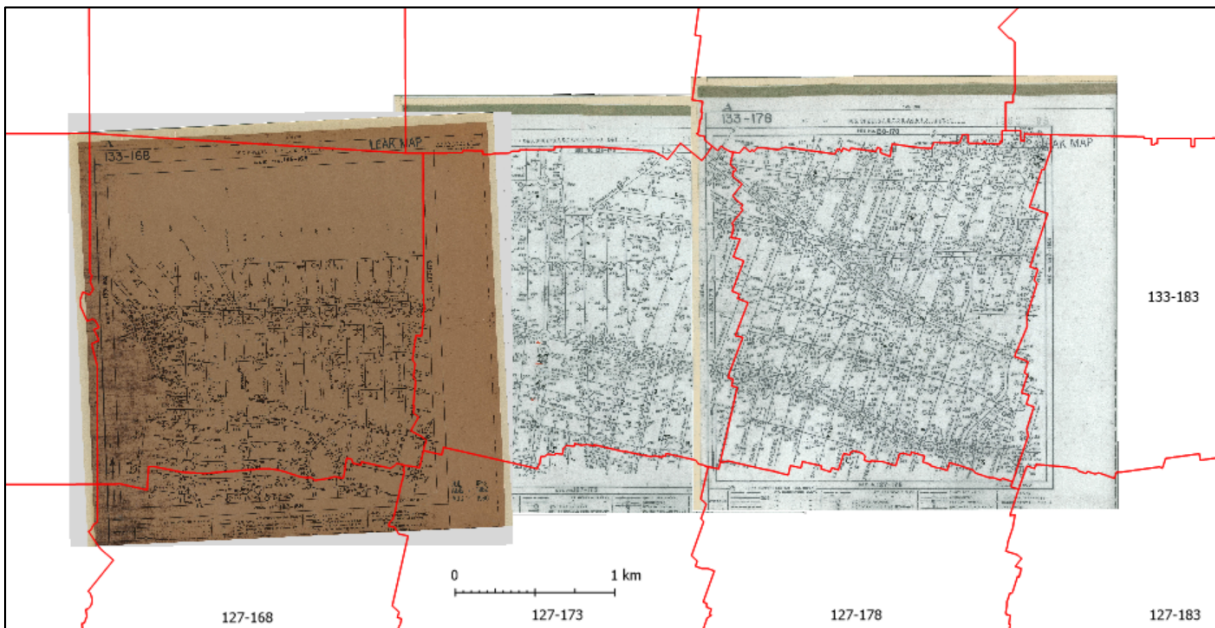


Figure 3-6. LADWP 1960-2000: Example Maps for Several Grid Cells, Maps from Different Lustra.

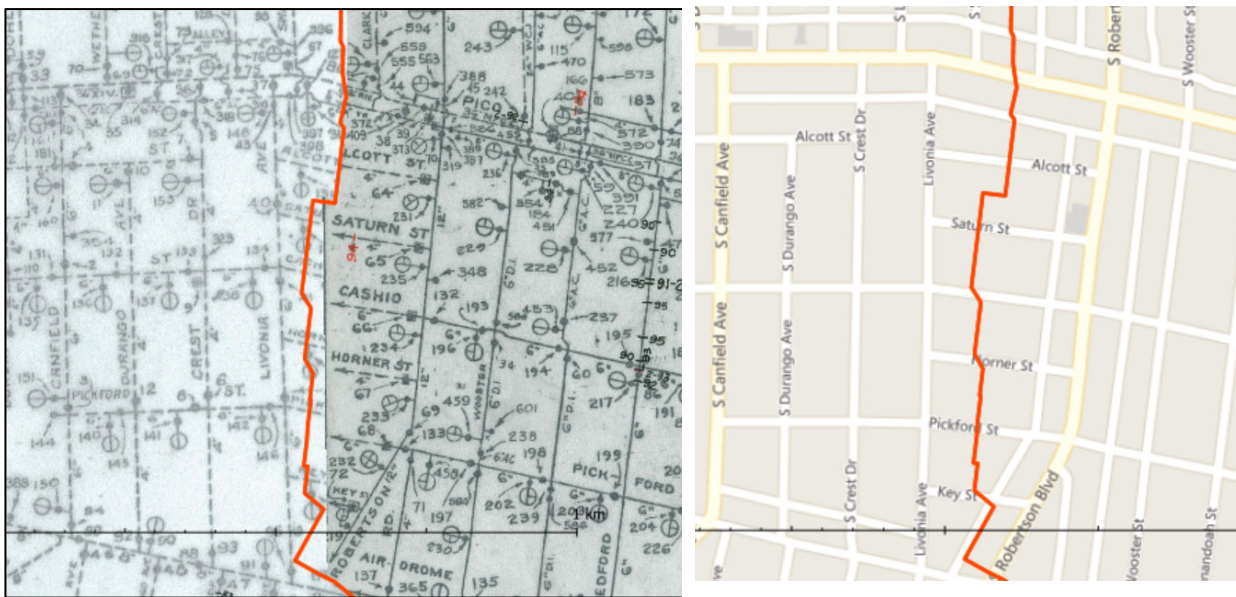


Figure 3-7. LADWP 1960-2000: Example Map Alignment across Cell Boundaries.

3.2.1.2 LADWP 2000-2017 Data

The format of data for repairs since 2000 was received from LADWP and was in the format shown in Table 3-1, with distribution as shown in Figure 3-8.

Table 3-1. LADWP Data Received.

FIELD	EXAMPLE
ID	280257
OBJECTID	1
WGS_FID	2602411
ORIENTATIO	0
SOURCE	LEAKRPT
OWNER	DWP
WSM_NBR	106-189
RENDER_SCA	1
LEAK_DOC_I	30314
LEAK_SYS_I	0
LEAK_STATU	HISTORIC
RPT_TYPE	MAIN
RPT_MONTH	38537
DISTRICT	H
RPT_DATE	38537
WK_ORDER	WHM11A
ADDRESS	6019 S 6TH AV
MAIN_ST	6TH AV
CROSS_ST	0
PIPE_SIZE	4
PIPE_TYPE	C.I.
YR_INST	1924
PLR_INST	0
LEAK_TYPE	RUST HOLE
LEAK_QUANT	1
ANOD_INST	0
COAT_TYPE	0
COAT_COND	PITTED
SOIL_TYPE	CLAY
SOIL_INDEX	0
FOREMAN	0
WSM_NBR_1	106-189
TBM_NBR	0
REPAIR_HRS	7
MAN_HRS	14
OLD_REMARK	Found rupture in main, replaced 3.5 ft of pipe, backfilled and cleaned up.
GIS_STATUS	PLOTTED
ACAD_HANDL	19F3A
ENTRY_DATE	39001

(Continued)

Table 3-1. Continued.

FIELD	EXAMPLE
NOPLOT_REA	0
MASTER_ID	0
CPS_ID	0
PLOT_DATE	36494
REMARKS	Found rupture in main, replaced 3.5 ft of pipe, backfilled and cleaned up.
Report_Fil	\\galaxy\watergis-GSM\Leak_Reports\2005\H\07-Jul\30314.pdf

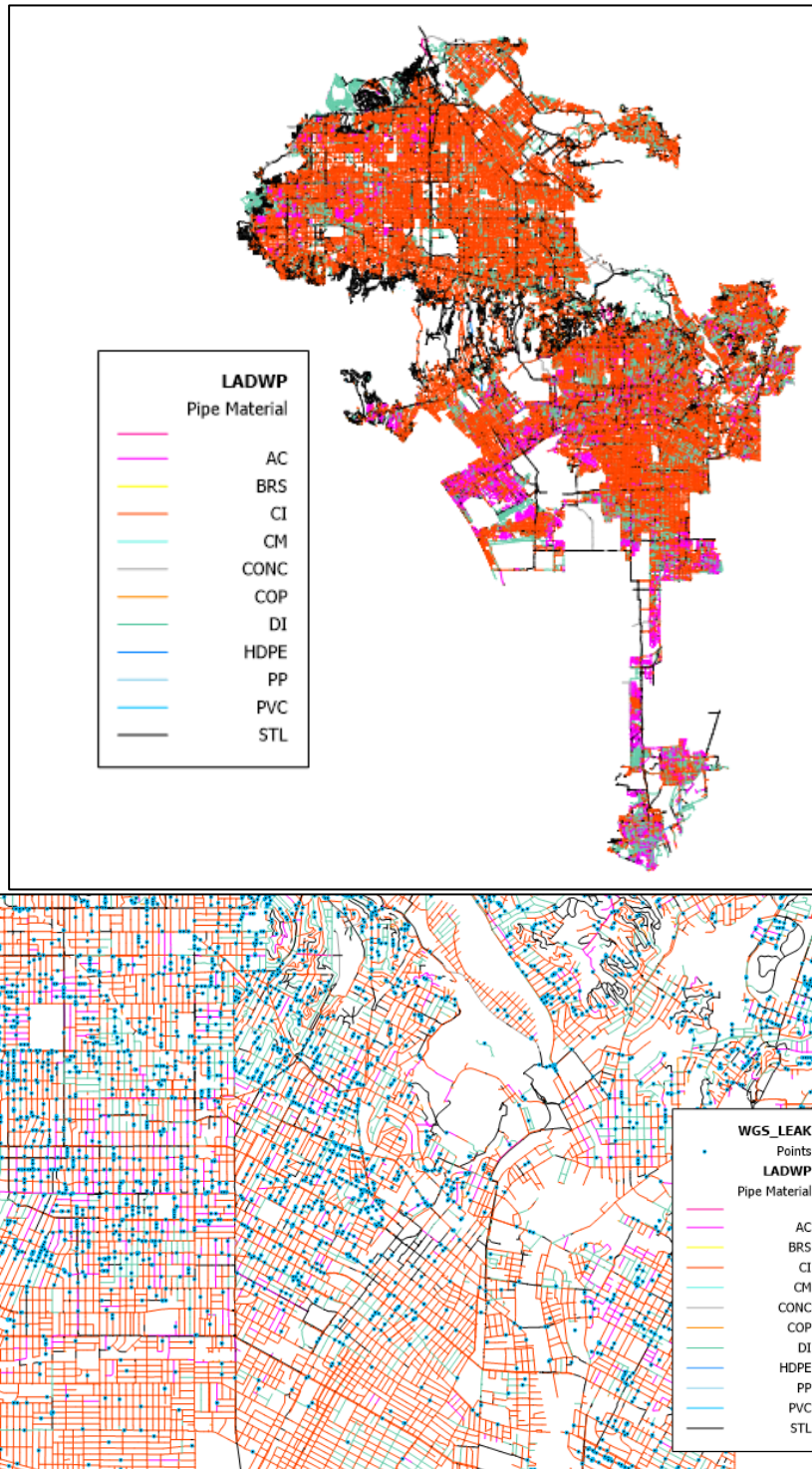


Figure 3-8. LADWP Pipe and Repair Data.

3.2.1.3 LADWP Northridge Repair Data

A third dataset received from LADWP is the record of repairs performed following the 1994 Mw 6.7 Northridge earthquake, isoseismals for which are shown in Figure 3-9 and repair data in Table 3-2.

Table 3-2. Number of Repairs by Pipe Diameter, 1994 Northridge Earthquake.

Diam	Number of repairs
0	5
2	14
4	218
6	415
8	203
10	3
12	72
16	9
18	1
20	3
22	1
Total	944

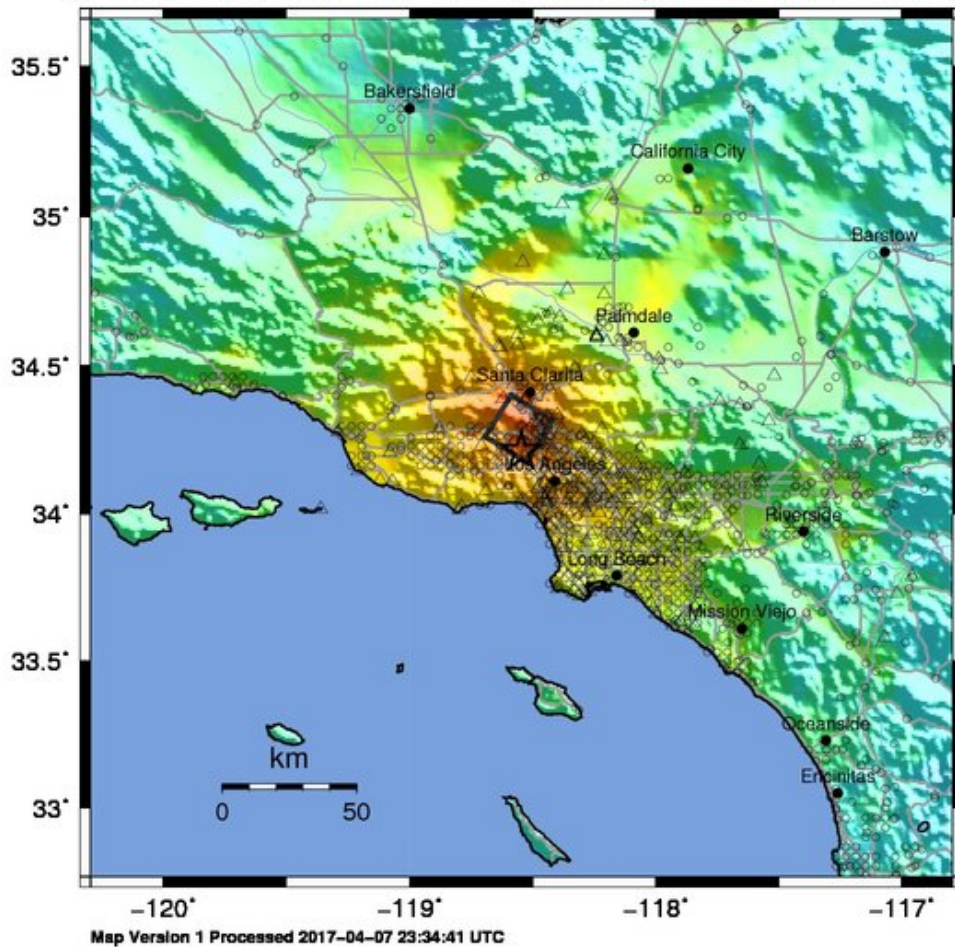
The Northridge earthquake forms a dividing line in repair record recording for LADWP. Prior to the mid-90s, repair records were recorded in paper records and geo-referenced in the form of paper maps, as discussed in section 3.2.1.1. During the Northridge earthquake, the large number of leaks and breaks that had to be immediately repaired overwhelmed this method of record-keeping, and only terse records were kept.

“The most significant damage to the distribution pipeline network was within the epicentral area. Preliminary reports there were approximately 1400 leak repairs by the water utilities in the San Fernando Valley and approximately 300 in the Simi and Santa Clarita Valleys. Pipes and fittings were broken by compression and tension, possibly resulting from permanent ground deformation or transient pressures. Some pipes weakened by corrosion were most likely to be vulnerable to ground vibration and displacement. The pipes most affected were older cast iron with rigid joints and old steel subjected to corrosion. Field supervisors reported that, although the usage was limited, ductile iron pipe performed very well.

“The repairs were time-consuming, requiring a process of draining prior to repair, the repair itself, filling the pipe for testing, and chlorination. Invariably, another leak was observed, requiring the same process to be repeated. In a number of cases, this process was repeated many times.” (Lund 1996)

USGS ShakeMap : Northridge, California

Jan 17, 1994 12:30:55 UTC M 6.6 N34.21 W118.55 Depth: 19.0km ID:19940117123055



PERCEIVED SHAKING	Not felt	Weak	Light	Moderate	Strong	Very strong	Severe	Violent	Extreme
POTENTIAL DAMAGE	none	none	none	Very light	Light	Moderate	Mod./Heavy	Heavy	Very Heavy
PEAK ACC.(%g)	<0.05	0.3	2.8	6.2	12	22	40	75	>139
PEAK VEL.(cm/s)	<0.02	0.1	1.4	4.7	9.6	20	41	86	>178
INSTRUMENTAL INTENSITY	I	II-III	IV	V	VI	VII	VIII	IX	X+

Scale based upon Worden et al. (2012)

Figure 3-9. 1994 M_w 6.7 Northridge Earthquake Isoseismal Distribution.

Source: USGS 1994

Data on nearly 1100 water-pipeline repairs after the Northridge earthquake, including location, pipe diameter and composition of the water-supply pipelines were collected and geocoded (O'Rourke, Toprak and Sano 1998; Toprak 1998) and analyzed (Jeon and O'Rourke 2005), Figure 3-10.

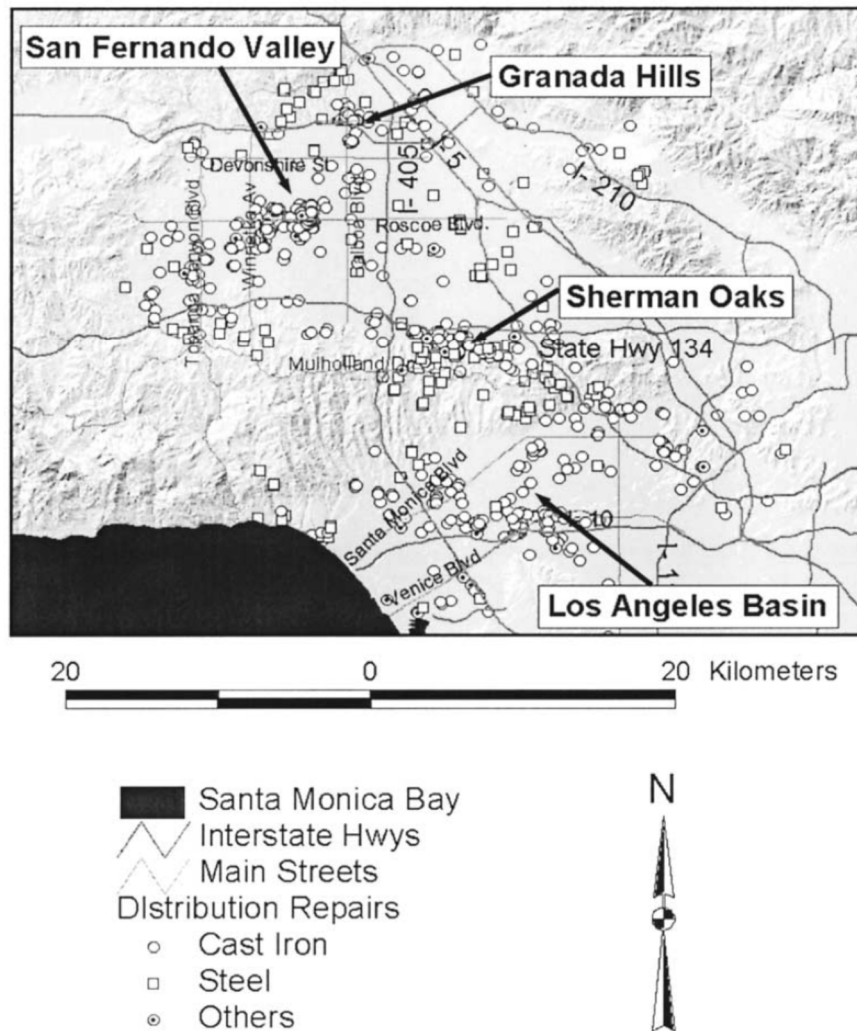


Figure 3-10. Water Distribution Line Repairs.

Source: Jeon and O'Rourke 2005

Davis also summarized the damage for LADWP as “...within the LADWP water system there were 14 repairs to the raw water supply conduits, 60 repairs to treated water transmission pipes, 1013 repairs to distribution pipe, over 200 service connection repairs, 7 damaged reservoirs, temporary suspension of half the treatment plant service, and other incidental damage.” (Davis et al. 2012)

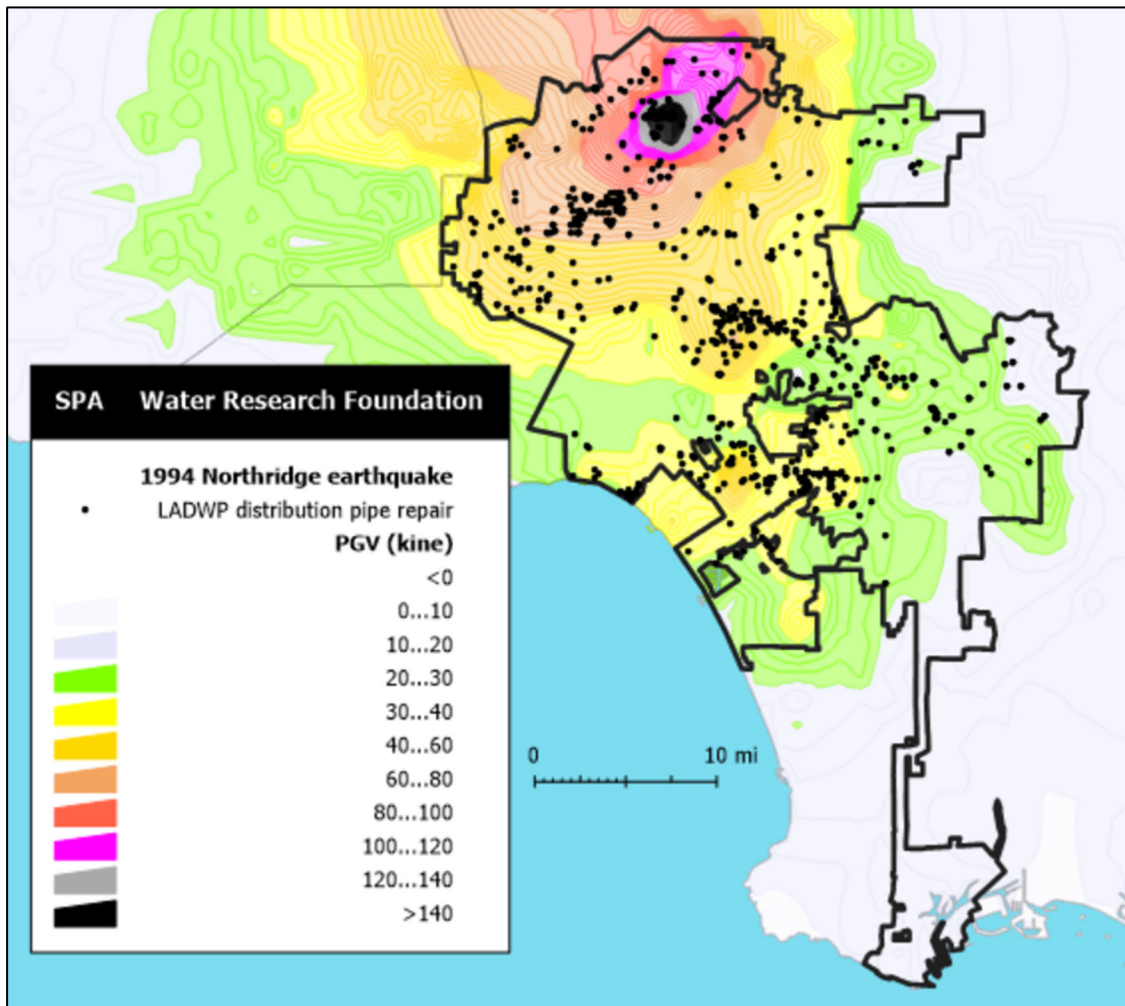


Figure 3-11. 1994 M_w 6.7 Northridge Earthquake and LADWP Water Distribution Pipe Repairs.

Data on the breaks were provided by LADWP for this study and is shown in Figure 3-11 and Figure 3-12. No information was available on date of repair, but presumably all these repairs were made within at most a few weeks following the earthquake (which occurred on Jan 17, 1994). Comparison of these repair locations with data from the scanned maps, Figure 3-12 and the digital database (which effectively begins in 2000) shows no agreement, implying the Northridge repair dataset is a separate and third dataset of repairs.

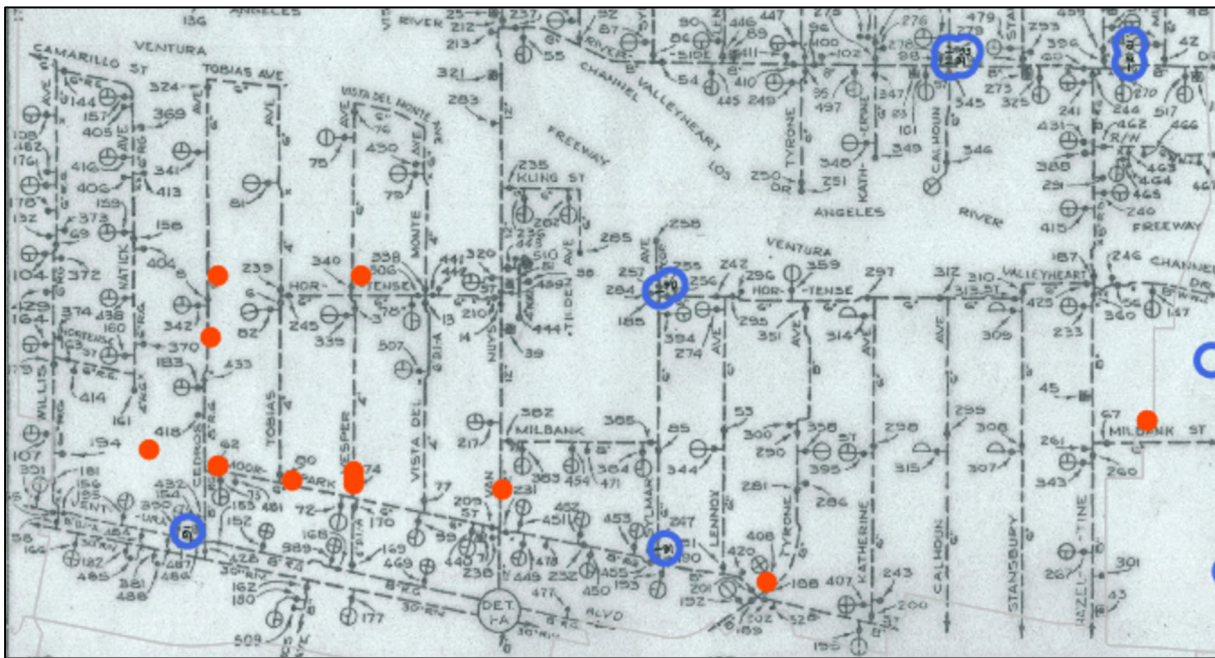


Figure 3-12. Comparison of Scanned Map Repair Locations (Blue) with 1994 Northridge Earthquake Repairs (Red), Showing No Correlation.

3.2.2 SFPUC Data Format

The format of data received from SFPUC is shown Figure 3-13 and Table 3-3.

Table 3-3. SFPUC Data Received.

MONTH	1
DAY	1
YEAR	1985
SYSTEM_	0
STREET	MARINA
DISTANCE1	11 W/WC
X_STREET	BEACH
DISTANCE2	24 N/NC
SIZE	6
BREAK_TYPE	TRANSVERSE

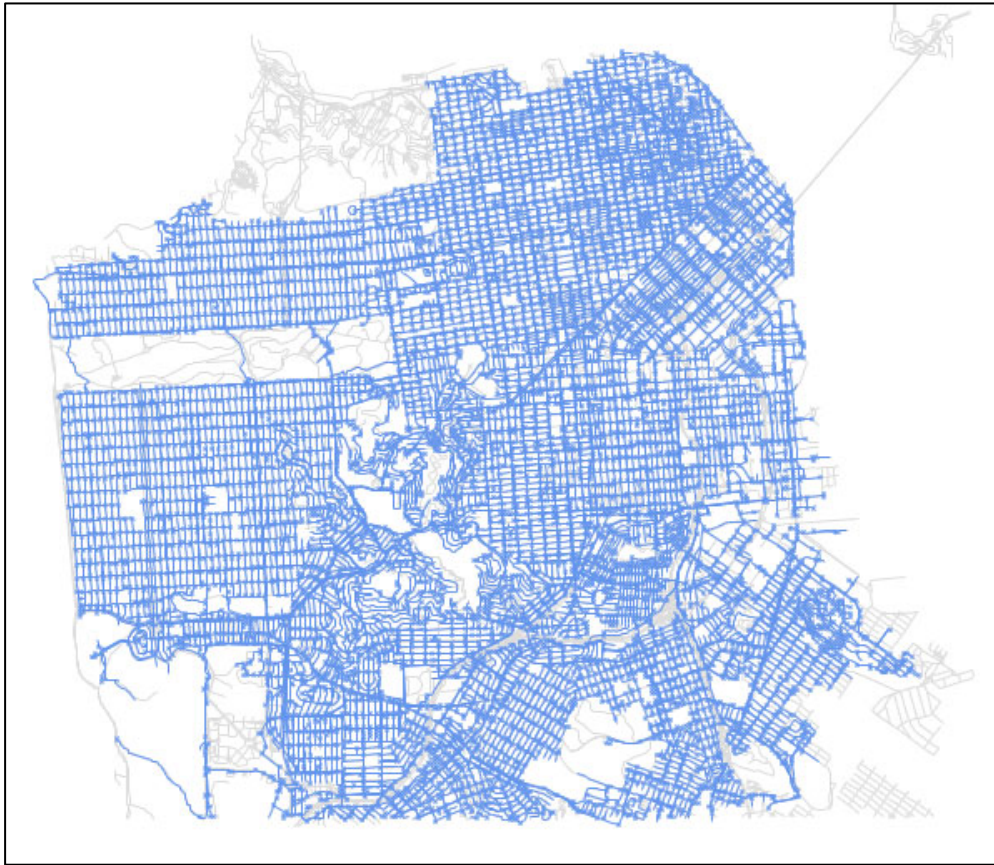


Figure 3-13. San Francisco Pipe Data.

3.2.3 EBMUD Data Format

The format of data received from SFPUC is shown in Table 3-4 and Figure 3-14.

Table 3-4. EBMUD Data Received.

FIELD	EXAMPLE
ID	121165
ID 2	98638
OBJECTID	65
REPORT_NU	346057
CANDIDATE_	0
LEAK_DATE	19910107
LEAK_YEAR	1991
BMAP	534B1473
COORD_EAST	1474480
COORD_NORT	534600
COORD_EA_1	6035848
COORD_NO_1	2175007
ADDRESS	5706 N ARLINGTON BL
STREET	ARLINGTON BL

(Continued)

Table 3-4. Continued.

FIELD	EXAMPLE
CITY	RICHMOND
MSLINK	0
PFID	25018
PIPE_EXTN_	34921
PIPE_DIAME	12
PIPE_TYPE	MM
YEAR_INST	59
PART_DAMAG	JOINT
CAUSE_OF_D	UNKNOWN
TYPE_OF_CO	NONE
PIPE_EXTN1	N
LEAK_TYPE	SMALL BLOWOUT HOLE <= 1"
CRSN_MTGTN	Y
DATA_SOURC	HIST
COORD_SOUR	TAP
GWO_COMMEN	0
LOCATION_C	0
CROSS_STRE	0
SERV_AREA	N
PRP_NOTES	0
FLAG	HIS
OLD_FLAG	HIS
OLD_REPORT	346057
WO_COMPLET	19910107
HIST_CAND_	1093
PFIDFLAG	GOOD_LINK

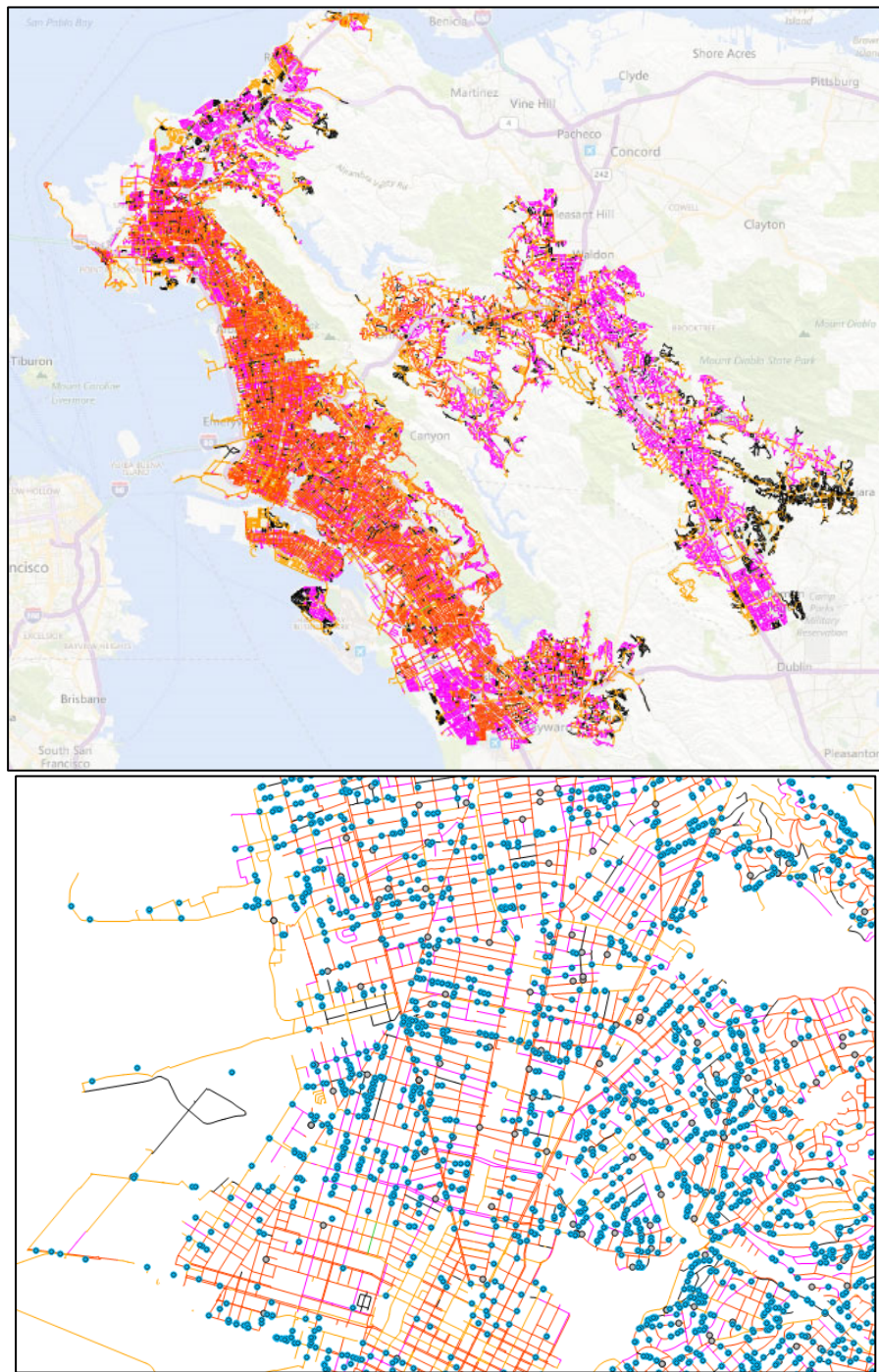


Figure 3-13. EBMUD Pipe and Repair Data.

3.2.4 PWB Data Format

The format of data received from PWB is shown Figure 3-15 and Table 3-5

Table 3-5. PWB Data Received.

FIELD	EXAMPLE
ID	619383
WORK_ORDER_NO	500215
WORK_DESC	REPAIR LEAK ON 2" GALV. MAIN IN FRONT OF 1407 NE GOLF CT.
STREET_ADDRESS	1407 NE Golf Court
CITY_STATE	Portland, OR
COMPLETE_ADDRESS	1407 NE Golf Court, Portland, OR
Latitude	45.592981
Longitude	-122.648242
Found Unique Coordinates (Yes, No)	---YES---
WORK_CLASS	MAIN_DIST
WORK_CATEGORY	REPAIR
WORK_STATUS	CLOSED
ACCOUNT_NO	153-180-42-304-0000
LABOR	0
EQUIP	0
MATRL	0
SUM1	0
QSEC	2032
ASSET_ID	419850
ASSET_DESC	2 Inch GALV DistributionMain
INSTALL_DATE	29221
ACTUAL_FINISH_DATE	38194.69353
COMPLETION_NOTES	0
SOIL_TYPE	0
RECOMMEND_REPLACEMENT	0
FAILURE_CODE	0
FAILURE_MODE	0
COMPONENT_CODE	0
ROOT_CAUSE	0
REPAIR_CODE	0
LONGITUDE	-122.648242
LATITUDE	45.592981
ASSET_DESC	2 Inch GALV DistributionMain
MATL	GALV
DIAM	2

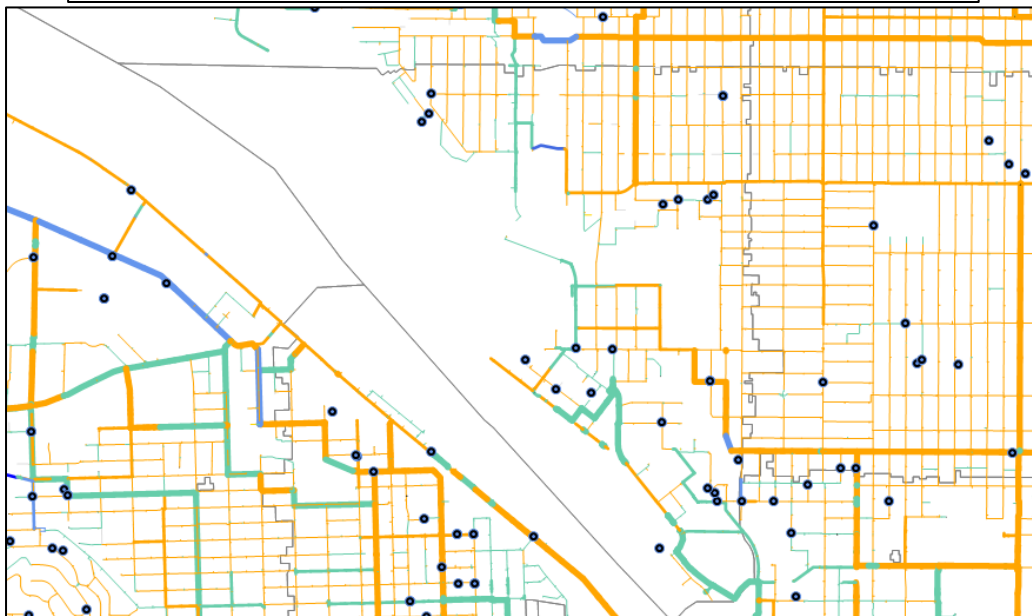
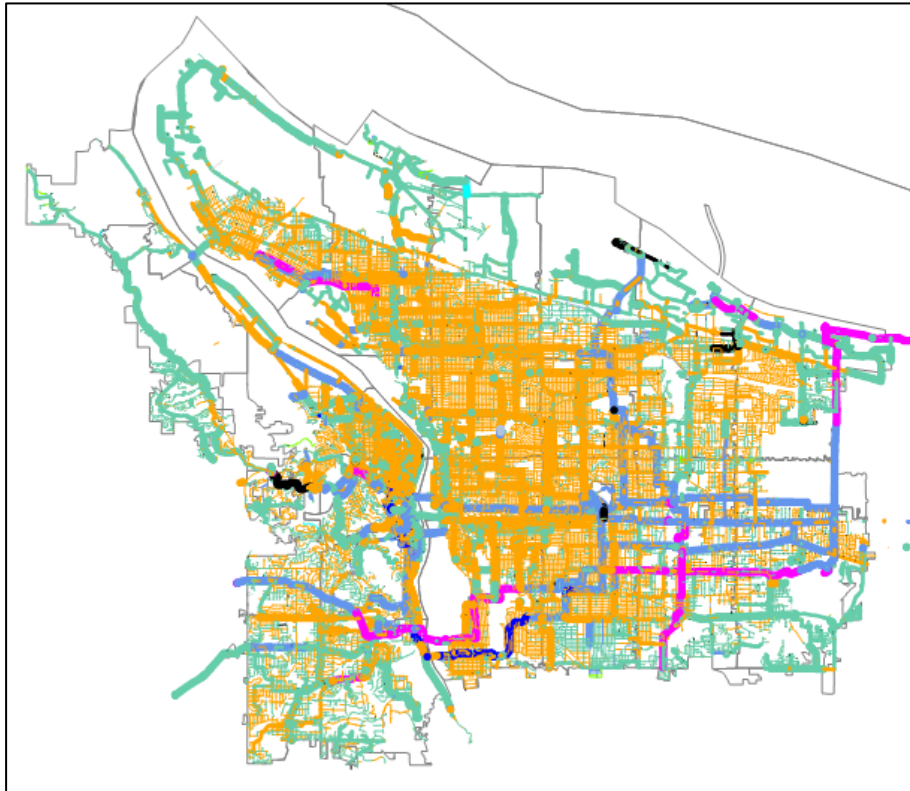


Figure 3-14. Portland, OR Pipe and Repair Data.

3.2.5 SPU Data Format

The format of data received from SPU is shown in Table 3-6 and Figure 3-16.

Table 3-6. SPU Data Received.

WO_ID	LOCATION	PROBLEM	REPAIR_DT	WMN_FEAKEDIAMETER	MATERIAL	NSTALL_YFLIFECYCLE	RETIRE_YR
477226	IN 44TH AVE SW 100'S OF SW 102ND ST	V BREAK	1/20/2000	5178543	4	CI	1939
477128	IN 35TH AVE SW 30'N OF SW 107TH ST	V BREAK	1/13/2000	5180990	6	CI	1939
477424	IN SW 115TH ST 44.5'E OF CL OF 27TH PL SW	V BREAK	1/30/2000	5183191	4	CI	1953
477399	IN S ANDOVER ST 1'W OF CL OF 7TH AVE S	PINHOLE	1/28/2000	5177329	8	CI	1957
477735	IN 39TH AVE SW 32'S OF NM OF SW HANFORD	UNKNOWN	2/15/2000	5170022	8	CI	1912
14891	IN HOWELL ST 75'E OF CL OF 8TH AVE	LD JOINT	6/8/2000	5159257	16	CI	1891
16787	IN S BAYVIEW ST 132'W OF WM OF 30TH AV S	UNKNOWN	7/23/2000	5171605	1.5	I	0
18267-A	IN EUCLID AV 65'N OF NM OF YESLER WY	PINHOLE	8/25/2000	5165512	2	GI	1962
16763-A	IN S CONCORD ST 167'E OF CL OF 7TH AV S	LD JOINT	7/21/2000	5202763	8	CI	1910
21573-A	IN PERKINS LN W 104'N OF GV OF W RAYE ST	V BREAK	11/17/2000	5146942	8	CI	1948
22571	IN LAKE WASHINGTON BV E 150'S OF 2"V OF E	UNKNOWN	12/20/2000	5158092	2	GI	1915
21842-A	IN SW SULLIVAN ST 119'W OF CL OF 42ND AVE	V BREAK	11/29/2000	5198397	6	CI	1957

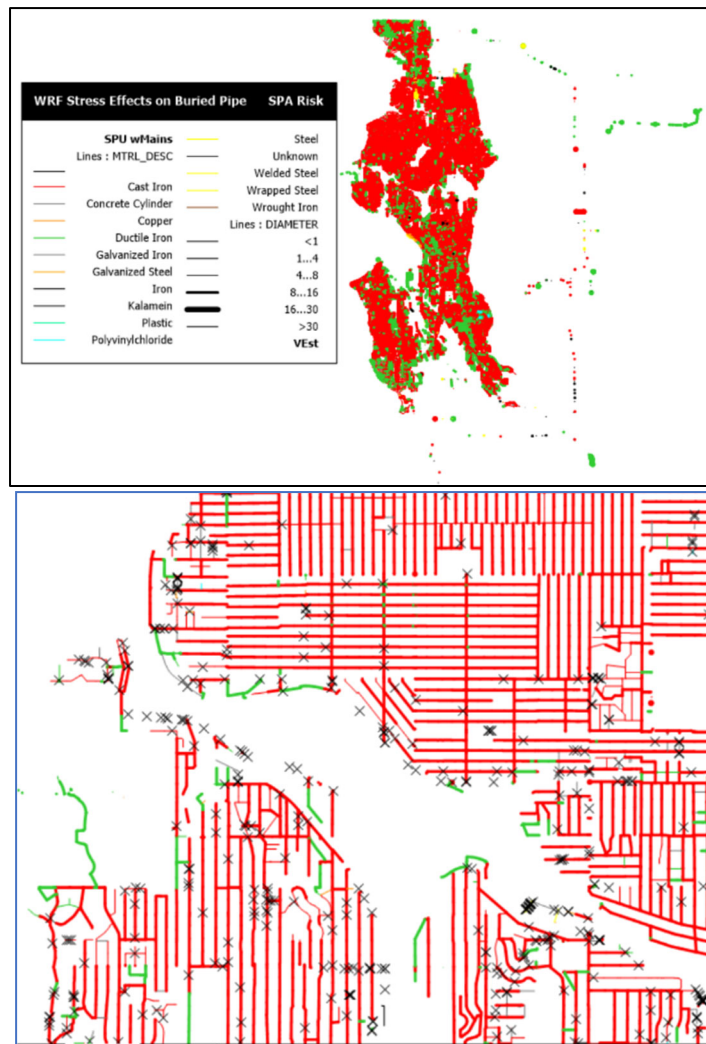


Figure 3-16. Seattle SPU Pipe Network with Detail Showing Break Locations.

3.2.6 Summary of Data

Table 3-7 summarizes the data collected.

Table 3-7. Summary of Data.

System	Total Length Pipe million ft.	Period of Repair data	No. Repair records
LADWP	39.7	1960-1997 1997-2017	Scanned maps, tbd 16982
SFPUC	21.6	1986-2008 2009-2010 2011 2012 2013-2015	2201 226 103 97 550
EBMUD	20.3	1990-2015 2016-2017	20856 1671
PWB	11.9	2004-2015	2176
SPU	7.4	1958-2018	5303

3.3 Data Processing and Covariate Data

This section first discusses the processing of the data received from the five agencies, and then discusses the collection and processing of *covariate* data – that is, for this study, possible repair-causing factors.

Processing of the data consisted of the following steps:

1. Initial review of the data to confirm essential data were provided– this was largely the subject of section 3.2
2. Review of the data to confirm validity and consistency of, and remove erroneous, data.
3. Creation of an initial GIS database consisting of pipe segments and repair data. Key covariates for each pipe segment include segment location, length, diameter, material and date of installation. The key repair covariate was the date of repair.
4. Assignment of repair data to the corresponding pipe segment.
5. Collection of ground elevation data (discussed in 3.3.6) and assignment of elevation, slope and aspect to each pipe segment.
6. Collection of weather records and assignment of key temperature covariates to each pipe segment having a repair, discussed in section 3.3.6
7. If affected by a major earthquake (LADWP, EBMUD, SFPUC yes, PWB and SPU no), determine the peak ground velocity (PGV, measured in kine) from that event for each pipe.
8. Compilation of this data in a table for each agency network, for analysis. Since each agency uses different terminology, convert to a consistent terminology.
9. Aggregation of the five resulting tables into one project dataset, for analysis.

3.3.1 LADWP

Processing of LADWP data consisted of two major tasks: (1) cleaning, and (2) assignment of covariates. This section discusses data cleaning which for LADWP data consisted of two subtasks: (a) conversion of scanned paper maps for repair data for 1960-2000, and (b) for the digital datasets for 2000-2017, removing clearly erroneous data. The first subtask was quite challenging, involving converting a massive amount of data from scanned paper maps to a digital database. We discuss this next. Collection and assignment of covariate data is discussed later.

3.3.1.1 LADWP 1960-2000 Data

The data received from LADWP was discussed above. This section discusses reduction of this data to a usable format. Merging of the 4800 individual maps into eight layers was accomplished using GIS

mosaic-ing algorithms. To extract the location of each repair from the scanned maps, each geo-referenced image for each lustrum was compiled into one large mosaic for each lustrum, Figure 3-17, using the grid polygon geometries as footprints to clip each image, Figure 3-18. There are some misalignments, Figure 3-19 and a few maps were corrupted and were omitted.

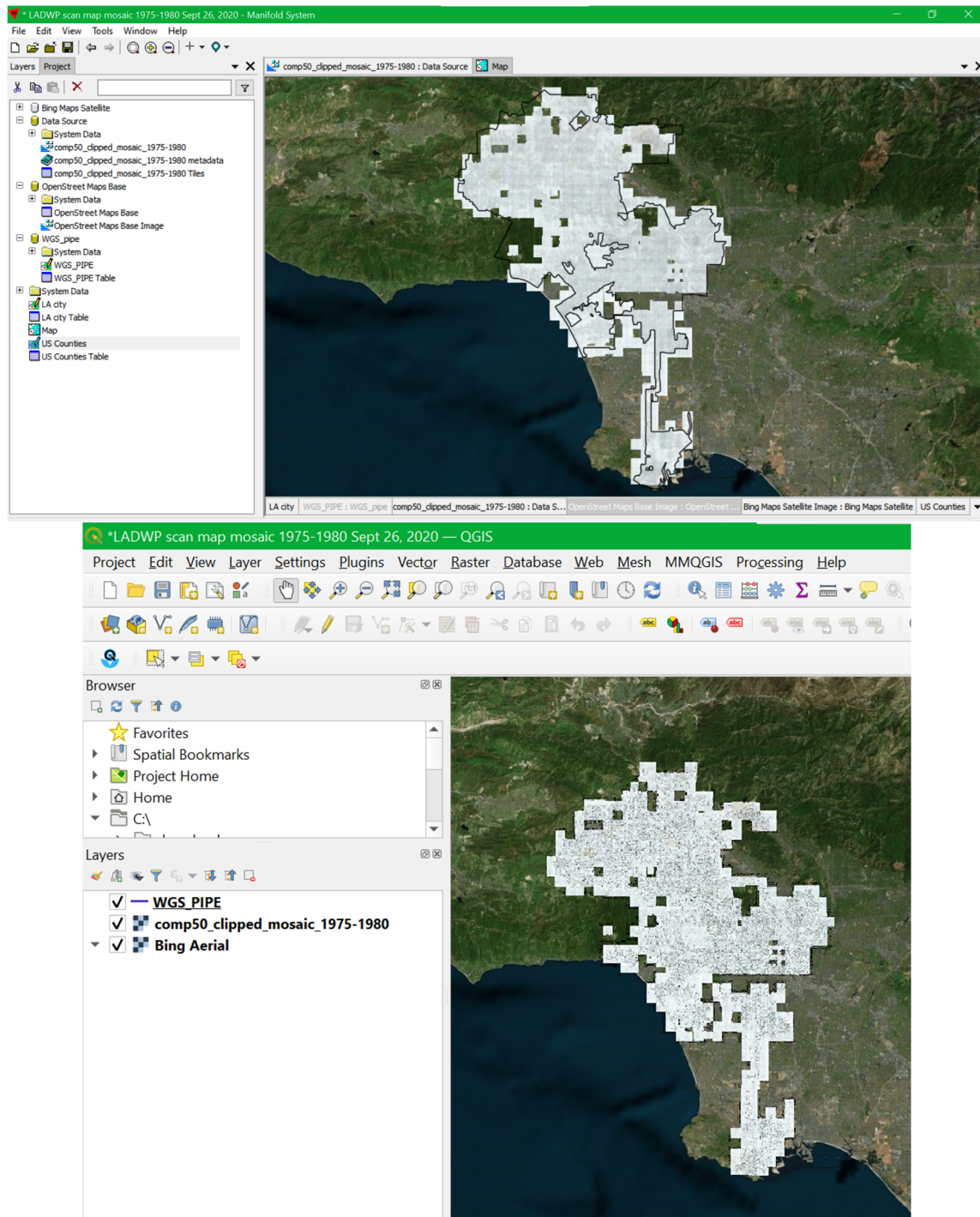


Figure 3-15. Entire Mosaic of 600 Scanned Maps for the 1975-80 Lustrum: (Top) Entire Mosaic with LA City Boundaries, in Manifold 9 GIS; (Bottom) Ditto, in QGIS 3.14.



Figure 3-16. Clipped Mosaic of Two Repair Maps.

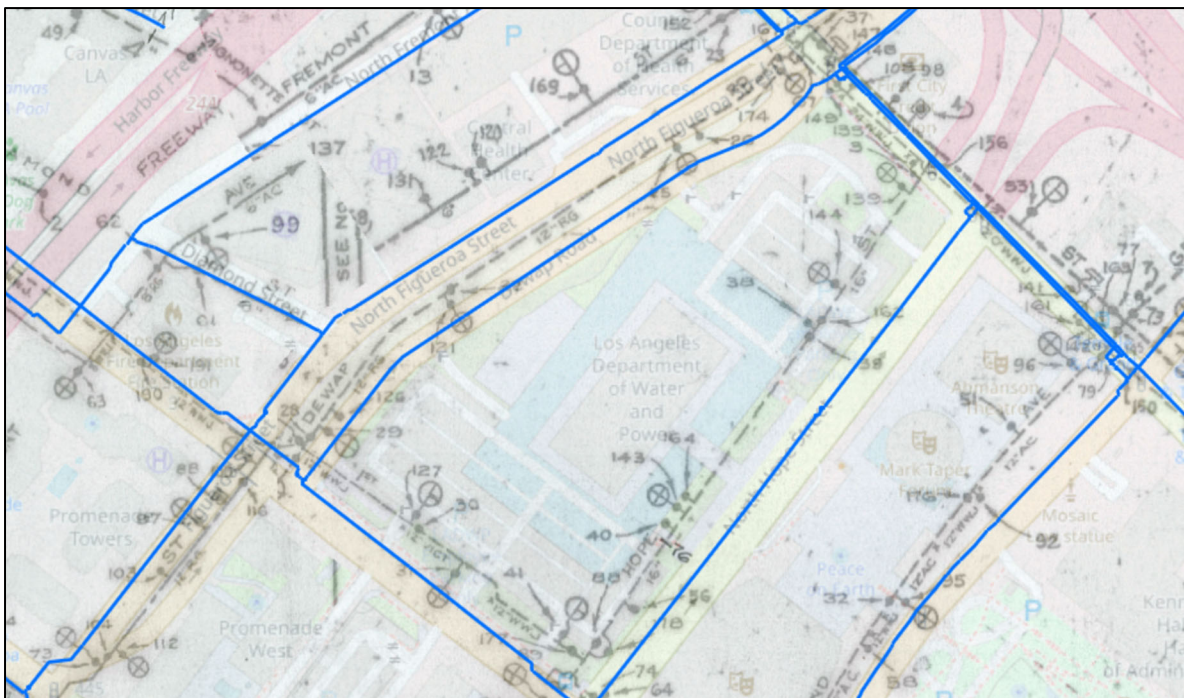


Figure 3-17. Mis-Alignment of Scanned Map with Pipe GIS Layer – the Blue Lines Are the Pipe Network from the GIS SHP Files and Align Very Well with Google Street Maps (Underlying Image – Note This Image is Centered on LADWP’s John Ferraro Building) While Pipelines in the Scanned Images (Dashed Lines) Are Here Displaced Several Tens of Feet to the West.

The full mosaic is a patchwork of more than 600 scanned images and is a 4 gb tif file for each lustrum. This size makes it difficult to work with so that batch processing of individual scanned map images was more feasible. In order to geo-reference the repair annotations, each image was thresholded to highlight the annotations so the background is suppressed and the annotations stand out, Figure 3-20

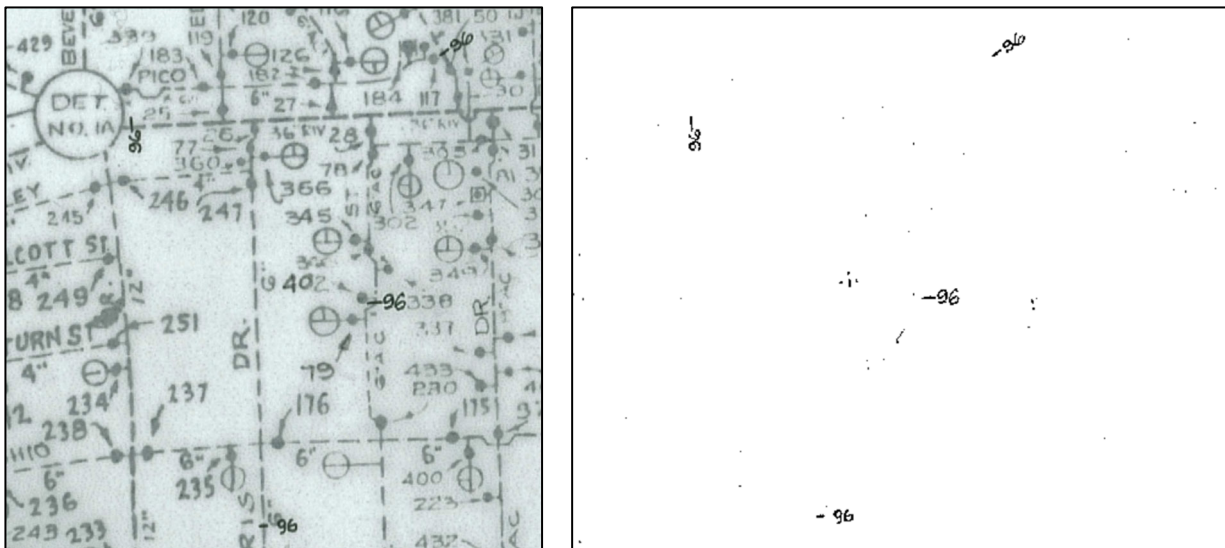


Figure 3-18. Detail of a Scanned Map on Left, with Background Thresholded Out, Revealing Only Annotations.

The annotations are then converted into objects or ‘nuggets’ and geolocated within the image. The resulting “nugget” objects (red irregular shapes) overlaid on the original scanned map is shown in Figure 3-21. Note that each “nugget” crosses a pipe, so each annotation can be assigned to a pipe from the pipe network shapefile (however, some of the pipes may be newer than the repair – that is, were replaced since the repair – so that the pipe material and other data may not correspond to the repaired pipe. This can be tested for by comparing date of repair versus the date of installation of the pipe in the network database. If the pipe installation date is more recent than the repair date, then that repair data point is “left-censored” in statistical terms).

At present, without significantly more processing, the year of the repair cannot be extracted from the annotation, but since each scanned map corresponds to one lustrum, if the median year (in the case of Figure 3-22, the lustrum is 1991-1995 so the median year is 1993) is assigned to the repair, there is at most a two year error, which is acceptable for regression and survival analysis purposes. Note that in Figure 3-23 the lower most annotation appears to be for 1985 (“85”) but on closer inspection is actually “95”.

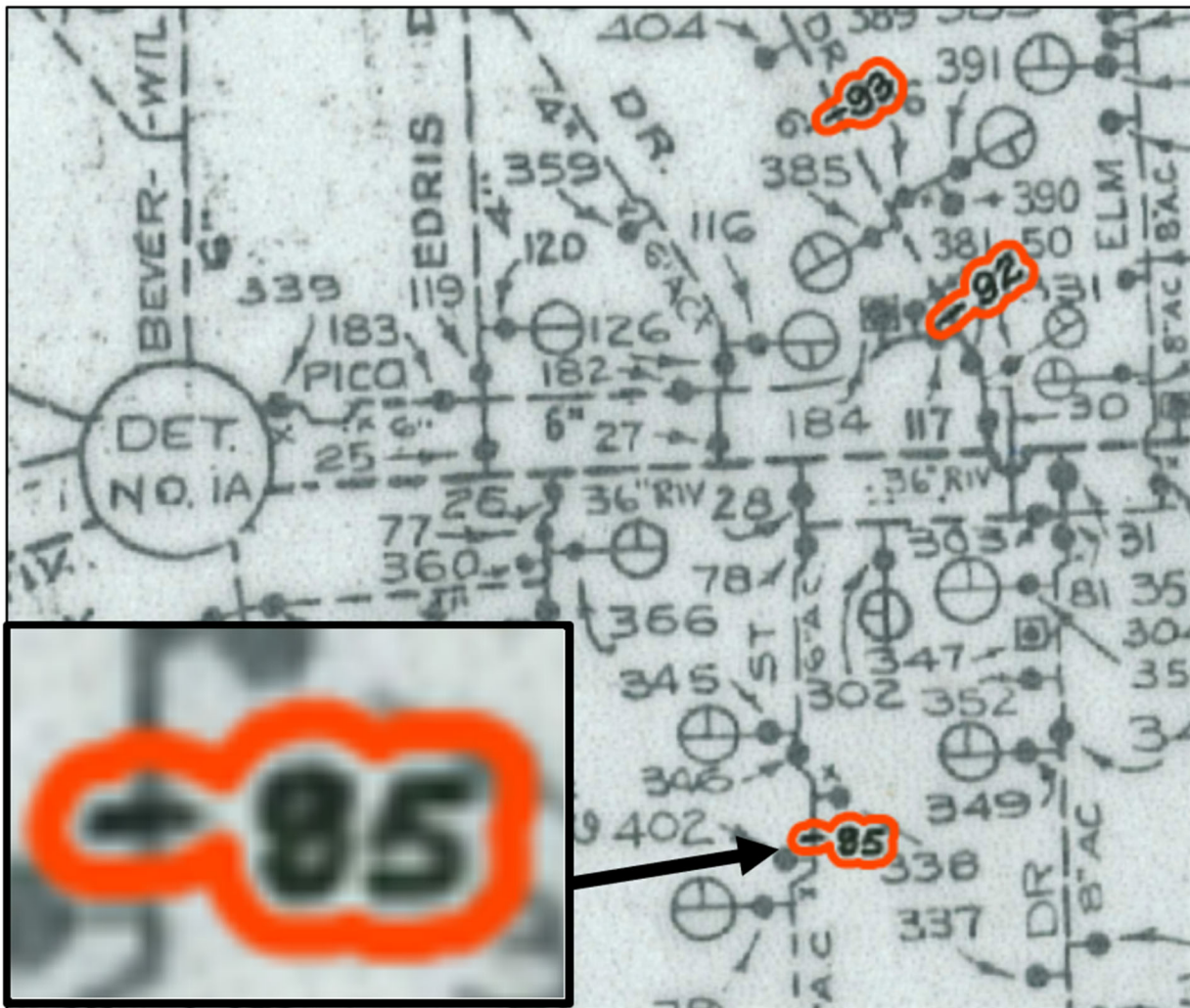


Figure 3-19. Detail of a Scanned Map on Annotations Geo-Located as “Nuggets” (Red). Detail Confirms Lower Annotation Is “95” and Not “85”.

For geo-location of each nugget, all image filenames were retrieved for a specific lustrum using the ‘glob’ python library which allows for use of wildcards in the retrieval. For example, specifying ‘*1996-2000.jpg’ will retrieve all filenames containing the trailing string of ‘1996-2000.jpg’. It was observed that some of the files were not relevant to the analysis, such as files containing detailed scans which were not georeferenced, and some images identified as having poor georeferencing information. These files were removed from the list of files for a specific lustrum.

Samples from each lustrum were interrogated to determine a range of valid pixel intensities for the red, green, and blue channels corresponding to the annotations on the scanned image. These ranges are summarized in Table 3-8 where it can be seen that all images from 1975-2000 are similar such that the same range of pixel intensities can be attributed to the annotations; images prior to 1975 are highly variable in tone of the scan and the annotation such that the intensity ranges are different, and variable compared to images from 1975-2000. These intensity values are henceforth referred to as the ‘annotation range’.

Table 3-8. Minimum and Maximum Red, Green, and Blue Pixel Intensities Specified to Threshold Scanned Maps from Each Lustrum. Note the Difference between Pre- and Post-1975 Data, Which Reflects the Difference in Tone between the Data.

Lustrum	Minimum [R,G,B]	Maximum [R,G,B]
1960-1965	[70,60,40]	[85,85,75]
1965-1970	[85,80,40]	[100,100,75]
1970-1975	[20,40,55]	[40,50,80]
1975-1980	[0,0,0]	[75,75,75]
1980-1985	[0,0,0]	[75,75,75]
1985-1990	[0,0,0]	[75,75,75]
1990-1995	[0,0,0]	[75,75,75]
1996-2000	[0,0,0]	[75,75,75]

The images were processed such that pixels with intensity values outside of the annotation range were suppressed and given a value of 0, and pixels with values within the annotation range were given a value of 1. This binary representation of the scanned image is now a mask where the mask contains areas of possible presence of annotations. These regions were identified using the scikit-image python library, which assigns to each region in the mask image a suite of attributes. In this work, the attributes ‘size’ and ‘centroid’ were used in subsequent steps. The ‘size’ attribute records the number of pixels present in a given region, and the ‘centroid’ attribute records the pixel X-Y coordinates of the geometric center for a given region.

Once all regions were identified, only regions meeting a set of specified requirements were retained, to minimize retention of small spurious regions. If the size threshold (25 pixels) was met, the centroid of that region was retained to convert to geographic X-Y coordinates in the same coordinate system as the source image. The pixel X-Y coordinates were converted to geographic X-Y coordinates using the affine transform of the associated source image. The affine transform is a 2-D array which provides the upper-left coordinates in geographic space as well as the pixel size in geographic units in both the X and Y dimension. It can be described in general as:

$$\text{Aff} = \begin{bmatrix} A & B \\ C & D \end{bmatrix}; \begin{bmatrix} E \\ F \end{bmatrix} \quad \text{Equation 3-1}$$

where the components in Equation 3-1 are defined as

- A: x-component of the pixel width
- B: x-component of the pixel height
- C: x-coordinate of the center of the original image's upper left pixel transformed to the map
- D: y-component of the pixel width
- E: y-component of the pixel height
- F: y-coordinate of the center of the original image's upper left pixel transformed to the map

The affine transform is provided for each source image in the form of a world file (for a JPG image, the extension is .jgw). Typically, it will take the form of:

- Line 1: A
- Line 2: D
- Line 3: B
- Line 4: E
- Line 5: C
- Line 6: F

Lines 2 and 3 are often 0, so the geographic coordinates for a given pixel X-Y coordinates can be computed simply as:

- $xg = C + Axp$
- $yg = F + Eyp$

The geographic coordinates are calculated for each corresponding pixel X-Y coordinate pair. This process is repeated for each source image for a specific lustrum and the final list of geographic coordinates corresponding to the possible locations of annotations are saved to a shapefile in the same coordinate system as the source images.

The shapefile containing the possible annotation locations for a specific lustrum were then analyzed for proximity to a pipe network provided as an additional shapefile. Each feature in the pipe network was a line feature, and we wished to assign the presence of an annotation extracted from the scans to the nearest pipeline feature within a specified distance. To support this, we created a new column in the pipe network attribute table corresponding to each lustrum (e.g., “L1975-1980”, “L1980-1985”, etc.) and gave each row an initial value of 0. The ‘Select Feature by Location’ tool in ArcGIS was used to select the pipe features which were within a specified distance of the possible annotation points. These rows were then given a value of 1 for the lustrum associated with the points. An example is shown in Figure 3-22 below, where the assignment of lustrum to the pipe features was specified as being within 50 feet of the point features for that lustrum.

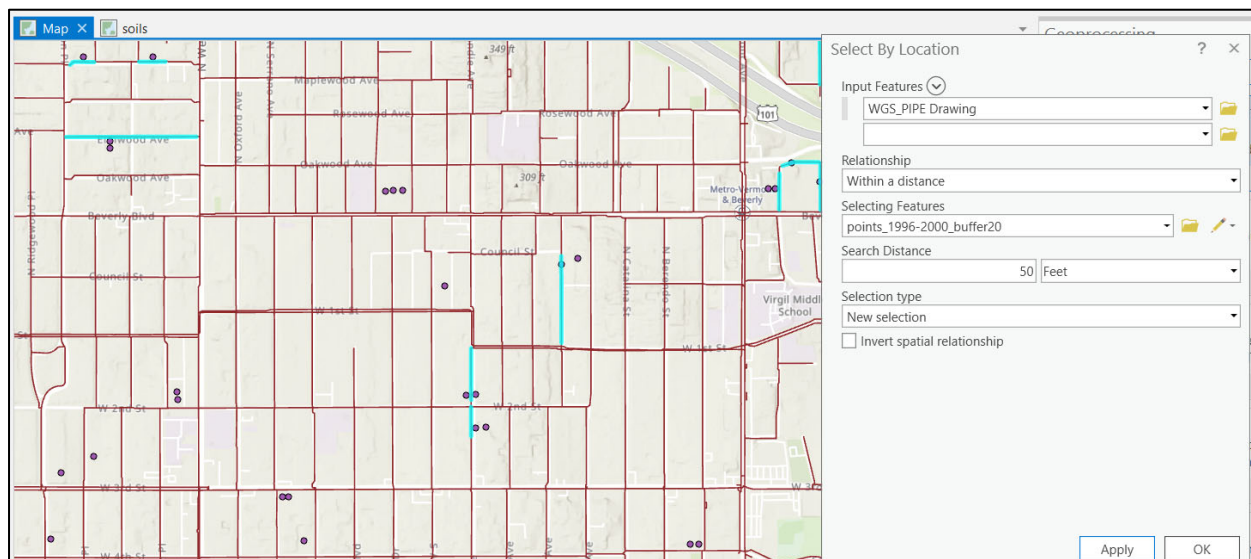


Figure 3-20. Example of ‘Select by Location’ to Determine Pipe Features within a Distance from the Annotation Features. Pipe Features Meeting This Criteria Are Highlighted in Cyan.

This workflow was not without error. There were many false annotation detections associated with the edges of the scans and the text “LEAK MAP” present on many of the scans. To mitigate these errors, the

images were clipped using the tile geometries in the file “GSMgrid-true.shp”. These features contained an attribute which was directly associable to the image filenames. Once the images were clipped to the associated geometry, these large errors were suppressed when processed with the same algorithm.

Finally, the annotation ranges identified for lustrums prior to 1975 proved insufficient to extract reliable information from images in those lustrums. A more sophisticated image analysis algorithm might be applied to the scanned maps prior to 1975 in order to extract the annotations, but this was beyond the scope of the present project. Further, it might be possible to extract the precise year associated with the annotation using number recognition algorithms. Number and digit recognition are not a simple task, and convolutional neural network approaches might be employed, although these require significant amounts of training data in the case of handwritten numbers. Google’s Vision AI API offers one approach to solve this problem and provides satisfactory recognition as shown in Figure 3-23. For the current project, the year of repair was taken as the mid-point of each lustrum (i.e., 1977 for the 1975-1980 lustrum – note the labeling of the lustrums as received from LADWP was imprecise in that the year-interval labels overlapped). This precision was adequate for the purposes of the project, and the specific year was not needed nor sought.

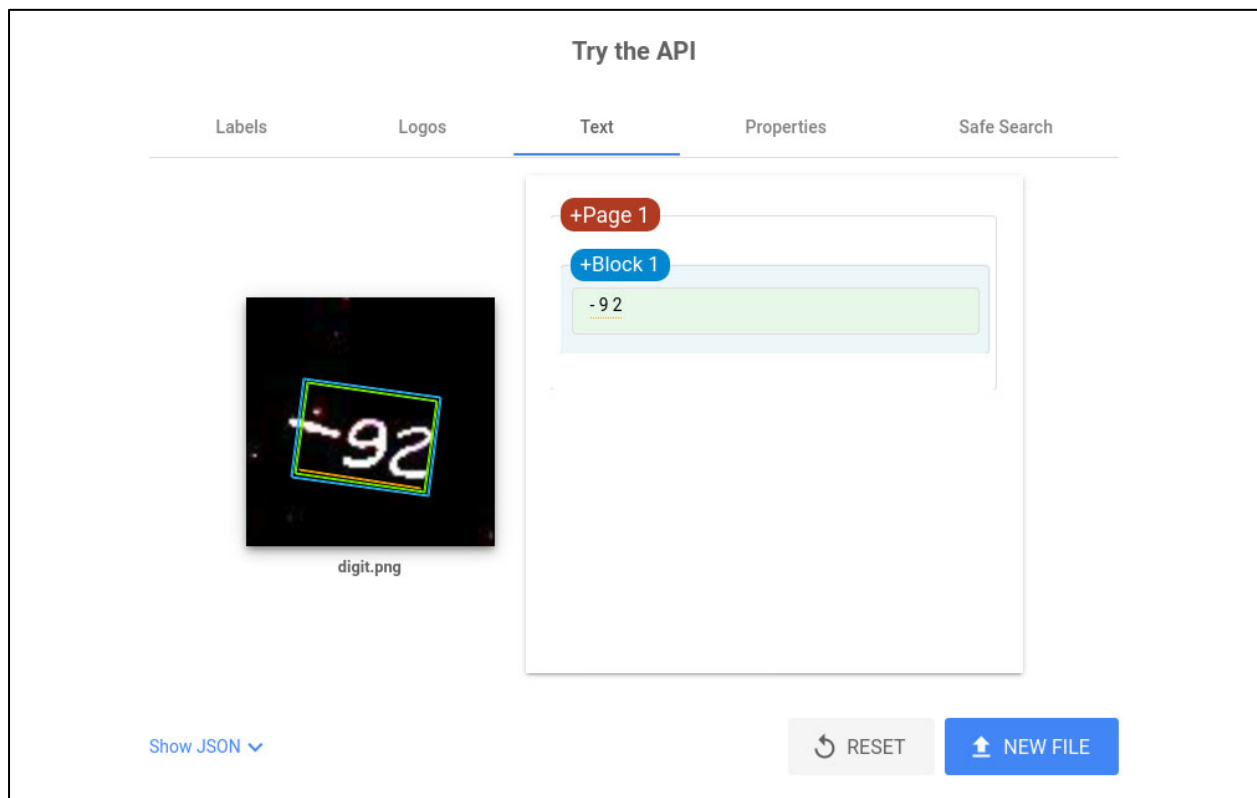


Figure 3-21. Google Vision AI Result on an Image Chip Containing One of the Annotations from an Image in the 1996-2000 Lustrum.

Figure 3-24 shows all 600+ scanned images for one lustrum, but these images overlap each other and require clipping and stitching together to constitute a usable single image of the system network and its repairs for that lustrum. To construct the stitched mosaic, the clipped images from the point processing algorithm were used to construct a stitched mosaic to represent the full set of images from a specific lustrum in a single file, a detail of which is shown in Figure 3-24.

The Geospatial Data Abstraction Library (GDAL) was the primary software used to produce the mosaicked data. The steps to build the mosaic from the individual image files can be summarized as:

- 1) *gdalbuildvrt*, used to build a virtual raster table from a list of input images
 - a) input: text file containing all image files contributing to the mosaic (.txt)
 - b) output: XML-like file containing locations of image files and spatial metadata (.vrt)
- 2) *gdal_translate*, used to convert the virtual raster (.vrt file) to a single mosaicked image file
 - a) input: VRT file from *gdalbuildvrt*
 - b) output: image file of specified format, here, TIF
- 3) *gdal_translate*, used to copy output file at 50% compression using JPEG compression
 - a) input: TIF file from previous command
 - b) output: TIF file at 50% compression

The resulting system-wide stitched mosaic file are quite large even when converted to TIF format. It would have been more desirable to save the mosaicked image as a single large JPEG which would have saved on file size. However, that was not possible due to the size constraints of the JPEG driver. The JPEG driver specifies a maximum image dimension of 65536 which was significantly exceeded for the full spatial coverage of the data – typical stitched mosaic files were about 3 gigabytes in size.

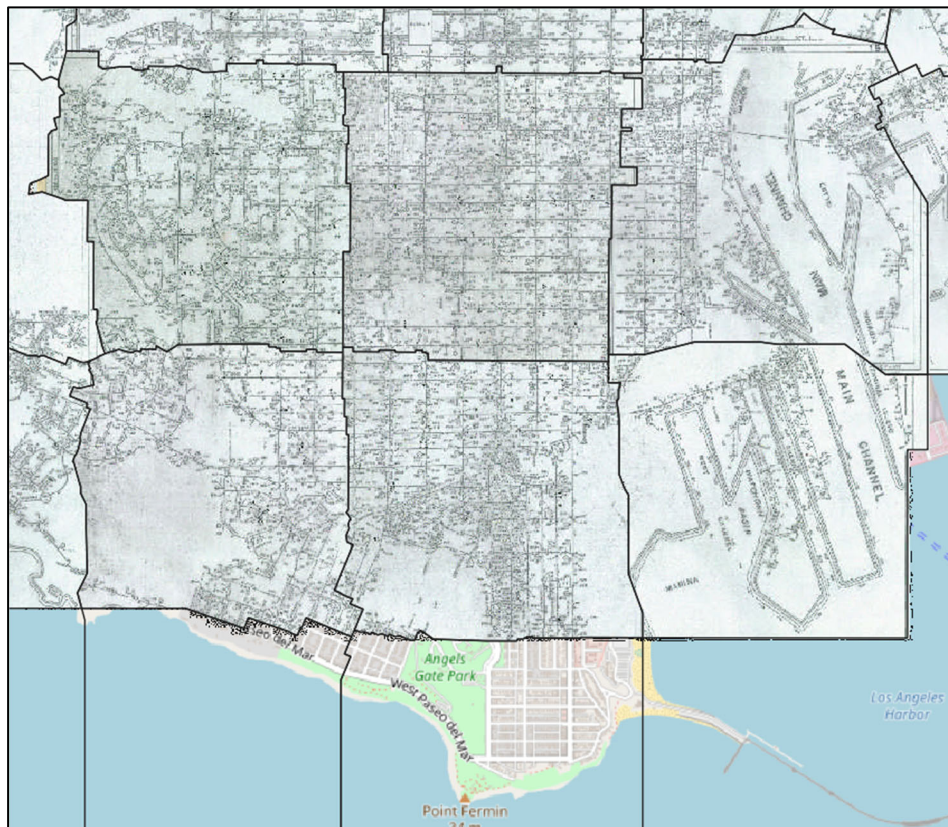


Figure 3-22. Detail of Stitched Mosaic, Port of Los Angeles, with Grid Boundaries (Black Lines) Overlaid.

This process was performed for the approximately 4,800 scanned maps, with “nuggets” (i.e., annotations) accumulated per lustrum. As noted, the image quality of maps for lustra 1960-1974 was inadequate for extraction of annotations, and data was retrieved only for the period 1975-2000. Review of the results revealed several patterns of false patterns, including creation of nuggets for certain words

in map titles, Figure 3-25, as well as some other reasons. These false positives are termed “problematic” and omitted from subsequent analyses.

The five lustra with satisfactory results (i.e., 1975-2000) were aggregated, resulting in identification of 19,235 repair locations for the 25 year period, Table 3-9 and Figure 3-26. An example in detail is shown in Figure 3-27.

The average number of repairs per year is shown in Table 3-9, averaging 769 which is generally consistent with the number determined for the era of digital data (2000-2017) which averaged 922 repairs per year. Note that the above dataset of repairs omits the repairs immediately in the aftermath of the 1994 Northridge earthquake (yet another dataset).

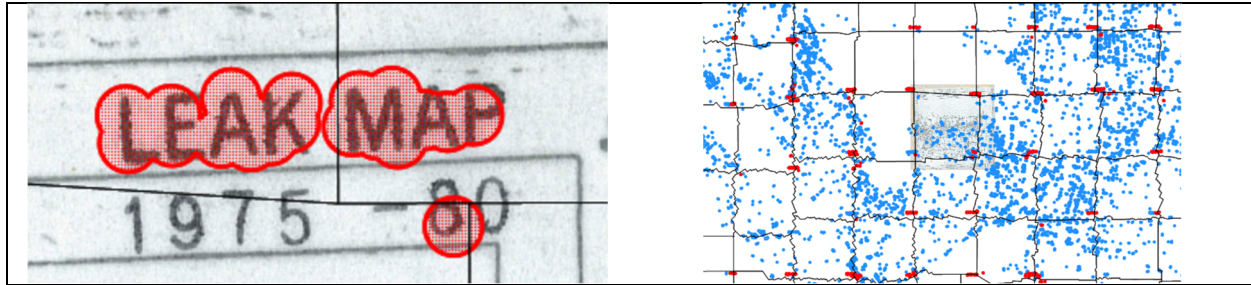


Figure 3-23. False Positives for Leak Annotations.

Table 3-9. Number of Repair Locations Identified from Scanned Maps for Period 1975-2000.

Lustrum	No. of "nuggets"	No. of problematic nuggets	Nuggets employed in analysis	Annual mean
1975-1980	6,355	2110	4245	849
1980-1985	4,233	4	4229	846
1985-1990	3,293	3	3290	658
1990-1995	5,503	47	5456	1,091
1996-2000	2,015	0	2015	403
Total	21,399	2,164	19,235	769

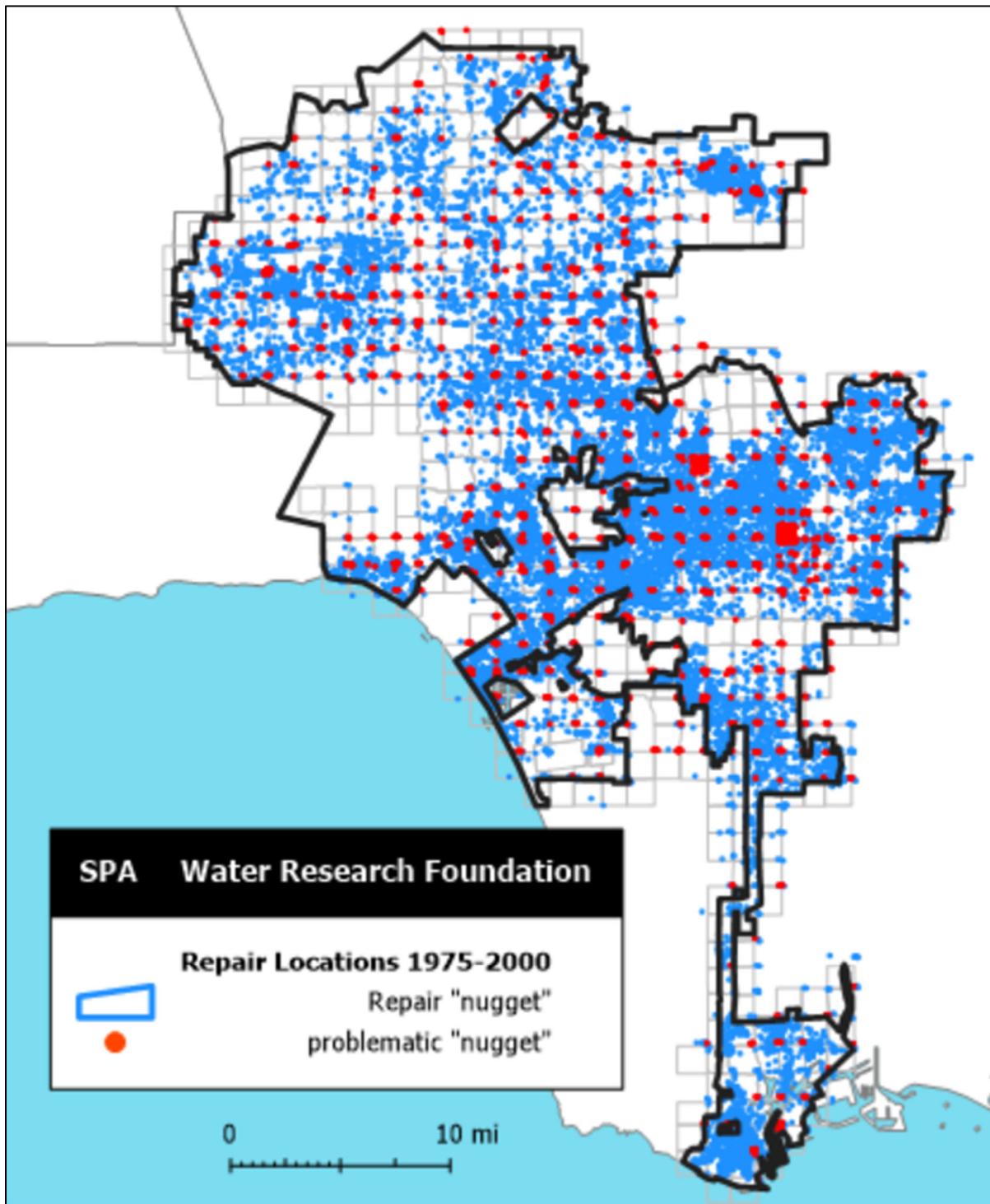


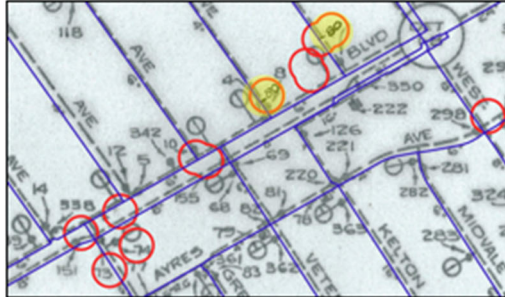
Figure 3-24. Repair Locations 1975-2000 Derived from Annotations on Scanned Maps.

Lustrum

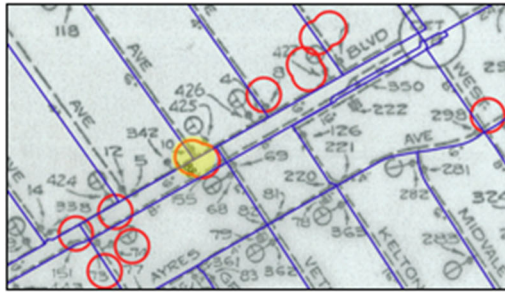
1975-1980



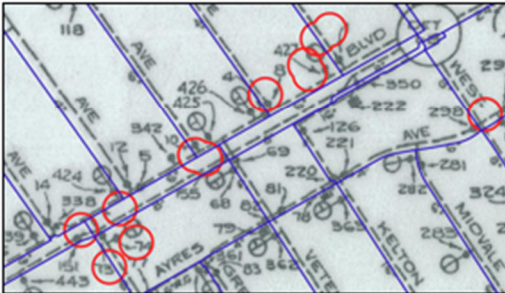
1980-1985



1985-1990



1990-1995



1996-2000



Figure 3-25. Example “Nuggets” Highlighted Yellow for Each of Five Lustra.

3.3.1.2 LADWP 2000-2017 Data

We next discuss data cleaning of the digital data for repairs since 2000. Cleaning is a typical and arduous task for any project involving data. For the digital datasets for 2000-2017, the task largely consisted of removing clearly erroneous data (e.g., date of pipe installation was listed as “3024”, or “24”) – such data was removed rather than an attempt being made to guess that the first either of those numbers might have been meant to be 1924. Another aspect of data cleaning was internal consistency – if a record was only partially complete (e.g., lacked material type, etc.) or a pipe was shown as having been installed in 2008 but the date of repair was 2004, this was interpreted as the pipe having been repaired in 2004 and replaced in 2008, so that the pipe data in the record (e.g., material, date of installation) was for the new replacement pipe rather than the pipe that had been repaired. That is, the repaired pipe was no longer in the record, in fact no longer existed. Such records were also removed. Of the approximately 19,000 records in the original repair database, cleaning removed approximately 2,500 or about 13%, which is not atypical for such databases. The remaining database (16,595, or an average of 922 repairs per year) is still large and useful.

3.3.1.3 Merged LADWP Dataset

The two LADWP datasets were processed and merged, resulting in 19 covariates as shown in Table 3-10. Some repair data omitted key information, so that the final merged dataset consists of 280,256 GIS pipe segments with a total of 46,621 repairs, consisting of 29,973 repairs for the period 1975-1999 (an average of 1,199 repairs pa) and 16,645 repairs for the period 2000-2017 (an average of 925 repairs pa).

The timeline of LADWP pipe repairs is shown in Figure 3-28 (note that due to repair records for 1975 to about 1998 only assignable to five year periods, that the graph depicts the average number of repairs per year for those lustra). Based on both graphs (number per year, and cumulative number per year) it can be seen that the repair record appears relatively complete for the 40 year period 1977 to 2017.

A “heatmap” of this repair dataset is shown in Figure 3-29 from which it can be seen that most repairs occur in an east-west “swath” running from Santa Monica to south of downtown. Figure 3-30 shows that this has some correspondence with the year of installation. It should be noted that the 1960s were more or less the transition from cast iron to ductile iron pipe.

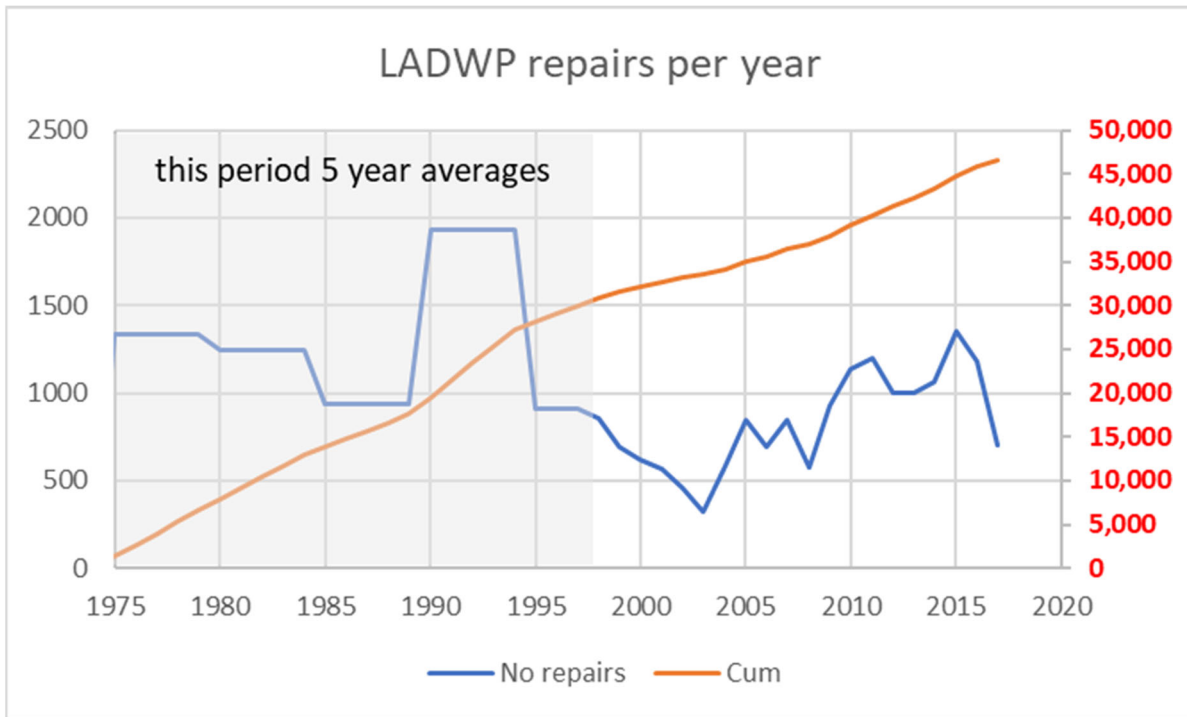


Figure 3-26. LADWP Pipe Repair Timeline: Blue Line Is Number of Repairs per Year (Right Axis) and Red Line Is Cumulative Repairs per Year (Right Axis).

As discussed above, the repair records for 1975 to about 1998 can only be assigned to five-year periods, so the graph depicts the average number of repairs per year for each lustrum.

Table 3-10. LADWP Dataset Covariates.

No.	Variable Name	Example value	Explanation
1	GISID	883636	An ID number for the pipe segment, from GIS database
2	pipeIDorig	1	A sequential number assigned to each pipe segment
3	WGS_FID	9800228	LADWP Facility ID number for the pipe segment
4	pDiam	6	Pipe diameter (inches)
5	pipeLft	5.75	Pipe length (ft)
6	pMatl	CI	Pipe material (CI, DI, AC, STL, X = other)
7	pipeYr	1969	Year of pipe installation
8	pipeAge	48	Pipe age as of 2017 (ie, 2017 - 1969 = 48)
9	leakYr	2012	The year of repair, for the period 2000-2017; if no repair then -999
10	repairYr	1977	The year of repair (mid-point of lustrum) for the period 1975-1999; if no repair then -999
11	PGVkine	16	Peak ground velocity at pipe location in 1994 Northridge earthquake
12	Slope_3DEP	0.27	Maximum gradient of the ground at mid-length of pipe (rise over run)
13	Aspect_3DEP	-112.1	Aspect of the slope (degrees from N, -180 <= Aspect <= 180)
14	Brg	1.4	Bearing from N of the pipe longitudinal axis (0 <= Brg <= 360)
15	SL	-0.11	Gradient parallel to pipe longitudinal axis (rise over run); sign depends on pipe start and end points and is inconsequential, only absolute value is employed
16	ST	0.25	Ditto for gradient transverse to pipe longit. Axis
17	TMIN	12	Minimum hourly temperature (degr. F) recorded on date of repair if known, else -999
18	dailyDiff	41	Difference between min and max hourly temperatures (degr. F), for day of repair if known, else -999
19	oneDayTminDiff	34	Difference between min hourly temperatures (degr. F) for day of repair and day before, if day is known, else -999

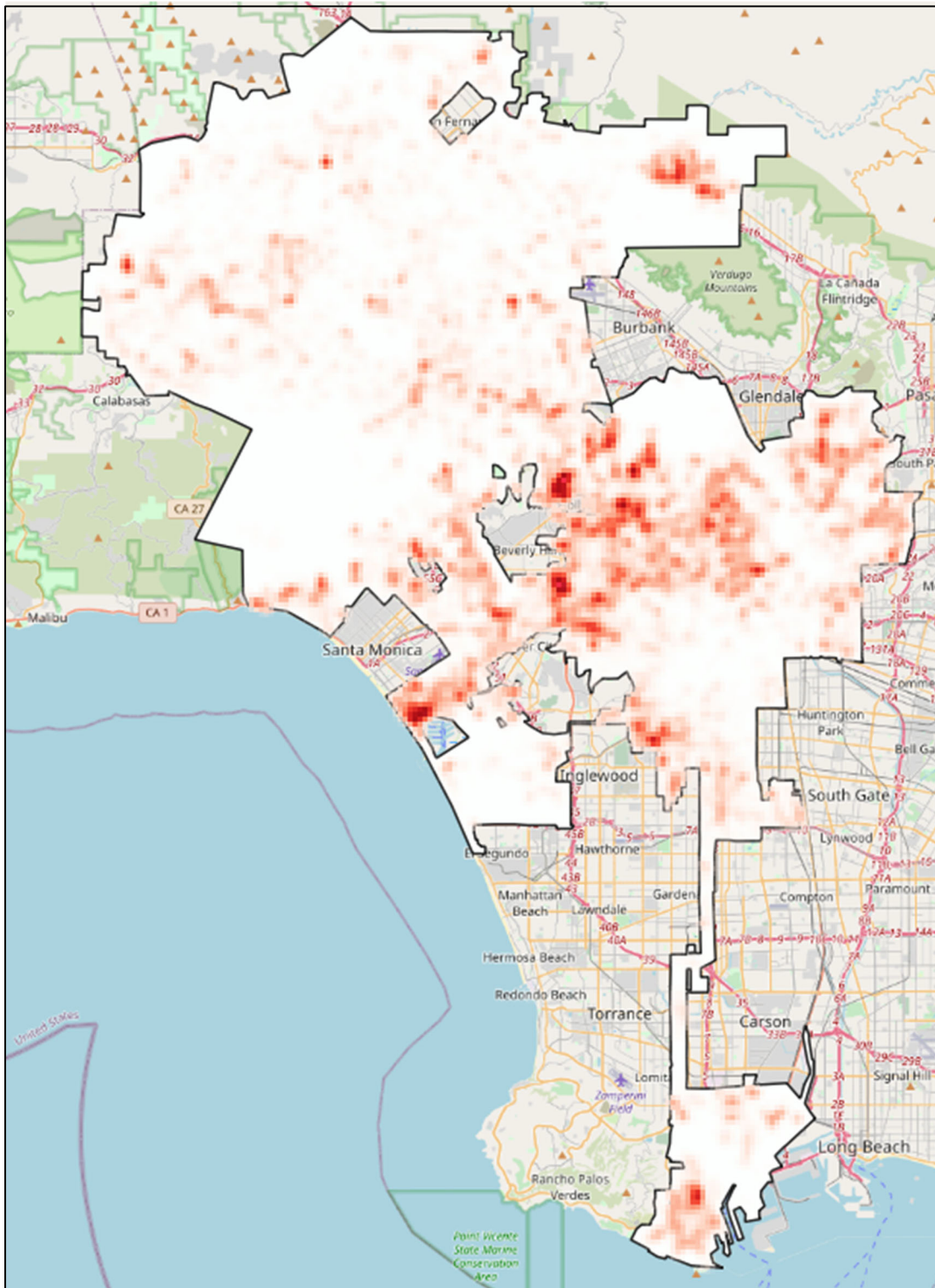


Figure 3-27. LADWP Pipe Repair Heatmap Showing Areas of Concentration of Repairs.

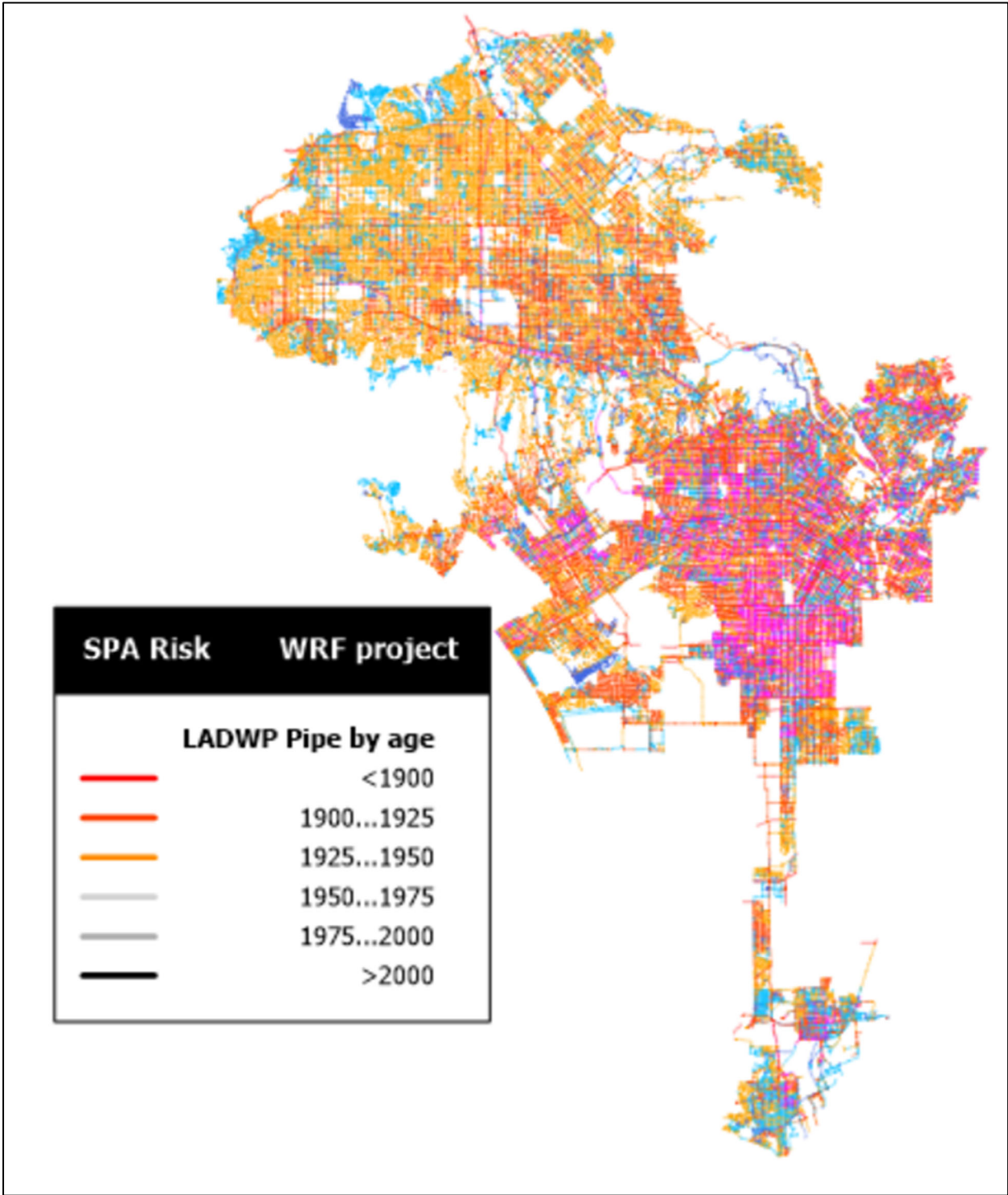


Figure 3-28. LADWP Pipe Network by Year of Installation.

3.3.2 SFPUC

Similar to the LADWP dataset, the SFPUC dataset was processed with 55,763 pipe segments having 3,325 repairs structured similarly to Table 3-8. The timeline of SFPUC pipe repairs is shown in Figure 3-31, from which it can be seen that the repair record appears relatively complete for the period 1980 to 2016. The repairs distribution is shown in a “heatmap” in Figure 3-32. Slope and aspect were extracted from the 3DEP DEM data and is discussed later.

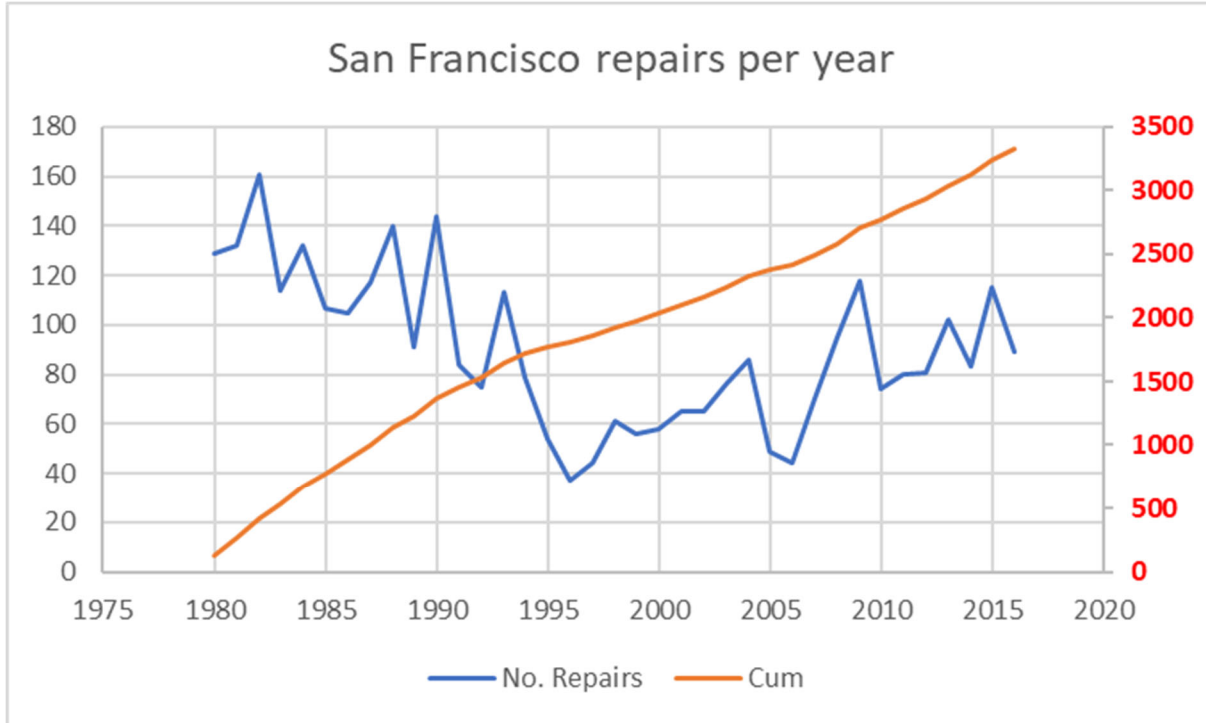


Figure 3-29. SFPUC Pipe Repair Timeline: Blue Line Is Number of Repairs per Year (Right Axis) and Red Line Is Cumulative Repairs per Year (Right Axis).

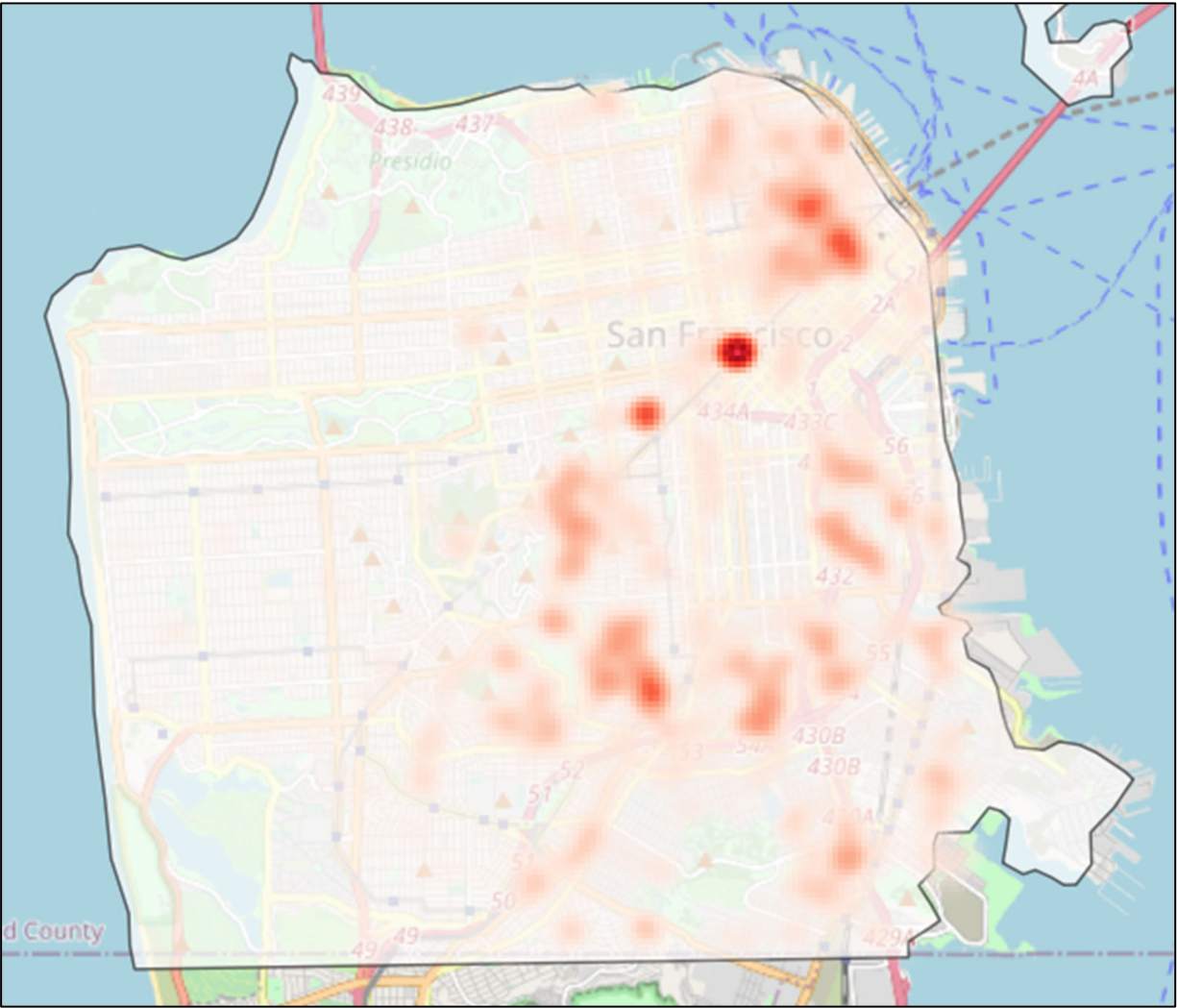


Figure 3-30. SFPUC Pipe Repair Heatmap Showing Areas of Concentration of Repairs.

3.3.3 EBMUD

Similar to the LADWP dataset, the EBMUD dataset was processed with 98,537 pipe segments having 20,856 repairs structured similarly to table 3-8. The timeline of EBMUD pipe repairs is shown in Figure 3-33, from which it can be seen that the repair record appears relatively complete for the period 1997 to 2016, with partial data before that. The repairs distribution is shown in a “heatmap” in Figure 3-34. Slope and aspect were extracted from the 3DEP DEM data and is discussed later.

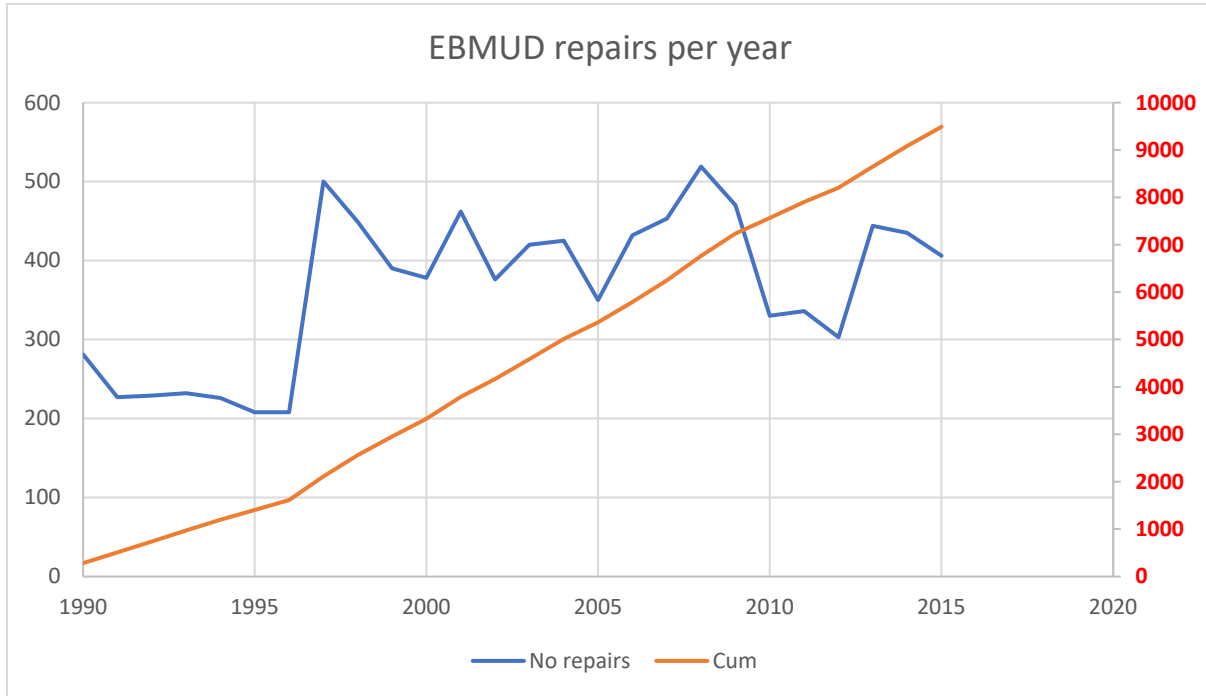


Figure 3-31. EBMUD Pipe Repair Timeline: Blue Line Is Number of Repairs per Year (Right Axis) and Red Line Is Cumulative Repairs per Year (Right Axis).

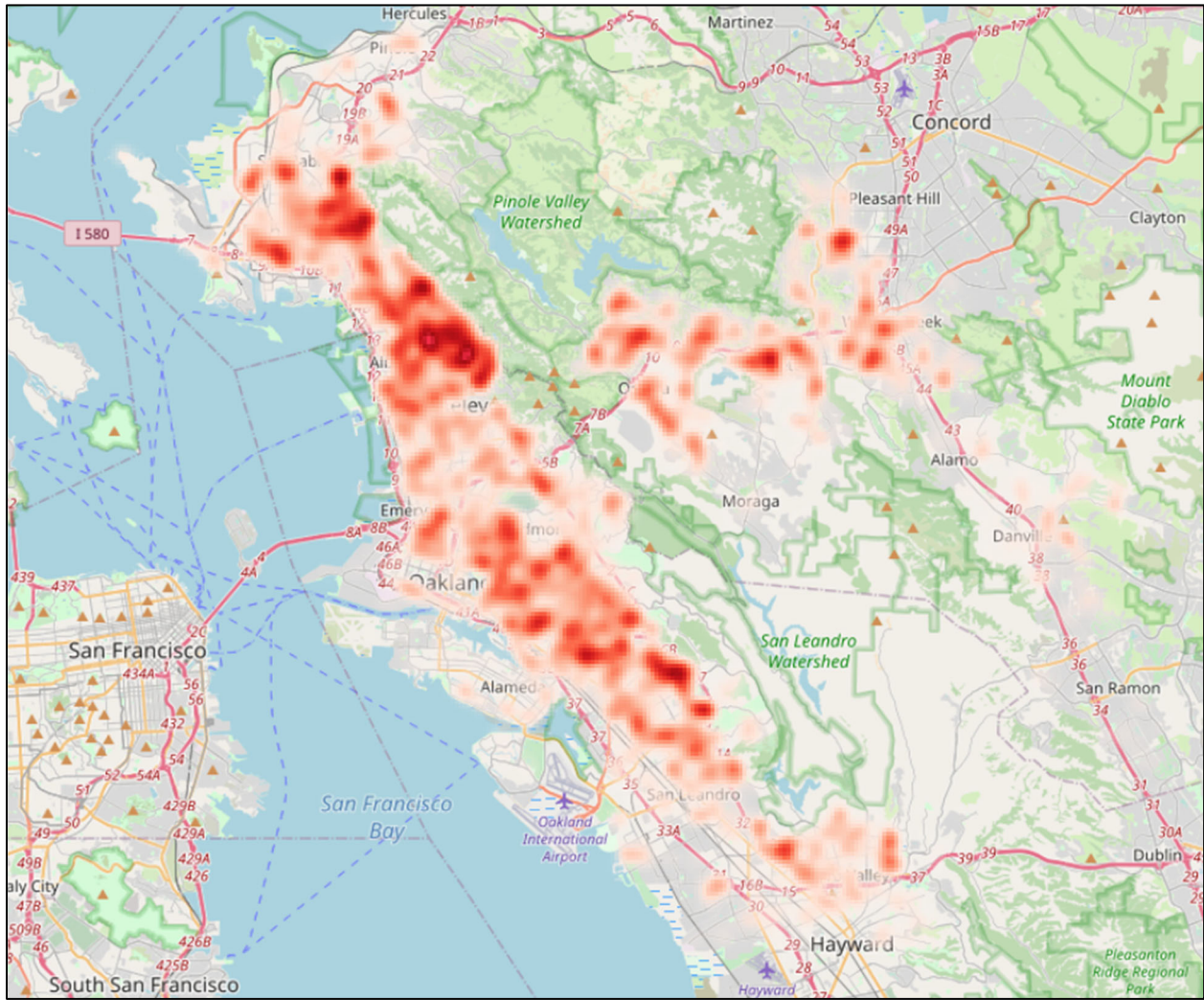


Figure 3-32. EBMUD Pipe Repair Heatmap Showing Areas of Concentration of Repairs.

3.3.4 PWB

Similar to the LADWP dataset, the PWB dataset was processed with 117,688 pipe segments having 1,337 repairs structured similarly to Table 3-8. The timeline of PWB pipe repairs is shown in Figure 3-35, from which it can be seen that the repair record appears relatively complete for the period 2006 to 2014, with partial data before after that. The repairs distribution is shown in a “heatmap” in Figure 3-36. Slope and aspect were extracted from the 3DEP DEM data and is discussed later. The 2001 Nisqually earthquake was felt in Portland but caused no damage in Portland, so that the PWB system is considered unaffected by major seismic stress events.

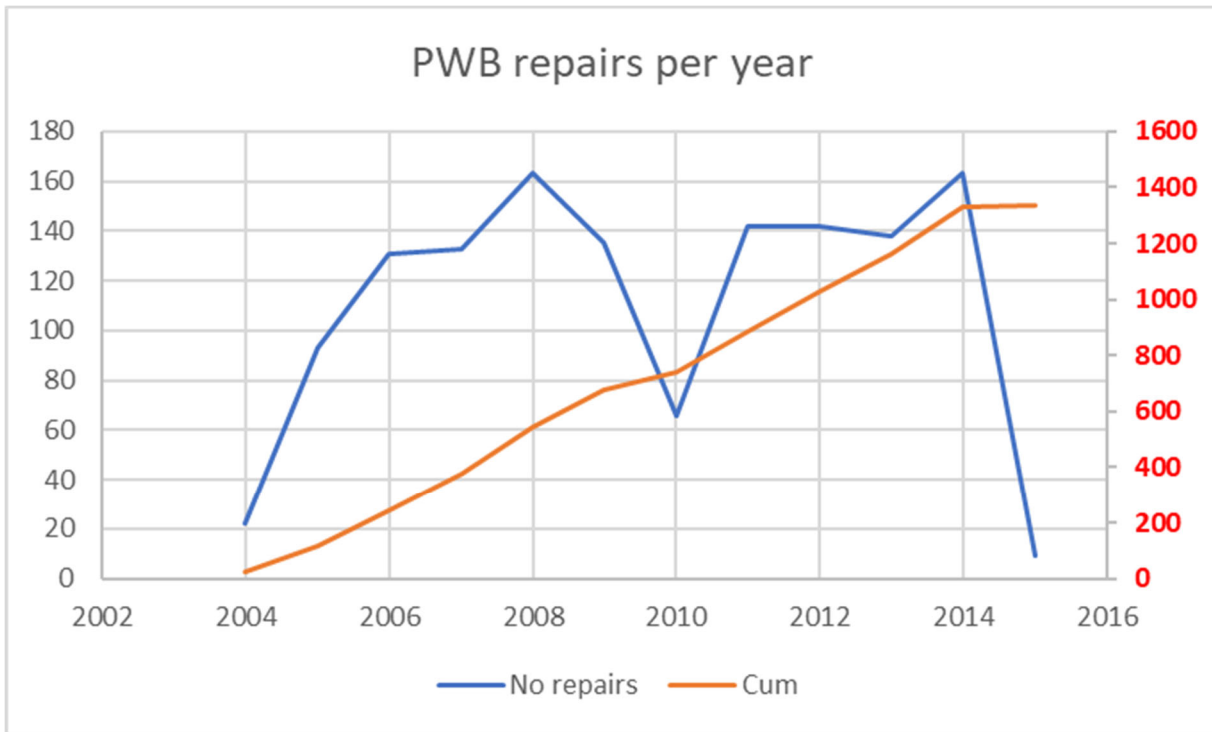


Figure 3-33. PWB Pipe Repair Timeline: Blue Line Is Number of Repairs per Year (Right Axis) and Red Line Is Cumulative Repairs per Year (Right Axis).

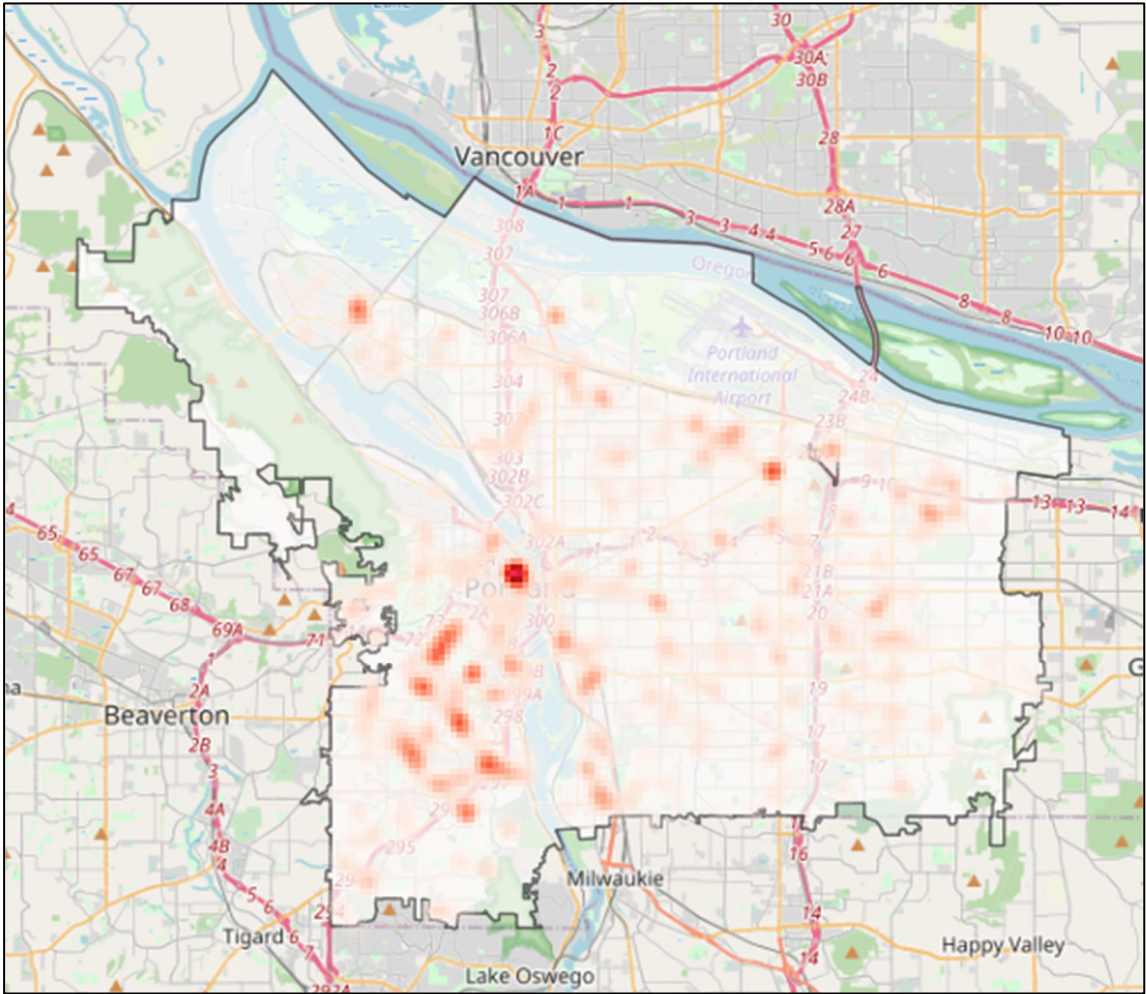


Figure 3-34. PWB Pipe Repair Heatmap Showing Areas of Concentration of Repairs.

3.3.5 SPU

Similar to the LADWP dataset, the SPU dataset was processed with 66,632 pipe segments having 5,303 repairs structured as shown Table 3-8. The timeline of SPU pipe repairs is shown in Figure 3-37, from which it can be seen that the repair record appears relatively complete for the period 2000 to 2017, with partial data before after that. The repairs distribution is shown in a “heatmap” in Figure 3-38, while Figure 3-39 show slope data for the service area.

While Seattle felt the 2001 Nisqually earthquake, in fact it caused very little damage in the city (or elsewhere, in fact) which is substantiated by the intensity distribution and PGV recording, Figure 3-40 and Figure 3-41 respectively. Not being subjected to a major earthquake, the PGV field 11 in Table 3-8 is not applicable, as is field 10 corresponding to the pre-2000 repairs for the LADWP dataset, extracted from the map scans.

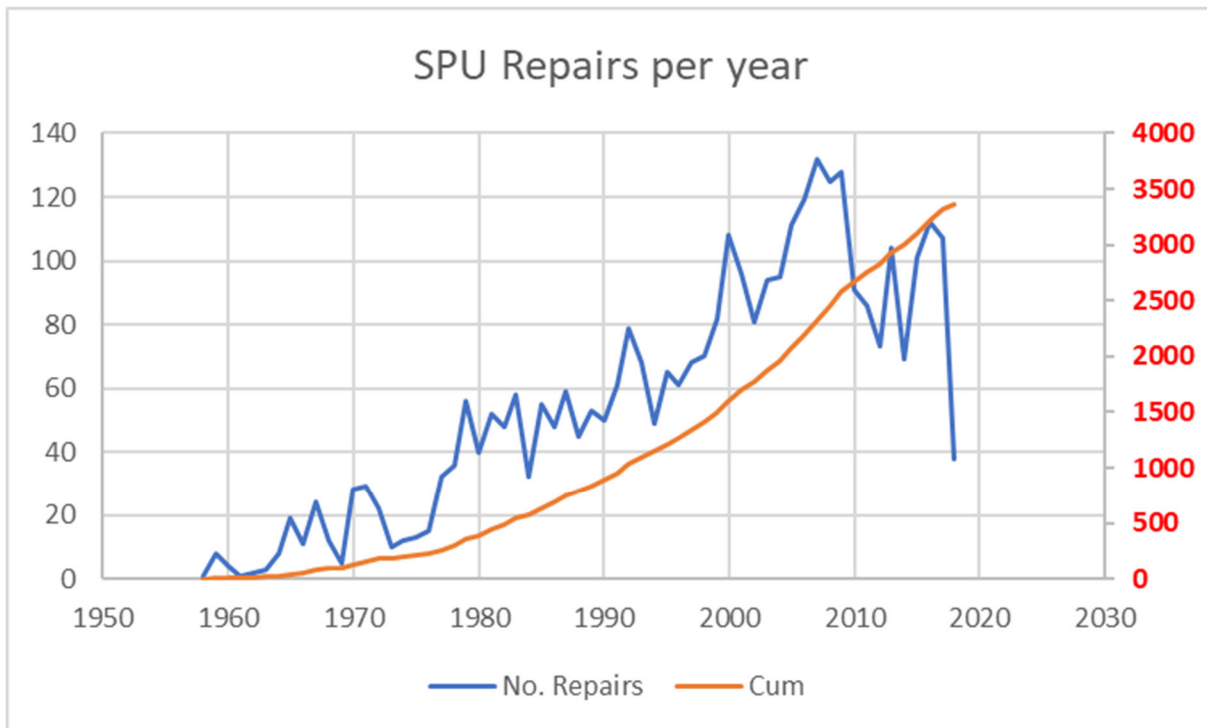


Figure 3-35. SPU Pipe Repair Timeline: Blue Line is Number of Repairs per Year (Right Axis) and Red Line is Cumulative Repairs per Year (Right Axis).

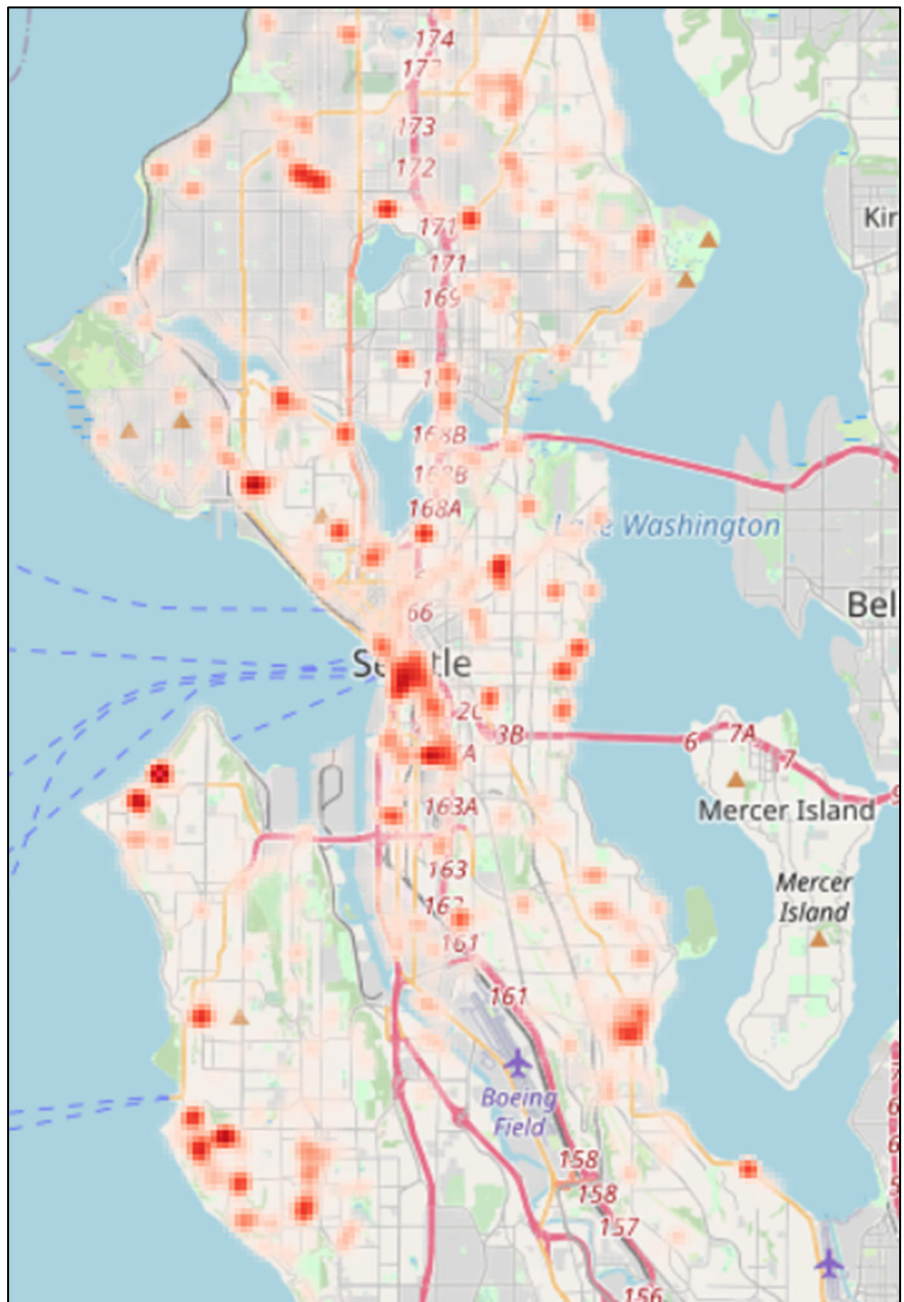


Figure 3-36. SPU Pipe Repair Heatmap Showing Areas of Concentration of Repairs.

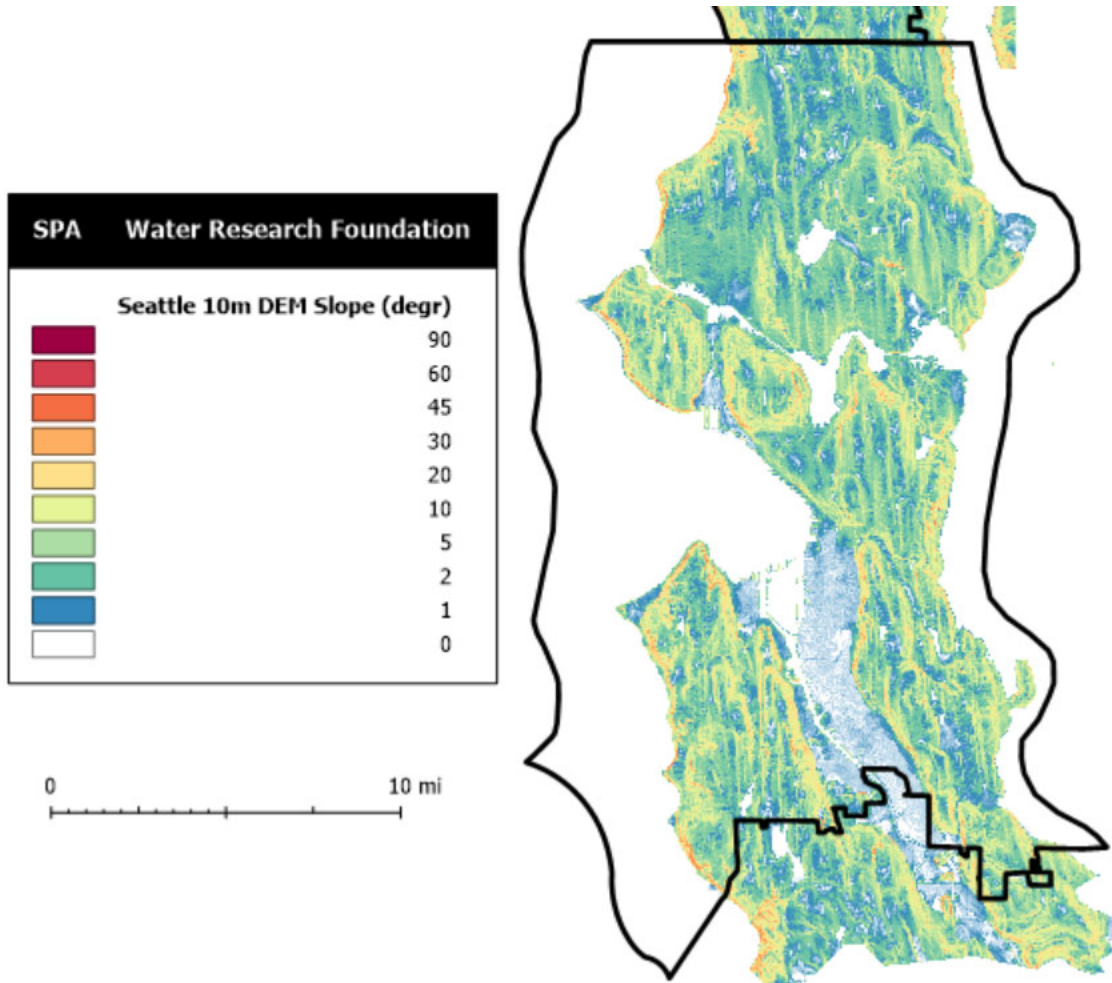
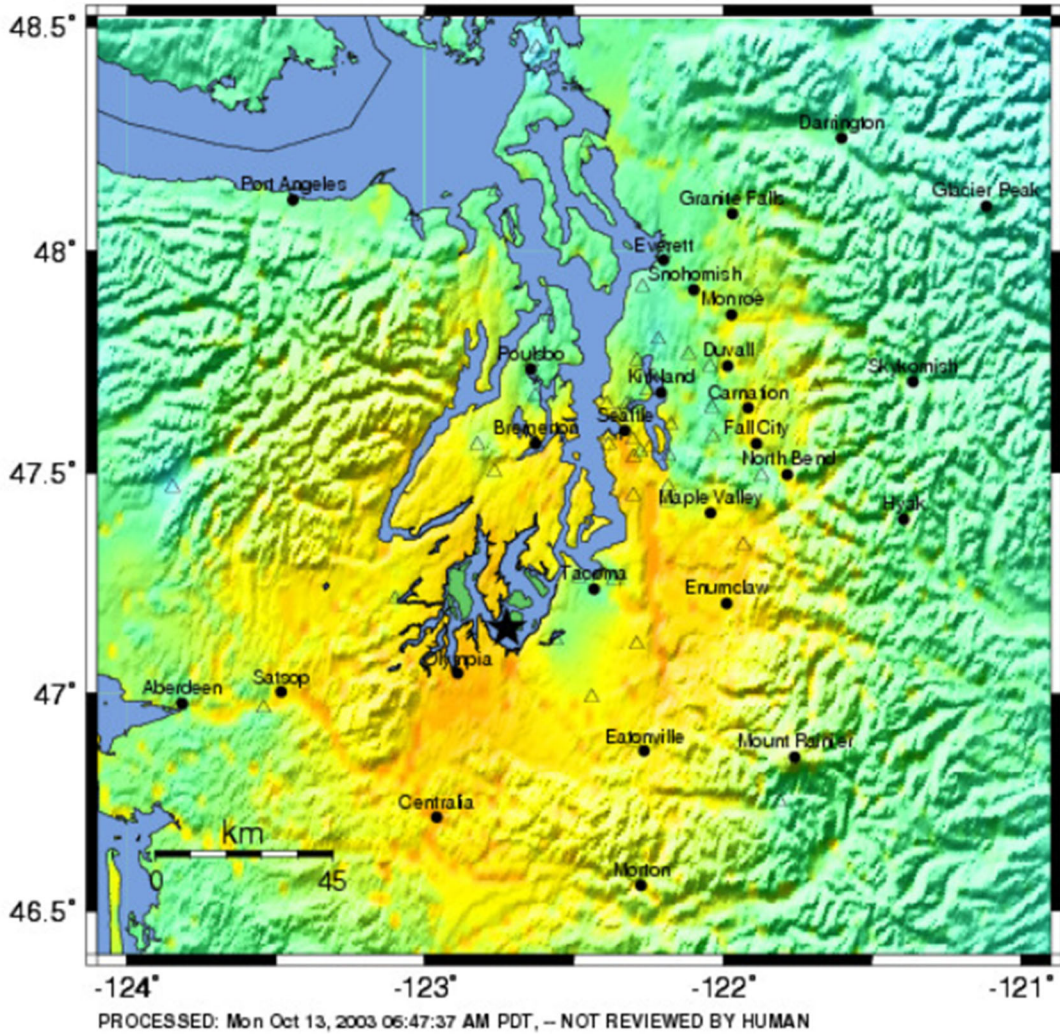


Figure 3-37. SPU Service Area within Which Is Displayed 10m Slope Data.

PNSN Rapid Instrumental Intensity Map Epicenter: 17.0 km NE of Olympia, WA
 Wed Feb 28, 2001 10:54:00 AM PST M 6.8 N47.15 W122.73 Depth: 51.9km ID:0102281854



PERCEIVED SHAKING	Not felt	Weak	Light	Moderate	Strong	Very strong	Severe	Violent	Extreme
POTENTIAL DAMAGE	none	none	none	Very light	Light	Moderate	Moderate/Heavy	Heavy	Very Heavy
PEAK ACC (%g)	<.17	.17-1.4	1.4-3.9	3.9-9.2	9.2-18	18-34	34-65	65-124	>124
PEAK VEL (cm/s)	<0.1	0.1-1.1	1.1-3.4	3.4-8.1	8.1-16	16-31	31-60	60-116	>116
INSTRUMENTAL INTENSITY	I	II-III	IV	V	VI	VII	VIII	IX	X+

Figure 3-38. 2001 Nisqually Earthquake Intensity Distribution.

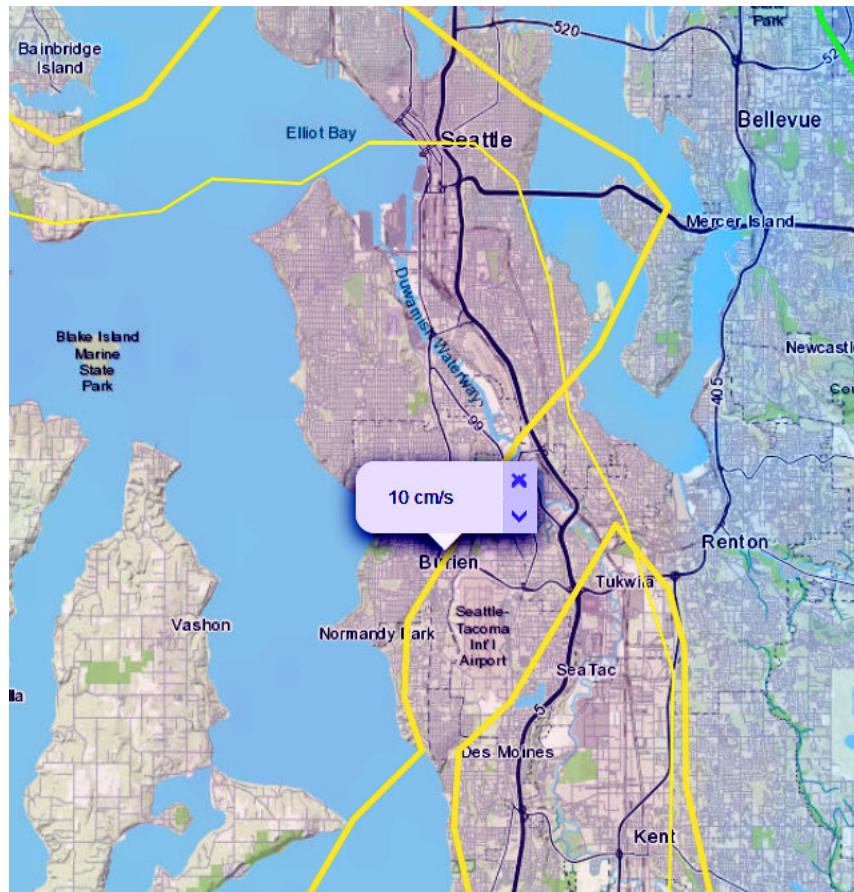


Figure 3-39. 2001 Nisqually Earthquake PGV Recorded in Central Seattle.

3.3.6 Geophysical Covariates

This section discusses this study’s collection and processing of geophysical covariates, using the Los Angeles data set for discussion purposes. Conclusions based on this examination are employed for all data sets.

Pipe damage can result from many factors, some natural such as down-slope ground movement or earthquake and others anthropogenic such as backhoe strikes or heavy truck traffic. Because our research question concerns major system-wide stress events such as an earthquake, we examine only natural factors.

Natural or geophysical factors selected for examination included geology, ground slope, a measure of surficial soil stiffness termed Vs30, temperature, and the stress event of interest to this study – earthquake strong ground motion. Geology, and Vs30 are measures of soil type which is the medium buried pipes are in and an important factor in buried pipe performance, for two reasons: soil type correlates with (a) ground movement, and (b) soil corrosivity. Correlation of soil type with ground movement or corrosivity is not especially strong (Melchers, Petersen and Wells 2019) but the measures employed here are at least consistent across the five data sets, particularly for corrosivity where we lack a uniform corrosivity database for the five data sets. The two measures examined for characterizing soil type were geology and Vs30. Geology, Vs30 and ground slope are of course inter-related, as discussed below.

3.3.6.1 Geology

Using GIS techniques, detailed surficial geology map data (Bedrossian et al. 2012) in Figure 3-42 was correlated with each pipe.

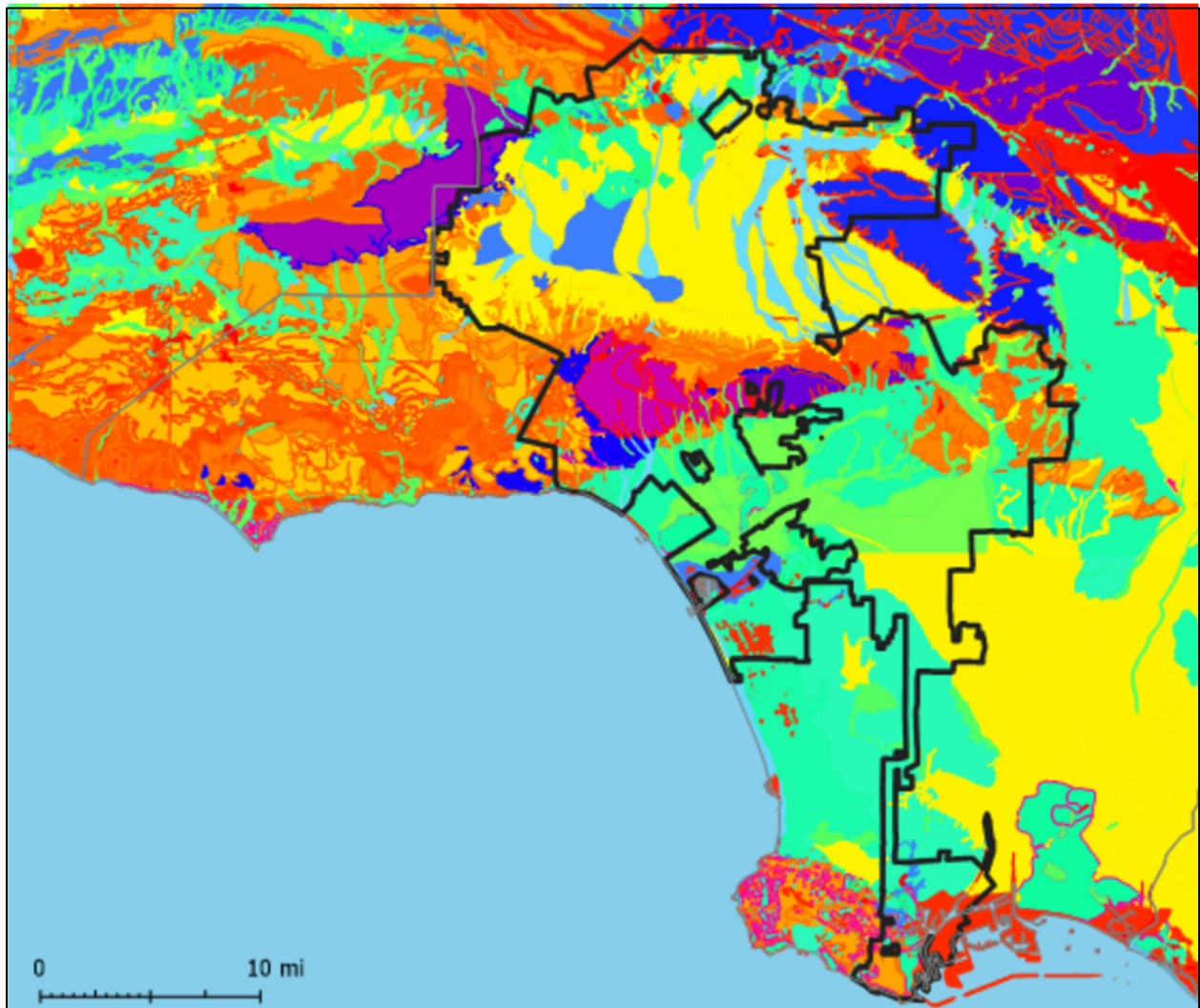


Figure 3-40. Geologic Compilation of Quaternary Surficial Deposits in Southern California.

Source: Data from Bedrossian et al. 2012

Because geological categories were too numerous for practical analysis, these were reduced to five major categories, Figure 3-43, consisting of:

- Af: artificial fill, typically very soft
- Qls: Quaternary landslide
- Qy: younger Quaternary deposits, typically softer
- Qo: older Quaternary deposits, typically firmer
- R: all other deposits, typically very firm materials

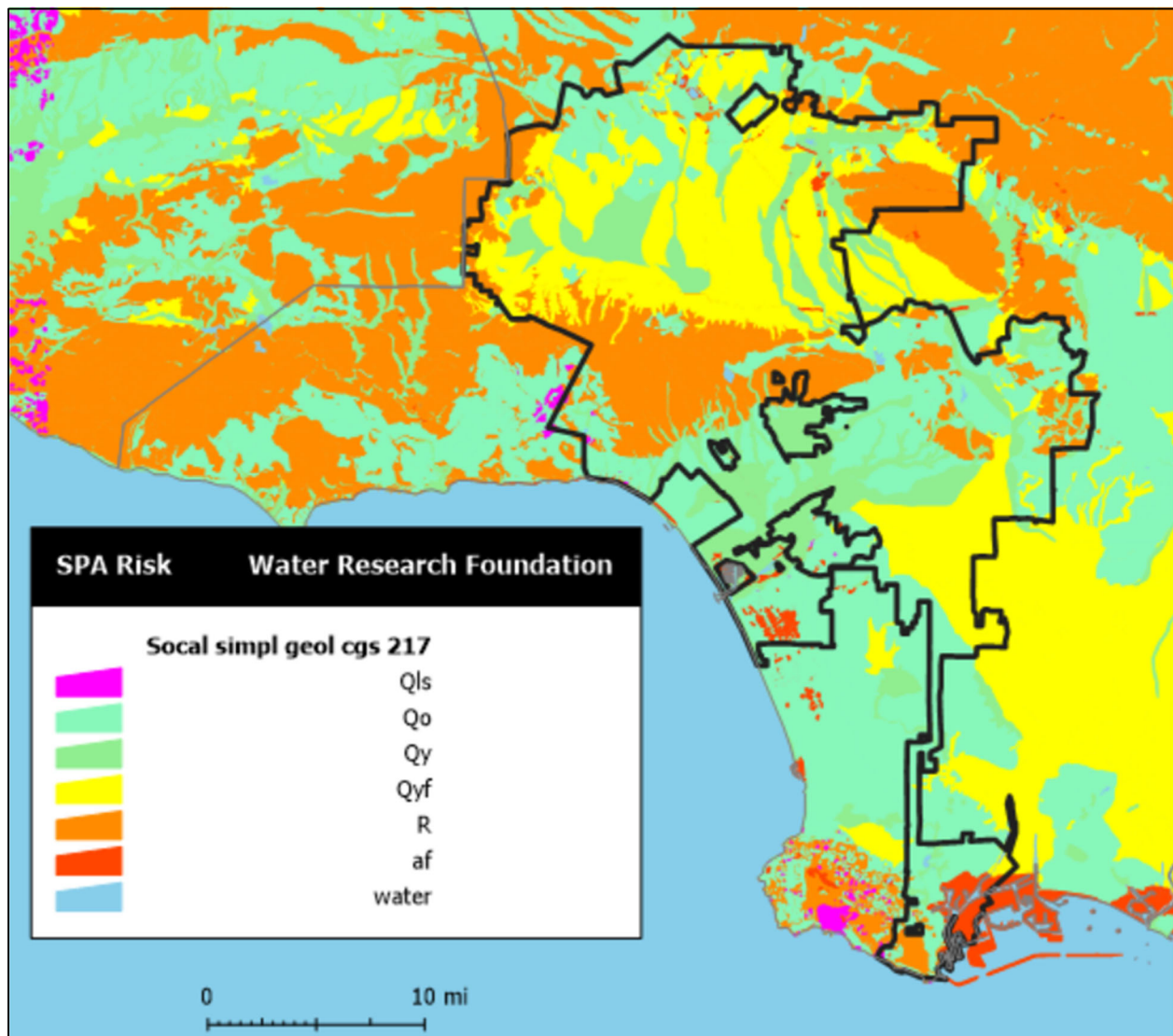


Figure 3-41. Simplified Surficial Deposits in Southern California This Study, After.

Source: Data from Bedrossian et al. 2012

The result is a designation for each pipe of its surrounding surficial geology.

3.3.6.2 Slope and Aspect

The *gradient* of a scalar field such as ground elevation is a vector field which points in the direction of the greatest rate of increase of the scalar field. *Slope* is the magnitude of the gradient vector and describes the surface's steepness and is relevant for several reasons - steeper slopes tend to sustain mass wasting (i.e., downward movement of material) and such movement damages pipe. Slope has also been found to correlate with surficial deposit stiffness (i.e., Vs30), which is discussed further below. The compass direction the surface faces (i.e., direction of the gradient vector) is termed the *aspect*. Aspect permits calculation of the slope relative to the pipe axis – that is, the pipe-relative longitudinal and transverse inclines, as shown in Figure 3-44 and the following equations.

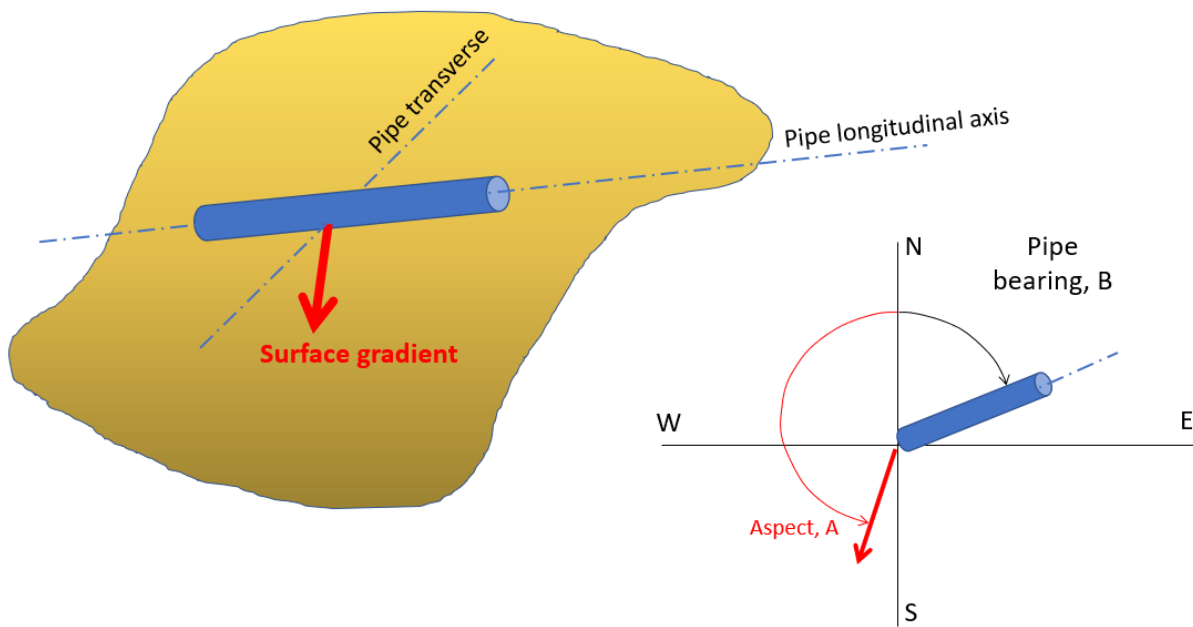


Figure 3-42. Pipe Axis Relative to Ground Surface Gradient.

If S is the slope (rise over run), A the aspect ($-180^\circ \leq A \leq 180^\circ$ counter-clockwise as measured from north) and B the bearing of the pipe (measured in degrees clockwise from north), then:

$$S_L = S[\cos(B - A)] \quad \text{Equation 3-2}$$

$$S_T = S[\sin(B - A)] \quad \text{Equation 3-3}$$

where S_L is the slope (rise over run) along the pipe axis (ie, longitudinal direction) and S_T is the slope transverse to the pipe.

A standard digital elevation model (DEM) data source, SRTM (USGS 2018) was examined as a source of slope data, Figure 3-45, from which slope data was derived, Figure 3-46. Slope can be measured in terms of angle (90° = vertical) or rise over run (45° slope has a rise over run of 1).

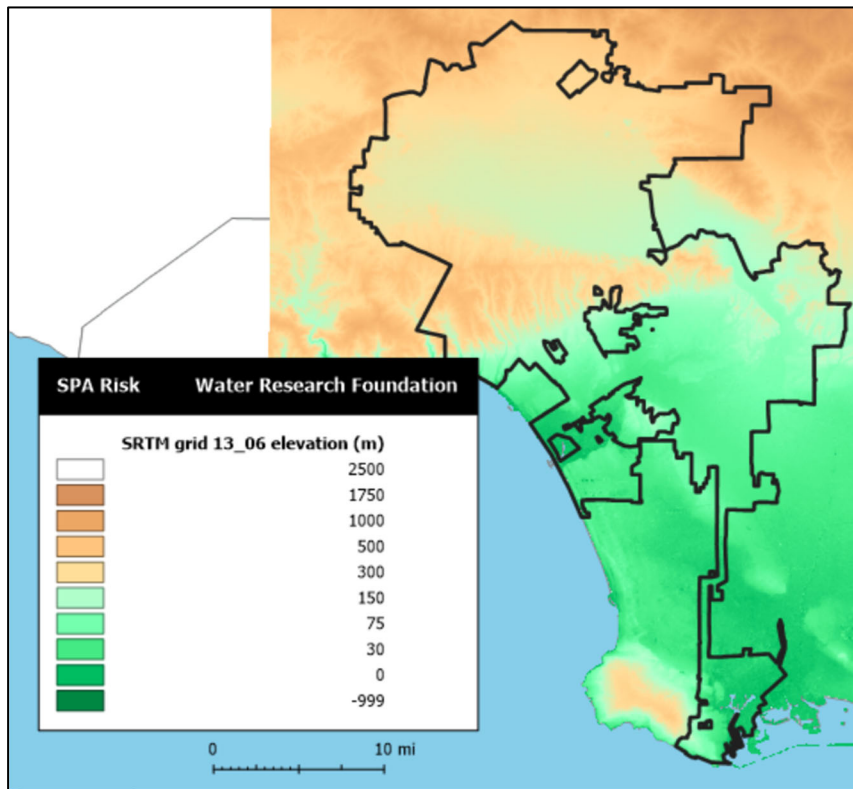


Figure 3-43. SRTM Digital Elevation Data.

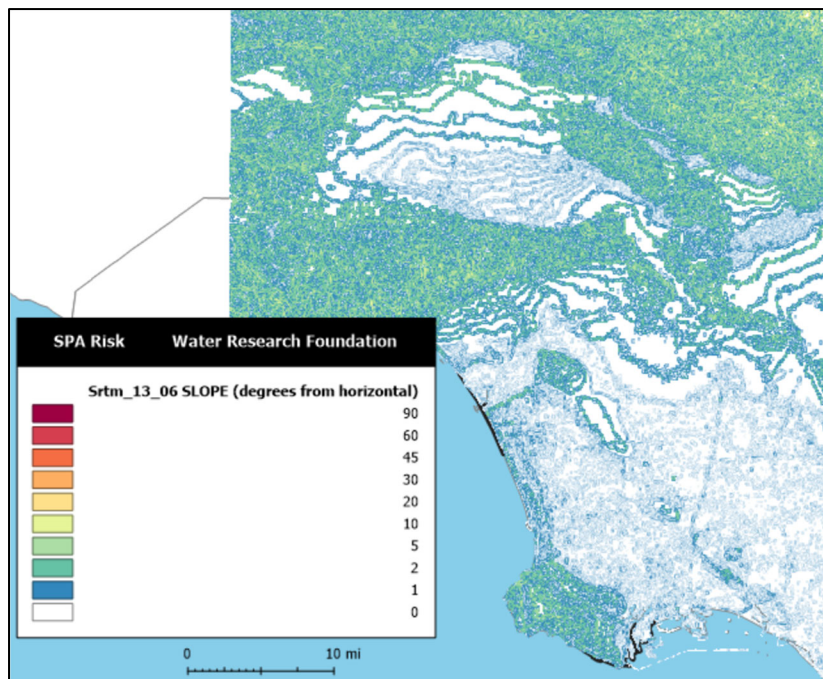


Figure 3-44. Slope as Derived SRTM Digital Elevation Data.

However, recently much more detailed DEM data has become available from the USGS based on lidar and related technology, Figure 3-47 and Figure 3-48. This data, termed Third Elevation Program or “3DEP” data, has a resolution of 1/3rd arc-second or equivalently about 10m, vs. 90m for the SRTM data, and allows derivation of much more detailed slopes, Figure 3-49. This 3DEP data is employed for slope and aspect all five data sets, Figure 3-50 to Figure 3-55.

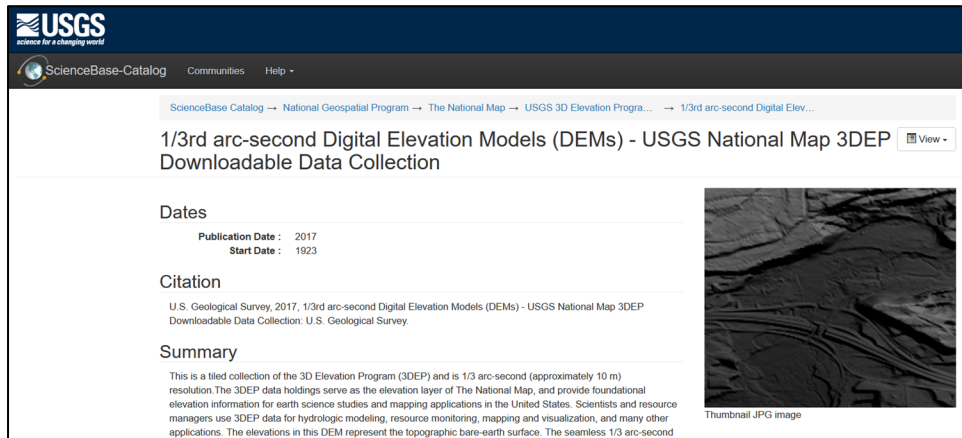


Figure 3-45. USGS 3DEP 1/3rd Arc-Second DEM Data Website.

Source: USGS 2020

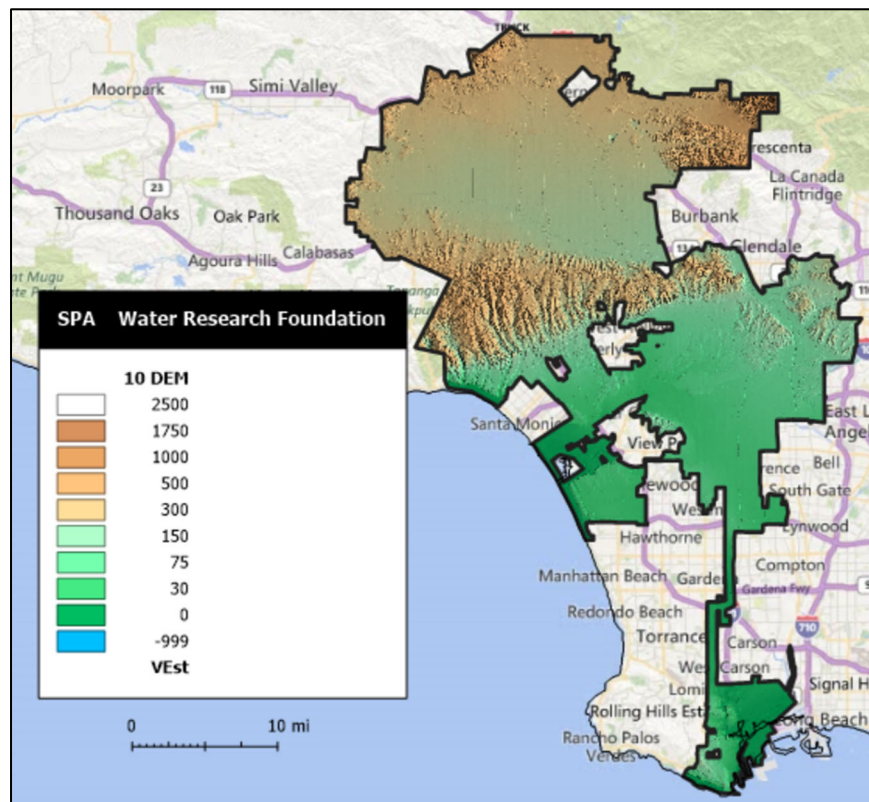


Figure 3-46. USGS 3DEP 1/3rd Arc-Second DEM Data for Los Angeles.

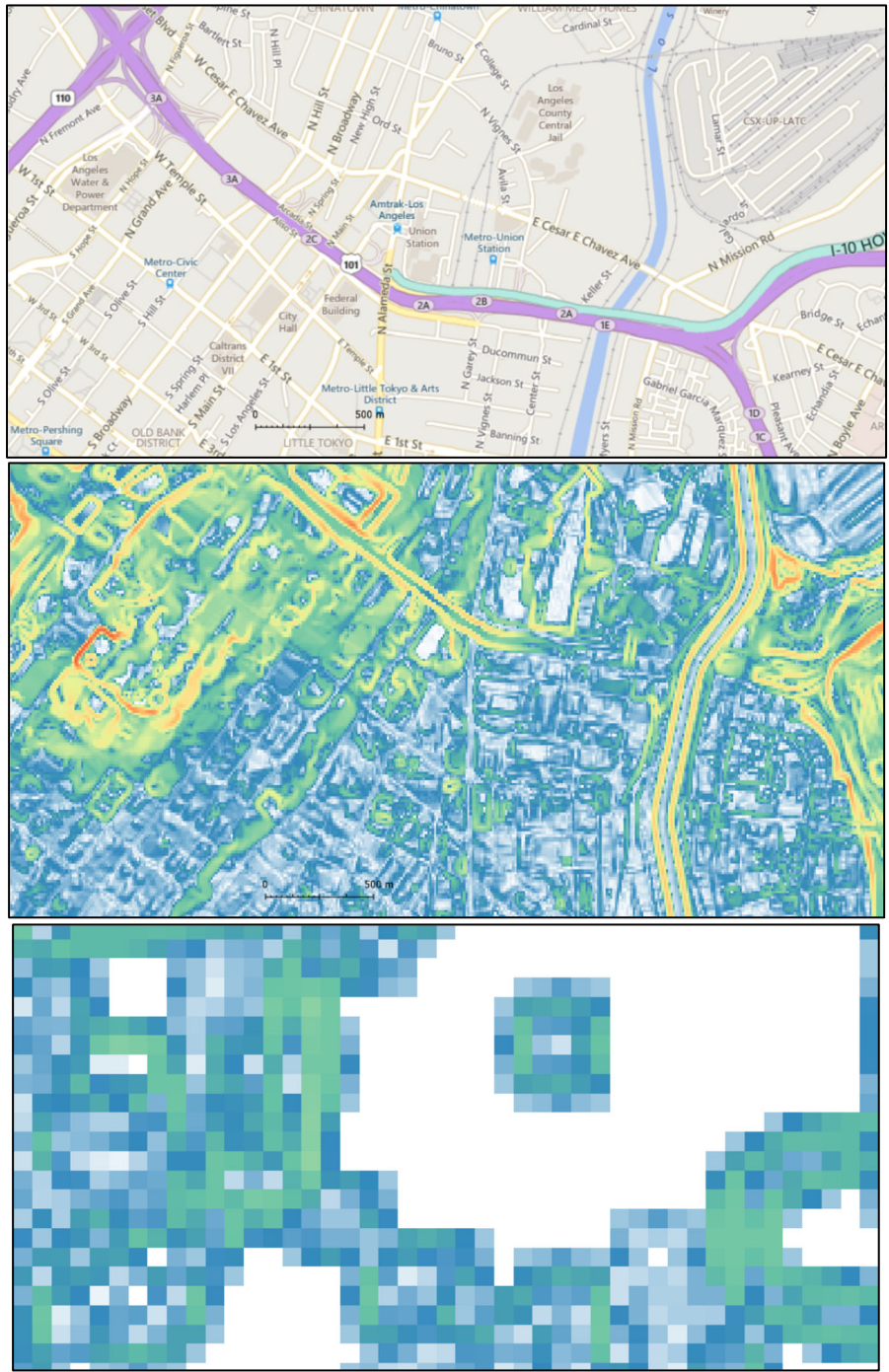


Figure 3-47. Slope Data Derived for Downtown Los Angeles: (Top) Map of Location; (Middle) Slope Data from 3DEP; (Bottom) Slope Data Derived from SRTM.

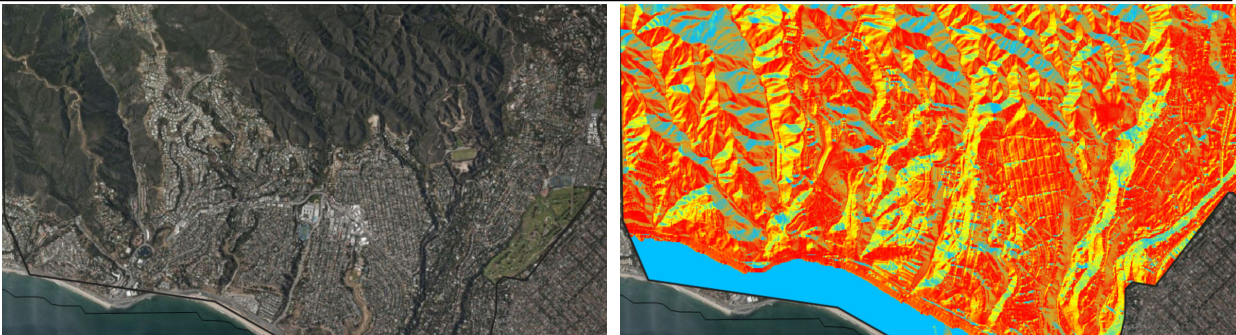
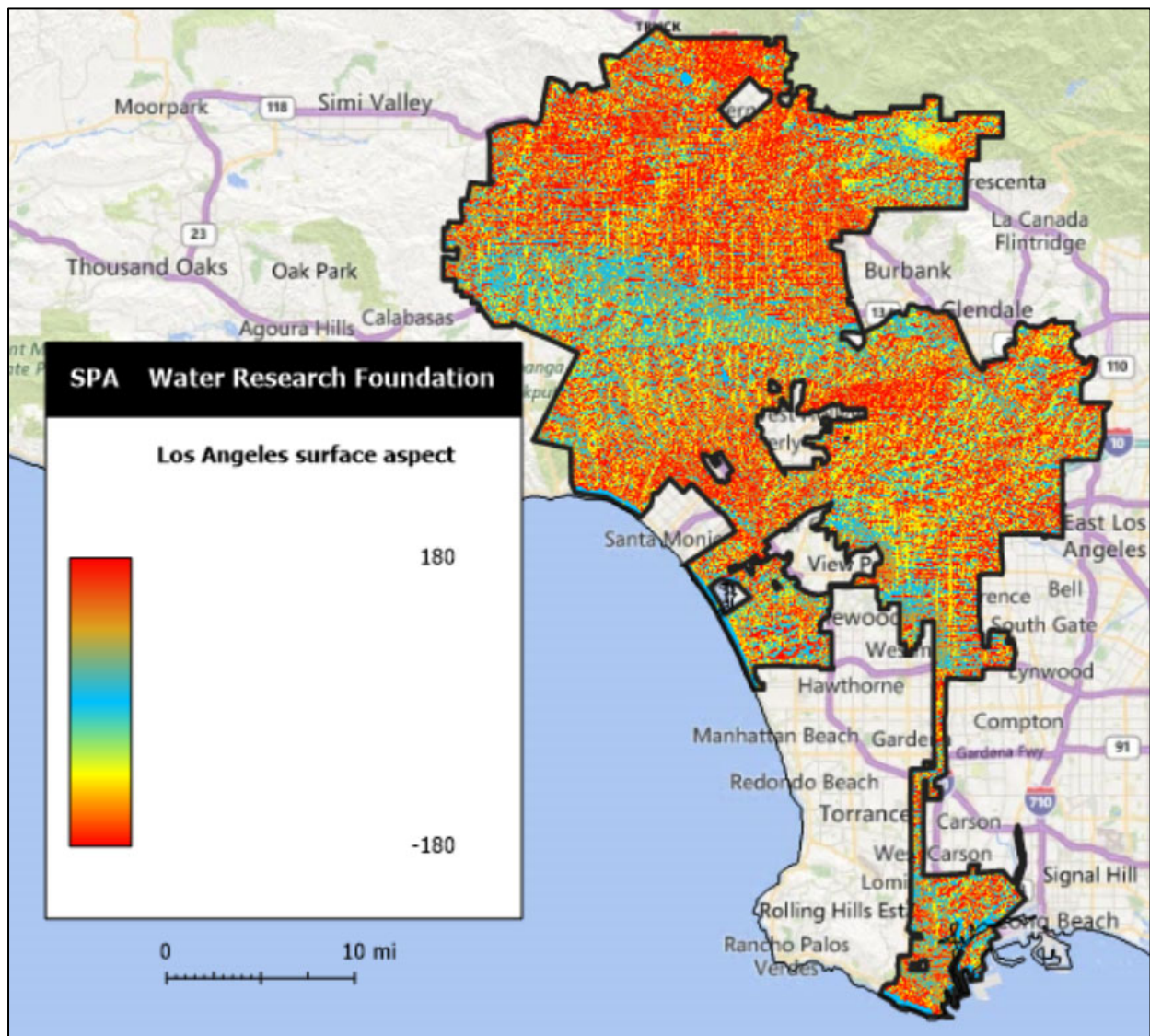


Figure 3-48. Aspect Data Derived for (Top) Los Angeles; (Bottom) Aerial Image and Aspect Detail Vicinity of Will Rogers State Historic Park.

Figure 3-51 shows the distribution of slope at the pipe centroid (ie, in general neither parallel nor perpendicular to the pipe’s longitudinal axis) for the LADWP dataset. It can be seen that about 20% of LADWP pipe are on slopes of more than 0.1 rise of run (equivalent to about 5°) and about 2% a slope greater than 0.6 (30°).

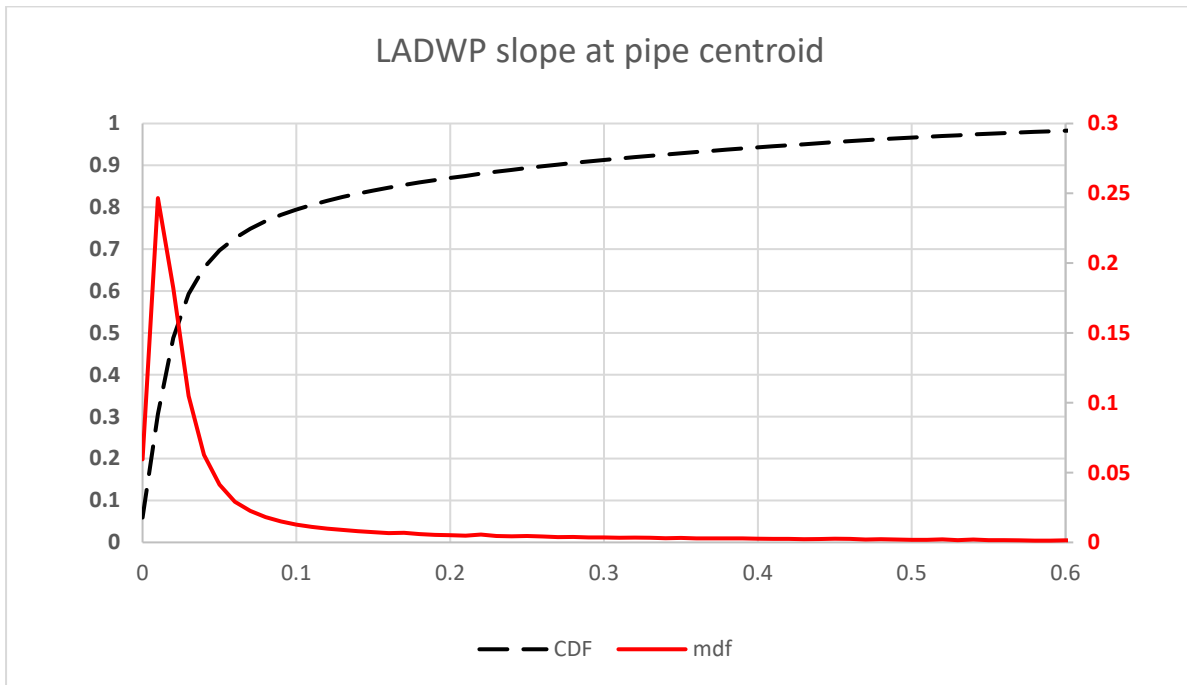


Figure 3-49. Distribution of Slope at Pipe Centroid for LADWP Dataset – CDF Axis Is on Left.

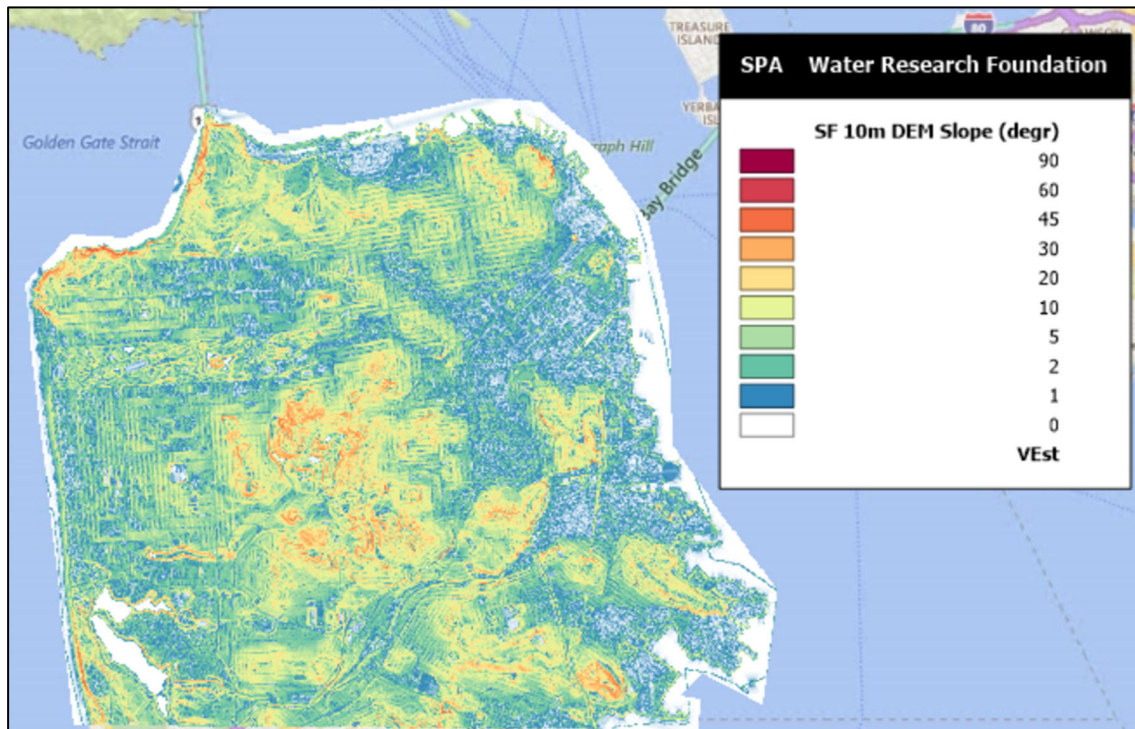


Figure 3-50. Slope Data for the SFPUC Service Area Derived from 3DEP Data.

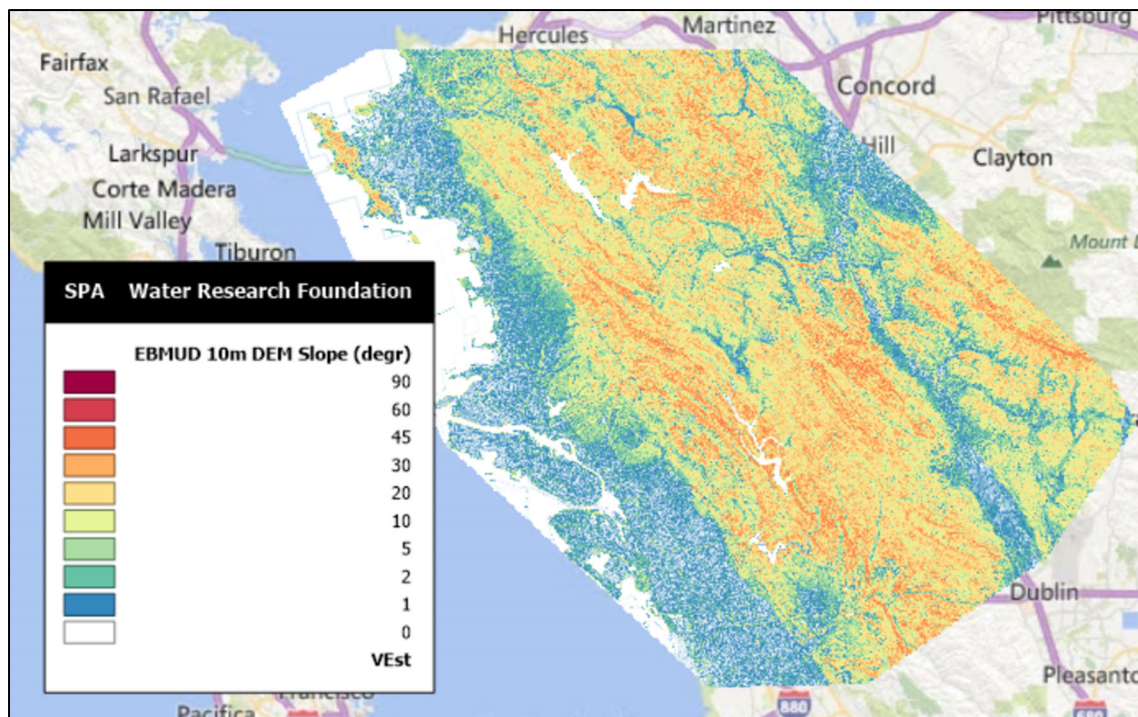


Figure 3-51. Slope Data for the EBMUD Service Area Derived from 3DEP Data.

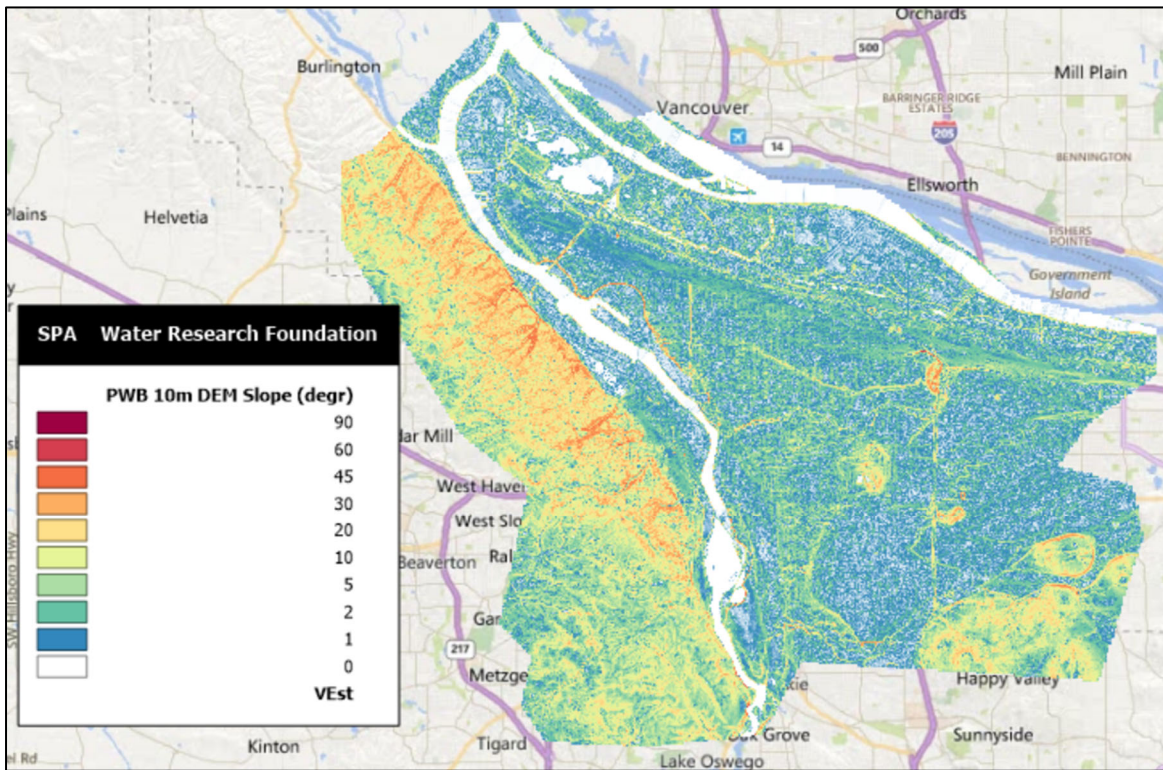


Figure 3-52. Slope Data for the PWB Service Area Derived from 3DEP Data.

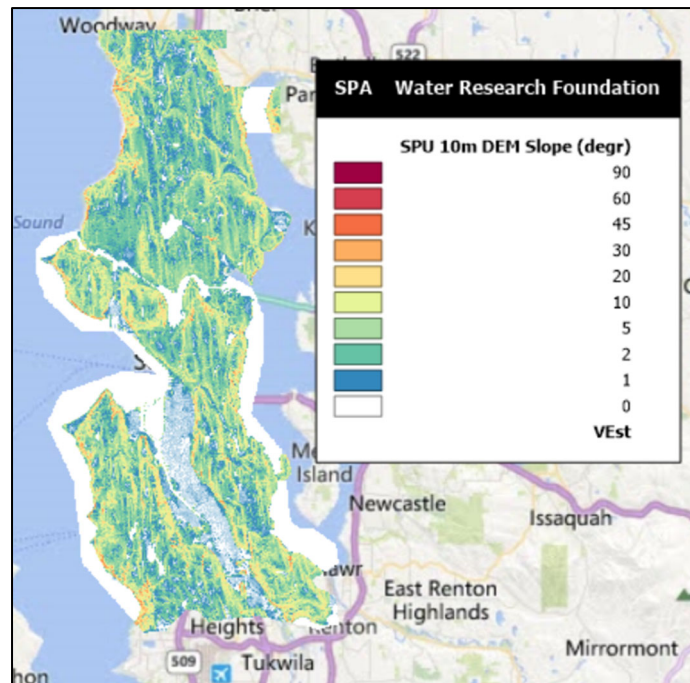


Figure 3-53. Slope Data for the SPU Service Area Derived from 3DEP Data.

3.3.6.3 Vs30

Because the geology assignments discussed above are relative crude and discontinuous, Vs30 data was also assigned to each pipe. Vs30, the shear wave velocity of the top 30 m of soil, is a measure of a site's relative stiffness and found to correlate well with earthquake strong ground motions (Borcherdt 2012;

Holzer et al. 2005). Soil stiffness, whether measured in terms of the above simple geologic categories or in terms of Vs30, is an approximate correlate with the potential for ground movement, whether gradual movement under normal conditions, or transient movement given an earthquake. The source of Vs30 data was the USGS (Allen and Wald 2007), Figure 3-56, with example data for the Los Angeles region shown in Figure 3-57.

However, the Allen and Wald Vs30 data are actually based on regression with slope as they discuss and which can be seen in Figure 3-58 and Table 3-11. Vs30 data were assigned to each pipe centroid and regressed against SRTM slope, Figure 3-58 and Figure 3-59, again confirming the correlation of Vs30 with slope (note that in one figure the slope is measured as rise over run, while in the other it is in terms of degrees from horizontal).

Because Vs30 and slope are correlated, particularly in a relatively linear relationship, inclusion of both covariates in multivariate regression will result in collinearity, which is to be avoided. We therefore drop Vs30 as an independent covariate and, for similar reasons, also drop the geologic categorization, and employ only slope as a characterization of soil type for this study's analyses. This discussion has been presented in order to clarify why only slope is employed as a characterization of soil and the geologic environment.

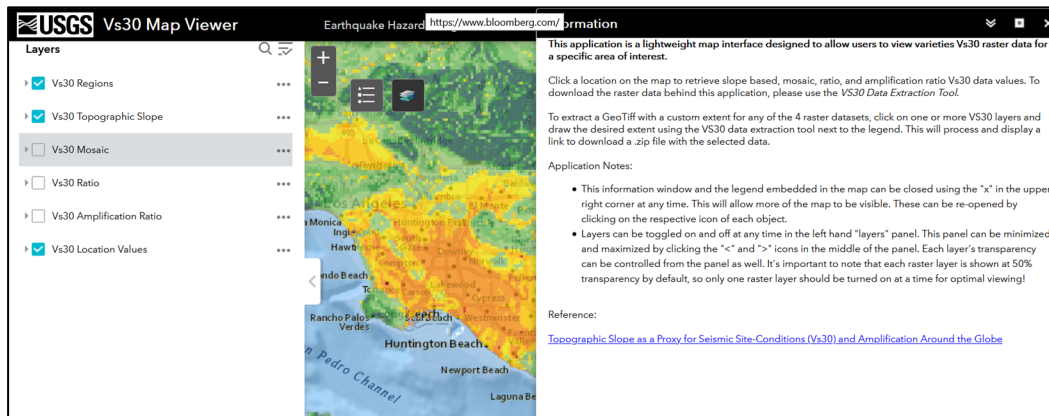


Figure 3-54. USGS Vs30 Map Viewer.

Source: USGS n.d.a.

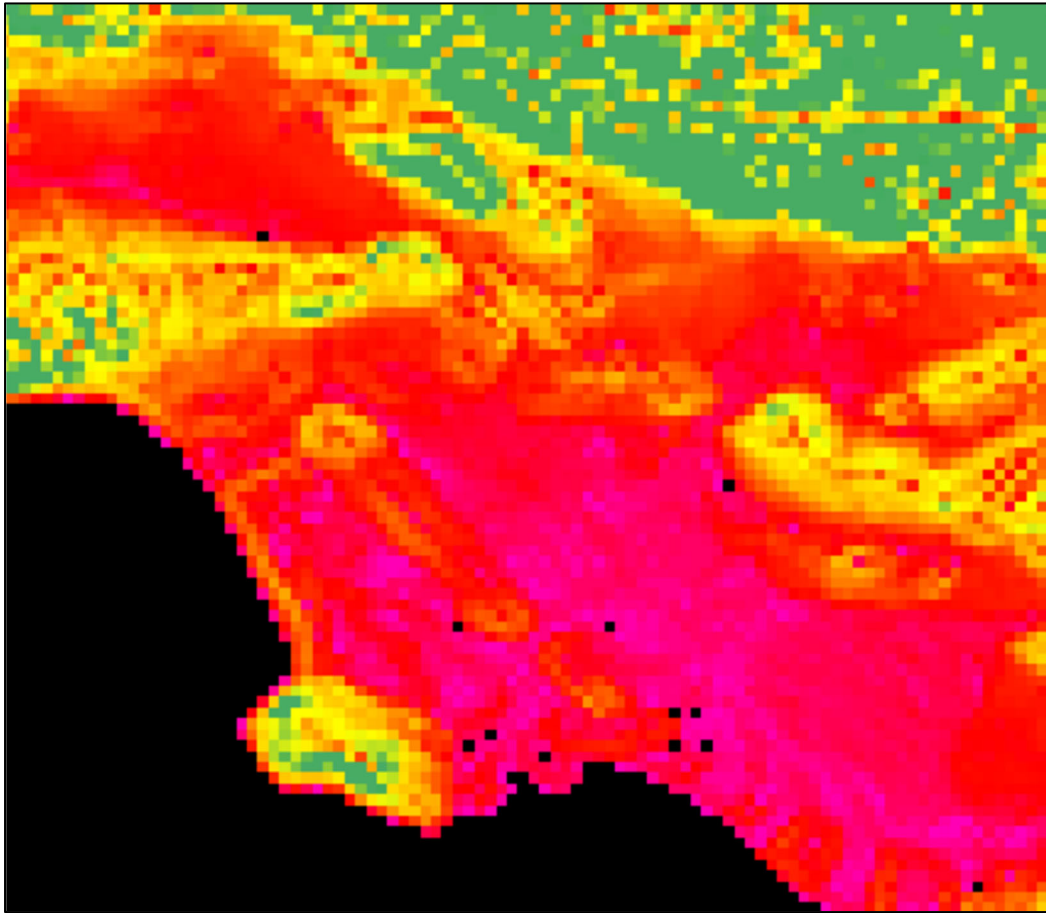


Figure 3-55. Los Angeles Vs30 (Upper 30m Shear Wave Velocity) is a Measure of Soil Stiffness and a Reasonable Proxy for Several Other Soil Proxies, Such as Corrosivity.

Table 3-11. Summary of Slope Ranges for Subdivided NEHRP Vs30 Categories.
 Source: Allen and Wald 2007

Class	V_s^{30} range (m/s)	Slope range (m/m) – (active tectonic)	Slope range (m/m) – (stable continent)
E	<180	<1.0E-4	<2.0E-5
	180–240	1.0E-4–2.2E-3	2.0E-5–2.0E-3
D	240–300	2.2E-3–6.3E-3	2.0E-3–4.0E-3
	300–360	6.3E-3–0.018	4.0E-3–7.2E-3
	360–490	0.018–0.050	7.2E-3–0.013
C	490–620	0.050–0.10	0.013–0.018
	620–760	0.10–0.138	0.018–0.025
B	>760	>0.138	>0.025

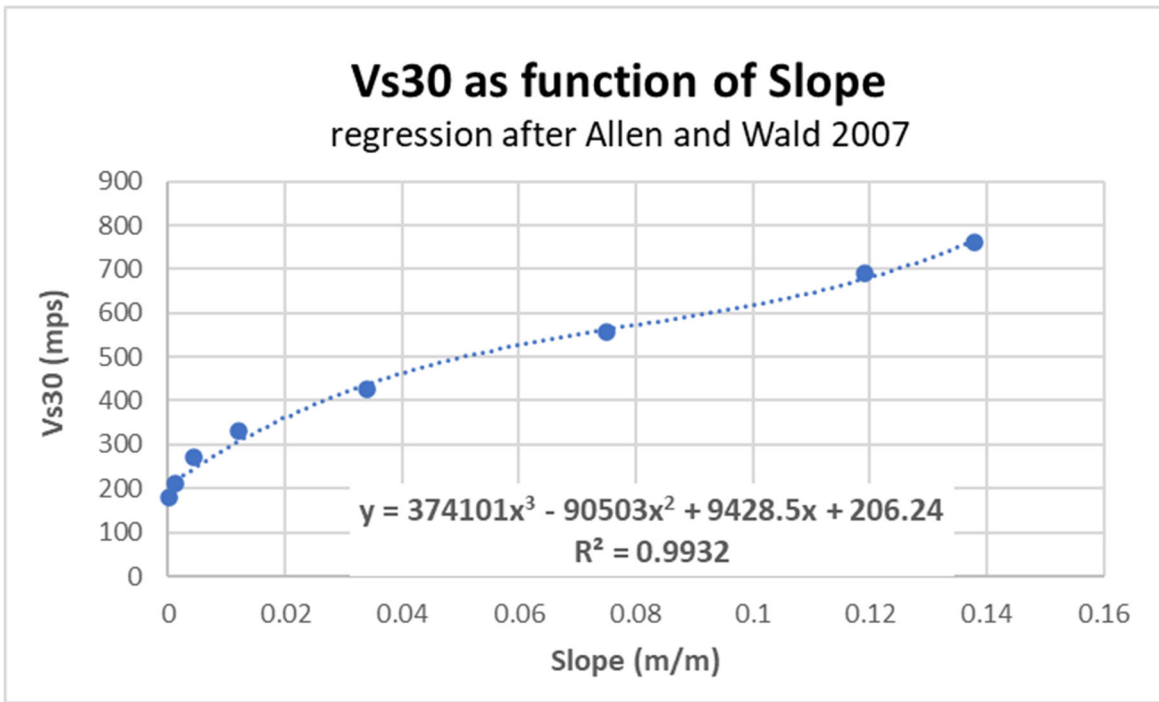


Figure 3-56. Correlation of Vs30 with Slope Back-Calculated from Data in Table 3-11. Note Slope Here Is Measured in Terms of Rise over Run (i.e., Tangent) Rather Than in Degrees.

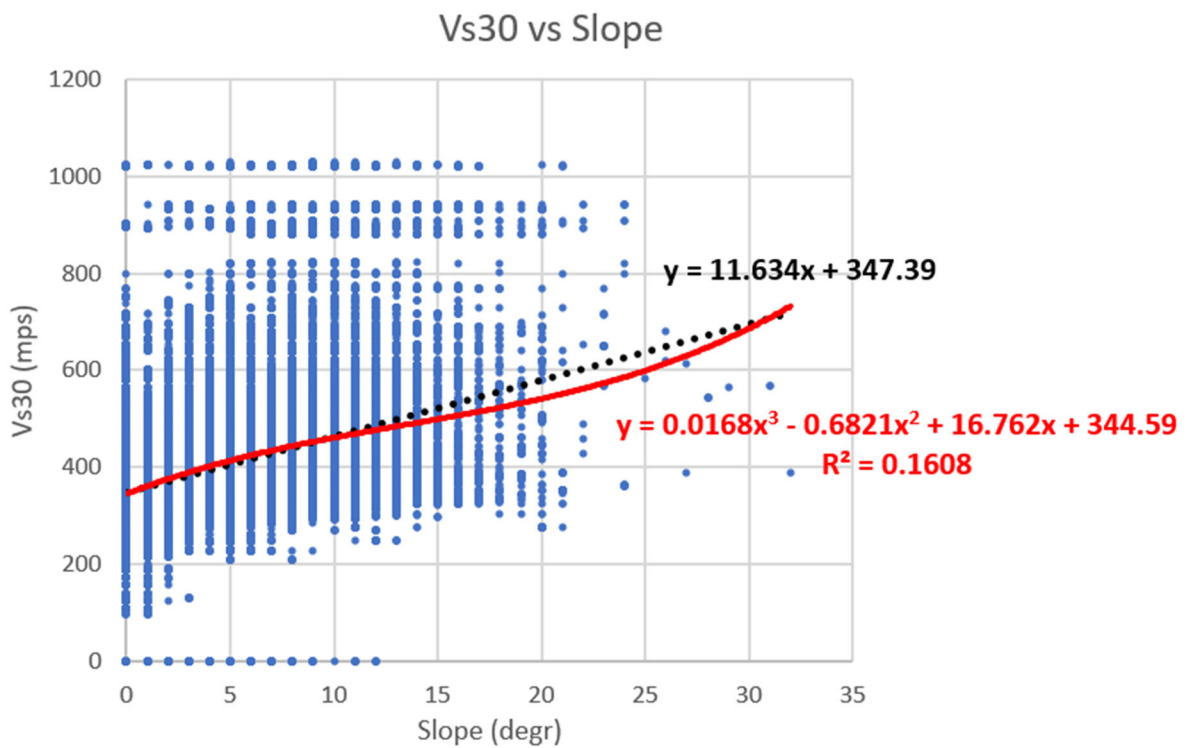


Figure 3-57. Los Angeles Pipe Centroid Vs30 (Upper 30m Shear Wave Velocity) versus Slope (Degrees of Inclination).

3.3.6.4 Temperature

Cold temperatures are known to correlate with increased numbers of pipe breaks (Rajani, Kleiner and Sink 2012) so three measures of temperature were assigned to each pipe:

- **Tmin:** the minimum temperature (F°) recorded in Los Angeles² on the day of the pipe repair.
- **Thilo:** the difference between the high and low temperature recorded in Los Angeles on the day of the pipe repair.
- **OneDayBefore:** the difference in low temperatures recorded in Los Angeles on the day of the pipe repair and the day before.

Temperature data is available from NOAA's NCEI, Figure 3-60 and was the record of daily weather recorded at USC (University of Southern California) station for the period 1950-2019, Figure 3-61 and Figure 3-62.

² As noted above, this discussion uses Los Angeles as the example of data processing – where “Los Angeles” is referred to, similar analyses were performed for all other datasets.

Climate Data Online

Climate Data Online (CDO) provides free access to NCDC's archive of global historical weather and climate data in addition to station history information. These data include quality controlled daily, monthly, seasonal, and yearly measurements of temperature, precipitation, wind, and degree days as well as radar data and 30-year Climate Normals. Customers can also order most of these data as certified hard copies for legal use.




- 
[Browse Datasets](#)
- 
[Certify Orders](#)
- 
[Check Status](#)
- 
[Find Help](#)

Figure 3-58. NOAA NCEI Data Website.
 Source: NOAA n.d.

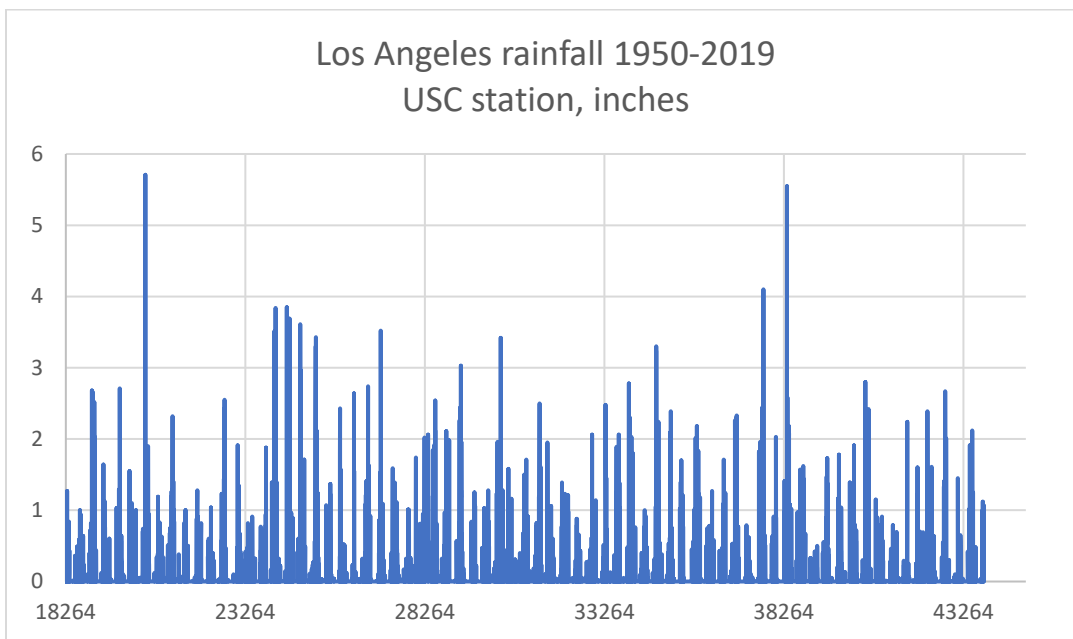


Figure 3-59. Los Angeles Daily Rainfall Data 1950-2019.

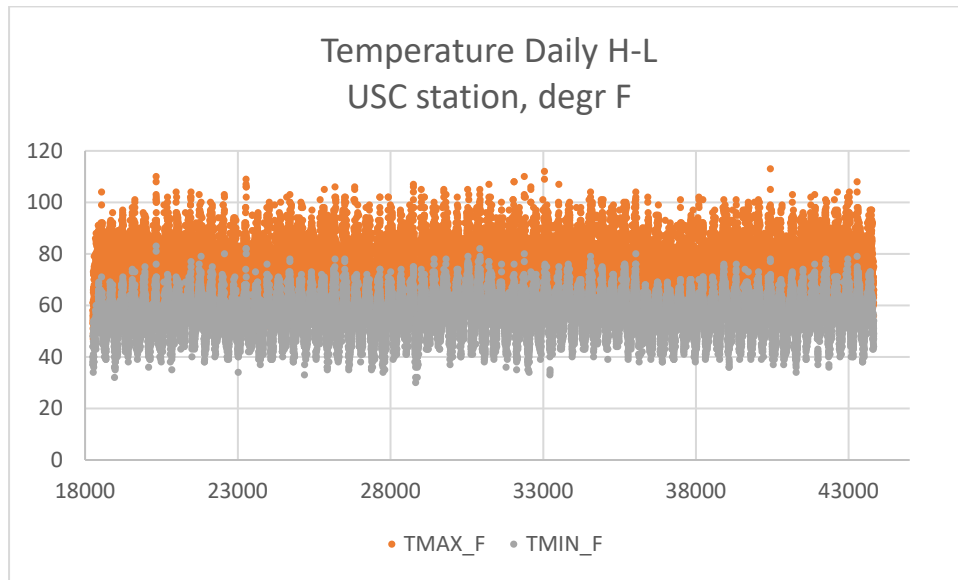


Figure 3-60. Los Angeles High-Low Temperature Data 1950-2019.

To examine the effect of temperature, we compare the minimum temperature on the day of repairs for over 16,000 repairs to the LADWP system during 1997-2017, Figure 3-63, and compare them with the seventy-year record of daily minimum temperatures, Figure 3-64. The minimum daily temperatures on the day of repairs have virtually the same distribution as the overall weather, from which we can infer that daily minimum temperature is not a significant factor for pipe repairs, at least in Los Angeles. That is, if daily minimum temperature were a factor for pipe repairs, the daily minimum temperature of the repair dataset would differ significantly (i.e., be lower) than the average for all days – it doesn't, so daily minimum temperature is a factor for pipe repairs.

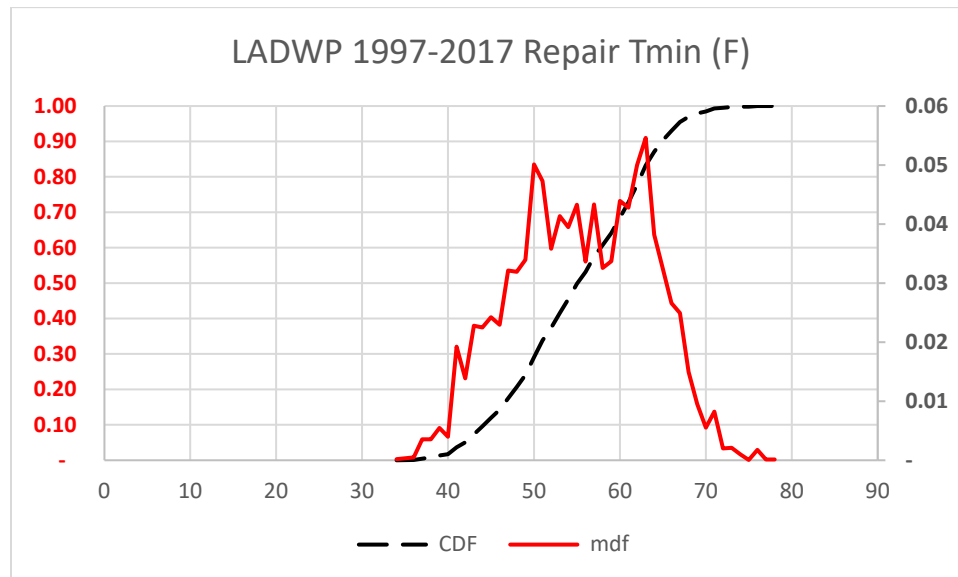


Figure 3-61. LADWP Minimum Temperature Distribution on Day of Repairs (1997-2017).

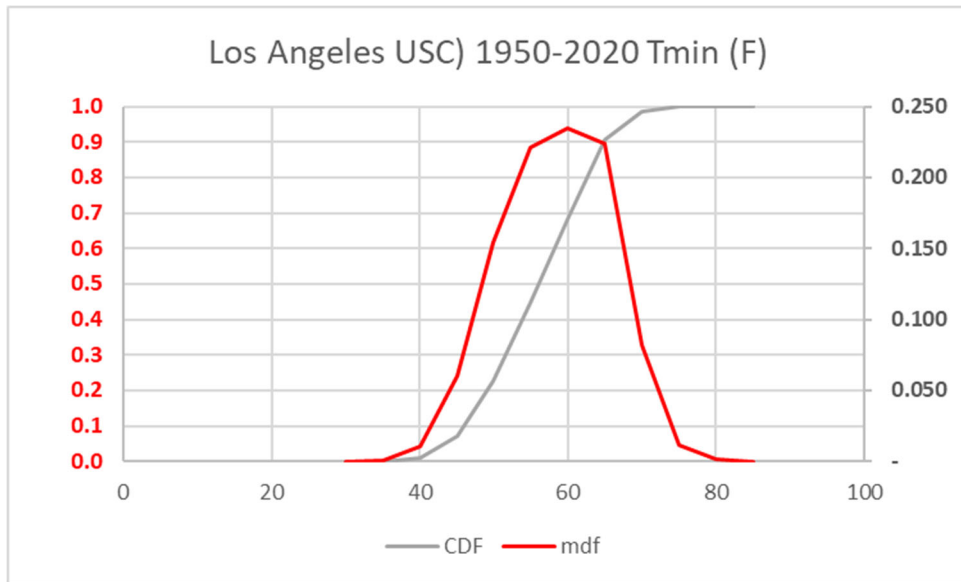


Figure 3-62. Los Angeles Daily Minimum Temperature Distribution 1950-2020.

3.3.6.5 Stress Events

Lastly, since the effect of earthquake is the key covariate of interest, the distribution of Peak Ground Velocity (PGV, measured in kine, that is, cm/s) was obtained from the USGS ShakeMap archive for the 1994 Mw 6.9 Northridge earthquake, Figure 3-65, which affected the LADWP system, and for the 1989 Mw 7.1 Loma Prieta earthquake, Figure 3-66, which affected the SFPUC and EBMUD pipe networks. PGV values for these events were assigned to each affected pipe segment.

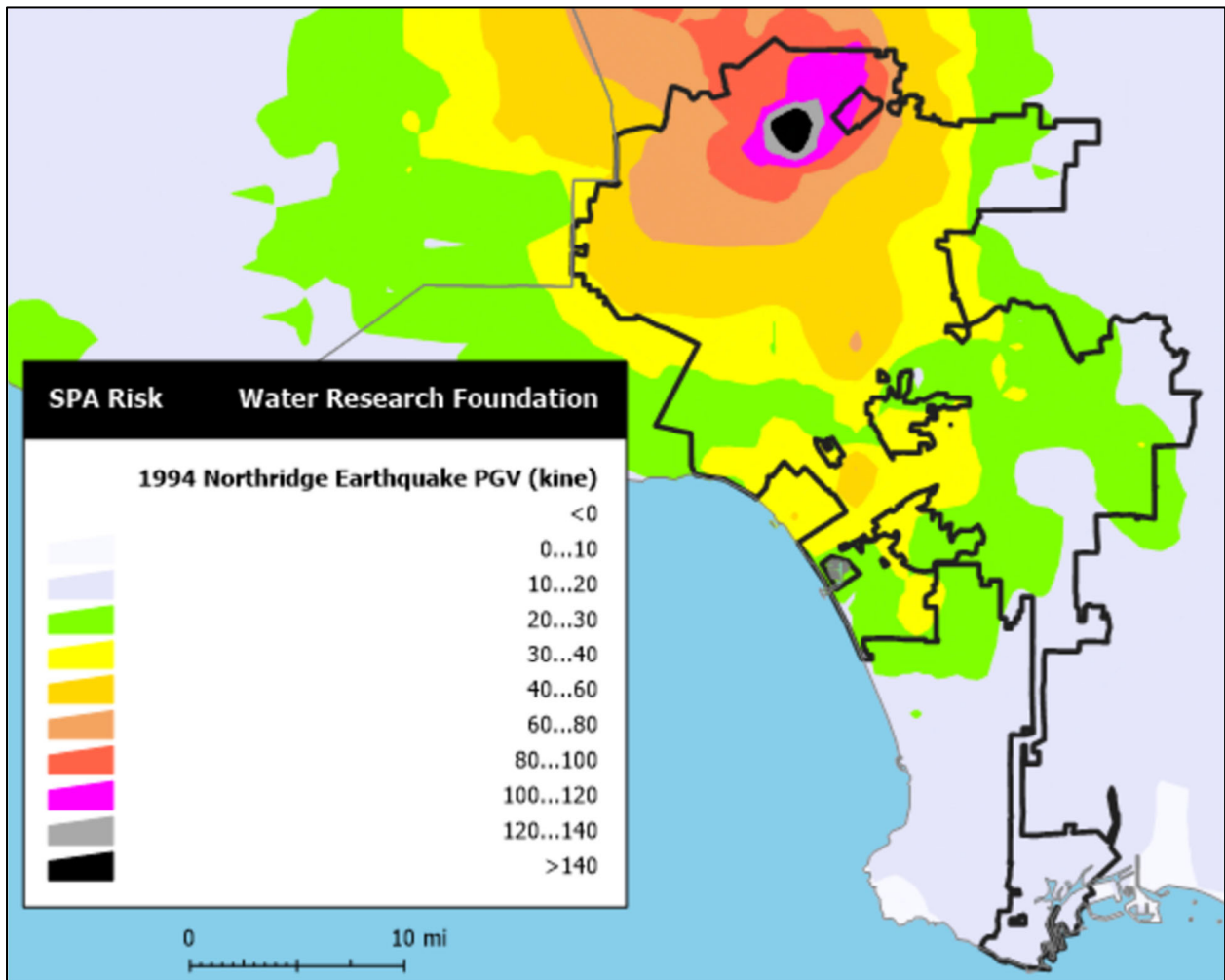


Figure 3-63. 1994 Northridge Earthquake Peak Ground Velocity (PGV) Distribution.
Data source: USGS 2020

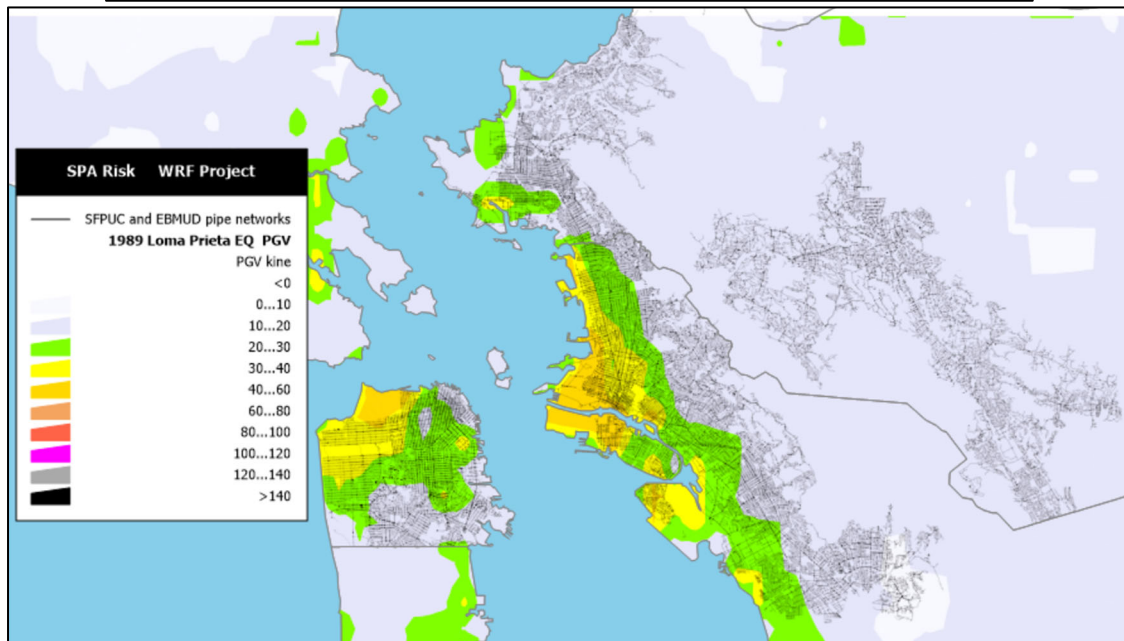
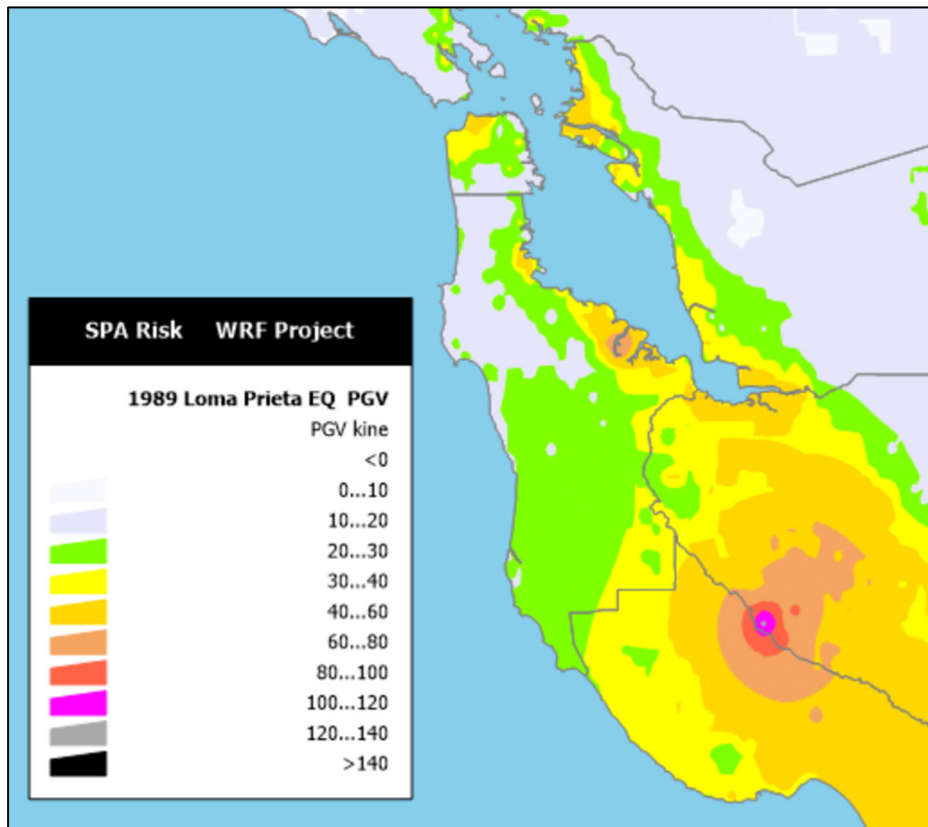


Figure 3-64. 1989 Loma Prieta Earthquake Peak Ground Velocity (PGV) Distribution.

3.4 Datasets for Analysis

This section summarizes the datasets as finally processed for analysis.

3.4.1 LADWP

The LADWP dataset consists of 279,799 GIS pipe segments totaling 39.6 million ft in length and ranging from 0 to 4,500 ft in length. It should be noted that a GIS pipe segment is not an actual pipe segment but rather is an artifact of data entry, whereas an actual CI or DI pipe segment will typically be perhaps 18 to 20 ft. in length.

A histogram of the dataset number of GIS pipe segments by material type is shown in Figure 3-67 and total length in feet by material type in Figure 3-68, both distributions being similar and showing the dataset is dominated by CI type pipe. Figure 3-69 shows a breakdown of repairs by year of occurrence. Figure 3-70 is a histogram of LADWP repairs by material type showing even greater dominance by CI. Figure 3-72 is actual leak rates per unit pipe length vs. materials. Note these are not annual rates, but rather for the entire 20 yr period (1997-2017) – the annual rate for CI for example would be approximately $0.16/20 = 0.008$ per year per foot of pipe. Since “other” material type of pipe, being a heterogenous mix of copper, HDPE, concrete, PVC etc., was a relatively small fraction of the total dataset, it was omitted from further consideration.

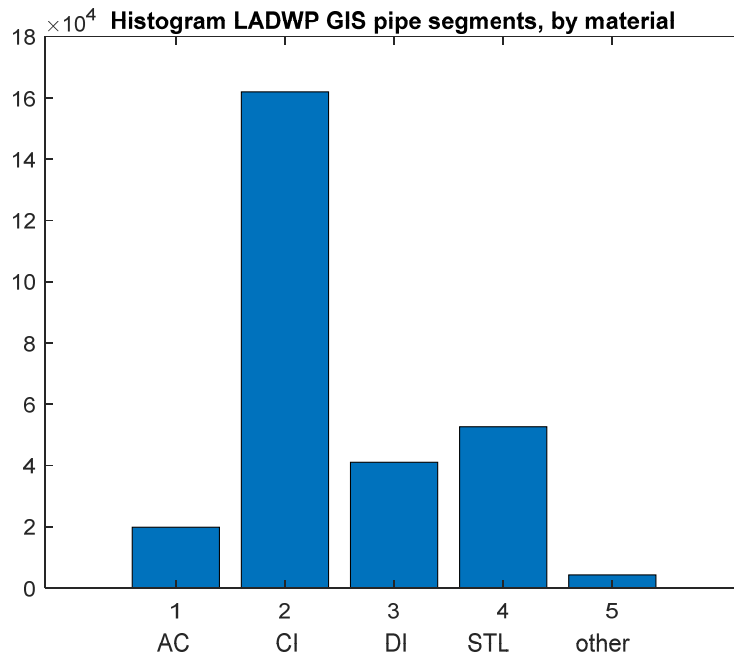


Figure 3-65. Histogram of LADWP GIS Pipe Segments by Material Type, LADWP Data.

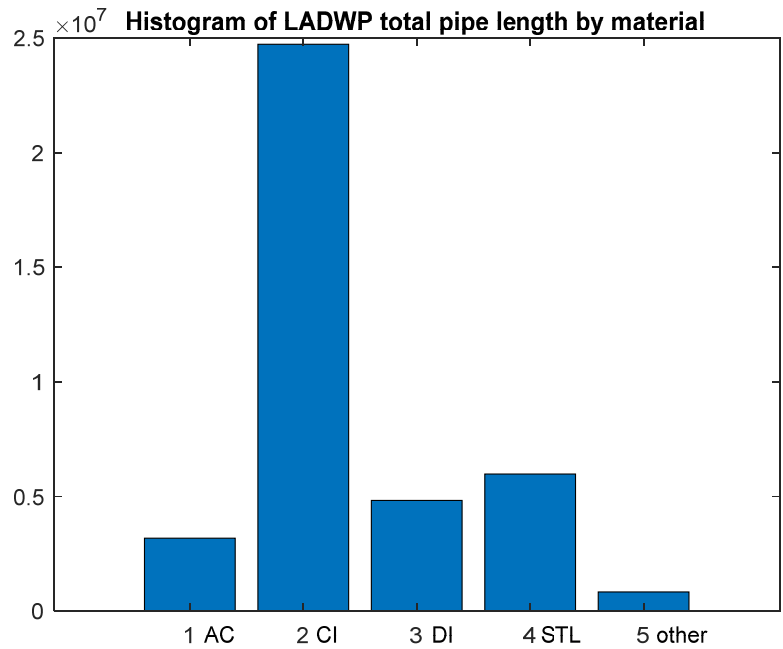


Figure 3-66. Histogram of LADWP GIS Total Pipe Length by Material Type, LADWP Data.

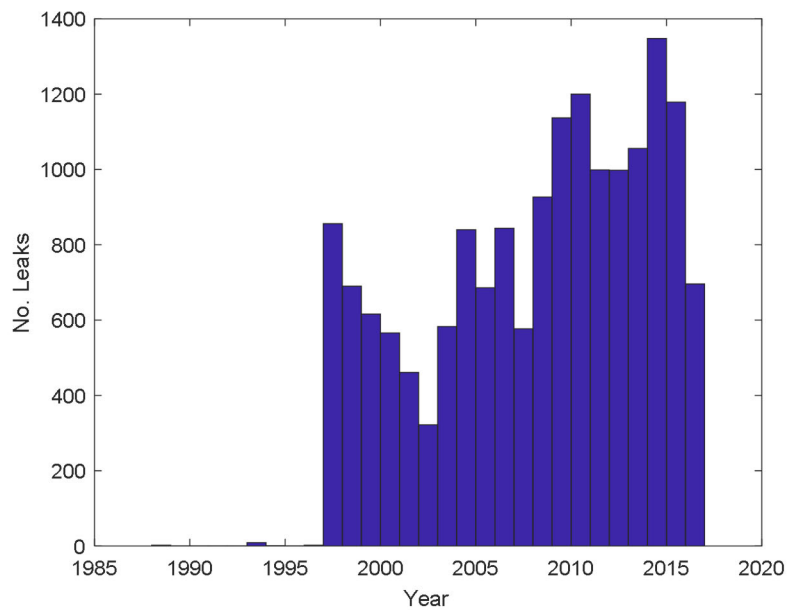


Figure 3-67. Histogram of LADWP GIS Repairs ("Leaks") by Year of Occurrence.

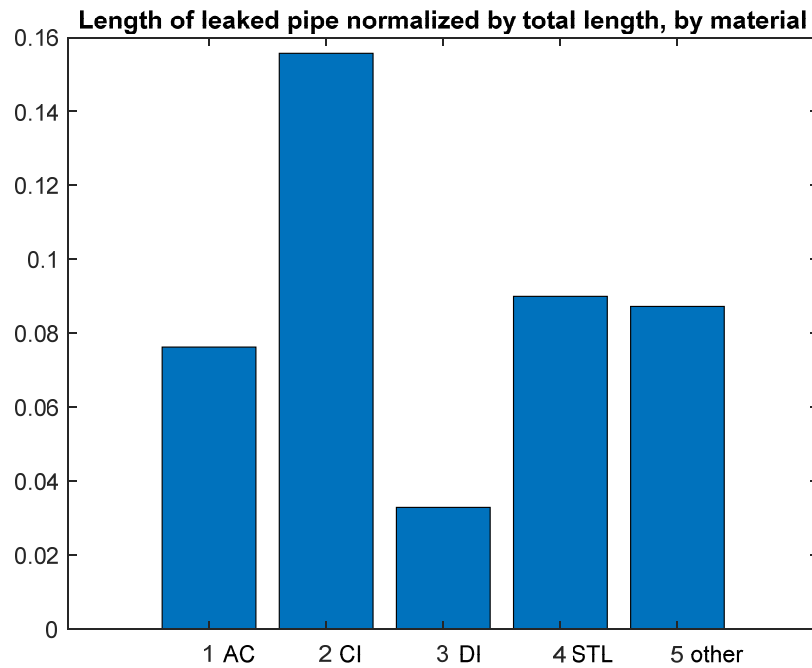


Figure 3-68. Histogram of Total Length of LADWP Repaired GIS Pipe Segments Normalized by Length of GIS Pipe Segments by Material Type.

3.4.2 SPU

This section presents some preliminary characterizations of the SPU data. Figure 3-71 is a plot of the raw SPU repair data by year of repair, which clearly shows non-homogeneity. Figure 3-72 is a histogram of number of SPU repairs by pipe material. Note y axis is logarithmic. Plot shows that about 81% of the SPU system by length is Cast Iron.

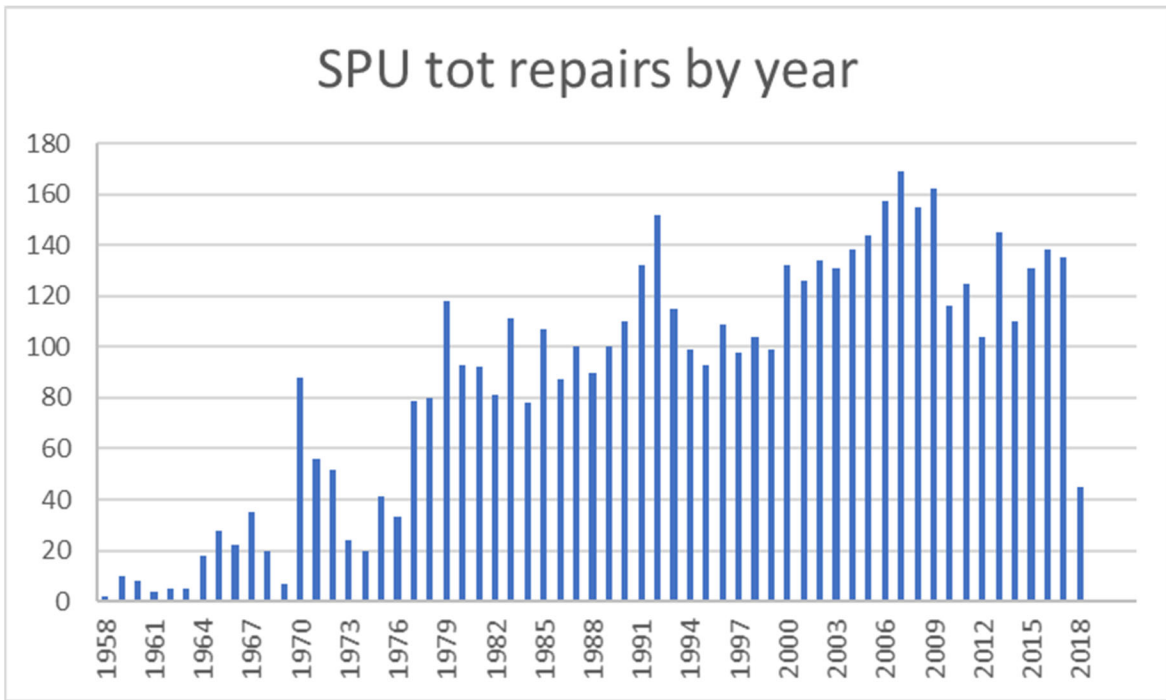


Figure 3-69. Plot of Number of SPU Repairs by Year – The Data Clearly Are Non-homogenous.

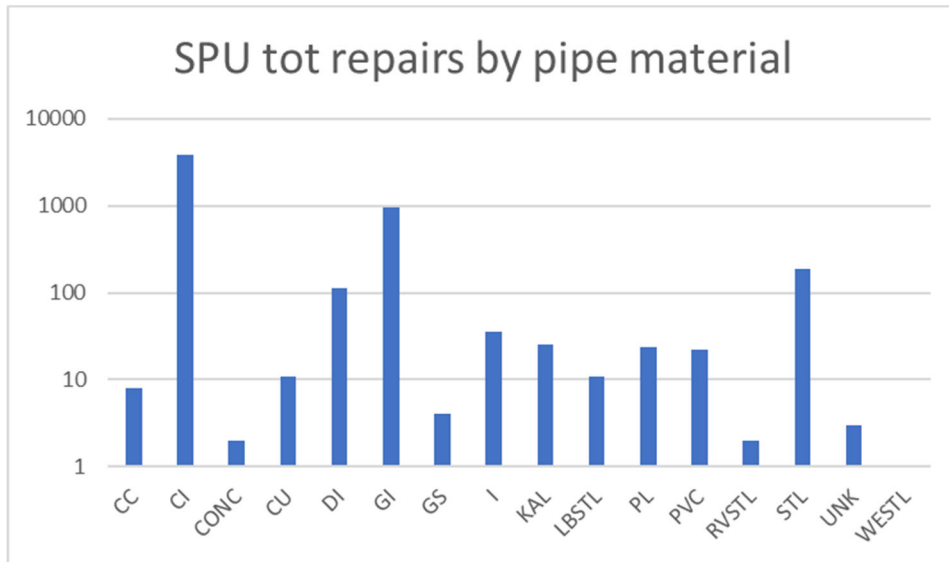


Figure 3-70. Histogram of Number of SPU Repairs by Pipe Material. Note Y Axis Is Logarithmic. Plot Shows That about 81% of the SPU System by Length Is Cast Iron, SPU Data.

3.4.3 SFPUC

The SFPUC dataset consists of 55,758 GIS pipe segments totaling 1,243 miles in length and ranging from 0 to 4,500 ft in length, Table 3-12. A histogram of the dataset number of GIS pipe segments by material type is shown in Figure 3-73.

Table 3-12. SFPUC Pipe Segments and Length by Material.

Material	No. GIS segments	Total Length (miles)
CI	26476	765.0
CU	56	0.7
DI	26229	358.7
LN	1246	48.5
ST	1732	70.1
TR	7	0.2
UN	12	0.2
Total	55758	1,243.4

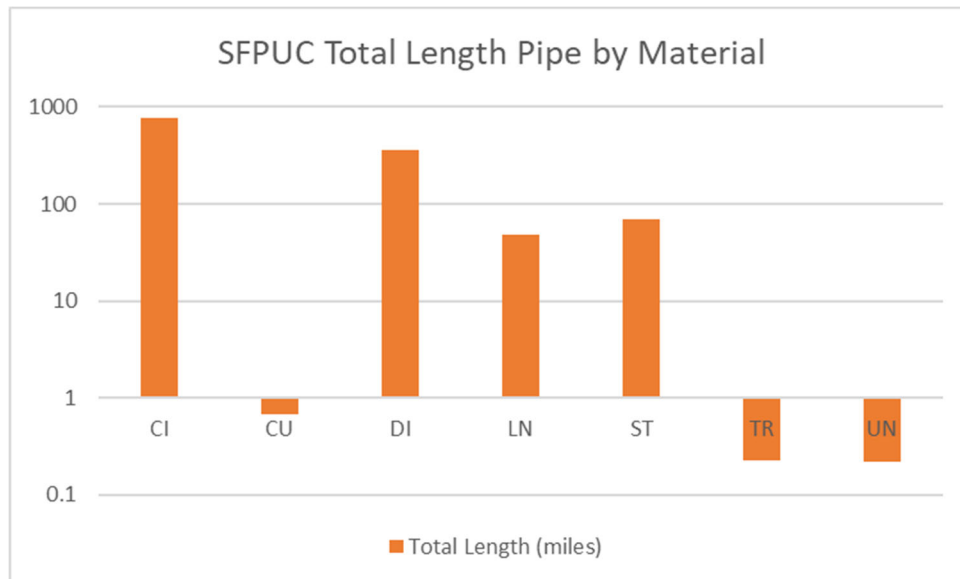


Figure 3-71. SFPUC Pipe Length by Material.

3.4.4 EBMUD

The EBMUD dataset consists of 98,637 GIS pipe segments totaling 3,833 miles in length and ranging from 0 to 4,500 ft in length, Table 3-13. A histogram of the dataset number of GIS pipe segments by material type is shown in Figure 3-74.

Table 3-13. EBMUD Pipe Segments and Length by Material.

Material	No. GIS segments	Total Length (miles)
AC	24,432	1,131
CI	32,826	1,285
DI	43	2
HDPE	220	11
other	154	4
PVC	8,985	398
STL	31,977	1,001
Total	98,637	3,833

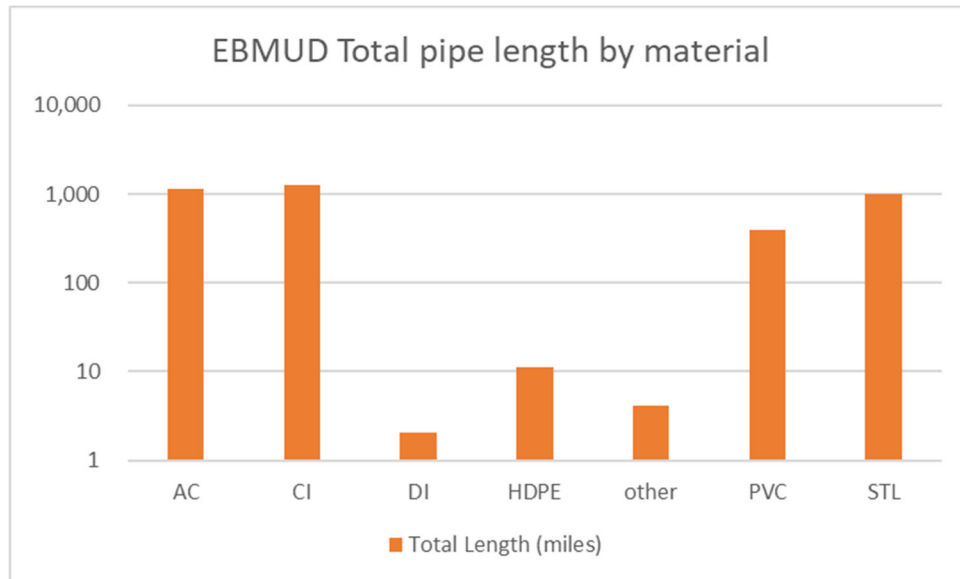


Figure 3-72. EBMUD Pipe Length by Material.

3.4.5 PWB

The PWB dataset consists of 117,688 GIS pipe segments totaling 2,248 miles in length, Table 3-14. A histogram of the dataset number of GIS pipe segments by material type is shown in Figure 3-75.

Table 3-14. PWB Pipe Segments and Length by Material.

Material	No. GIS segments	Total Length (miles)
AC	44	1
CC	337	25
CI	63279	1,379
DI	48245	705
HDPE	82	2
other	1905	11
PVC	151	9
STL	3645	116
Total	117688	2,248

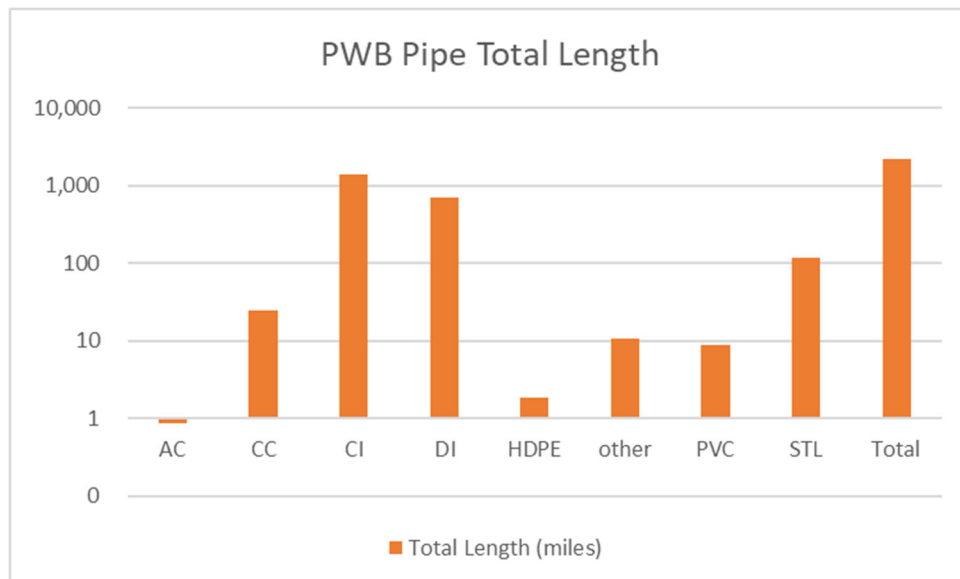


Figure 3-73. PWB Pipe Length by Material.

3.4.6 Summary of Datasets

Five datasets were the result of the above processing, each consisting of 17 fields with the exception of the LADWP dataset which has two additional fields due to the scanned maps, as explained in Table 3-13. Each utility dataset was saved as a comma-separated variable (CSV) file with name xxDataset.csv where xx = la, sf, eb, pwb or spu, and consisted of the fields shown in Table 3-15. For all records, if data is missing or not applicable, -999 is listed.

Table 3-16 summarizes the repair record data for the five utilities, from which it can be seen that the data is for more than 16,000 miles of buried water distribution pipe composed of more than 600,000 GIS segments that required more than 64,000 repairs. The period during which those repairs occurred varied for each utility, but the record period averaged about 34 years. However, this time period is a simple average, not weighted by system size, and is not reflective of the fact that some of the records are only partial, as was seen in the various repair timelines presented above. Even so, a simple statistic for the full data set is that collectively these systems averaged 11.2 repairs per 100 miles per year, which agrees well with a survey of 308 water utilities which found that *“Between 2012 and this 2018 report, overall water main break rates increased by 27% from 11.0 to 14.0 breaks/(100 miles)/year”* (Folkman 2018). and Figure 3-76 provide repair timelines for all five datasets. The LADWP system has a total pipe length approximately equal to the other four datasets combined, and more than twice the number of repairs. When normalized for system pipe length and duration of record, the LADWP system still has a somewhat higher repair rate than the other systems, Table 3-17.

This repair data was supplemented by three types of geophysical covariate data: (1) slope and slope aspect, which are causally related to mass wasting (ie, down slope movement) and serves as a reasonable proxy for settlement and other types of chronic ground movement as well as corrosion; (2) temperature, and (3) PGV, for the stress event. Temperature covariates are measured in three ways: peak on the day of the repair, temperature range on that day, and differential in daily low from that day to the day before.

Table 3-15. Repair Record Data Fields.

No	field	comment	example
1	laNo	a sequential number for each record (GIS pipe segment)	16
2	laFID	either the Facility ID from the utility, or the Manifold GIS ID number of that pipe segment	3323092
3	pDiam	pipe diameter (inches)	8
4	pipeLft	length of pipe segment, in ft	53.2079
5	pMatl	pMaterial, typically CI, DI, AC, STL or other - in a couple of the tabs, more detail such as HDPE, PVC etc	CI
6	pipeYr	year of pipe installation	1962
7	pipeAge	difference between last year of leak record (diff for each dataset) and year of pipe installation,	55
8	leakYr	year of the leak - we also have day and month for all datasets except LA 1975-1997, but d/m not included in final dataset	2008
9	repairYr	this field exists ONLY for LA , and is the year of repairs between 1975-1997, which was obtained from scanned maps	-999
10	repairYrProb	this field exists ONLY for LA , and is 0 if no problem and 1 is the data was problematic - typ. problematic data will not be used	0
11	PGVkine	PGV in cm/s at centroid of pipe, due to 1989 Loma Prieta, 1994 Northridge or 2001 Nisqually events	18
12	Slope_ror	slope (rise over run) at centroid of pipe as determined from USGS 3DEP 10m resolution data	0.3
13	Aspect	aspect of the slope as determined from USGS 3DEP 10m resolution data, where aspect is -180<= degrees <= 180 from N	91.9
14	Brg	bearing of pipe's longitudinal axis in degrees from N (ie, azimuth, 0 to 360)	34.8
15	SL	Slope parallel to pipe's longitudinal axis, calculated as $SL = \text{Slope_ror} * \cos(\text{Brg} - \text{Aspect})$	0.16
16	ST	Slope transverse to pipe's longitudinal axis, calculated as $SL = \text{Slope_ror} * \sin(\text{Brg} - \text{Aspect})$	-0.25
17	TMIN	minimum temperature (F) day of repair, as determined from NOAA NCEI records for closest station	66
18	dailyDiff	diff bet min and max temperatures (F) on day of repair	19
19	oneDayTminDiff	diff bet min temp (F) on day of repair, and min temp on day before day of repair	-1

Table 3-16. Summary of Repair Record Data.

Utility	Tot. Length		No. Segments	Leak Record		No. Repairs	Repairs per year	
	miles	km		Period	no. Year		per 100 miles	per 100 km
LADWP	7,512.5	12,093.3	280,256	1977-2017	40	46,621	15.5	9.6
SFPUC	1,243.4	2,001.6	55,763	1980-2016	36	3,325	7.4	4.6
SPU	1,409.1	2,268.4	66,652	1958-2018	60	3,364	4.0	2.5
PWB	2,247.6	3,618.1	117,688	2004-2015	11	1,337	5.4	3.4
EBMUD	3,832.6	6,169.6	98,637	1990-2015	25	9,489	9.9	6.2
sum	16,245.3	26,151.0	618,996			64,136		
average					34.4		11.2	6.9

Table 3-17. No. Repairs per Year per Agency.

Year	LA	SF	PWB	EB	SPU
1958	1	1	1	1	1
1959	0				8
1960	0				4
1961	0				1
1962	0				2
1963	0				3
1964	0				8
1965	0				19
1966	0				11
1967	0				24
1968	0				12
1969	0				5
1970	0				28
1971	0				29
1972	0				22
1973	0				10
1974	0				12
1975	1333.2				13
1976	1333.2				15
1977	1333.2				32
1978	1333.2				36
1979	1333.2				56
1980	1329	129			40
1981	1329	132			52
1982	1329	161			48
1983	1329	114			58
1984	1329	132			32
1985	935.6	107			55
1986	935.6	105			48
1987	935.6	117			59
1988	935.6	140			45
1989	935.6	91			53
1990	1932	144		281	50
1991	1932	84		227	61

Year	LA	SF	PWB	EB	SPU
1992	1932	75		229	79
1993	1932	113		232	68
1994	1932	79		226	49
1995	908	54		208	65
1996	908	37		208	61
1997	908	44		500	68
1998	471	61		449	70
1999	467	56		390	82
2000	400	58		378	108
2001	376	65		462	96
2002	342	65		376	81
2003	222	76		420	94
2004	371	86	22	425	95
2005	583	49	93	350	111
2006	498	44	131	432	119
2007	566	70	133	453	132
2008	423	95	163	519	125
2009	676	118	135	470	128
2010	875	74	66	330	91
2011	873	80	142	336	86
2012	774	81	142	303	73
2013	717	102	138	444	104
2014	782	83	163	435	69
2015	1027	115	9	406	101
2016	878	89			112
2017	531				107
2018					38
Tot No. Repairs	42226	3326	1338	9490	3364
Tot Length Pipe (miles)	7512	1243	2247	3832	1409
no. Years	40	36	11	25	60
No repairs/yr/mile	0.14	0.07	0.05	0.10	0.04

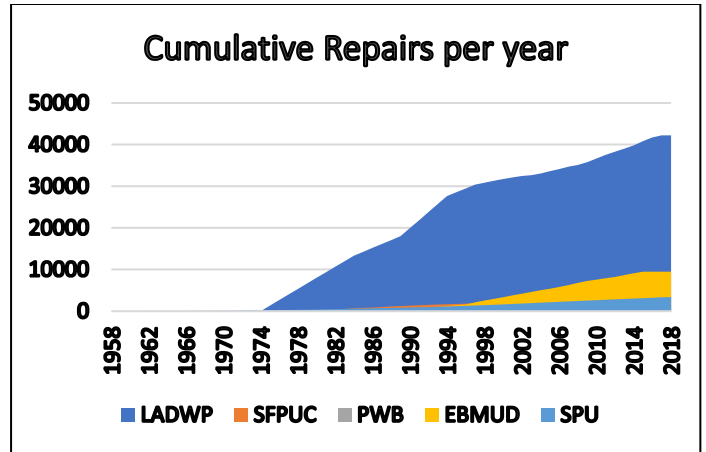
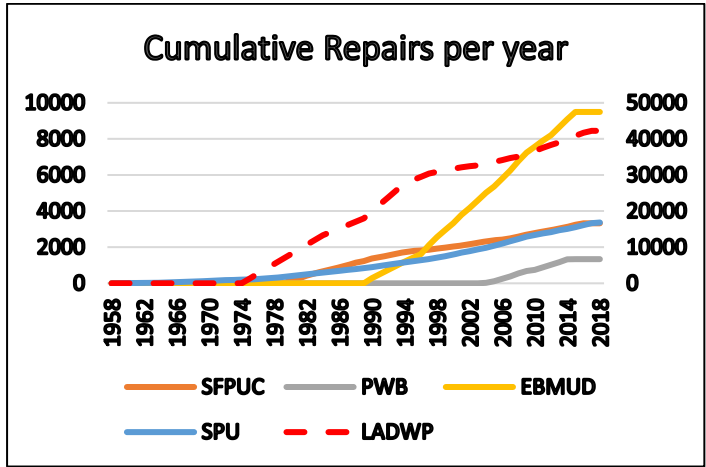
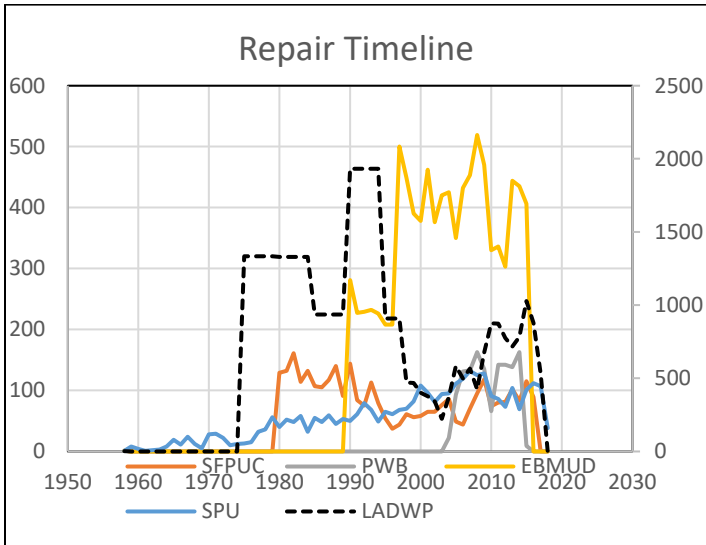


Figure 3-74. Timeline and Cumulative Repairs per Year, Five Agencies.

3.5 Completeness

A key issue for the datasets is that of *completeness* – that is, over what period is the data complete, with negligible missing data. This issue is fundamental for statistical analysis and many approaches exist to assess data completeness. Table 3-18 shows the number of repairs per year for the LADWP digital dataset (i.e., not including the scanned maps data). It is readily apparent by inspection that not all repairs had been yet recorded for 2017, and that from about 1999 to 2008 probably not all repairs are in the record (alternatively, 2010-2016 were quite bad years for repairs, which is unlikely). The median and standard deviation for the years 1998-2016 (unshaded years) are shown in the table to be 848 and 281 repairs, respectively. Assuming a normal distribution the upper plot in Figure 3-77 shows that 1,000 or more repairs should occur in about 1 in 3 years, and 1,200 in about 1 in 10 years, while if only the years 2010-2016 are employed, it can be seen that the probability of less than 900 repairs is negligible. So, the question exists – which is more representative 1998-2016, or 2010-2016?

To answer that question, we employ a method originally developed for application in seismology (Stepp 1972) which is based on assuming the repair sequence can be modeled as a Poisson distribution. Plotting the standard deviation of the estimate of the mean vs. $\log T$ for any period (where T is the period prior to the last year of the record) it can be shown that the portion of the record with slope $T^{-1/2}$ can be considered temporally homogeneous. Figure 3-78 plots this approach for data from 1994 to 2014, from which it can be seen that the period from about 2013 to 2006 is complete, and incomplete prior to then, which can also be generally seen by inspection of the data in Table 3-18.

Table 3-18. LADWP No. Repairs per Year, 1988-2017.

Yr	No Repairs
2017	699
2016	1180
2015	1350
2014	1061
2013	1003
2012	1001
2011	1200
2010	1139
2009	932
2008	579
2007	848
2006	690
2005	846
2004	584
2003	322
2002	462
2001	567
2000	617
1999	692
1998	859
1997	2
1995	1
1994	9
1988	2
Median 1998-2016	281
St. Dev. 1998-2016	848

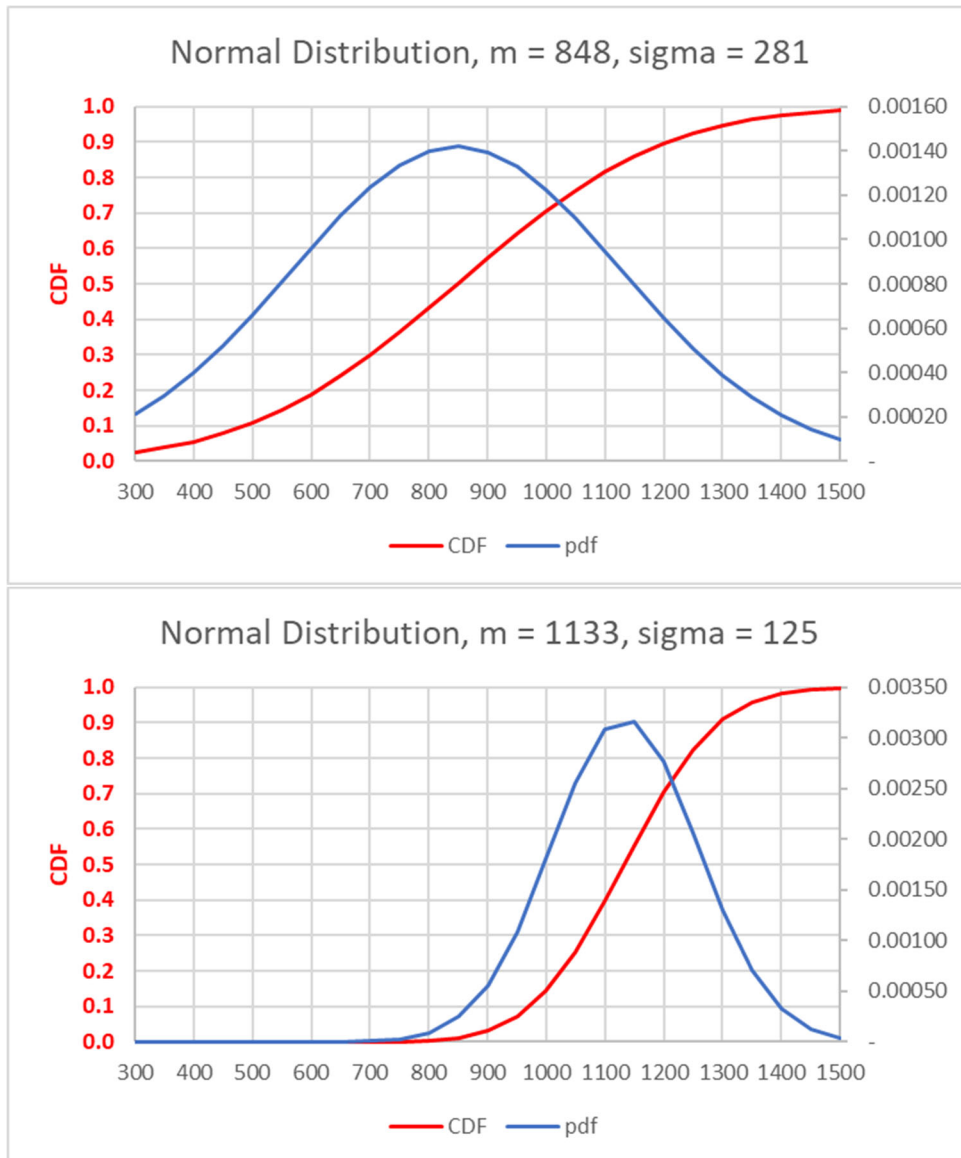


Figure 3-75. Normal Distribution Given (Top) Mean = 848 Repairs and Standard Deviation = 281 Repairs Corresponding to Years 1996-2016 and (Bottom) Mean = 1133 and St. Dev. = 125 Corresponding to Years 2010-2016.

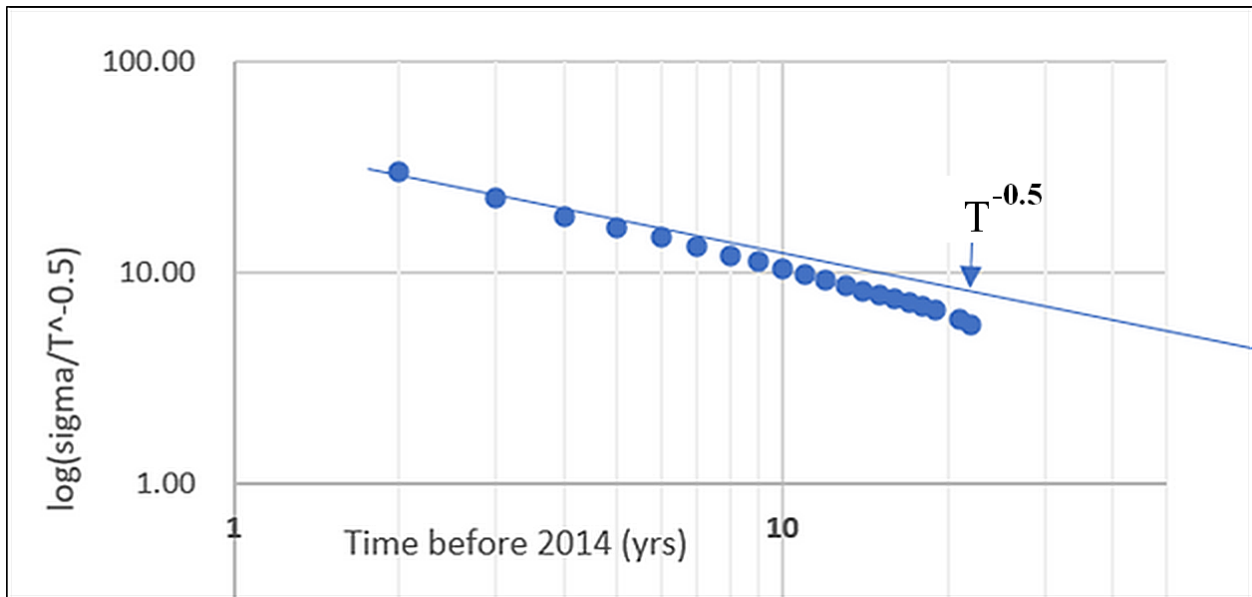


Figure 3-76. Examination of Data Completeness, Showing Relative Completeness for Period 2-8 Years before 2014 (i.e., 2013-2006) and Drop Off in Repairs Prior to Then.

However, examination of Figure 3-26 shows that including the scanned map data for LADWP represents a relatively complete 40-year period, and this period will be used as data-complete. Similar examination of comparable plots for the other agencies shows that the number of years for leak records shown in Table 3- are valid periods of completeness, with the exception of the SPU data, where we shall use 20 years rather than 60 as the period of completeness.

CHAPTER 4

Analysis

4.1 Introduction

The research hypothesis is that there is a long-term effect of stress events such as earthquake, which reduces the useful service life of buried pipe, and that such stress events play a greater role in decreasing service life than has been previously recognized. Factors affecting service life of buried pipe were discussed in Chapter 2. This chapter presents statistical analysis of data discussed in Chapter 3 to answer this question. The basic regression models employed are based on the factors discussed in Chapter 2 and are variations on Equation 4-1:

$$\begin{aligned} & \text{Leak rate / 1000 ft =} \\ & f [pDiam, material, pipeAge, A_L, PGV_kine \text{ (if subject to EQ), slope,} \\ & \quad \text{temperature}] \end{aligned} \qquad \text{Equation 4-1}$$

where A_L is the age of pipe at time of leak if it had a leak, and temperature measures are:

- -999 if no leak
- Min temp on day of leak
- (max-min) temp on day of leak
- Min temp day before – min temp day of leak

The dataset for analysis is structured as shown in Table 4-1.

Analysis is divided into two parts: regression analysis of repair rates, and survival analysis. Within the regression analysis we first analyze two datasets individually, but each taken as one block of repairs spread over a number of years. That analysis is below and is only for the LADWP and SPU datasets. The LADWP dataset is only for the years 1997-2017.

Subsequently, in the next section, datasets for all five entities, LADWP, SPU, EBMUD, PWB and SFPUC are each analyzed for annual repair frequencies, individually and in combination.

Table 4-1. Analysis Dataset Structure.

field	example
agency	LA, EB, SF, PW, SPU
pipeID	Numbering scheme, 1,2,...
pipeYr	Year pipe installed, 1927
pipeMatl	CI, DI, AC, STL, other
pipeDiam	6"
PipeL	12 ft
leakID	The agency's leak report number
leakYr	1982
leakYrInstalled	If reported, year of installation of pipe (may differ from pipeYr)
Lat / lon	of GIS object centroid
pgvKine	Pgv for major stress event (NR for LA, LP for EB and SF)
slope	7°, calc'd from USGS 3DEP 10M DEM data
pipeAge	Calc from pipeYr to yr of database
temperature	Any one of: <ul style="list-style-type: none"> • -999 if no leak • Min temp on day of leak • (max-min) temp on day of leak • Min temp day before – min temp day of leak

4.2 Regression Analysis of Repair Rates as a Whole

This section analyzes two of the data sets each as a whole for the block of years the dataset represents. The LADWP dataset is for the years 1997-2017 only – that is, the digital repair dataset. Later, that dataset is merged with the scanned map dataset so that the LADWP dataset is then analyzed on an annual frequency basis for the period 1977-2017, as are also the other datasets.

4.2.1 LADWP: Analysis of 1997-2017

The LADWP pipe record data set consists of 279,799 GIS pipe segments³ totaling 39.5 million feet in length, varying in date of installation from 1885 to 2017, with 16,609 recorded leaks for the period 2 Feb 1994 to 30 Aug 2017 (plus, inexplicably, two records from 1988). We begin with the simplest analysis.

4.2.1.1 Leak Frequency per GIS Pipe Segment as a Function of Pipe Diameter and Material

The first analysis is simply for raw leak frequency (f) per GIS pipe segment as a function of pipe diameter and material, using a linear model. Results are:

³ Note that GIS pipe segments are not physical segments of pipe but rather are individual line objects in the GIS file. For the 39.5 million ft of pipe in the data set, the 279,799 GIS segments result in an average GIS segment length of about 140 ft.

```
regress leak vs diam and matl
y=la.leak;
X=[la.pDiam,la.AC,la.CI,la.DI,la.STL];
```

regr =

Linear regression model:

$$y \sim 1 + x1 + x2 + x3 + x4 + x5$$

Estimated Coefficients:

	Estimate	SE	tStat	pValue
(Intercept)	0.099389	0.0037196	26.721	4.2781e-157
x1	-0.0016724	5.8479e-05	-28.598	1.3083e-179
x2	-0.046264	0.0040023	-11.559	6.7332e-31
x3	-0.010117	0.0036773	-2.7513	0.0059363
x4	-0.072397	0.0038093	-19.005	1.7348e-80
x5	-0.028676	0.003738	-7.6715	1.7051e-14

Number of observations: 279799, Error degrees of freedom: 279793

Root Mean Squared Error: 0.235

R-squared: 0.0124, Adjusted R-Squared: 0.0123

F-statistic vs. constant model: 700, p-value = 0

Reviewing results we see that repair frequency decreases with increasing diameter and that CI has least reduction in repair frequency, as we would expect. These results are shown Figure 4-1. Note these results and all frequencies in this section are for the 20 year dataset, and should be divided by 20 for annual frequencies.

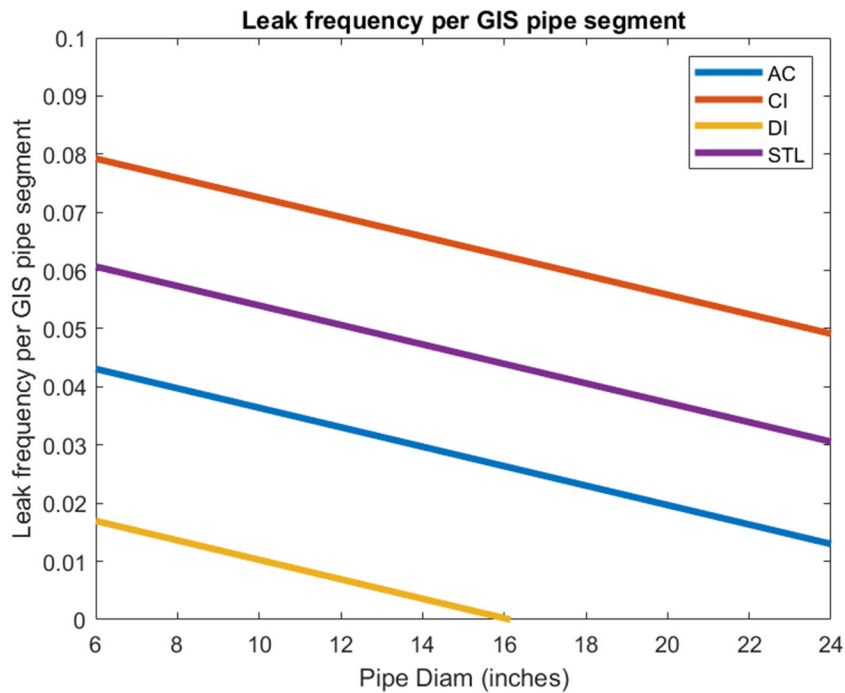


Figure 4-1. Raw Leak Frequency per GIS Pipe Segment, by Material and Diameter, LADWP Data.

4.2.1.2 Leak Frequency per Thousand Foot of Pipe as a Function of Pipe Diameter and Material

However, GIS segment is an artifact of data entry and is of limited use, so we next normalize break rates by pipe length. Results are shown in Figure 4-2.

normalize leak by pipe length and regress leak vs diam and matl

$y = y.*la.pipeLft./1000;$

$X=[la.pDiam,la.AC,la.Cl,la.Dl,la.STL];$

regr =

Linear regression model:

$y \sim 1 + x1 + x2 + x3 + x4 + x5$

Estimated Coefficients:

	Estimate	SE	tStat	pValue
(Intercept)	0.023218	0.0016841	13.787	3.1614e-43
x1	-0.00038813	2.6477e-05	-14.659	1.2341e-48
x2	-0.0084145	0.0018121	-4.6435	3.4279e-06
x3	0.0034756	0.001665	2.0875	0.036843
x4	-0.016303	0.0017247	-9.4523	3.3405e-21
x5	-0.0074829	0.0016924	-4.4214	9.8104e-06

Number of observations: 279799, Error degrees of freedom: 279793

Root Mean Squared Error: 0.106

R-squared: 0.00621, Adjusted R-Squared: 0.00619

F-statistic vs. constant model: 349, p-value = 0

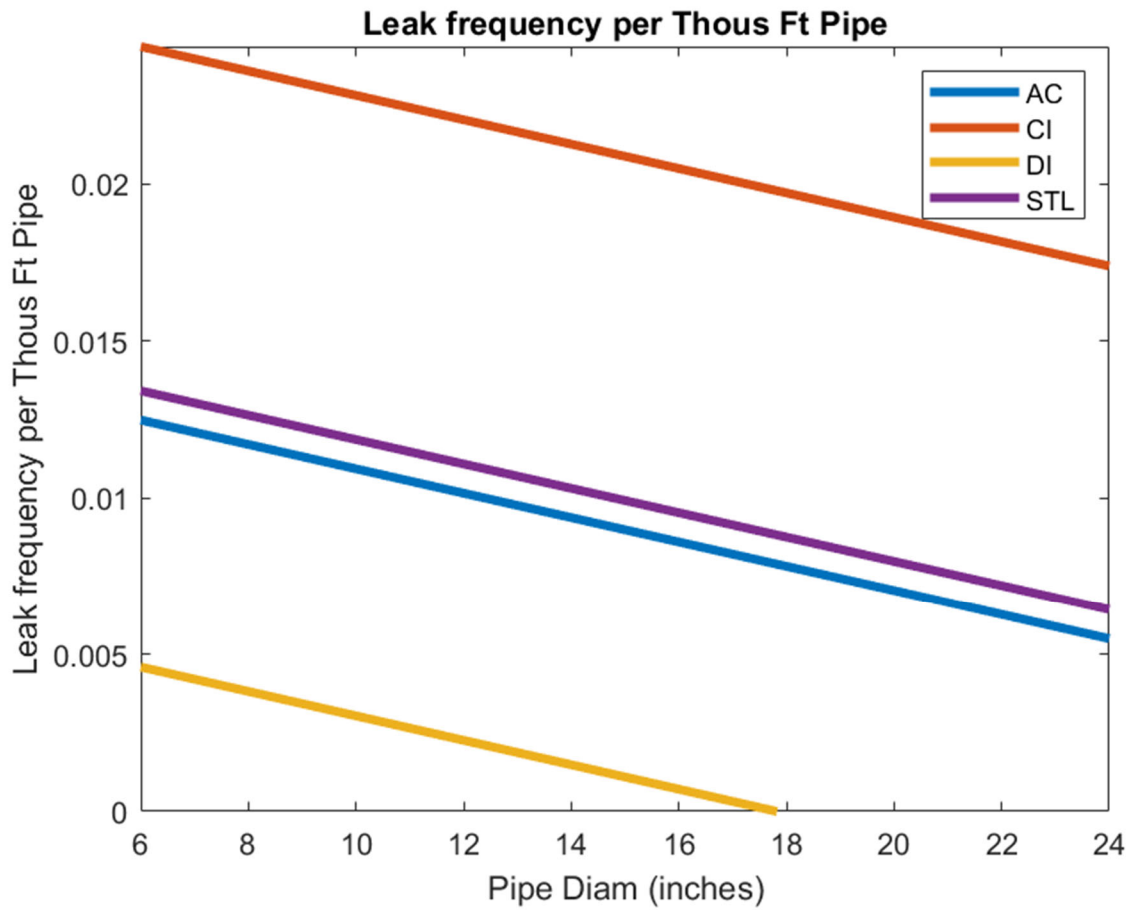


Figure 4-2. Leak Frequency per Thousand Foot of Pipe as a Function of Pipe Diameter and Material, LADWP Data.

4.2.1.3 Considering Pipe Age: Linear and Log Models

Age is an important factor in pipe deterioration. The age distribution of LADWP GIS pipe segments (where known) is shown in the following figure:

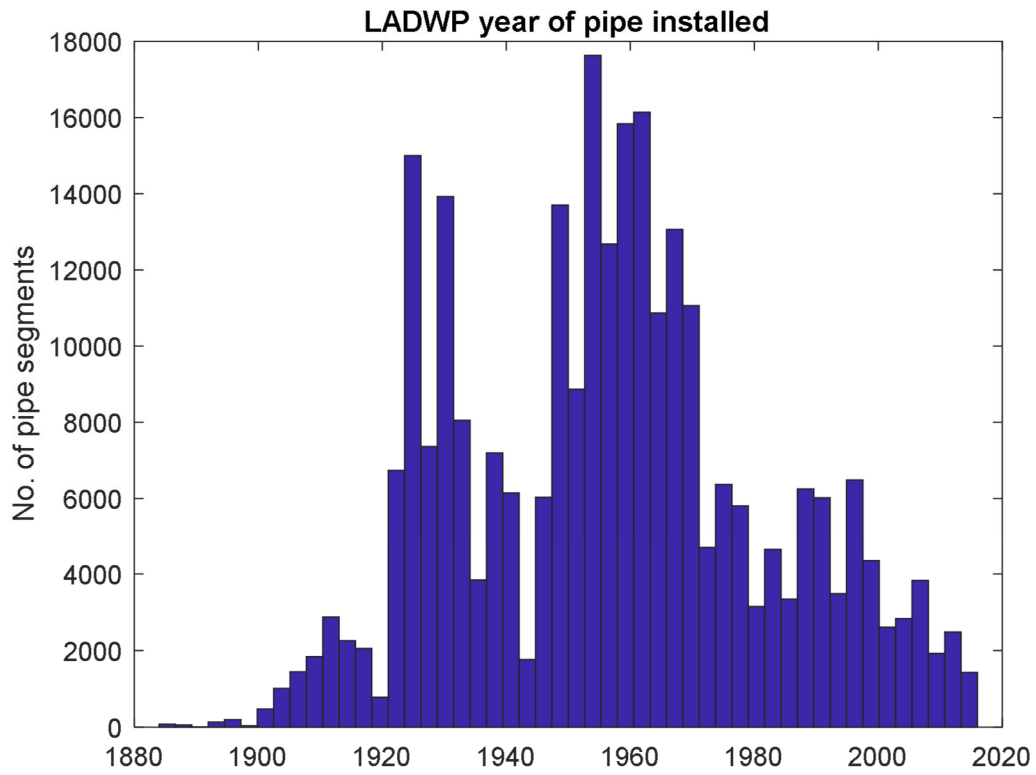


Figure 4-3. Histogram of LADWP Pipe GIS Segments by Year of Installation.

so that the simplest linear regression to consider pipe age would be a linear model, with results here and in the figure below:

Leak freq./th ft considering age

$y = y.*t.pipeLft./1000;$

$X=[t.pDiam,t.AC,t.Cl,t.Dl,t.STL,t.pipeAge];$

regrAge =

Linear regression model:

$y \sim 1 + x1 + x2 + x3 + x4 + x5 + x6$

Estimated Coefficients:

	Estimate	SE	tStat	pValue
(Intercept)	0.0014027	0.001786	0.78534	0.43225
x1	-0.00052747	2.8119e-05	-18.758	1.8482e-78
x2	-0.013624	0.0018397	-7.4056	1.3088e-13
x3	-0.010771	0.0017233	-6.25	4.1101e-10
x4	-0.0046884	0.0017739	-2.643	0.0082172
x5	-0.010305	0.0017266	-5.968	2.405e-09
x6	0.00050888	1.1655e-05	43.664	0

Number of observations: 278878, Error degrees of freedom: 278871

Root Mean Squared Error: 0.106

R-squared: 0.013, Adjusted R-Squared: 0.013

F-statistic vs. constant model: 614, p-value = 0

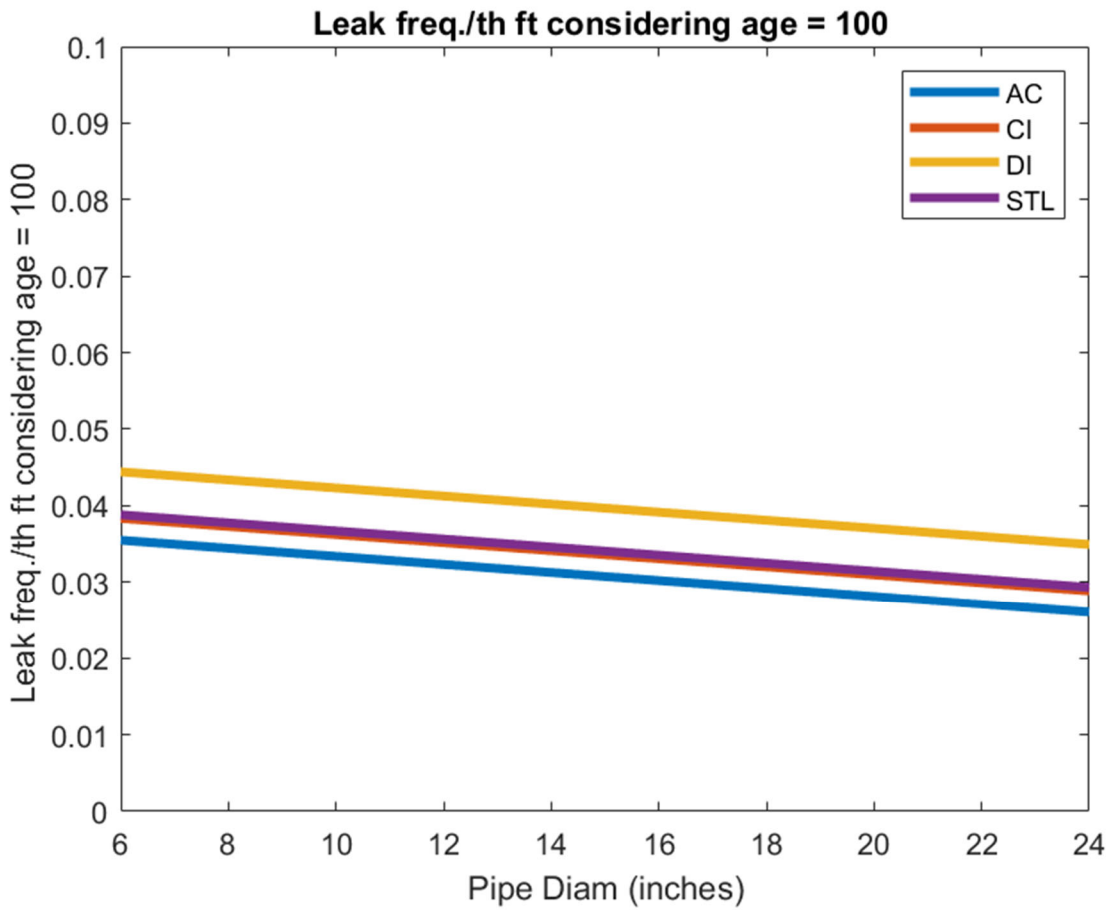


Figure 4-4. Repair Frequency per Thousand Feet of Pipe Considering Material, Age, and Diameter, Based on a Linear Model. Plot Is an Example for Pipe Age Equal to 100 Years, LADWP Data.

As expected, increasing age results in higher repair frequencies (positive coefficient in x6). However, age is more typically an exponential decay phenomenon rather than linear, so we employ a log-log model:

Leak freq./th ft considering age

$$y = \ln(y.*t.pipeLft./1000);$$

$$X=\ln[t.pDiam,t.AC,t.Cl,t.Dl,t.STL,t.pipeAge];$$

regr = Linear regression model:

$$y \sim 1 + x1 + x2 + x3 + x4 + x5 + x6$$

Estimated Coefficients:

	Estimate	SE	tStat	pValue
(Intercept)	-0.017234	0.0018134	-9.5033	2.0487e-21
x1	-0.0074223	0.00028174	-26.344	9.2325e-153
x2	-0.0089236	0.0018937	-4.7123	2.4509e-06
x3	0.00036417	0.0017694	0.20582	0.83694
x4	0.00038476	0.0018464	0.20838	0.83493
x5	-0.0042081	0.0018092	-2.3259	0.020026
x6	0.011768	0.00035575	33.08	1.6603e-239

Number of observations: 278878, Error degrees of freedom: 278871

Root Mean Squared Error: 0.0755

R-squared: 0.013, Adjusted R-Squared: 0.0129

F-statistic vs. constant model: 611, p-value = 0

Results for a pipe age of 100 years are shown in Figure 4-5. Comparing that figure and Figure 4-1, we see that the repair rates for an age of 100 years are about 50% of those derived from a linear model, implying a higher rate for younger pipe.

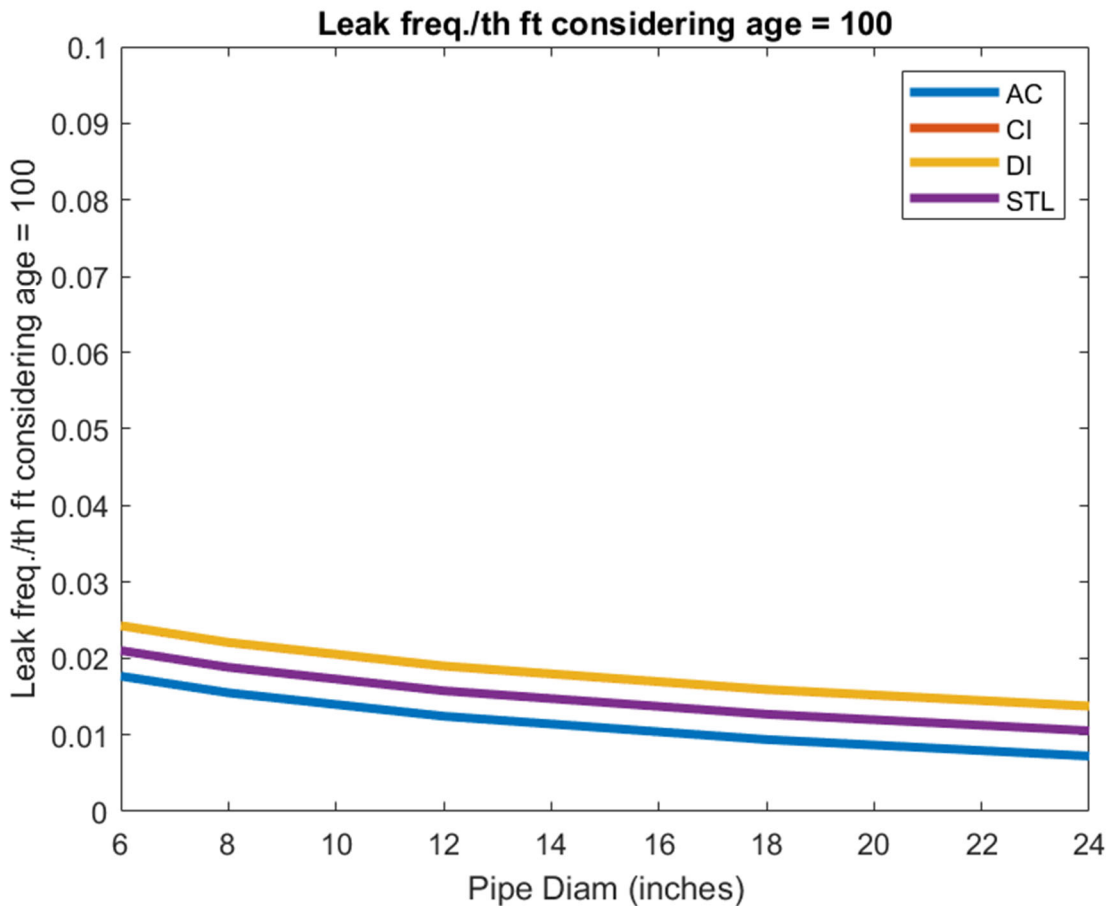


Figure 4-5. Repair Frequency per Thousand Feet of Pipe Considering Material, Age, and Diameter, Based on a Log-Log Model. Plot Is an Example for Pipe Age Equal to 100 Years, LADWP Data.

4.2.1.4 Considering Slope and Soil Vs30

Lastly in this section we consider slope and soil Vs30. As discussed in (Allen and Wald 2007), their Vs30 data is a correlation based on slope, so that we would expect slope and soil Vs30 to be correlated. If closely correlated and both employed in a regression, we would expect a rank deficiency and poor or infeasible correlation. To investigate this point prior to attempting a regression, we plot Vs30 vs. slope for our dataset, as shown in Figure 4-6. While there is substantial scatter, the correlation coefficient is still acceptable at 5% confidence bounds, so we may have a problem. Referring to (Allen and Wald 2007) we find their correlation as shown in Figure 4-7 we see substantial scatter and that the correlation is log-log (which is what we are employing). Nevertheless, we proceed as discussed next and find a feasible regression.

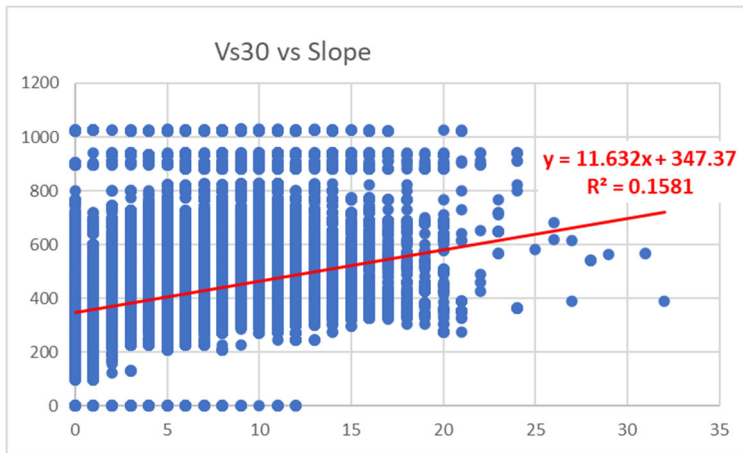


Figure 4-6. Scattergram of Vs30 vs. Slope (Degrees).

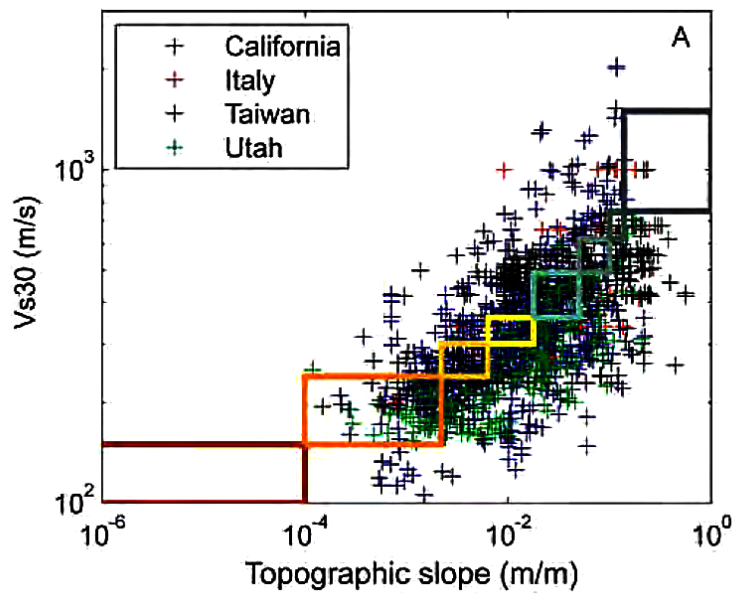


Figure 4-7. Correlations of Measured Vs30 (M/S) Versus Topographic Slope (M/M) for Active Tectonic Regions.

Source: Allen and Wald 2007

Leak freq./th ft considering age = 100, Vs30 and Slope

$$y = \ln(1+y.*t.pipeLft./1000)$$

$$X=\ln([t.pDiam,(1+t.AC),(1+t.Cl),(1+t.Dl),(1+t.STL),t.pipeAge, t.Vs30,(1+t.Slope_degr)])$$

regr = Linear regression model:

$$y \sim 1 + x1 + x2 + x3 + x4 + x5 + x6 + x7 + x8$$

Estimated Coefficients:

	Estimate	SE	tStat	pValue
(Intercept)	-0.095153	0.004167	-22.835	2.6556e-115
x1	-0.0068637	0.00028338	-24.221	1.8387e-129
x2	-0.0071895	0.0018978	-3.7884	0.00015163
x3	0.0023439	0.0017719	1.3229	0.18588
x4	0.0012311	0.0018476	0.66632	0.50521
x5	-0.0056784	0.0018112	-3.1352	0.0017178
x6	0.01175	0.00035583	33.023	1.1115e-238
x7	0.012817	0.00063873	20.066	1.6895e-89
x8	0.00072797	0.00017754	4.1003	4.1278e-05

Number of observations: 278394, Error degrees of freedom: 278385

Root Mean Squared Error: 0.0755

R-squared: 0.0149, Adjusted R-Squared: 0.0149

F-statistic vs. constant model: 526, p-value = 0

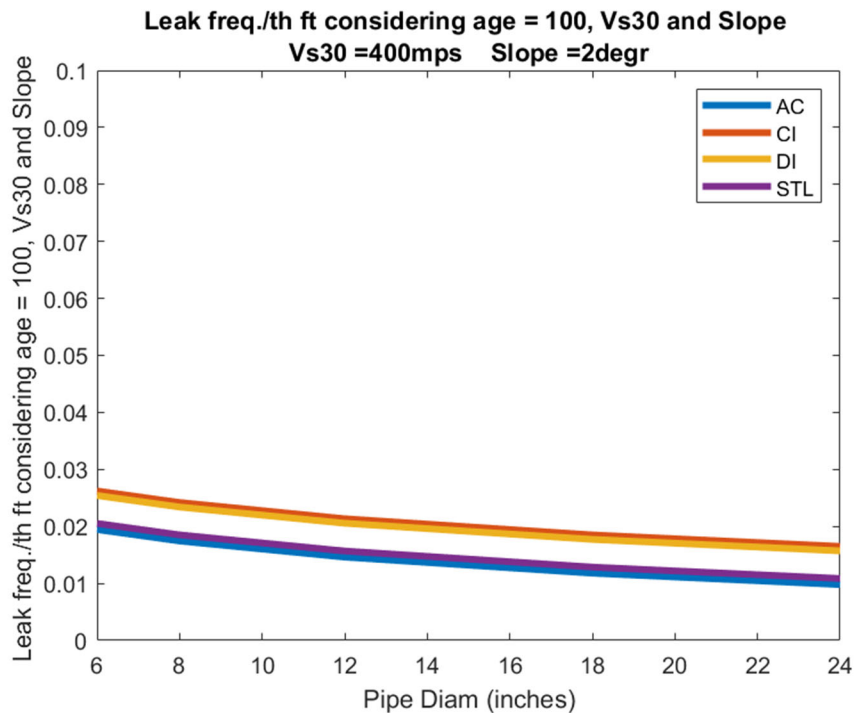


Figure 4-8. Repair Frequency per Thousand Feet of Pipe Considering Material, Age, Diameter, Vs30, and Slope, Based on a Log-Log model. Plot Is an Example for Pipe Age Equal to 100 Years Vs30 = 400 Mps and Slope of 2 Degrees, LADWP Data.

Results are shown in Figure 4-8 above. Surprisingly, while increasing slope increases repair frequency, increasing Vs30 (increasing soil firmness) also increases repair frequency, which is counter to expectations. This aspect will be investigated further.

4.2.2 SPU Data as a Whole

The SPU pipe record data set consists of 64,654 GIS pipe segments (fewer than reported above due to some data being incomplete) totaling 7.24 million feet in length, varying in date of installation from 1890 to 2017, with 3,272 recorded leaks for the period 1958 to 2017. The SPU system has no AC pipe, so that material type is omitted in the analysis. We begin with the simplest analysis.

4.2.2.1 Leak Frequency per GIS Pipe Segment as a Function of Pipe Diameter and Material

The first analysis is simply for raw leak frequency (f) per GIS pipe segment as a function of pipe diameter and material, using a linear model. Results are:

regress leak vs diam and matl

y=spuC.leak;

X=[spuC.pDiam,spuC.CI,spuC.DI,spuC.STL];

regr = Linear regression model:

$$y \sim 1 + x1 + x2 + x3 + x4$$

Estimated Coefficients:

	Estimate	SE	tStat	pValue
(Intercept)	0.061209	0.0045502	13.452	3.4095e-41
x1	0.00027876	0.00039036	0.71411	0.47516
x2	-0.018381	0.0049039	-3.7482	0.00017826
x3	0.0013783	0.0051422	0.26804	0.78867
x4	-0.014408	0.015493	-0.92995	0.3524

Number of observations: 64654, Error degrees of freedom: 64649

Root Mean Squared Error: 0.219

R-squared: 0.00162, Adjusted R-Squared: 0.00156

F-statistic vs. constant model: 26.2, p-value = 9.49e-22

Reviewing results we are surprised to find that repair frequency increases modestly with increasing diameter and that CI has most reduction in repair frequency, contrary to expectations. These results are shown in Figure 4-9. These results are contrary to the LADWP results and warrant further investigation. Note these results and all frequencies in this section are for the duration of the dataset and should be divided by that duration for annual frequencies.

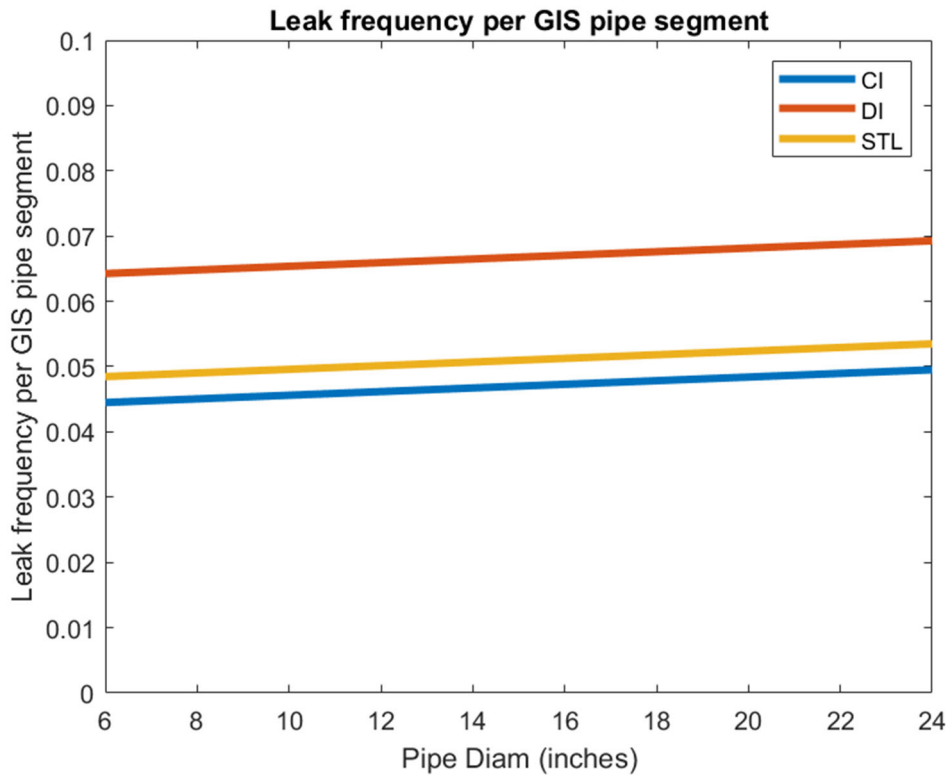


Figure 4-9. Raw SPU Leak Frequency per GIS Pipe Segment, by Material and Diameter, SPU Data.

4.2.2.2 Leak Frequency per Thousand Foot of Pipe as a Function of Pipe Diameter and Material

However, GIS segment is an artifact of data entry and is of limited use, so we next normalize break rates by pipe length. Results are shown in Figure 4-10. Results still increase with pipe diameter, contrary to expectation, but DI at least has a lower leak frequency than CI.

normalize leak by pipe length and regress leak vs diam and matl

$y = y \cdot \text{spuC.pipeLft.}/1000;$

$X = [\text{spuC.pDiam}, \text{spuC.Cl}, \text{spuC.DI}, \text{spuC.STL}];$

regr = Linear regression model:

$y \sim 1 + x1 + x2 + x3 + x4$

Estimated Coefficients:

	Estimate	SE	tStat	pValue
(Intercept)	0.0033941	0.00084046	4.0384	5.3885e-05
x1	0.00011352	7.2102e-05	1.5745	0.11539
x2	0.0021127	0.00090578	2.3324	0.019681
x3	-9.9474e-06	0.00094981	-0.010473	0.99164
x4	0.0064942	0.0028617	2.2693	0.023253

Number of observations: 64654, Error degrees of freedom: 64649

Root Mean Squared Error: 0.0405

R-squared: 0.000685, Adjusted R-Squared: 0.000624

F-statistic vs. constant model: 11.1, p-value = 5.48e-09

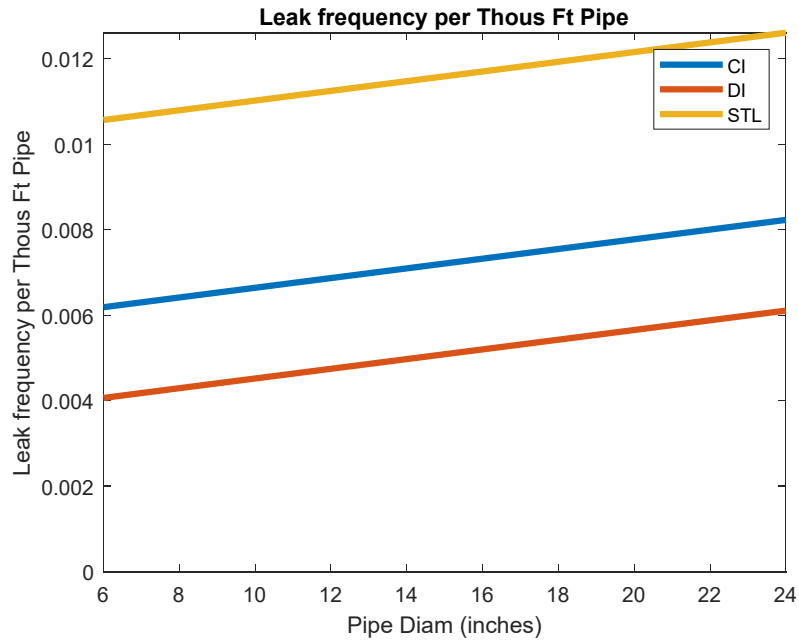


Figure 4-10. Raw SPU Leak Frequency per 1000 Ft. of GIS Pipe Segment, by Material and Diameter, SPU Data.

Because these results appear anomalous, we examine the distribution of pipe diameters by material in the SPU system, finding almost all pipe is 8" diameter, Figure 4-11. Therefore, diameter is poorly distributed in this data set, and not a robust covariate.

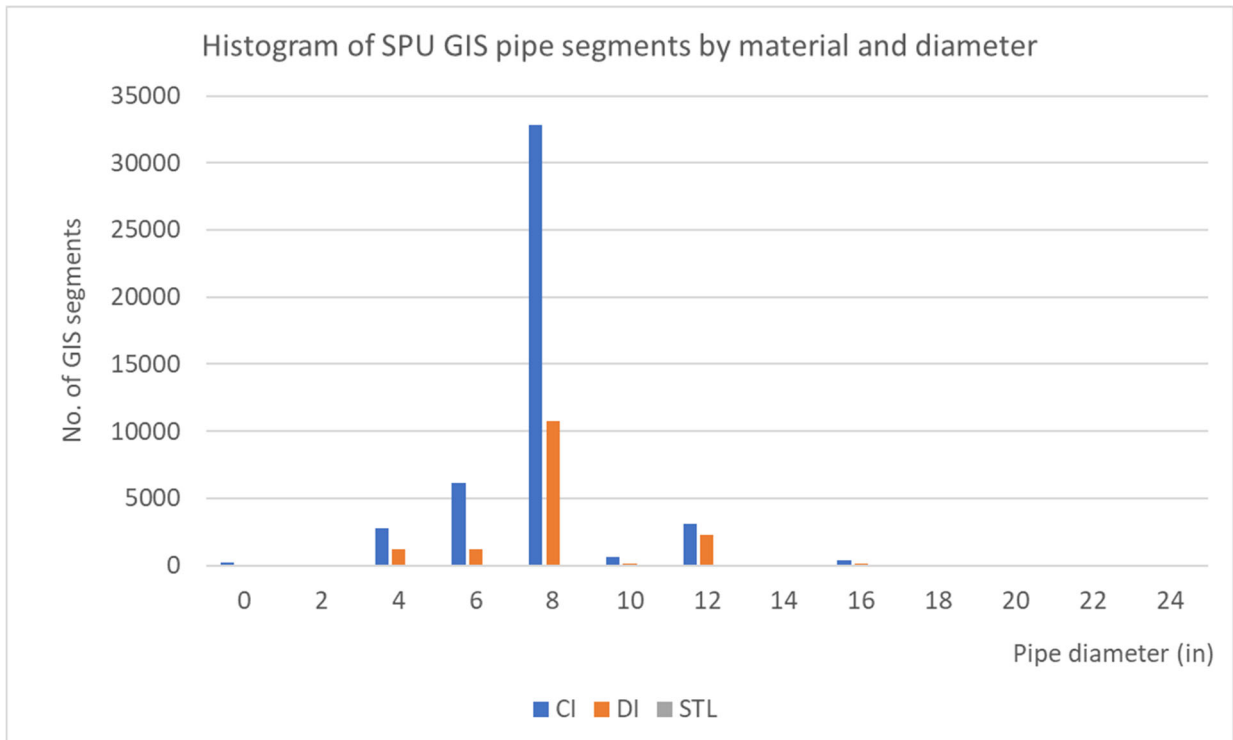


Figure 4-11. Histogram of SPU GIS Pipe Segments by Material and Diameter.

4.2.2.3 Considering Pipe Age: Linear and Log Models

Age is an important factor in pipe deterioration. The age distribution of LADWP GIS pipe segments (where known) is shown in the following figure:

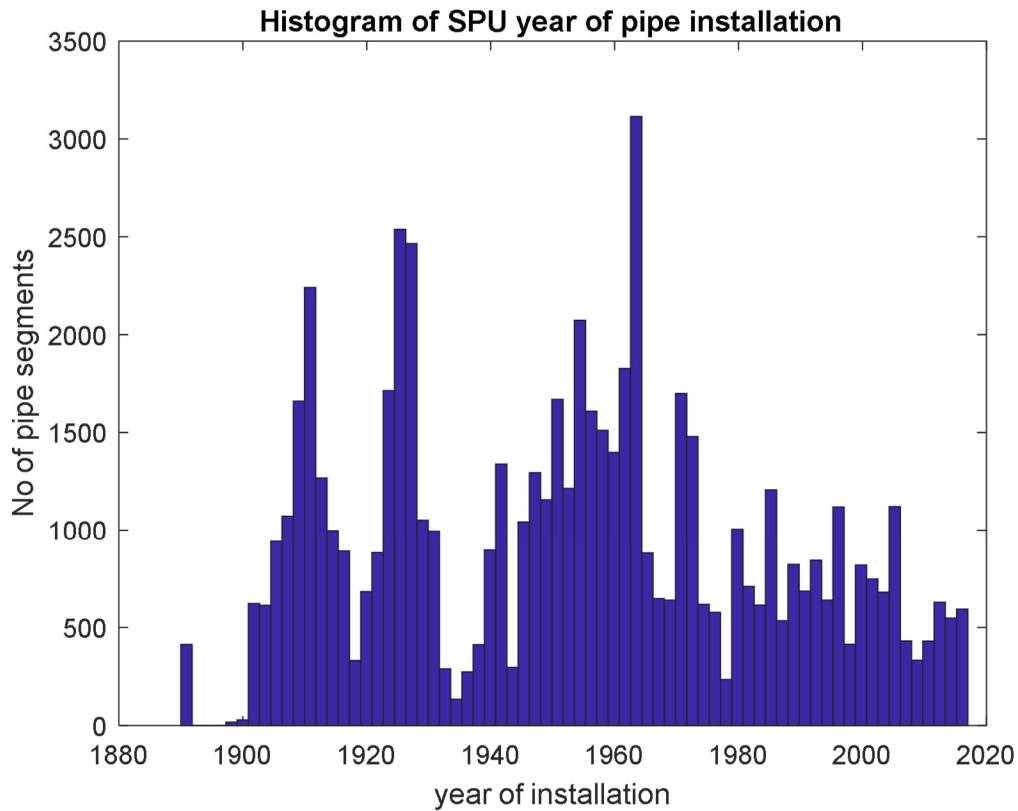


Figure 4-12. Histogram of SPU Pipe GIS Segments by Year of Installation.

so that the simplest linear regression to consider pipe age would be a linear model, with results here and in Figure 4-12.

Leak freq./th ft considering age

$y = y.*\text{pipeLft.}/1000;$

$X = [\text{spuC.pDiam}, \text{spuC.Cl}, \text{spuC.DI}, \text{spuC.STL}, \text{spuC.pipeAge}];$

regrAge =

Linear regression model:

$y \sim 1 + x1 + x2 + x3 + x4 + x5$

Estimated Coefficients:

	Estimate	SE	tStat	pValue
(Intercept)	0.0026065	0.00096938	2.6889	0.0071712
x1	0.00010556	7.2267e-05	1.4607	0.1441
x2	0.0019662	0.00091021	2.1602	0.03076
x3	0.0005351	0.0010069	0.53143	0.59512
x4	0.0065783	0.0028622	2.2984	0.021544
x5	1.2607e-05	7.7329e-06	1.6303	0.10303

Number of observations: 64654, Error degrees of freedom: 64648

Root Mean Squared Error: 0.0405

R-squared: 0.000727, Adjusted R-Squared: 0.000649

F-statistic vs. constant model: 9.4, p-value = 5.72e-09

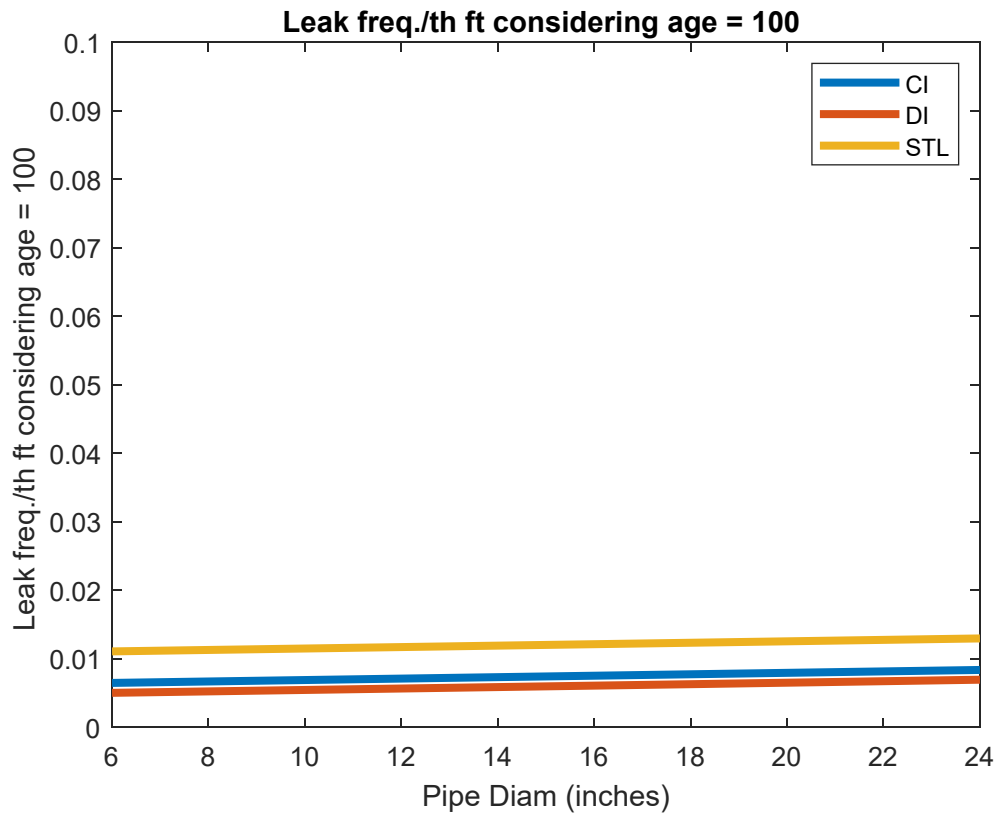


Figure 4-13. Repair Frequency per Thousand Feet of Pipe Considering Material, Age, and Diameter, Based on a Linear Model. Plot Is an Example for Pipe Age Equal to 100 Years, SPU Data.

For this dataset, increasing age results has a relatively weak effect on repair frequencies (positive coefficient in x5). However, age is more typically an exponential decay phenomenon rather than linear, so we employ a log-log model:

Leak freq./th ft considering age

$$y = \ln(y.\text{spuC.pipeLft.}/1000);$$

$$X = \ln[\text{spuC.pDiam}, \text{spuC.Cl}, \text{spuC.DI}, \text{spuC.STL}, \text{spuC.pipeAge}];$$

regr =

Linear regression model:

$$y \sim 1 + x1 + x2 + x3 + x4 + x5$$

Estimated Coefficients:

	Estimate	SE	tStat	pValue
(Intercept)	0.0021863	0.0013361	1.6363	0.10177
x1	0.00058021	0.0005031	1.1533	0.2488
x2	0.0021596	0.0013288	1.6253	0.10411
x3	-3.1377e-05	0.0014061	-0.022315	0.9822
x4	0.005822	0.0035474	1.6412	0.10076
x5	0.00017791	0.0002718	0.65457	0.51275

Number of observations: 64654, Error degrees of freedom: 64648

Root Mean Squared Error: 0.0344

R-squared: 0.00062, Adjusted R-Squared: 0.000543

F-statistic vs. constant model: 8.02, p-value = 1.42e-07

Results for a pipe age of 100 years are shown in Figure 4-14. Comparing that figure and Figure 4-13, we see that the repair rates for an age of 100 years are slightly less than those derived from a linear model.

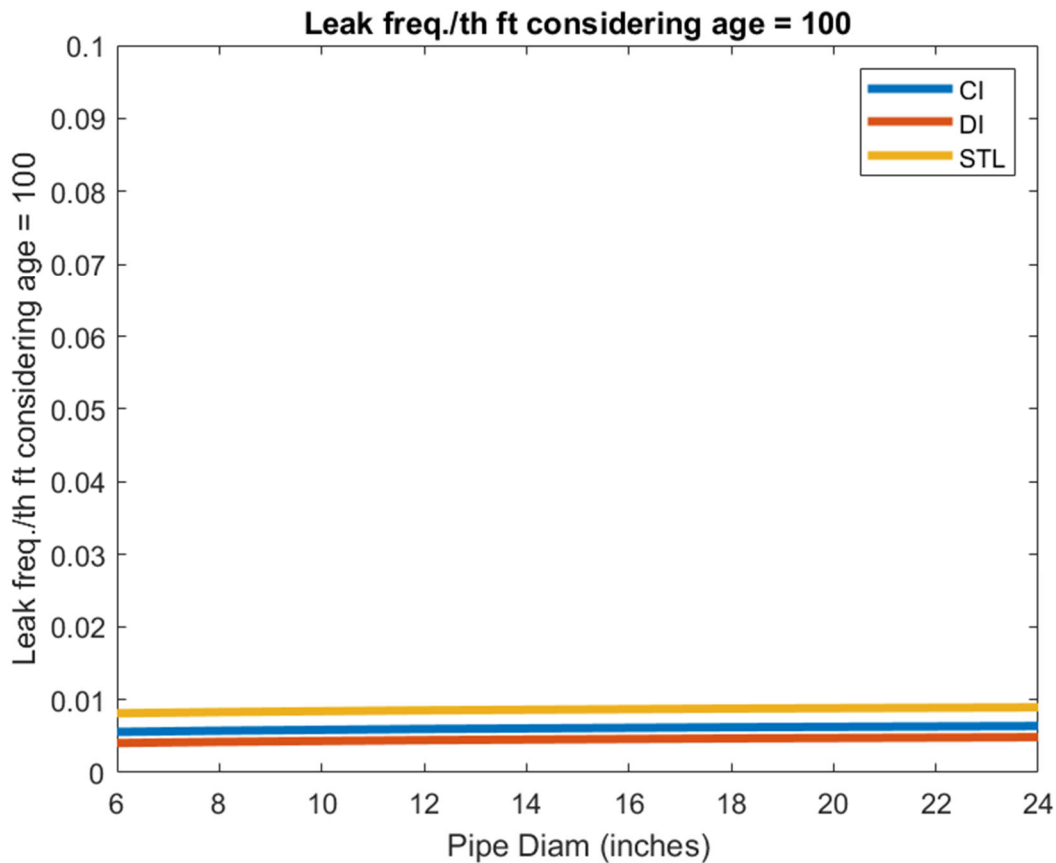


Figure 4-14. Repair Frequency per Thousand Feet of Pipe Considering Material, Age, and Diameter, Based on a Log-Log Model. Plot Is an Example for Pipe Age Equal to 100 Years, SPU Data.

4.3 Regression Analysis of Repair Rate Annual Frequencies

This section analyzes the five data sets each on an annualized basis for the block of years the dataset represents, as opposed to the previous section where breaks were analyzed for the entire period of the LADWP and SPU datasets. The LADWP dataset is for the years 1977-2017– that is, the digital and scanned map repair dataset. Lastly, we present the same analysis for all five datasets merged into one large dataset.

4.3.1 LADWP: Analysis of 1975-2017 Dataset

4.3.1.1 Leak Frequency per GIS Pipe Segment as a Function of Pipe Diameter and Material

The first analysis is simply for raw leak frequency (f) per GIS pipe segment as a function of pipe diameter and material, using a linear model. Results are:

LADWP repair freq pa per GIS pipe segment = f(diam, matl)

regress repair vs diam and matl

y=xx.leak

X=[xx.pDiam,xx.AC,xx.Cl,xx.Dl,xx.STL]

regr = Linear regression model:

$$y \sim 1 + x1 + x2 + x3 + x4 + x5$$

Estimated Coefficients:

	Estimate	SE	tStat	pValue
(Intercept)	0.19826	0.0056398	35.153	4.063e-270
x1	-0.00097211	8.709e-05	-11.162	6.3326e-29
x2	-0.054347	0.0060572	-8.9723	2.9201e-19
x3	-0.050374	0.0055712	-9.0418	1.5507e-19
x4	0.037882	0.0057573	6.5798	4.7202e-11
x5	-0.071333	0.0056546	-12.615	1.7837e-36

Number of observations: 280256, Error degrees of freedom: 280250

Root Mean Squared Error: 0.354

R-squared: 0.0106, Adjusted R-Squared: 0.0105

F-statistic vs. constant model: 598, p-value = 0

Reviewing results, we see that repair frequency decreases with increasing diameter and that CI has the highest repair frequency, as we would expect. These results are shown in Figure 4-15.

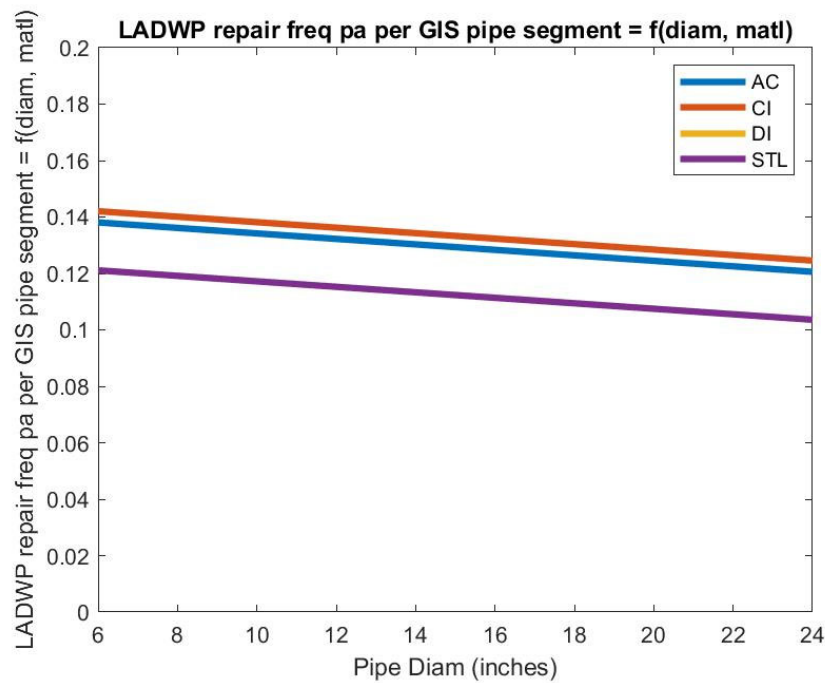


Figure 4-15. Raw Leak Frequency per GIS Pipe Segment, by Material and Diameter, LADWP Data.

4.3.1.2 Leak Frequency per GIS Pipe Segment as a Function of Pipe Diameter, Material, and Slope

We add the variable of slope of the ground where the pipe is located – this is not the slope parallel or perpendicular to the pipe axis but rather the gradient of the ground at the centroid of the pipe (later we examine slope parallel or perpendicular to the pipe axis). Results are shown in Figure 4-16.

LADWP repair freq pa per GIS pipe segment = f(diam, matl, abs(slope))
 repair freq pa per GIS pipe segment vs diam, matl, Slope
 $y = \text{xx.leak}$
 $[\text{xx.pDiam}, \text{xx.AC}, \text{xx.CI}, \text{xx.DI}, \text{xx.STL}, \text{abs}(\text{xx.Slope_ror})]$

regr = Linear regression model:
 $y \sim 1 + x1 + x2 + x3 + x4 + x5 + x6$

Estimated Coefficients:

	Estimate	SE	tStat	pValue
(Intercept)	0.18513	0.0058405	31.697	4.2757e-220
x1	-0.00078684	8.9294e-05	-8.8118	1.2387e-18
x2	-0.048812	0.0062471	-7.8135	5.581e-15
x3	-0.046185	0.0057407	-8.0452	8.6425e-16
x4	0.040481	0.0059214	6.8364	8.1389e-12
x5	-0.078048	0.0058224	-13.405	5.8482e-41
x6	0.10955	0.0048581	22.551	1.6694e-112

Number of observations: 272150, Error degrees of freedom: 272143
 Root Mean Squared Error: 0.354

R-squared: 0.0125, Adjusted R-Squared: 0.0124

F-statistic vs. constant model: 573, p-value = 0

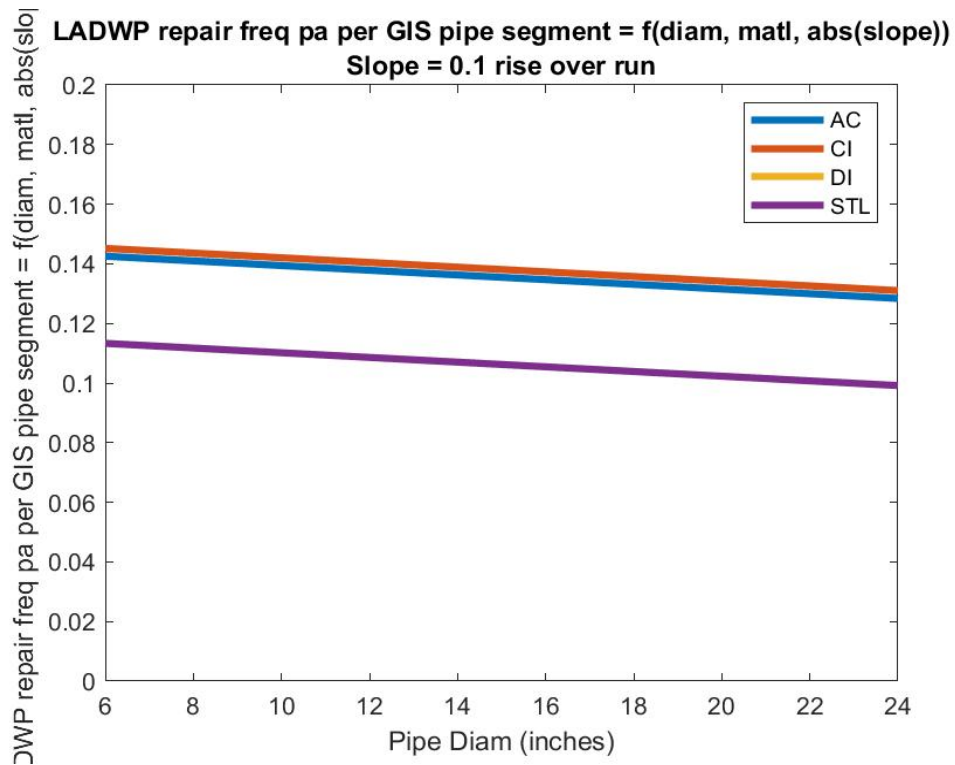


Figure 4-16. Leak Frequency per GIS Pipe Segment as a Function of Pipe Diameter, Material, and Slope, LADWP Data.

4.3.1.3 Leak Frequency per Thousand Feet of Pipe as a Function of Pipe Diameter, Material, and Slope

We normalize the repair frequency to a thousand feet of pipe and retain the variable of slope of the ground where the pipe is located. Again, this is not the slope parallel or perpendicular to the pipe axis but rather the gradient of the ground at the centroid of the pipe (later we examine slope parallel or perpendicular to the pipe axis). Results are shown in Figure 4-17.

LADWP repair freq pa per th ft = f(diam, matl, abs(slope)), Slope = 0.1

repair freq pa per th ft vs diam, matl, abs(slope)

$y = y.*xx.pipeLft./1000$

$X=[xx.pDiam,xx.AC,xx.Cl,xx.Dl,xx.STL]$

regr = Linear regression model:

$y \sim 1 + x1 + x2 + x3 + x4 + x5 + x6$

Estimated Coefficients:

	Estimate	SE	tStat	pValue
(Intercept)	0.024398	0.0024177	10.091	6.0848e-24
x1	0.0016299	3.6963e-05	44.095	0
x2	-0.0035558	0.002586	-1.375	0.16913
x3	-0.0035051	0.0023764	-1.475	0.14022
x4	0.0092113	0.0024512	3.7579	0.00017136
x5	-0.023795	0.0024102	-9.8724	5.5302e-23
x6	0.030218	0.002011	15.026	5.1913e-51

Number of observations: 272150, Error degrees of freedom: 272143

Root Mean Squared Error: 0.147

R-squared: 0.00952, Adjusted R-Squared: 0.00949

F-statistic vs. constant model: 436, p-value = 0

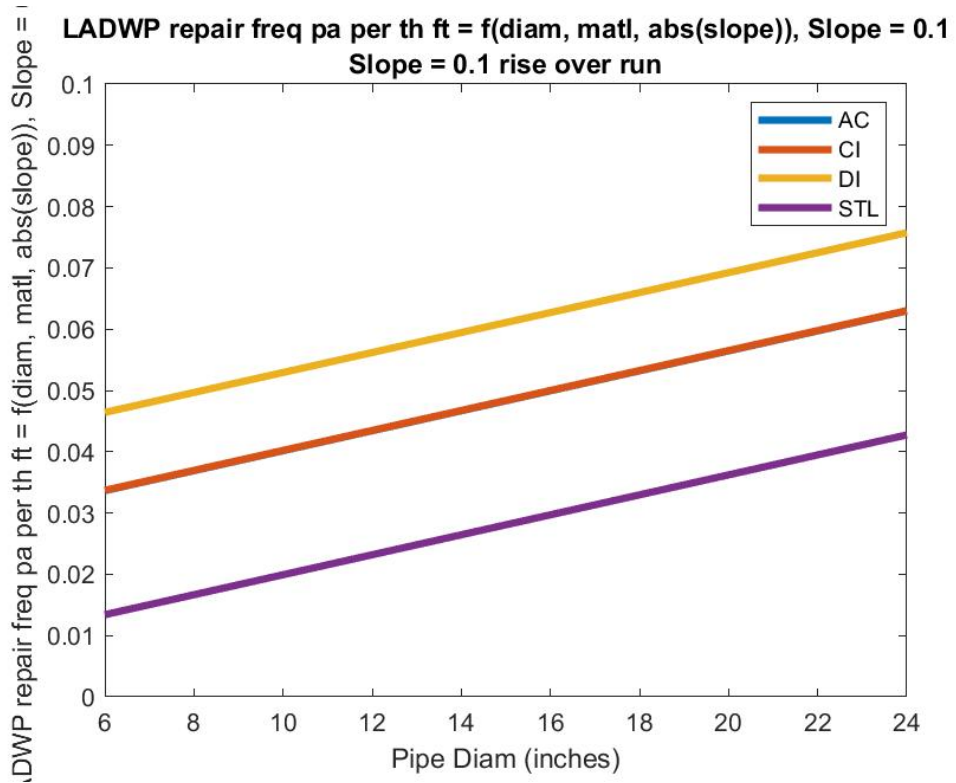


Figure 4-17. Leak Frequency per GIS Pipe Segment as a Function of Pipe Diameter, Material, and Slope, LADWP Data.

4.3.1.4 Considering Pipe Age in a Linear Model

Age is an important factor in pipe deterioration. The simplest linear regression to consider pipe age would be a linear model, with results here and in Figure 4-18:

LADWP repair freq pa per th ft vs diam, matl, age, age = 100

repair freq. per th ft considering age = 100

$y = y.*t.pipeLft./1000;$

$X=[t.pDiam,t.AC,t.Cl,t.Dl,t.STL,t.pipeAge]$

regr = Linear regression model:

$y \sim 1 + x1 + x2 + x3 + x4 + x5 + x6$

Estimated Coefficients:

	Estimate	SE	tStat	pValue
(Intercept)	0.024398	0.0024177	10.091	6.0848e-24
x1	0.0016299	3.6963e-05	44.095	0
x2	-0.0035558	0.002586	-1.375	0.16913
x3	-0.0035051	0.0023764	-1.475	0.14022
x4	0.0092113	0.0024512	3.7579	0.00017136
x5	-0.023795	0.0024102	-9.8724	5.5302e-23
x6	0.030218	0.002011	15.026	5.1913e-51

Number of observations: 272150, Error degrees of freedom: 272143

Root Mean Squared Error: 0.147

R-squared: 0.00952, Adjusted R-Squared: 0.00949

F-statistic vs. constant model: 436, p-value = 0

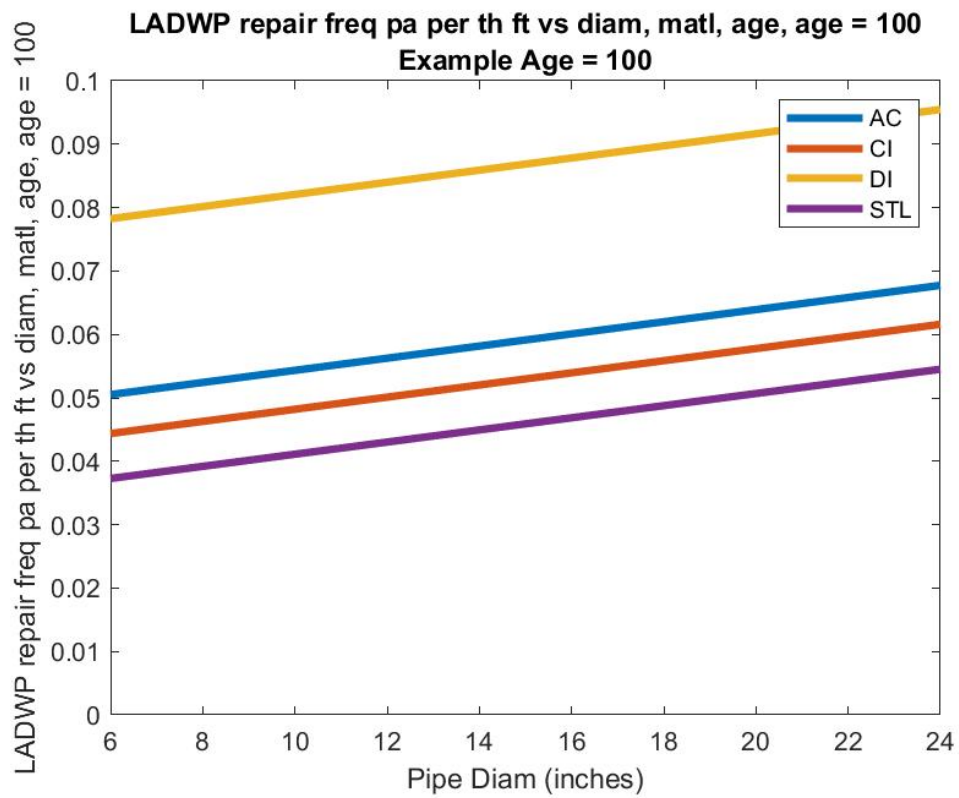


Figure 4-18. Repair Frequency per Thousand Feet of Pipe Considering Material, Age, and Diameter, Based on a Linear Model. Plot Is an Example for Pipe Age Equal to 100 Years, LADWP Data.

4.3.1.5 Considering Pipe Age in a Log-Log Model

As expected, increasing age results in higher repair frequencies (positive coefficient in x6). However, age is more typically an exponential decay phenomenon rather than linear, so we employ a log-log model:

LADWP log repair freq pa per th ft vs log(diam, matl, age)

LADWP log repair freq pa per th ft vs log(diam, matl, age)

$$y = \ln(y.*t.pipeLft./1000);$$

$$X = \ln[t.pDiam, (1+t.AC), (1+t.Cl), (1+t.Dl), (1+t.STL), t.pipeAge]$$

regr = Linear regression model:

$$y \sim 1 + x1 + x2 + x3 + x4 + x5 + x6$$

Estimated Coefficients:

	Estimate	SE	tStat	pValue
(Intercept)	0.0017555	0.0024404	0.71936	0.47192
x1	0.0045559	0.00038346	11.881	1.5105e-32
x2	-0.013222	0.0025943	-5.0966	3.4609e-07
x3	-0.014397	0.0024271	-5.9318	3e-09
x4	0.013901	0.0025232	5.5092	3.6071e-08
x5	-0.026418	0.0024777	-10.662	1.5435e-26
x6	0.0065683	0.00047483	13.833	1.6649e-43

Number of observations: 279272, Error degrees of freedom: 279265

Root Mean Squared Error: 0.103

R-squared: 0.00442, Adjusted R-Squared: 0.0044

F-statistic vs. constant model: 207, p-value = 3.28e-264

Results for a pipe age of 100 years are shown in Figure 4-19. Comparing that figure and previous results we see that the repair rates for an age of 100 years are about 50% of those derived from a linear model, implying a higher rate for younger pipe.

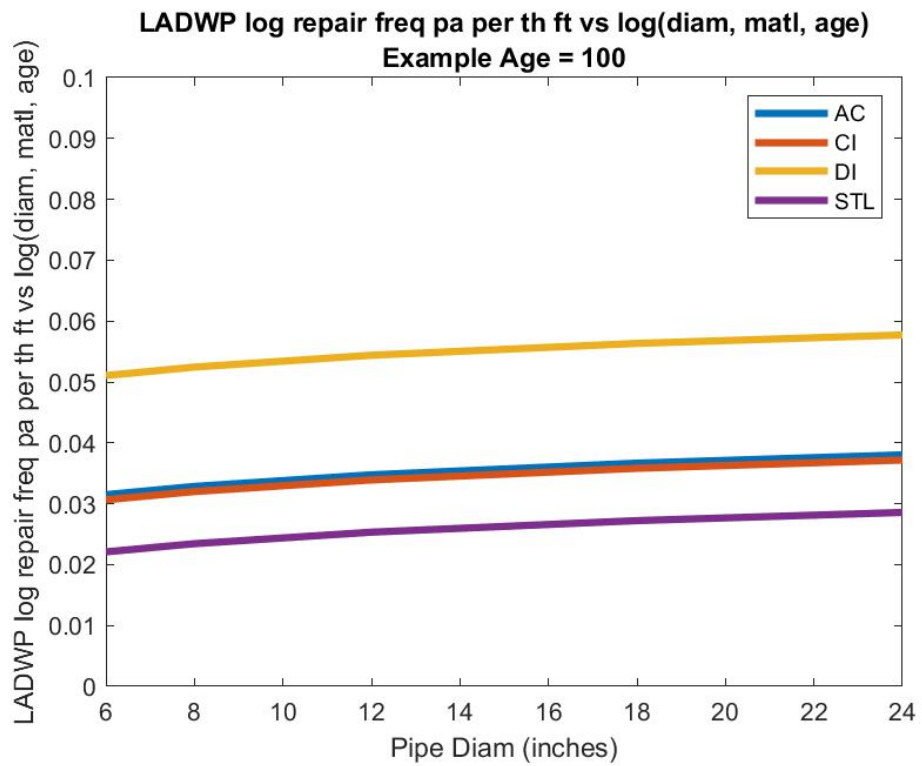


Figure 4-19. Repair Frequency per Thousand Feet of Pipe Considering Material, Age, and Diameter, Based on a Log-Log Model. Plot Is an Example for Pipe Age Equal to 100 Years, LADWP Data.

4.3.1.6 Considering Slope and Age

In this section we consider slope and age of the pipe. Results are shown in Figure 4-20.

LADWP log repair freq pa per th ft vs log(diam, matl, age, abs(slope))

repair freq. per th ft considering age = 100, and Slope

$$y = \ln(1+y.*t.pipeLft./1000)$$

$$X=\ln([t.pDiam,(1+t.AC),(1+t.CI),(1+t.DI),(1+t.STL),t.pipeAge, \text{abs}(1+t.Slope_ror)])$$

regr = Linear regression model:

$$y \sim 1 + x1 + x2 + x3 + x4 + x5 + x6 + x7$$

Estimated Coefficients:

	Estimate	SE	tStat	pValue
(Intercept)	-0.0028119	0.0025115	-1.1196	0.26287
x1	0.0050824	0.00039282	12.938	2.8064e-38
x2	-0.012214	0.0026782	-4.5606	5.1019e-06
x3	-0.014159	0.002503	-5.6569	1.543e-08
x4	0.014327	0.0025978	5.5151	3.4887e-08
x5	-0.029476	0.0025558	-11.533	9.1463e-31
x6	0.0069358	0.00048392	14.333	1.4228e-46
x7	0.030876	0.001784	17.308	4.4839e-67

Number of observations: 271360, Error degrees of freedom: 271352

Root Mean Squared Error: 0.103

R-squared: 0.00555, Adjusted R-Squared: 0.00552

F-statistic vs. constant model: 216, p-value = 8.94e-322

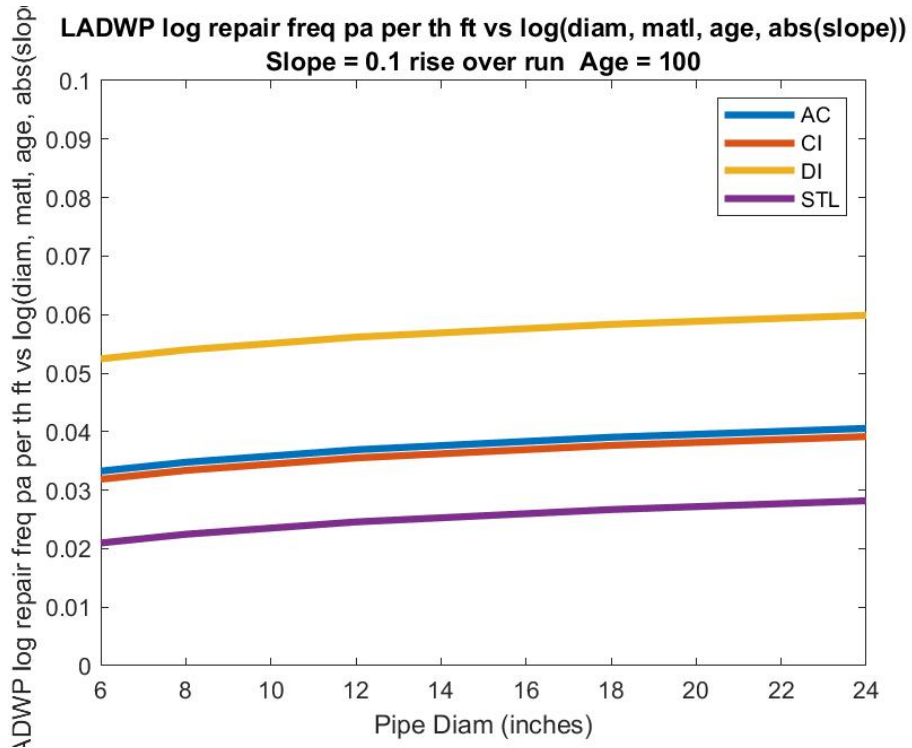


Figure 4-20. Repair Frequency per Thousand Feet of Pipe Considering Material, Age, Diameter and Slope Parallel and Perpendicular to the Pipe’s Longitudinal Axis, Based on a Log-Log model. Plot Is an Example for Pipe Age Equal to 100 Years, LADWP Data.

4.3.1.7 Considering Age as Well as Slope, Diameter, and Material

In this section we determine repair frequency per thousand feet of pipe considering material, age, diameter and slope parallel and perpendicular to the pipe’s longitudinal axis, based on a log-log model. Plot is an example for pipe age equal to 100 years. Results are shown in Figure 4-21.

LADWP log repair freq pa per th ft vs log(diam, matl, age, abs(SL), abs(ST))

repair freq. per th ft considering age = 100, and Slope

$$y = \ln(1+y.*t.pipeLft./1000)$$

$$X=\log([t.pDiam,(1+t.AC),(1+t.CI),(1+t.DI),(1+t.STL),t.pipeAge, (1+abs(t.SL)), (1+abs(t.ST))]);$$

regr = Linear regression model:

$$y \sim 1 + x1 + x2 + x3 + x4 + x5 + x6 + x7 + x8$$

Estimated Coefficients:

	Estimate	SE	tStat	pValue
(Intercept)	-0.0030926	0.0024549	-1.2597	0.20777
x1	0.0050441	0.0003843	13.125	2.422e-39
x2	-0.010857	0.0025964	-4.1815	2.8972e-05
x3	-0.012858	0.0024273	-5.2972	1.1771e-07
x4	0.01528	0.002523	6.056	1.397e-09
x5	-0.027982	0.0024781	-11.292	1.4613e-29
x6	0.0068336	0.00047481	14.392	6.0128e-47
x7	0.015191	0.0027652	5.4937	3.9396e-08
x8	0.03038	0.0027442	11.071	1.7631e-28

Number of observations: 279272, Error degrees of freedom: 279263

Root Mean Squared Error: 0.103

R-squared: 0.00552, Adjusted R-Squared: 0.0055

F-statistic vs. constant model: 194, p-value = 0

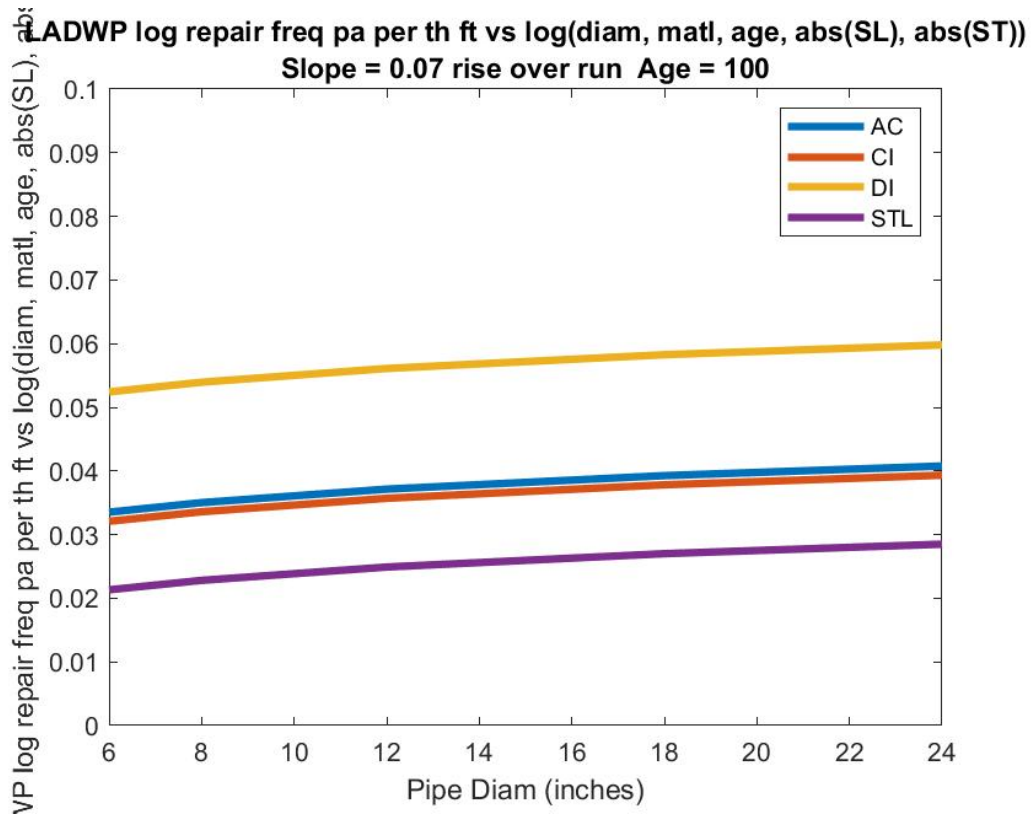


Figure 4-20. Repair Frequency per Thousand Feet of Pipe Considering Material, Age, Diameter, and Slope Parallel and Perpendicular to the Pipe's Longitudinal Axis, Based on a Log-Log Model. Plot Is an Example for Pipe Age Equal to 100 Years, LADWP Data.

4.3.1.8 Summary

The intercept and regression coefficients for the above seven models are summarized in Table 4-2.

Table 4-2. LADWP Regression Coefficients for Seven Models.

Regression Coefficients	1. linear model: repair = f(diam, matl)	2. linear model: repair = f(diam, matl, slope)	3. linear model: repair/length = f(diam, matl, slope)	4. linear model: repair/length = f(diam, matl, age)	5. log-log model: $\ln(1 + \text{repair}/\text{length}) = f[\ln(\text{diam}, 1 + \text{matl}, \text{age})]$	6. log-log model: $\ln(1 + \text{repair}/\text{length}) = f[\ln(\text{diam}, 1 + \text{matl}, \text{age}, 1 + \text{slope})]$	7. log-log model: $\ln(1 + \text{repair}/\text{length}) = f[\ln(\text{diam}, 1 + \text{matl}, \text{age}, 1 + \text{SL}, 1 + \text{ST})]$
1	0.1983	0.1851	0.0244	0.0120	0.0018	-0.0028	-0.0031
2	-0.0010	-0.0008	0.0016	0.0010	0.0046	0.0051	0.0050
3	-0.0543	-0.0488	-0.0036	-0.0069	-0.0132	-0.0122	-0.0109
4	-0.0504	-0.0462	-0.0035	-0.0131	-0.0144	-0.0142	-0.0129
5	0.0379	0.0405	0.0092	0.0208	0.0139	0.0143	0.0153
6	-0.0713	-0.0780	-0.0238	-0.0202	-0.0264	-0.0295	-0.0280
7		0.1096	0.0302	0.0004	0.0066	0.0069	0.0068
8						0.0309	0.0152
9							0.0304

4.3.2 EBMUD

Comparable results for the EBMUD data set are provided below – similar comments apply, with results presented in Figure 4-22 to Figure 4-28 and Table 4-3:

Table 4-3. EBMUD Regression Coefficients for Seven Models.

Regression Coefficients	1. linear model: repair = f(diam, matl)	2. linear model: repair = f(diam, matl, slope)	3. linear model: repair/length = f(diam, matl, slope)	4. linear model: repair/length = f(diam, matl, age)	5. log-log model: $\ln(1 + \text{repair}/\text{length}) = f[\ln(\text{diam}, 1 + \text{matl}, \text{age})]$	6. log-log model: $\ln(1 + \text{repair}/\text{length}) = f[\ln(\text{diam}, 1 + \text{matl}, \text{age}, 1 + \text{slope})]$	7. log-log model: $\ln(1 + \text{repair}/\text{length}) = f[\ln(\text{diam}, 1 + \text{matl}, \text{age}, 1 + \text{SL}, 1 + \text{ST})]$
1	0.0630	0.0403	0.0073	0.0185	0.0244	0.0130	0.0146
2	-0.0063	-0.0060	-0.0017	-0.0020	-0.0190	-0.0177	-0.0180
3	0.0697	0.0736	0.0307	0.0239	0.0236	0.0261	0.0263
4	0.1677	0.1705	0.0649	0.0546	0.0590	0.0614	0.0610
5	0.0249	0.0347	0.0075	-0.0008	-0.0026	0.0033	0.0025
6	0.0246	0.0206	0.0062	0.0067	0.0076	0.0050	0.0052
7		0.2945	0.1625	0.0001	0.0060	0.0059	0.0059
8						0.1421	0.0411
9							0.1601

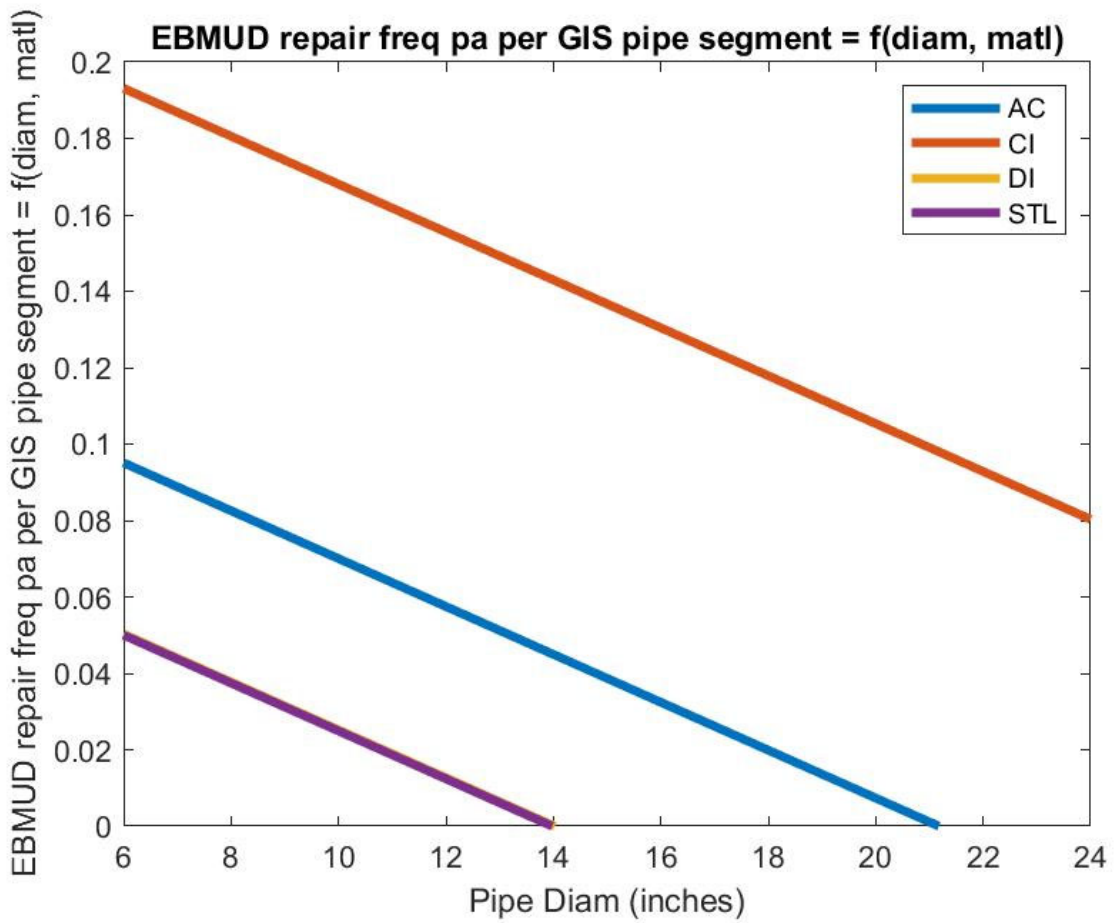


Figure 4-21. Raw Leak Frequency per GIS Pipe Segment, by Material and Diameter, EBMUD Data.

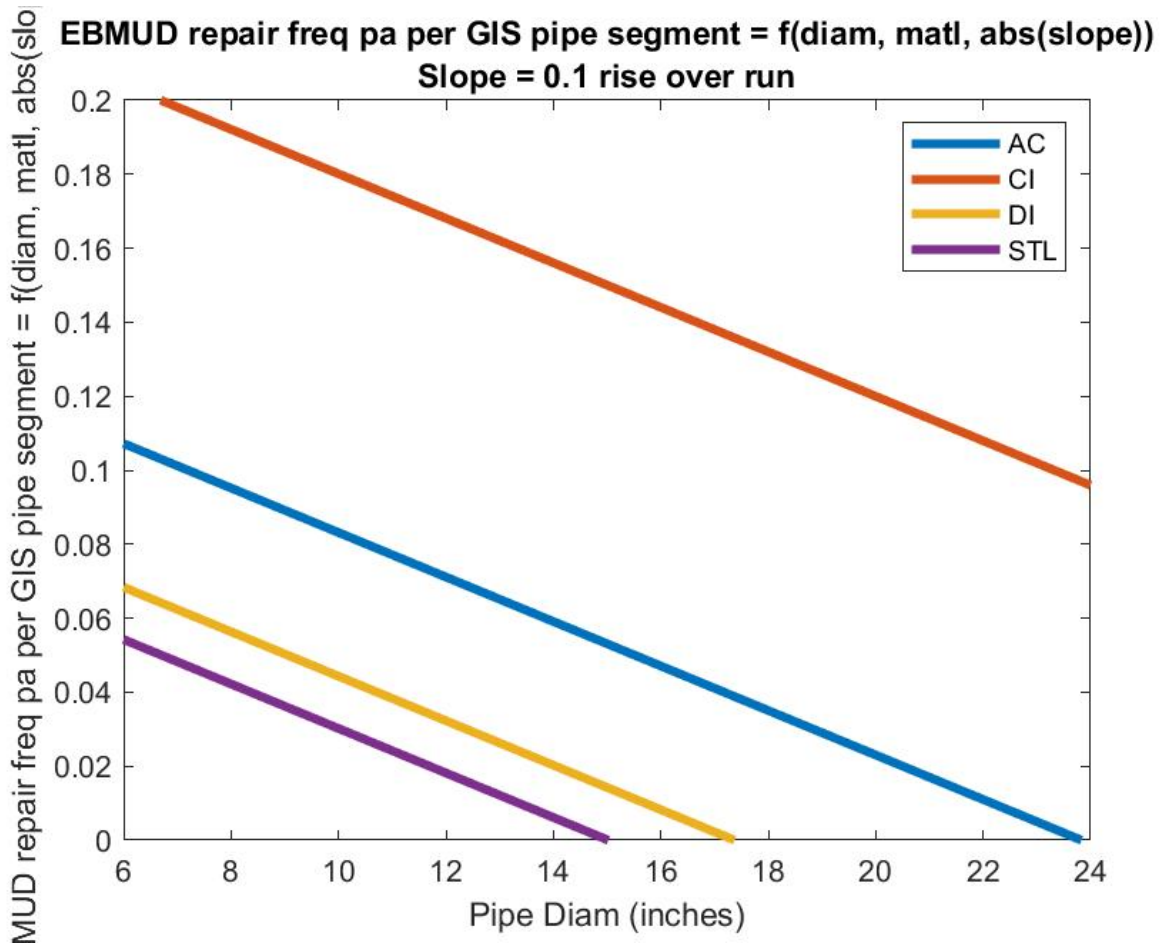


Figure 4-22. Leak Frequency per GIS Pipe Segment as a Function of Pipe Diameter, Material, and Slope, EBMUD Data.

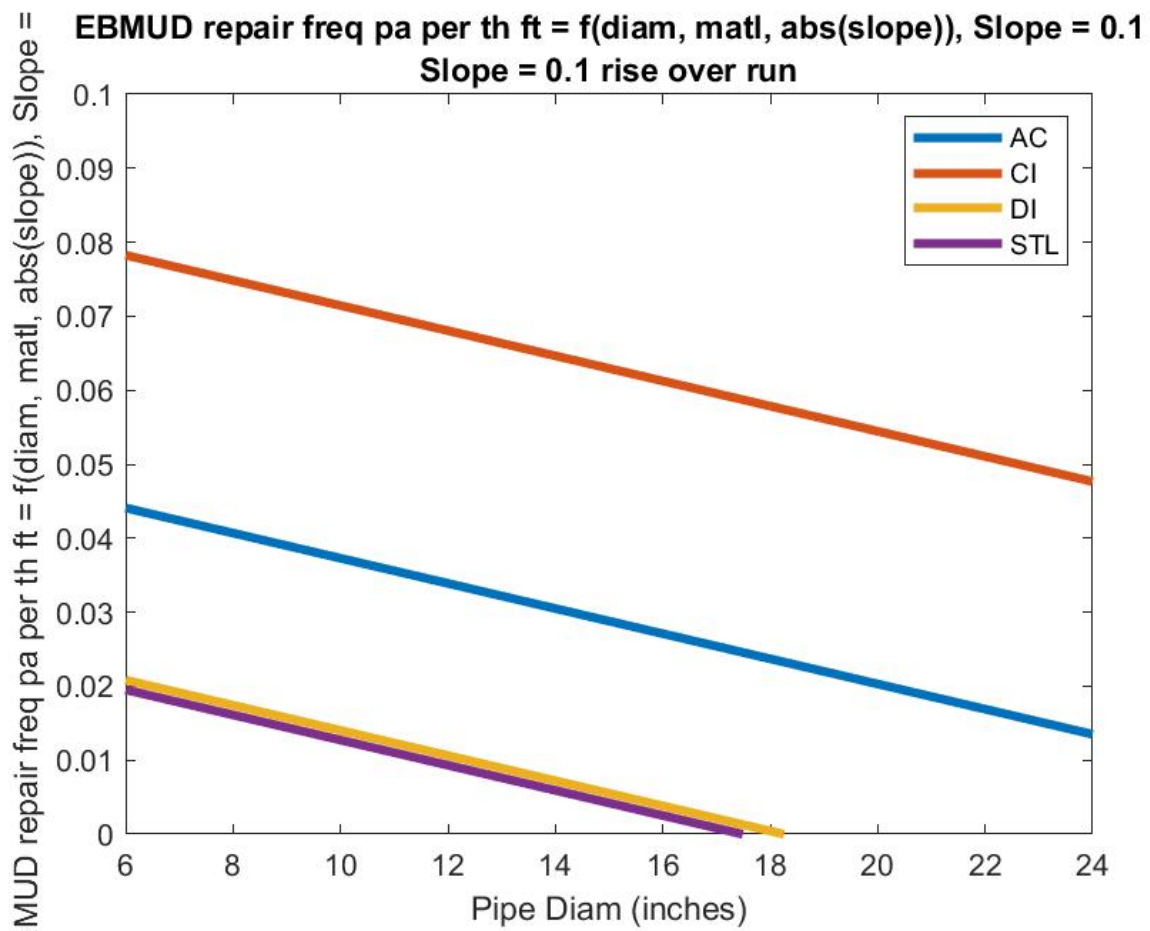


Figure 4-23. Leak Frequency per GIS Pipe Segment as a Function of Pipe Diameter, Material, and Slope, EBMUD Data.

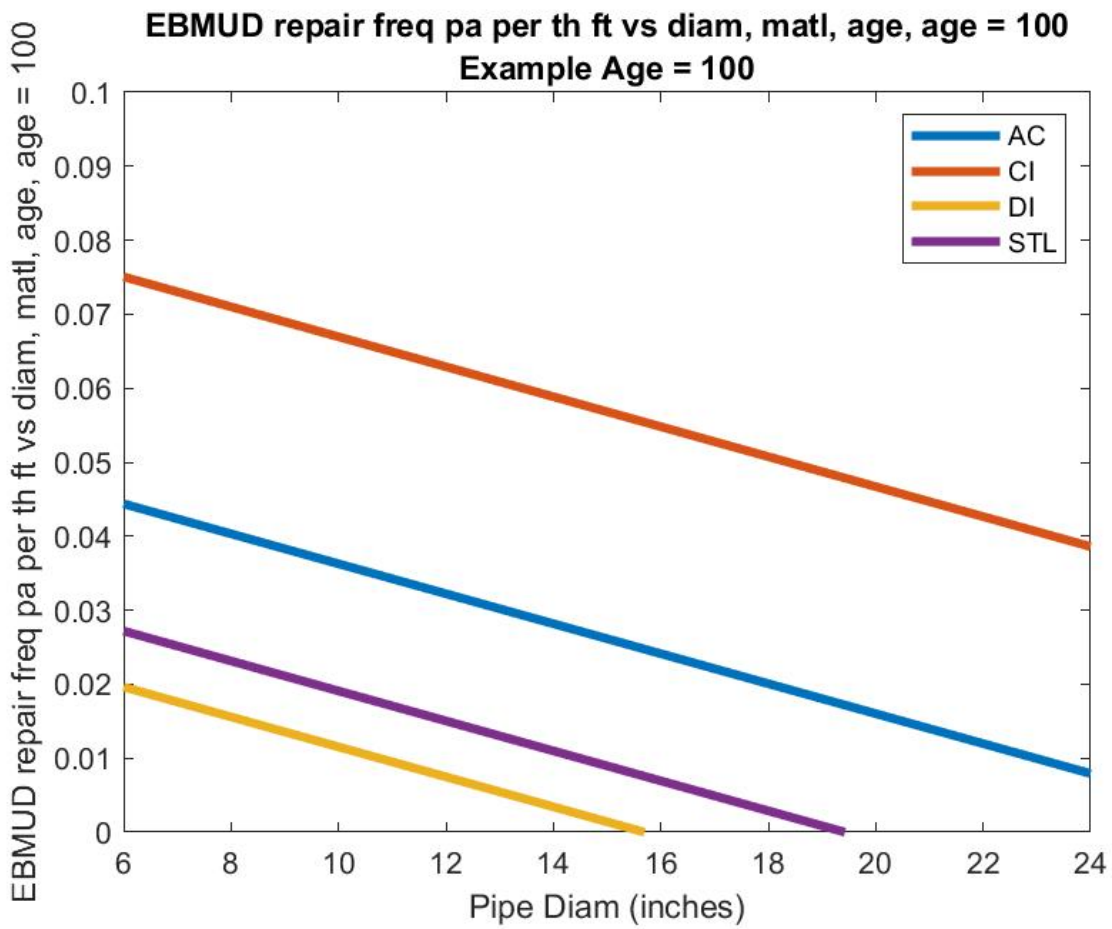


Figure 4-24. Repair Frequency per Thousand Feet of Pipe Considering Material, Age, and Diameter, Based on a Linear Model. Plot Is an Example for Pipe Age Equal to 100 Years, EBMUD Data.

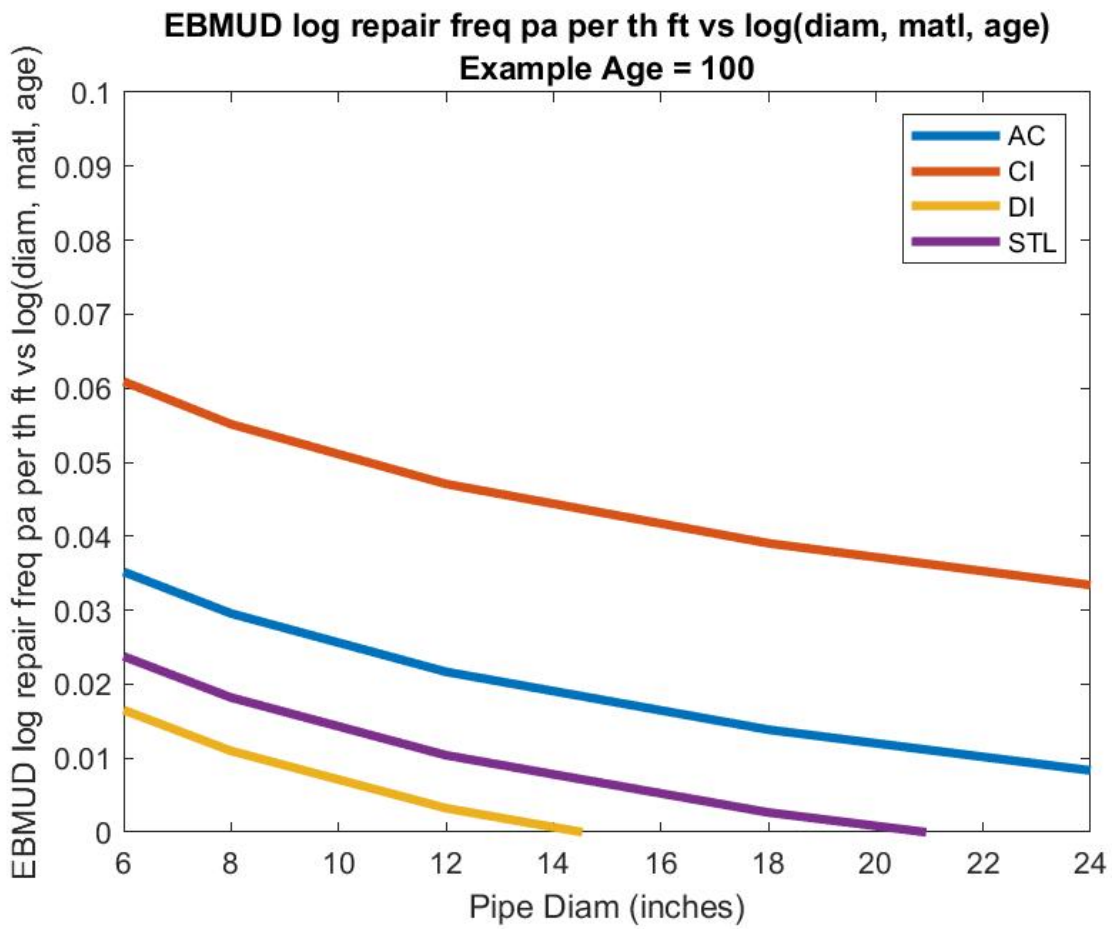


Figure 4-25. Repair Frequency per Thousand Feet of Pipe Considering Material, Age, and Diameter, Based on a Log-Log Model. Plot Is an Example for Pipe Age Equal to 100 Years, EBMUD Data.

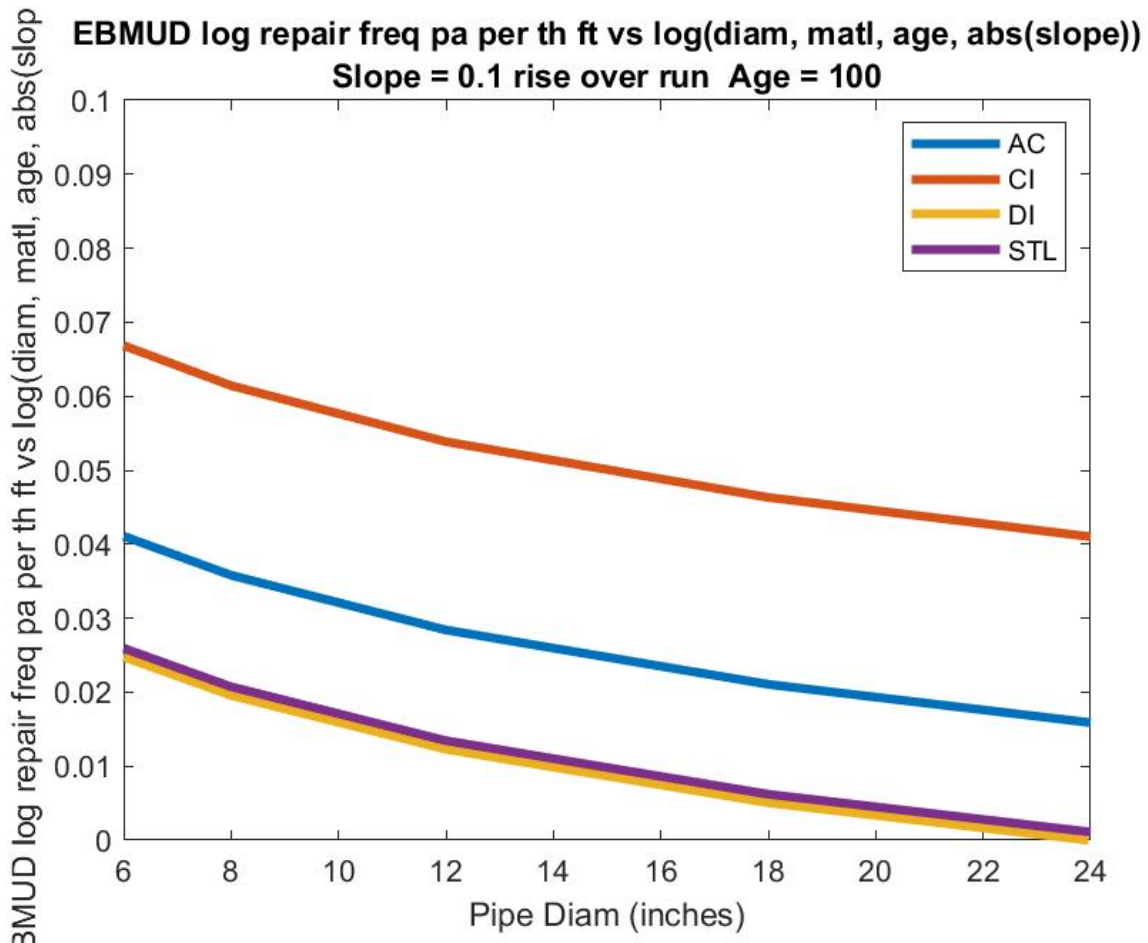


Figure 4-26. Repair Frequency per Thousand Feet of Pipe Considering Material, Age, Diameter, and Slope Parallel and Perpendicular to the Pipe’s Longitudinal Axis, Based on a Log-Log Model. Plot Is an Example for Pipe Age Equal to 100 Years, EBMUD Data.

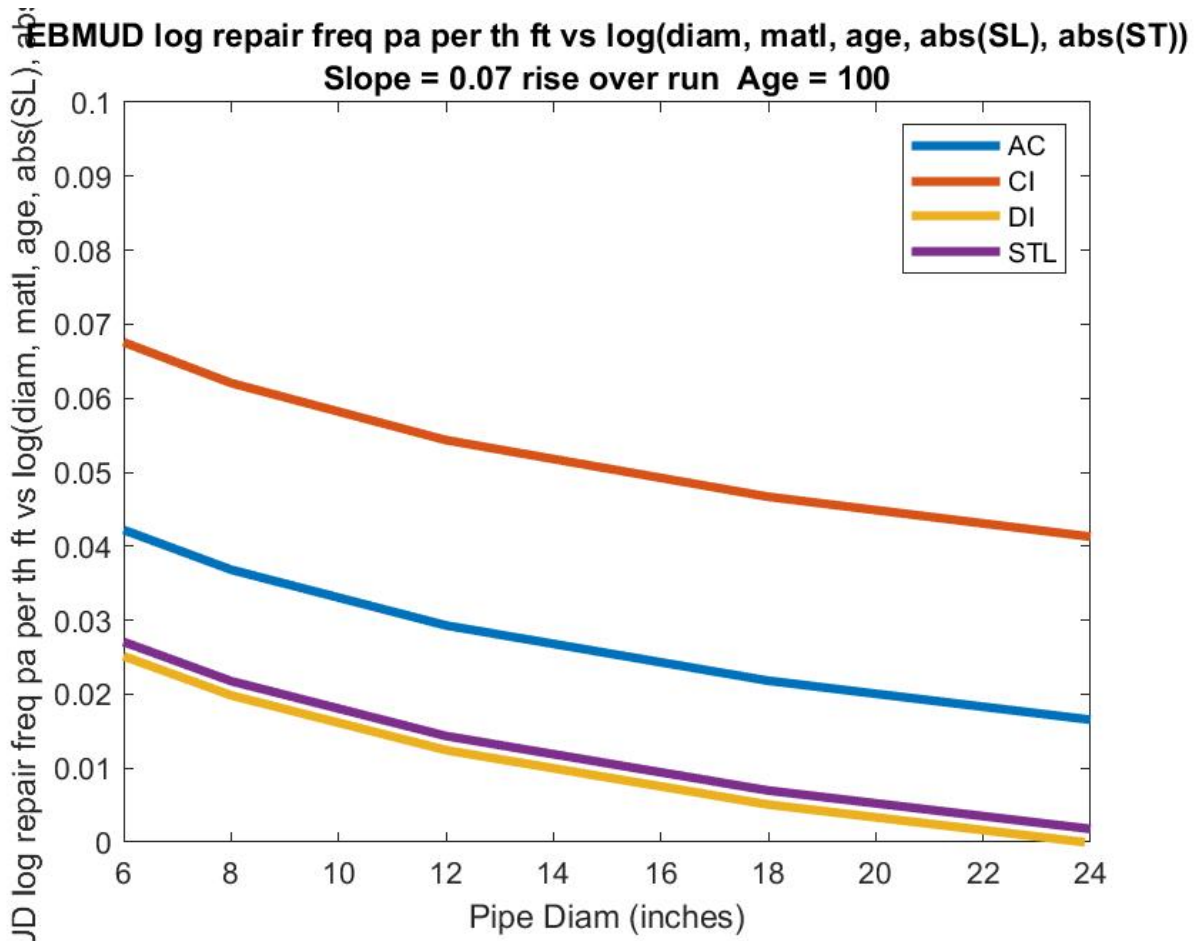


Figure 4-27. Repair Frequency per Thousand Feet of Pipe Considering Material, Age, Diameter, and Slope Parallel and Perpendicular to the Pipe's Longitudinal Axis, Based on a Log-Log Model. Plot Is an Example for Pipe Age Equal to 100 Years, EBMUD Data.

4.3.3 SFPUC

Comparable results for the SFPUC data set are provided below – similar comments apply, with results presented in Figure 4-29 to Figure 4-35 and Table 4-4:

Table 4-4. SFPUC Regression Coefficients for Seven Models.

Regression Coefficients	1. linear model: repair = f(diam, matl)	2. linear model: repair = f(diam, matl, slope)	3. linear model: repair/length = f(diam, matl, slope)	4. linear model: repair/length = f(diam, matl, age)	5. log-log model: $\ln(1 + \text{repair}/\text{length}) = f[\ln(\text{diam}, 1 + \text{matl}, \text{age})]$	6. log-log model: $\ln(1 + \text{repair}/\text{length}) = f[\ln(\text{diam}, 1 + \text{matl}, \text{age}, 1 + \text{slope})]$	7. log-log model: $\ln(1 + \text{repair}/\text{length}) = f[\ln(\text{diam}, 1 + \text{matl}, \text{age}, 1 + \text{SL}, 1 + \text{ST})]$
1	0.0773	0.0657	0.0017	0.0116	0.0129	0.0028	0.0032
2	-0.0016	-0.0014	0.0001	0.0000	-0.0008	0.0010	0.0010
3	-0.0772	-0.0656	-0.0018	-0.0116	-0.0212	-0.0006	-0.0014
4	0.0139	0.0155	0.0062	0.0078	0.0058	0.0074	0.0074
5	-0.0206	-0.0173	-0.0026	-0.0060	-0.0075	-0.0044	-0.0046
6	-0.0011	-0.0035	-0.0027	-0.0008	-0.0009	-0.0027	-0.0027
7		0.1334	0.0848	-0.0001	-0.0008	-0.0006	-0.0006
8						0.0758	0.0486
9							0.0677

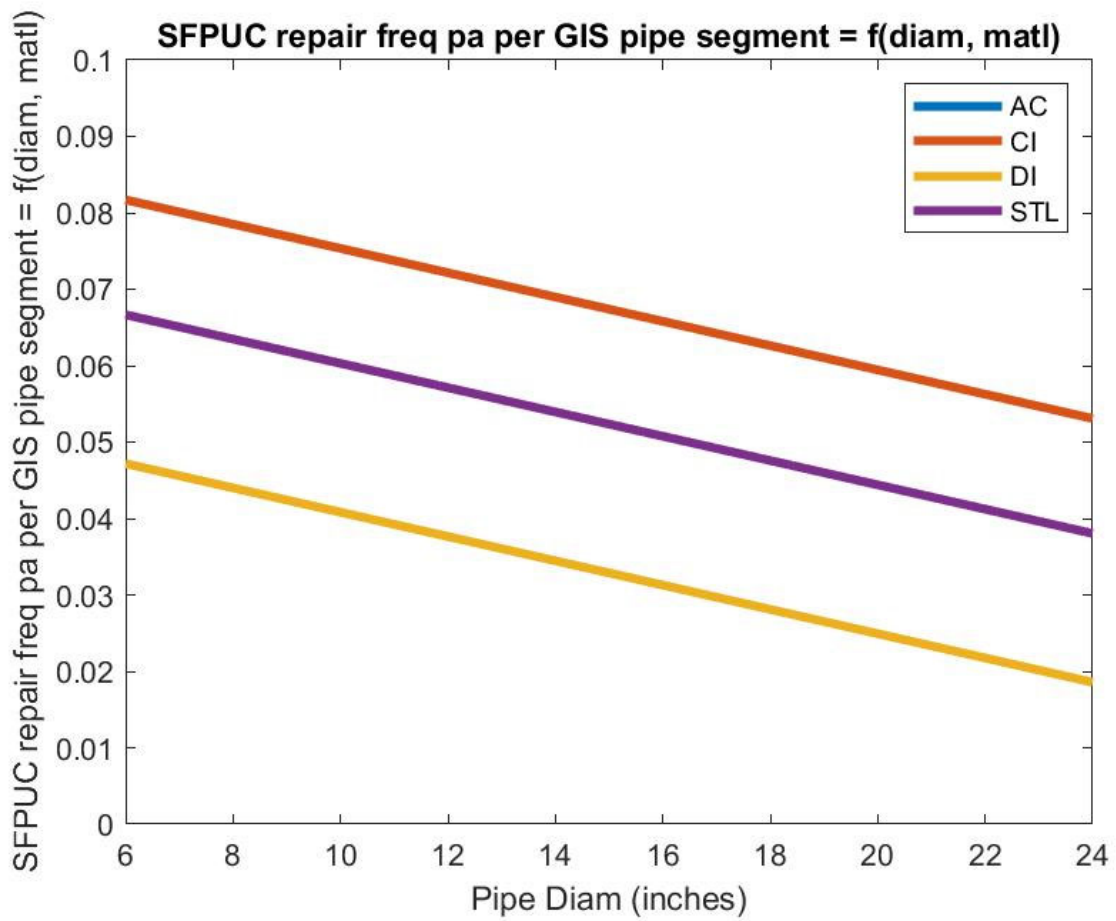


Figure 4-28. Raw Leak Frequency per GIS Pipe Segment, by Material and Diameter, SFPUC Data.

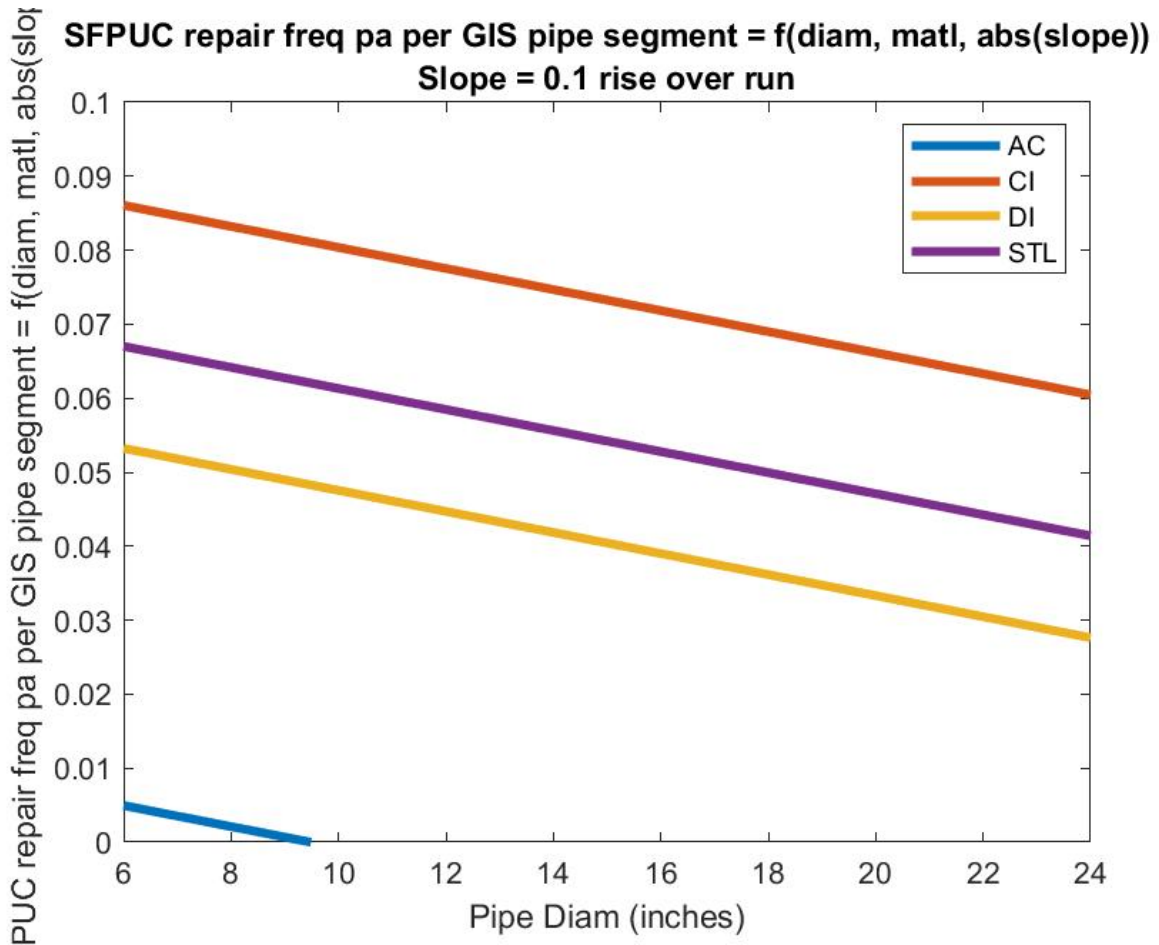


Figure 4-29. Leak Frequency per GIS Pipe Segment as a Function of Pipe Diameter, Material, and Slope, SFPUC Data.

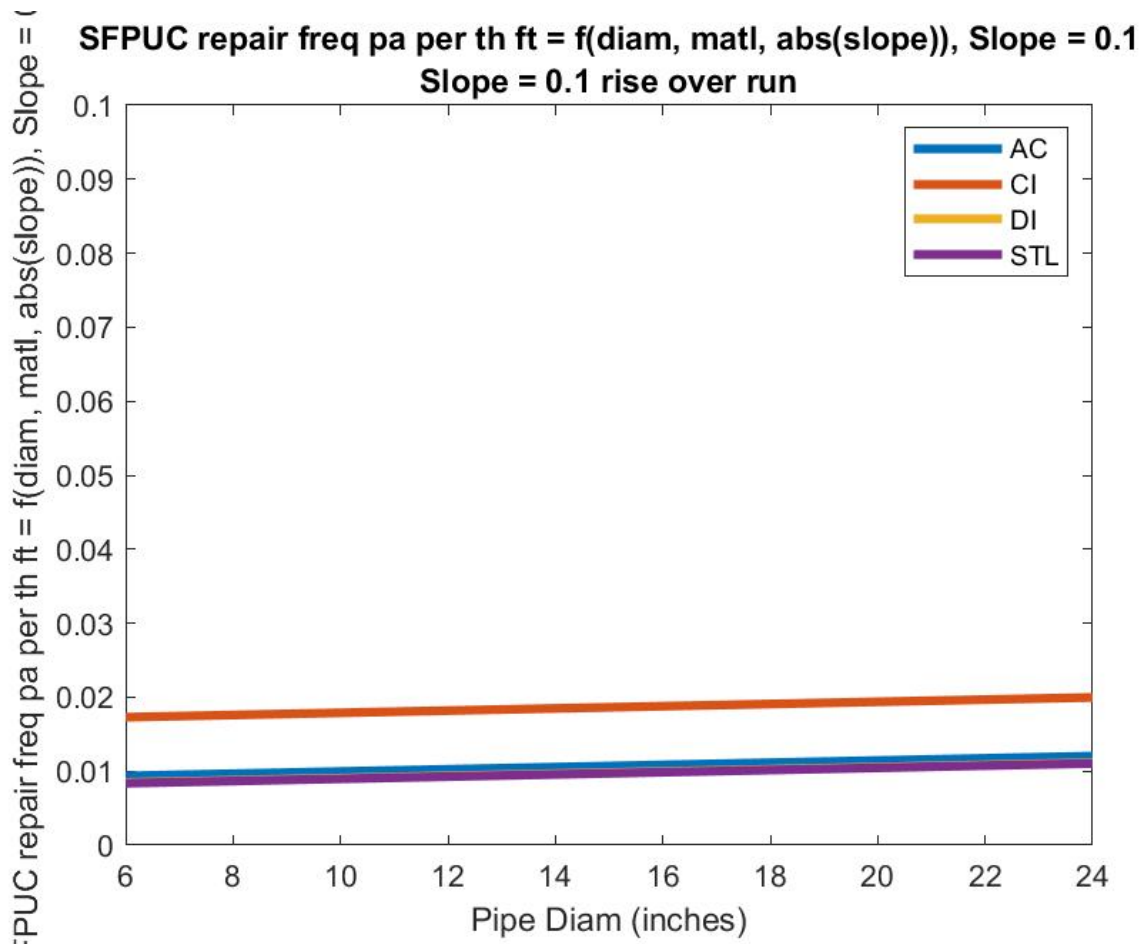


Figure 4-30. Leak Frequency per GIS Pipe Segment as a Function of Pipe Diameter, Material, and Slope, SFPUC Data.

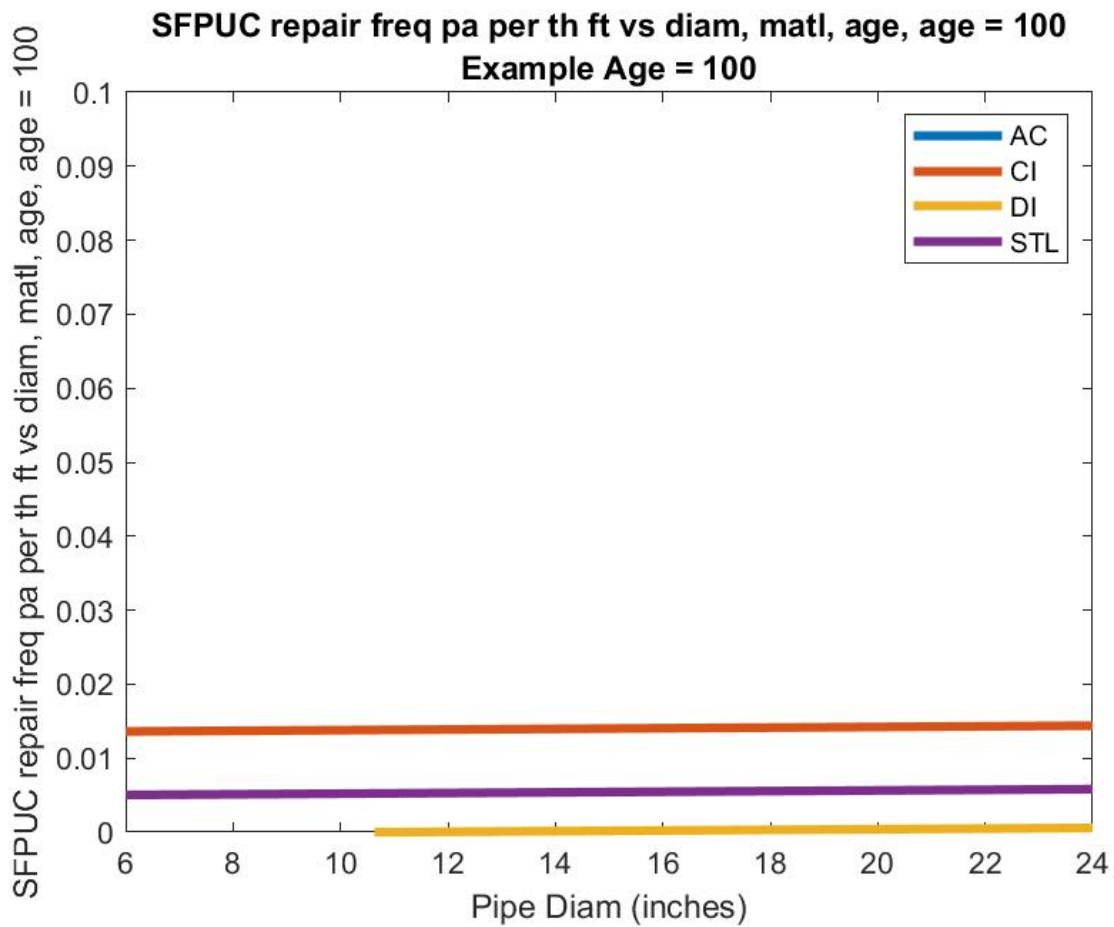


Figure 4-31. Repair Frequency per Thousand Feet of Pipe Considering Material, Age, and Diameter, Based on a Linear Model. Plot Is an Example for Pipe Age Equal to 100 Years, SFPUC Data.

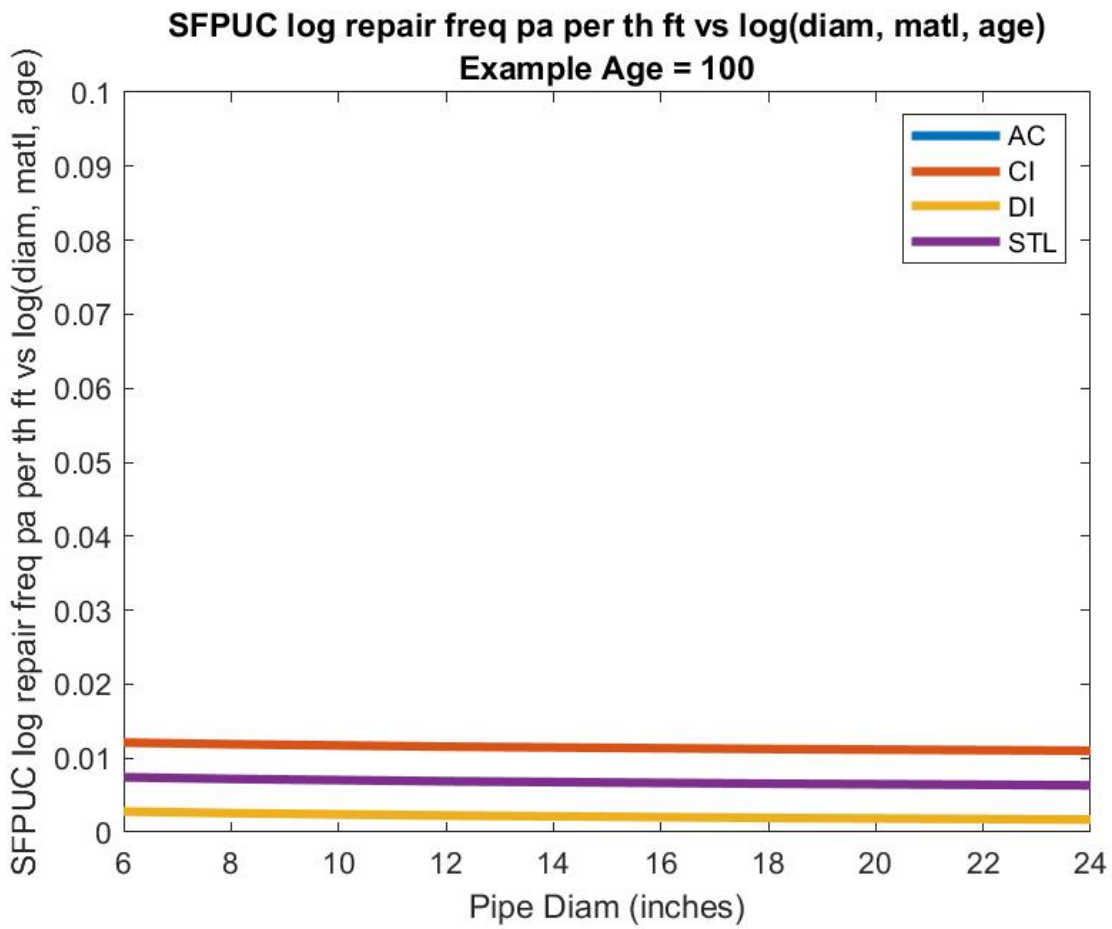


Figure 4-32. Repair Frequency per Thousand Feet of Pipe Considering Material, Age, and Diameter, Based on a Log-Log Model. Plot Is an Example for Pipe Age Equal to 100 Years, SFPUC Data.

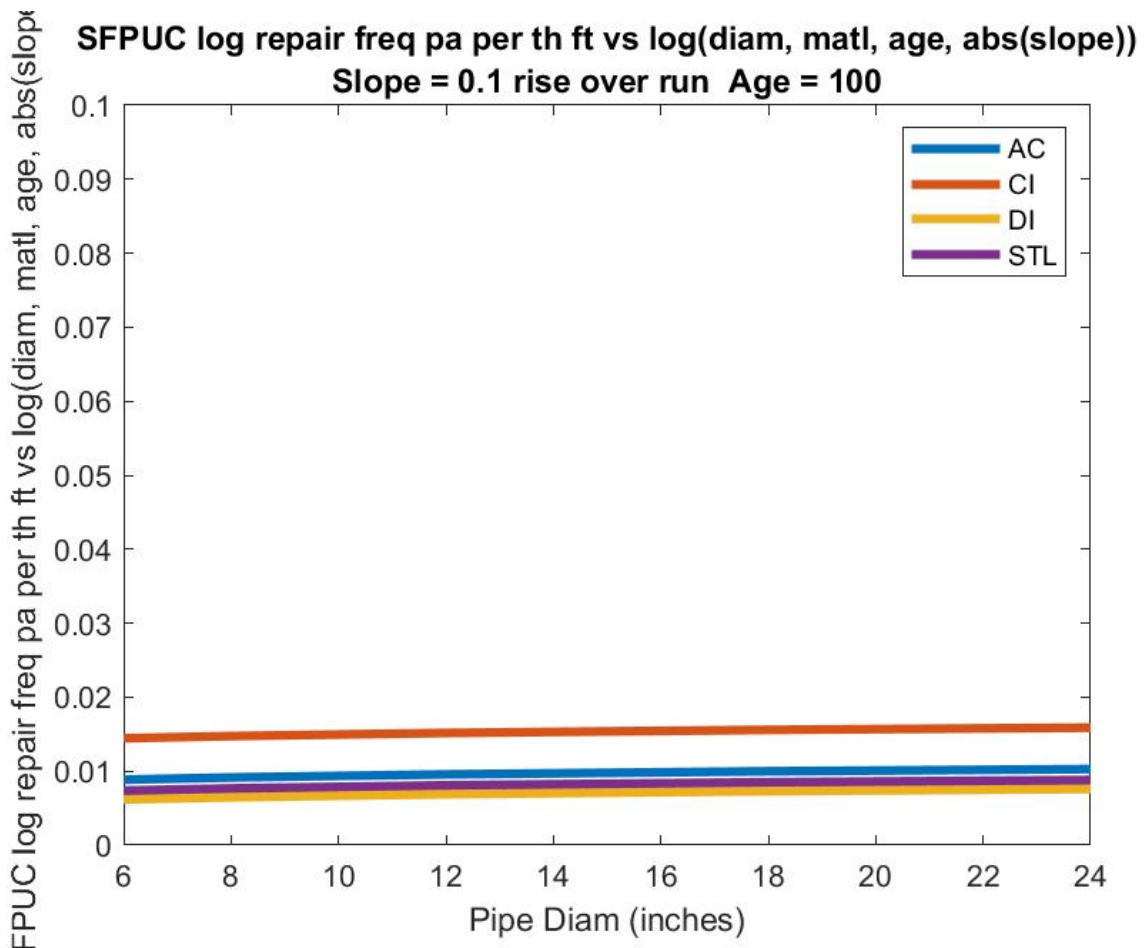


Figure 4-33. Repair Frequency per Thousand Feet of Pipe Considering Material, Age, Diameter, and Slope Parallel and Perpendicular to the Pipe's Longitudinal Axis, Based on a Log-Log Model. Plot Is an Example for Pipe Age Equal to 100 Years, SFPUC Data.

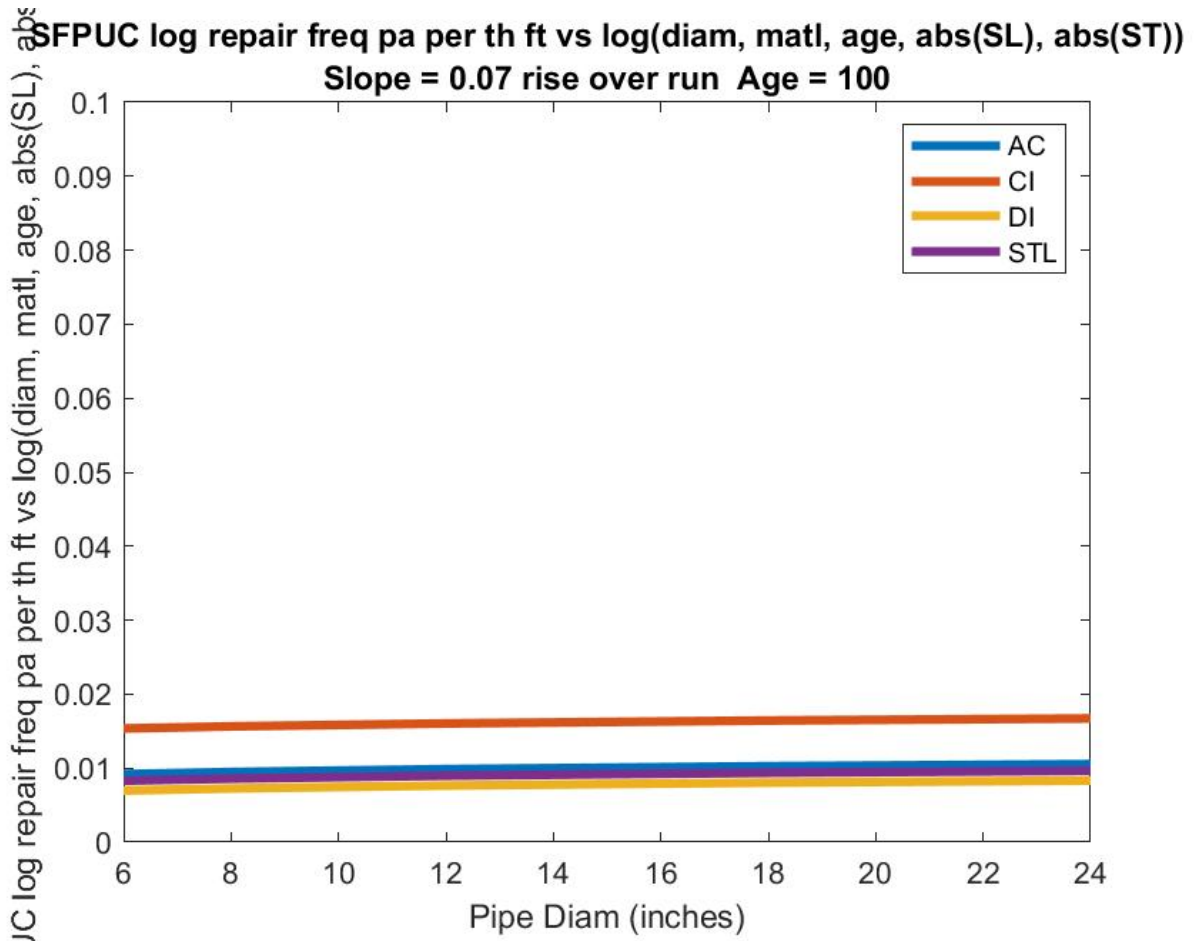


Figure 4-34. Repair Frequency per Thousand Feet of Pipe Considering Material, Age, Diameter, and Slope Parallel and Perpendicular to the Pipe's Longitudinal Axis, Based on a Log-Log Model. Plot Is an Example for Pipe Age Equal to 100 Years, SFPUC Data.

4.3.4 PWB

Comparable results for the PWB data set are provided below – similar comments apply, with results presented in Figure 4-36 to Figure 4-42 and Table 4-5:

Table 4-5. PWB Regression Coefficients for Seven Models.

Regression Coefficients	1. linear model: repair = f(diam, matl)	2. linear model: repair = f(diam, matl, slope)	3. linear model: repair/length = f(diam, matl, slope)	4. linear model: repair/length = f(diam, matl, age)	5. log-log model: $\ln(1 + \text{repair}/\text{length}) = f[\ln(\text{diam}, 1 + \text{matl}, \text{age})]$	6. log-log model: $\ln(1 + \text{repair}/\text{length}) = f[\ln(\text{diam}, 1 + \text{matl}, \text{age}, 1 + \text{slope})]$	7. log-log model: $\ln(1 + \text{repair}/\text{length}) = f[\ln(\text{diam}, 1 + \text{matl}, \text{age}, 1 + \text{SL}, 1 + \text{ST})]$
1	0.0106	0.0085	0.0007	0.0032	0.0034	0.0023	0.0025
2	-0.0008	-0.0008	-0.0001	-0.0001	-0.0020	-0.0019	-0.0019
3	-0.0054	-0.0042	-0.0007				
4	0.0124	0.0132	0.0055	0.0095	0.0085	0.0094	0.0091
5	-0.0019	-0.0017	-0.0005	-0.0011	0.0008	0.0009	0.0007
6	0.0585	0.0604	0.0153	0.0149	0.0171	0.0176	0.0170
7		0.0290	0.0169	-0.0001	0.0002	0.0001	0.0001
8						0.0169	0.0042
9							0.0194

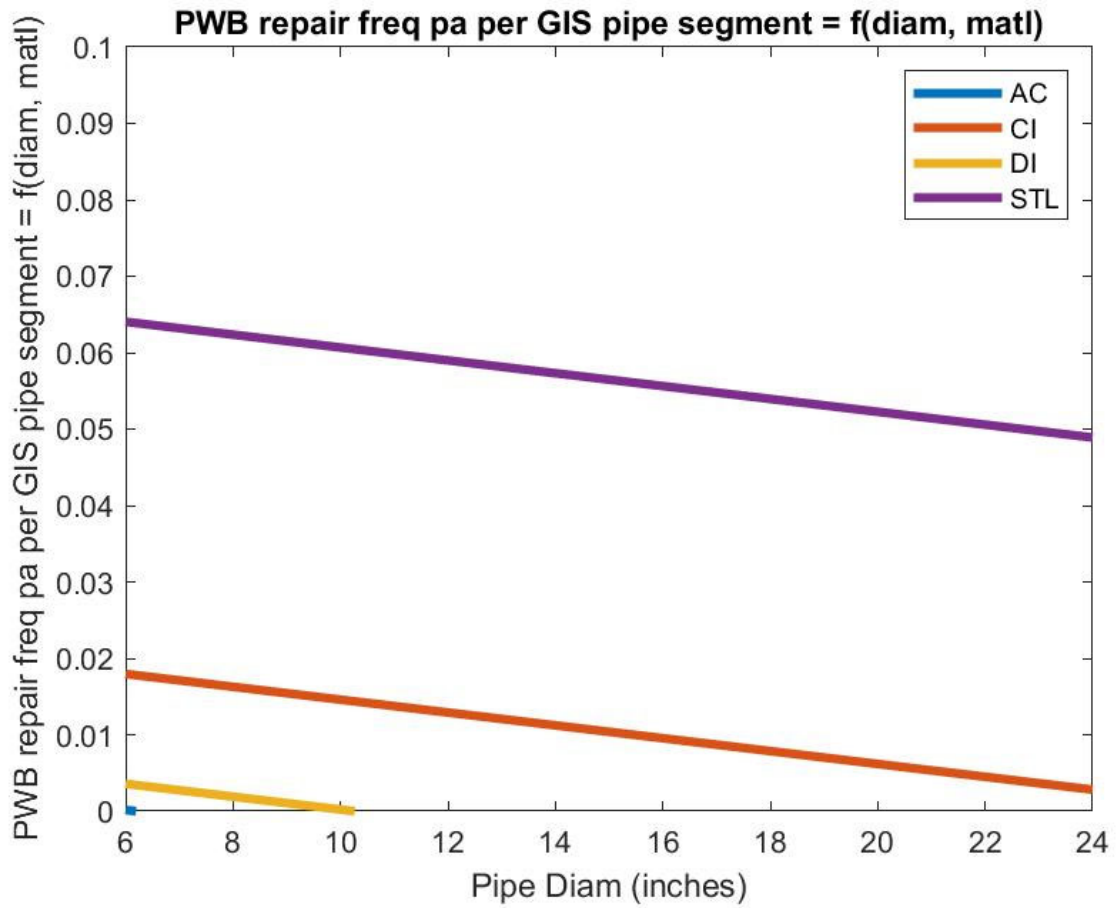


Figure 4-35. Raw Leak Frequency per GIS Pipe Segment, by Material and Diameter, PWB Data.

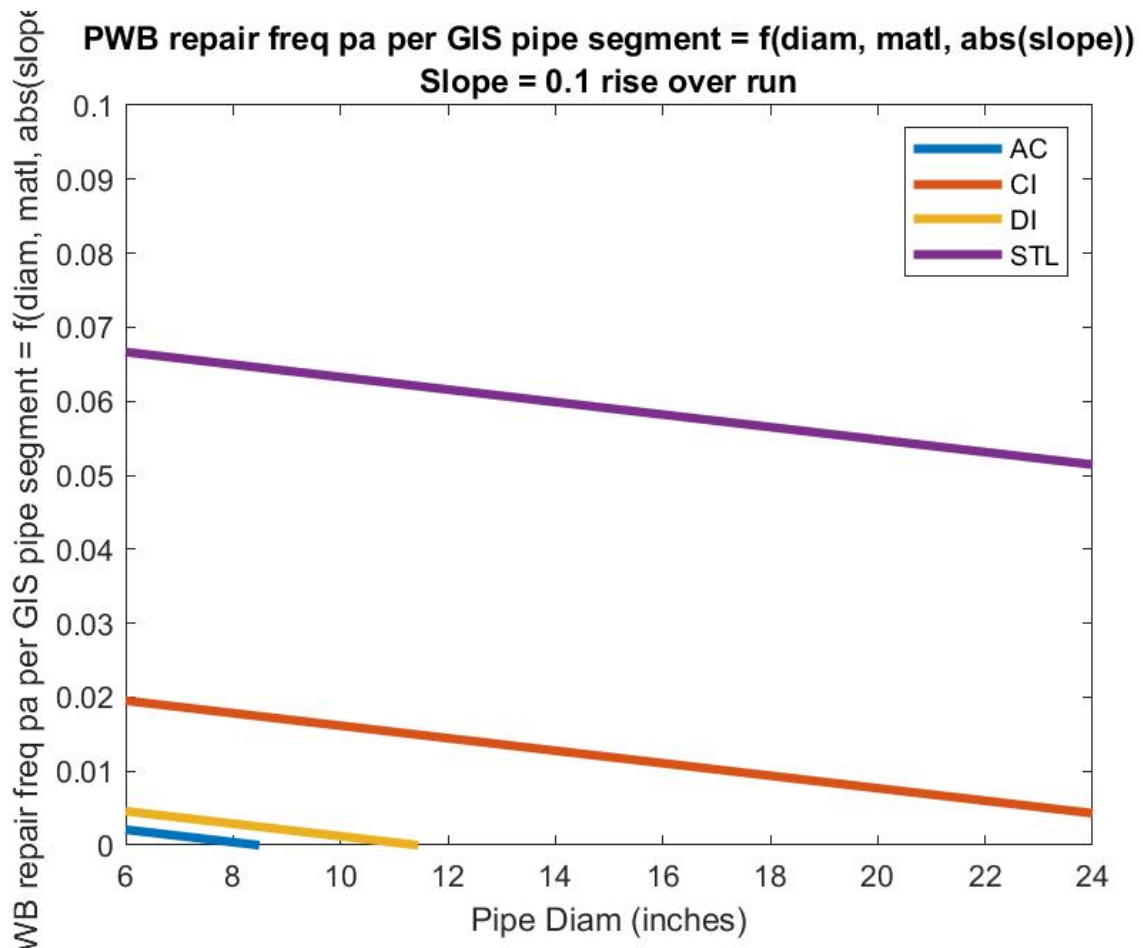


Figure 4-36. Leak Frequency per GIS Pipe Segment as a Function of Pipe Diameter, Material, and Slope, PWB Data.

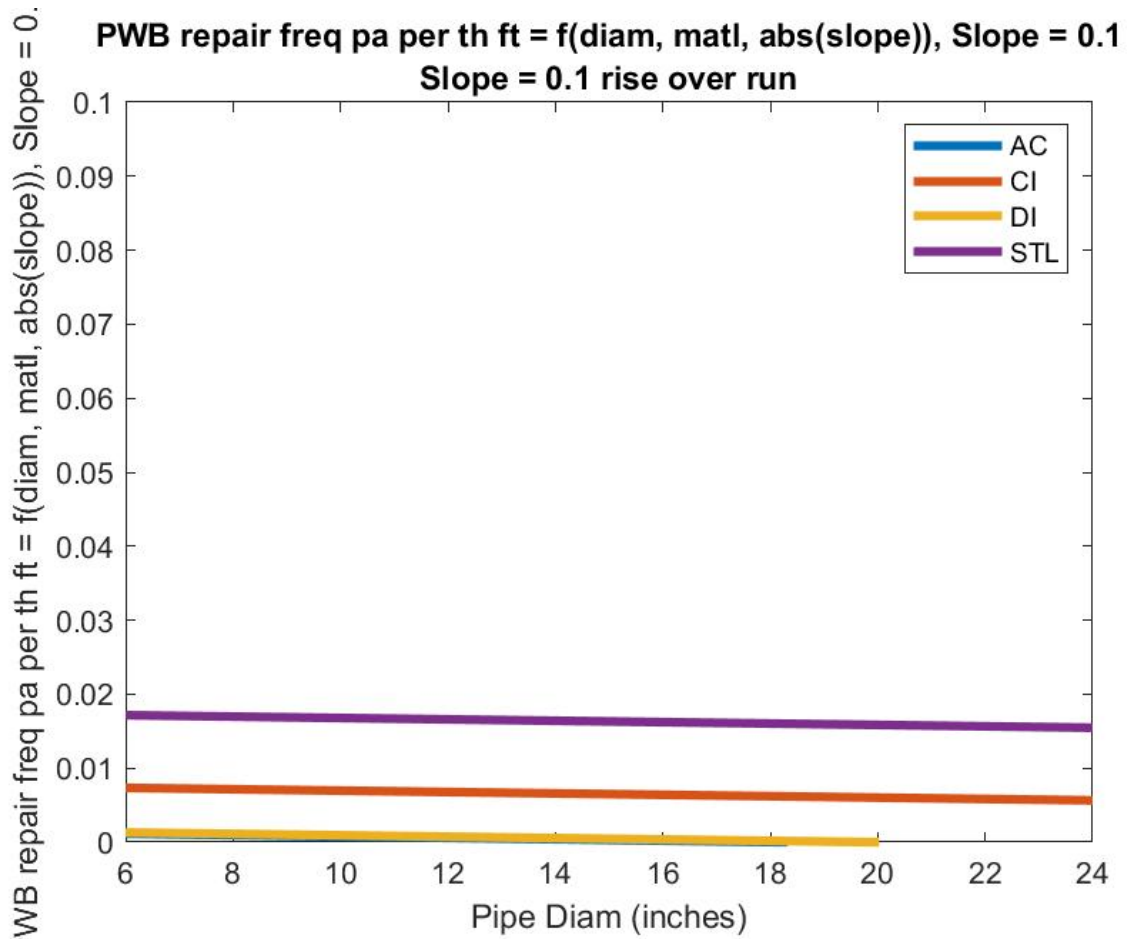


Figure 4-37. Leak Frequency per GIS Pipe Segment as a Function of Pipe Diameter, Material, and Slope, PWB Data.

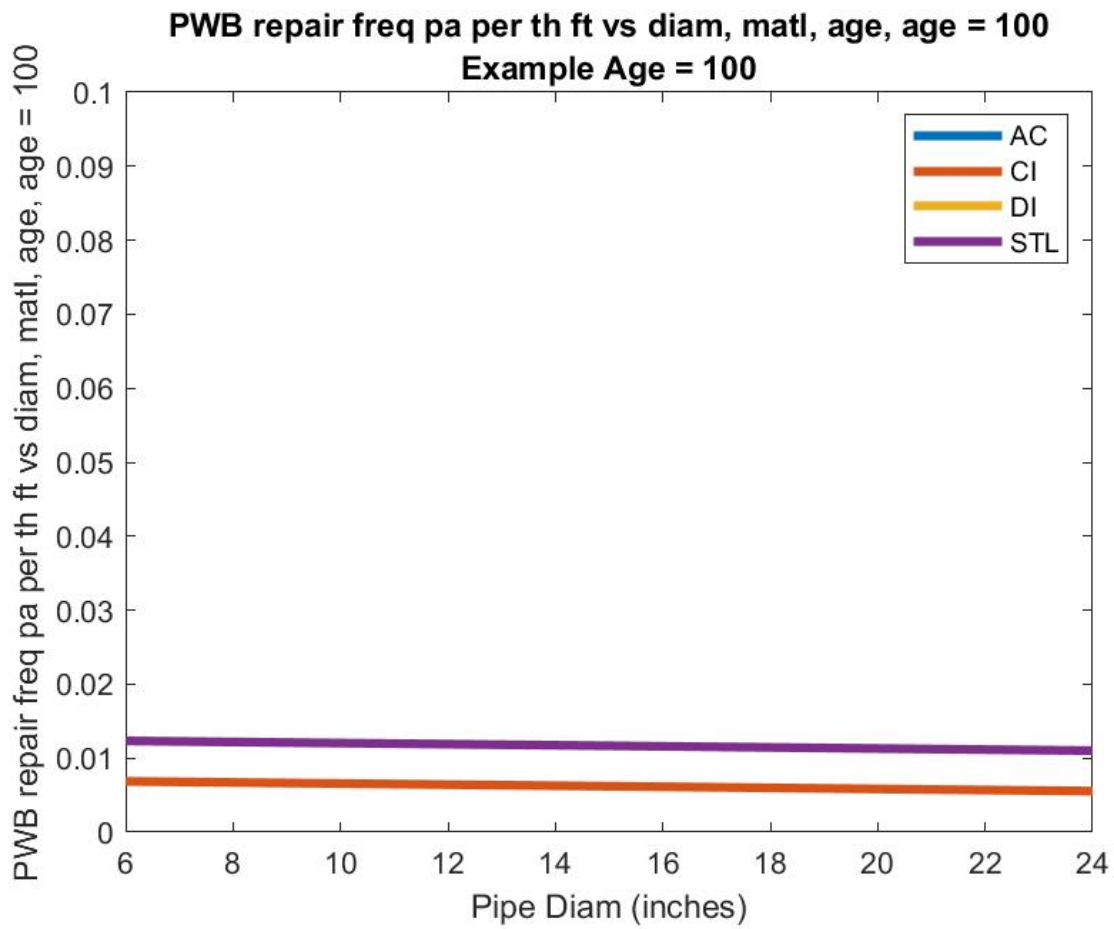


Figure 4-38. Repair Frequency per Thousand Feet of Pipe Considering Material, Age, and Diameter, Based on a Linear Model. Plot Is an Example for Pipe Age Equal to 100 Years, PWB Data.

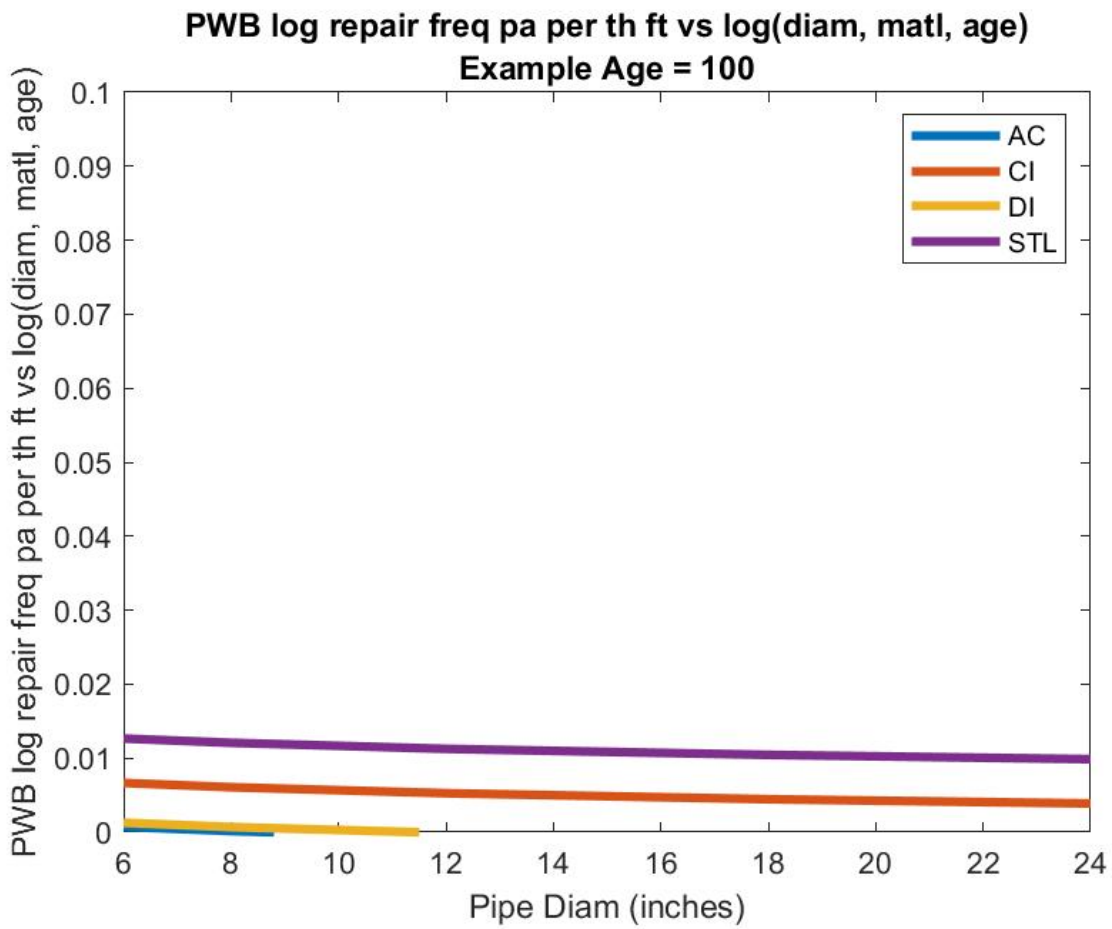


Figure 4-39. Repair Frequency per Thousand Feet of Pipe Considering Material, Age, and Diameter, Based on a Log-Log Model. Plot Is an Example for Pipe Age Equal to 100 Years, PWB Data.

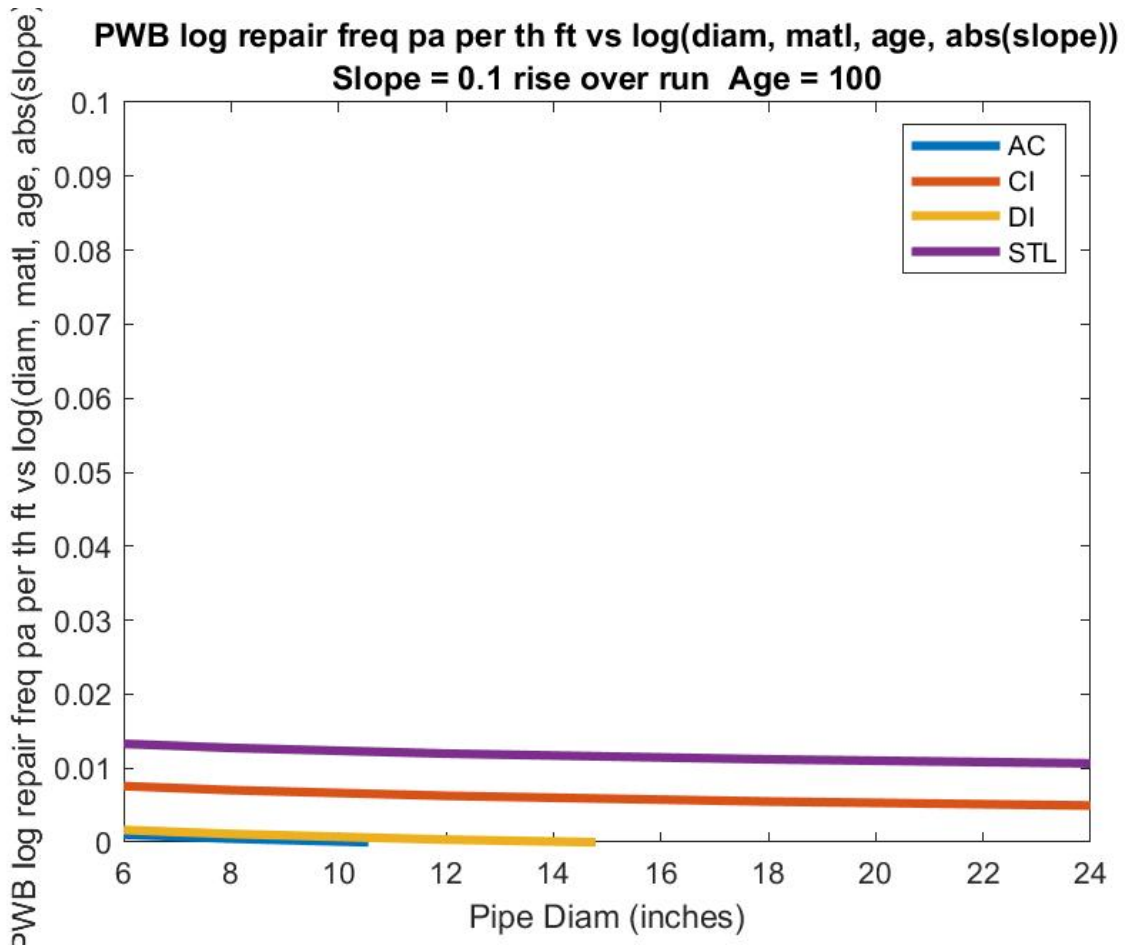


Figure 4-40. Repair Frequency per Thousand Feet of Pipe Considering Material, Age, Diameter, and Slope Parallel and Perpendicular to the Pipe's Longitudinal Axis, Based on a Log-Log Model. Plot Is an Example for Pipe Age Equal to 100 Years, PWB Data.

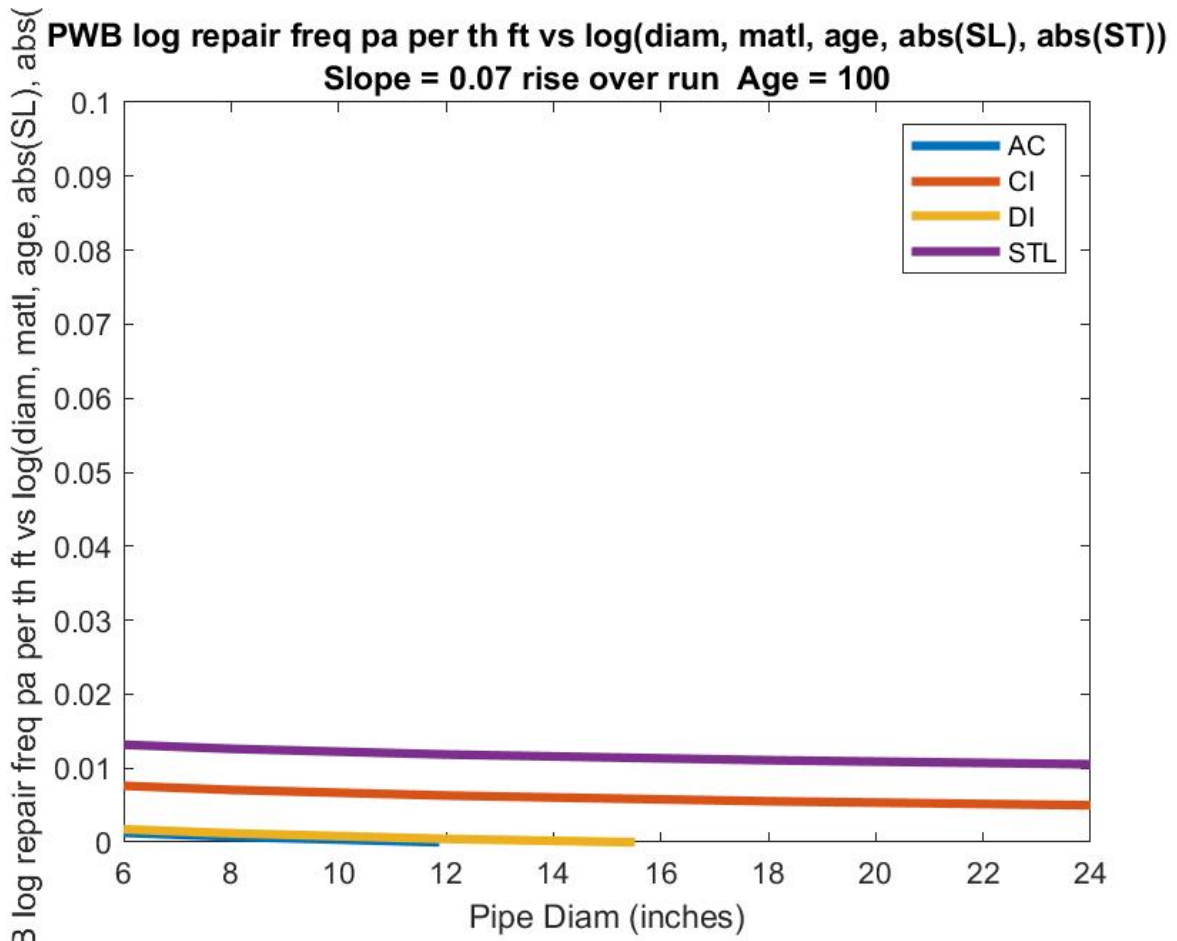


Figure 4-41. Repair Frequency per Thousand Feet of Pipe Considering Material, Age, Diameter, and Slope Parallel and Perpendicular to the Pipe's Longitudinal Axis, Based on a Log-Log Model. Plot Is an Example for Pipe Age Equal to 100 Years, PWB Data.

4.3.5 SPU

Comparable results for the SPU data set are provided below – similar comments apply, with results presented in Figure 4-43 to Figure 4-49 and Table 4-6:

Table 4-6. SPU Regression Coefficients for Seven Models.

Regression Coefficients	1. linear model: repair = f(diam, matl)	2. linear model: repair = f(diam, matl, slope)	3. linear model: repair/length = f(diam, matl, slope)	4. linear model: repair/length = f(diam, matl, age)	5. log-log model: $\ln(1 + \text{repair}/\text{length}) = f[\ln(\text{diam}, 1 + \text{matl}, \text{age})]$	6. log-log model: $\ln(1 + \text{repair}/\text{length}) = f[\ln(\text{diam}, 1 + \text{matl}, \text{age}, 1 + \text{slope})]$	7. log-log model: $\ln(1 + \text{repair}/\text{length}) = f[\ln(\text{diam}, 1 + \text{matl}, \text{age}, 1 + \text{SL}, 1 + \text{ST})]$
1	0.1713	0.1713	0.0203	0.0179	0.0104	0.0104	0.0104
2	0.0006	0.0006	0.0002	0.0002	0.0014	0.0014	0.0014
3	-0.1713	-0.1714	-0.0203	-0.0181	-0.0129	-0.0128	-0.0128
4	-0.1199	-0.1199	-0.0153	-0.0155	-0.0199	-0.0199	-0.0199
5	-0.1680	-0.1680	-0.0207	-0.0208	-0.0267	-0.0267	-0.0267
6	-0.0328	-0.0327	-0.0034	-0.0030	-0.0041	-0.0041	-0.0041
7					0.0016	0.0016	0.0016
8						0.0001	-0.0022
9							0.0022

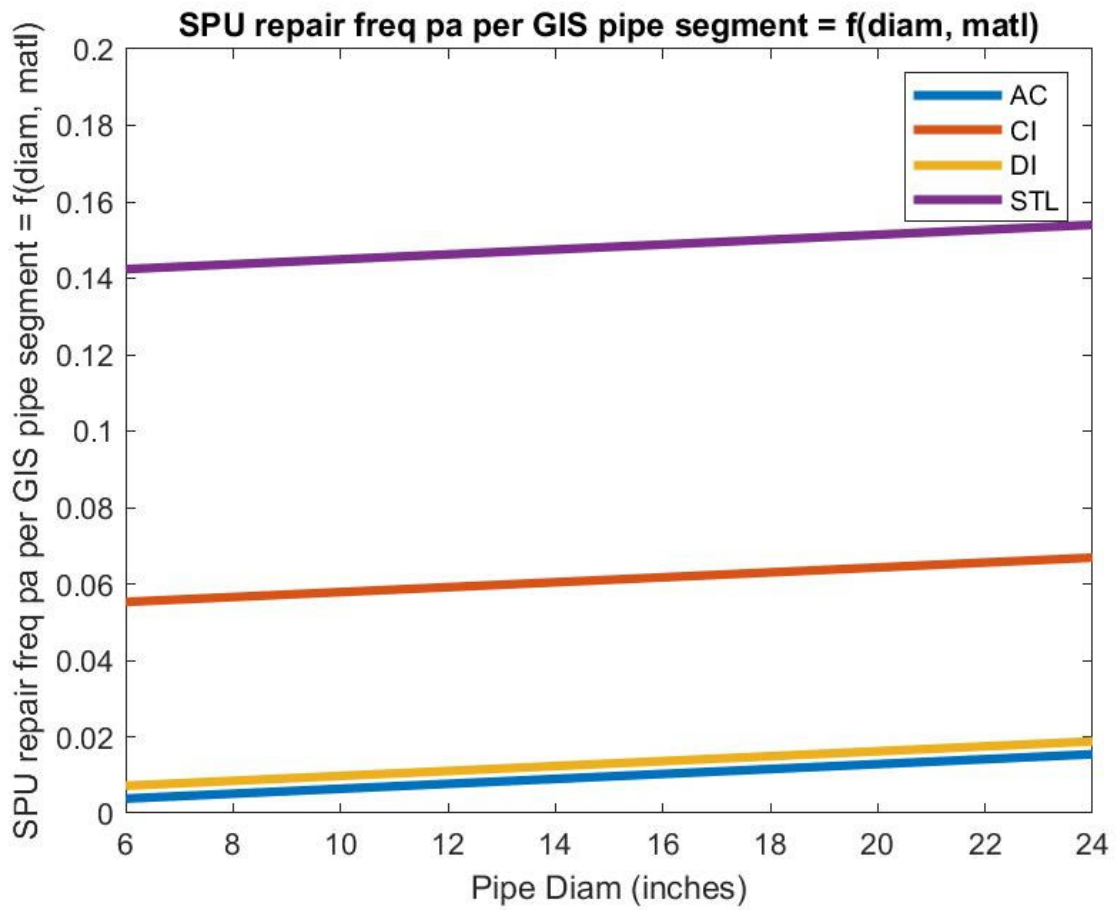


Figure 4-42. Raw Leak Frequency per GIS Pipe Segment, by Material and Diameter, SPU Data.

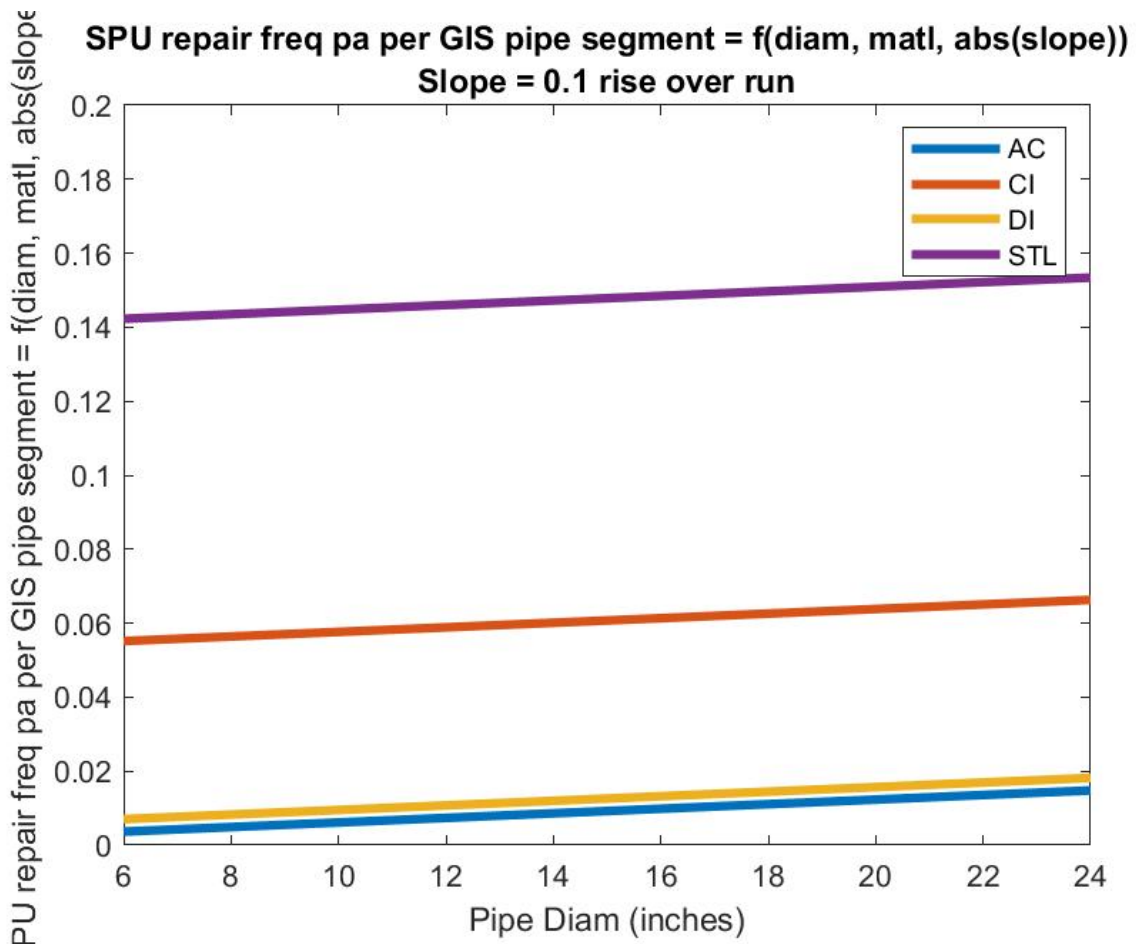


Figure 4-43. Leak Frequency per GIS Pipe Segment as a Function of Pipe Diameter, Material, and Slope, SPU Data.

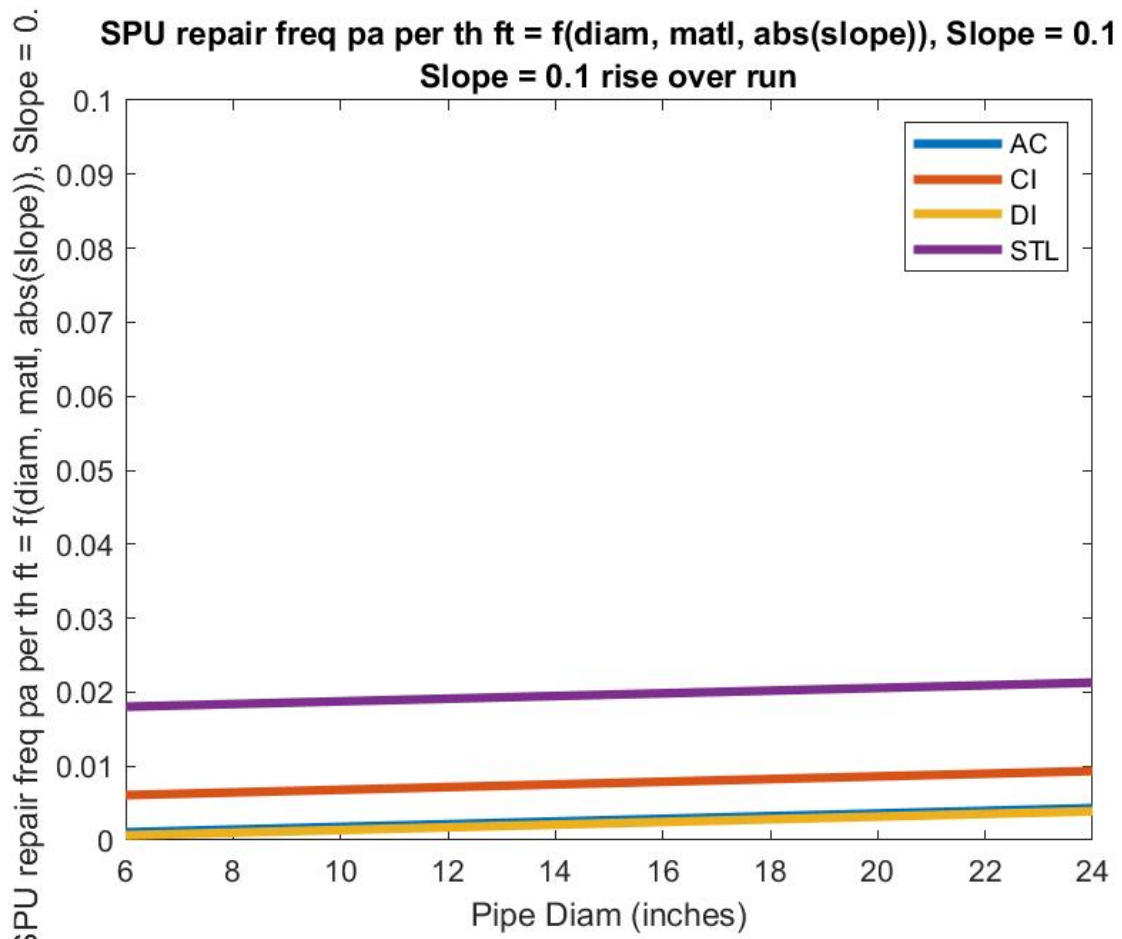


Figure 4-44. Leak Frequency per GIS Pipe Segment as a Function of Pipe Diameter, Material, and Slope, SPU Data.

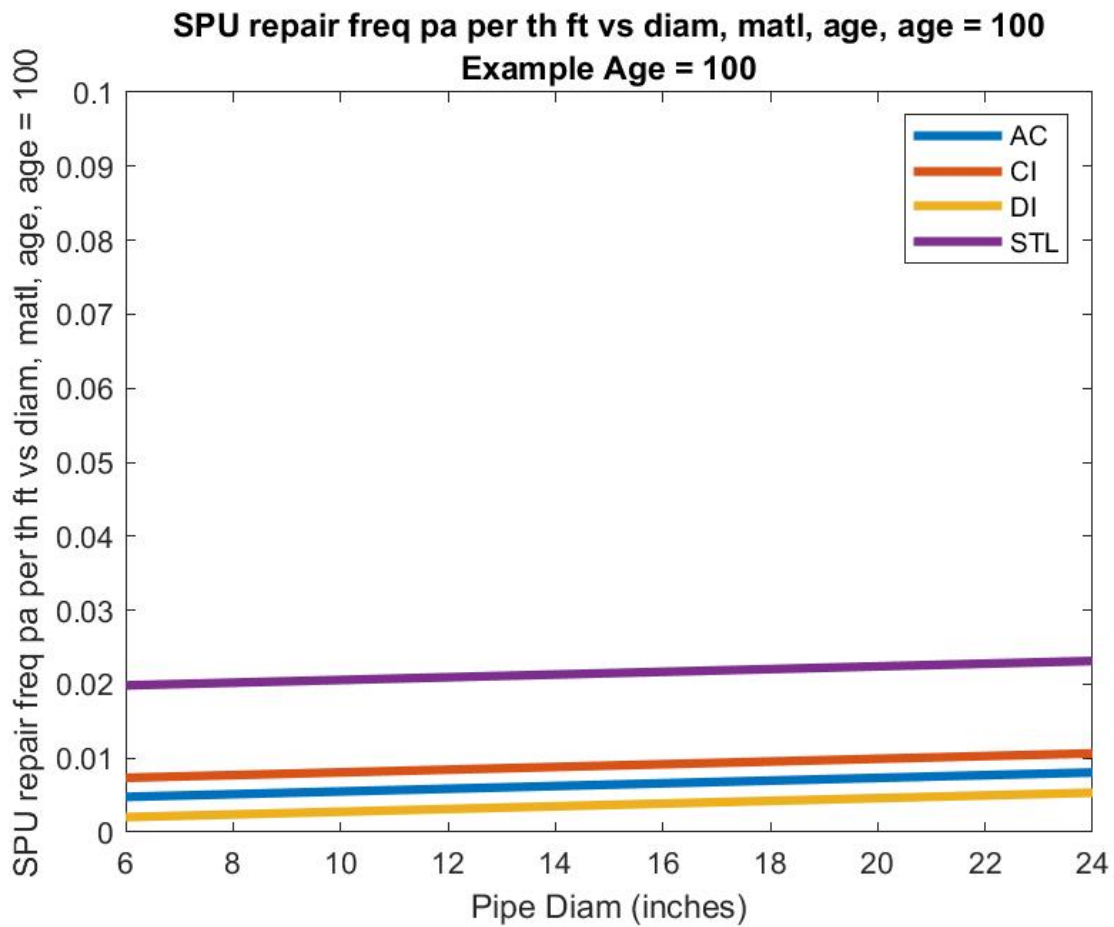


Figure 4-45. Repair Frequency per Thousand Feet of Pipe Considering Material, Age, and Diameter, Based on a Linear Model. Plot Is an Example for Pipe Age Equal to 100 Years, SPU Data.

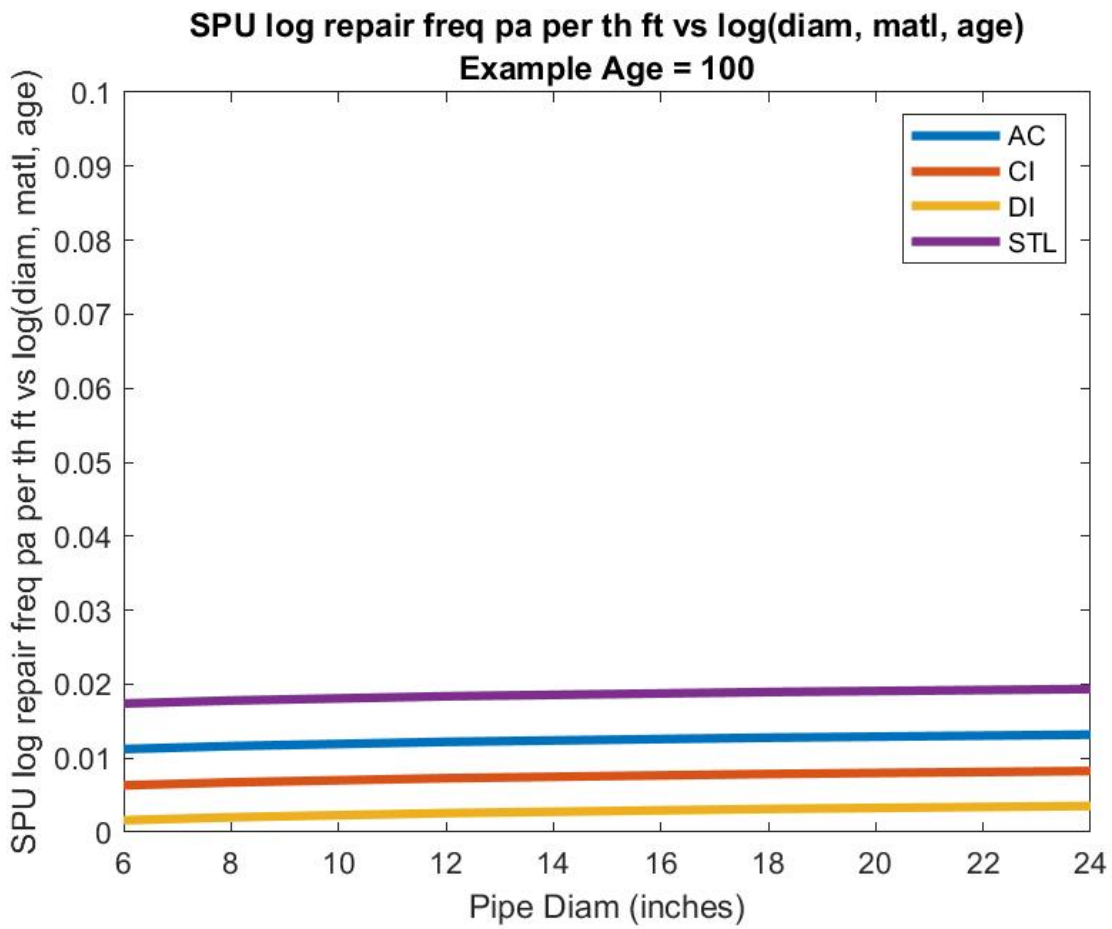


Figure 4-46. Repair Frequency per Thousand Feet of Pipe considering Material, Age and Diameter, Based on a Log-Log Model. Plot Is an Example for Pipe Age Equal to 100 Years, SPU Data.

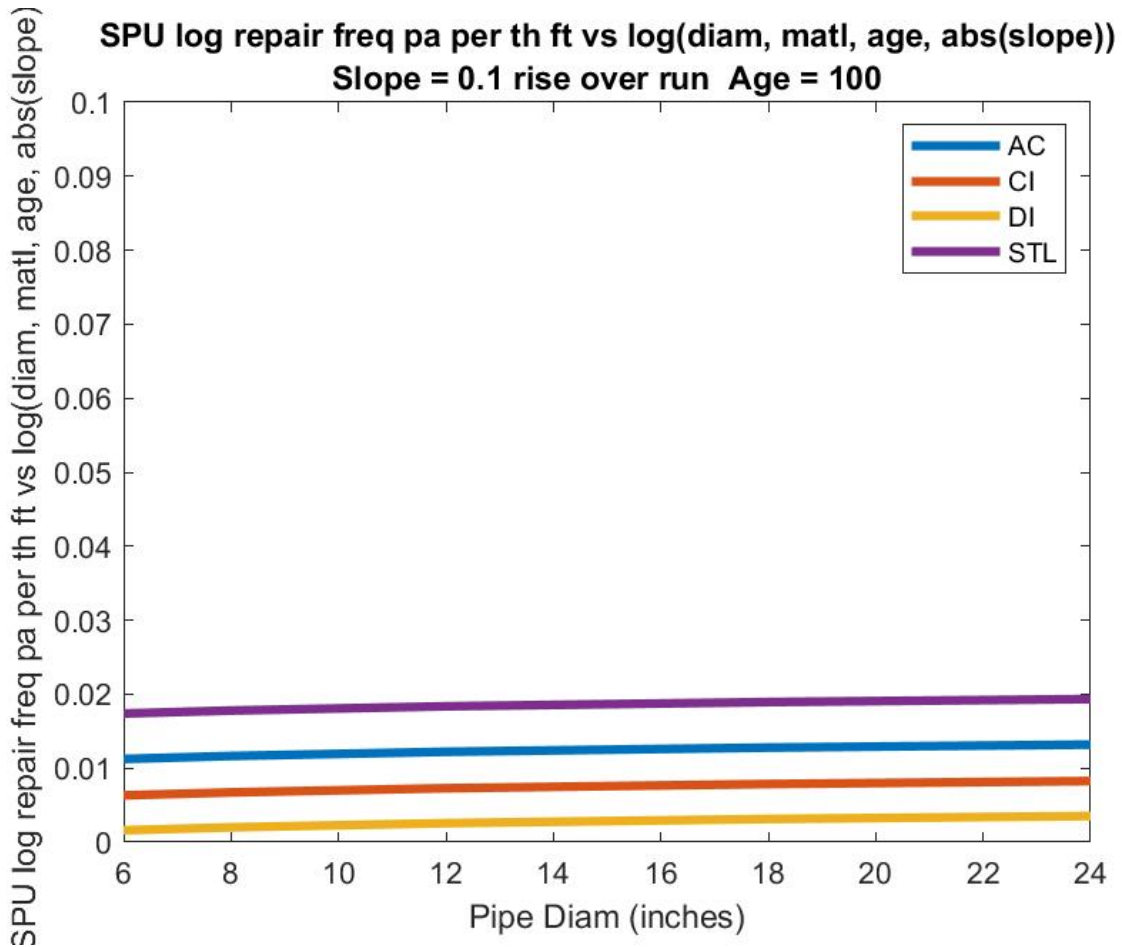


Figure 4-47. Repair Frequency per Thousand Feet of Pipe Considering Material, Age, Diameter, and Slope Parallel and Perpendicular to the Pipe's Longitudinal Axis, Based on a Log-Log Model. Plot Is an Example for Pipe Age Equal to 100 Years, SPU Data.

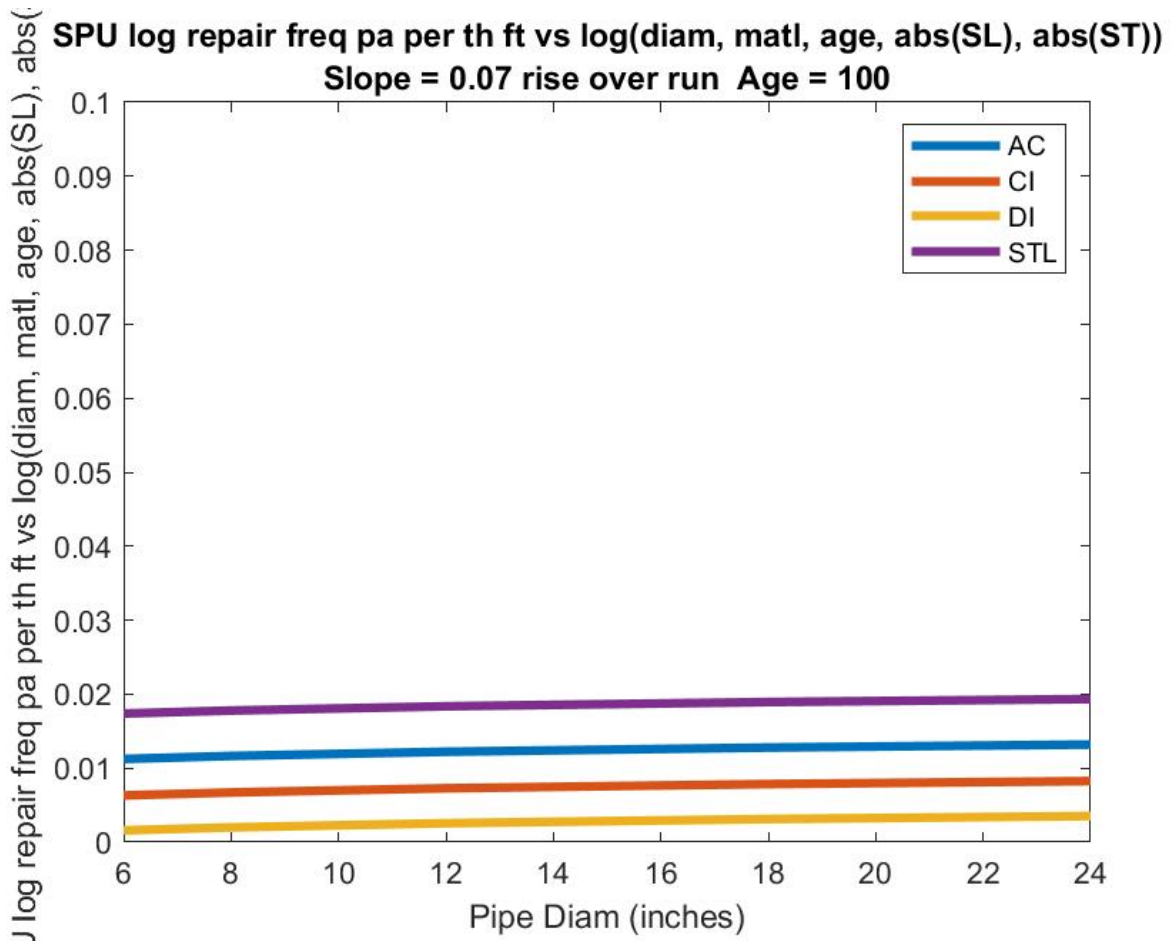


Figure 4-48. Repair Frequency per Thousand Feet of Pipe Considering Material, Age, Diameter, and Slope Parallel and Perpendicular to the Pipe's Longitudinal Axis, Based on a Log-Log Model. Plot Is an Example for Pipe Age Equal to 100 Years, SPU Data.

4.3.6 Merged Dataset

Comparable results for the merged data set are provided below – similar comments apply, with results presented in Figure 4-50 to Figure 4-56 and Table 4-7:

Table 4-7. Merged Regression Coefficients for Seven Models.

Regression Coefficients	1. linear model: repair = f(diam, matl)	2. linear model: repair = f(diam, matl, slope)	3. linear model: repair/length = f(diam, matl, slope)	4. linear model: repair/length = f(diam, matl, age)	5. log-log model: $\ln(1 + \text{repair}/\text{length}) = f[\ln(\text{diam}, 1 + \text{matl}, \text{age})]$	6. log-log model: $\ln(1 + \text{repair}/\text{length}) = f[\ln(\text{diam}, 1 + \text{matl}, \text{age}, 1 + \text{slope})]$	7. log-log model: $\ln(1 + \text{repair}/\text{length}) = f[\ln(\text{diam}, 1 + \text{matl}, \text{age}, 1 + \text{SL}, 1 + \text{ST})]$
1	0.0852	0.0862	0.0078	0.0062	0.0029	0.0032	0.0028
2	-0.0009	-0.0009	0.0010	0.0006	-0.0018	-0.0019	-0.0018
3	0.0323	0.0305	0.0199	0.0167	0.0165	0.0163	0.0165
4	0.0264	0.0248	0.0118	0.0080	0.0095	0.0093	0.0096
5	0.0060	0.0040	0.0007	0.0032	0.0040	0.0036	0.0040
6	0.0058	0.0047	0.0004	-0.0005	0.0007	0.0006	0.0007
7		0.0000	0.0000	0.0002	0.0043	0.0042	0.0043
8						0.0015	-0.0177
9							0.0180

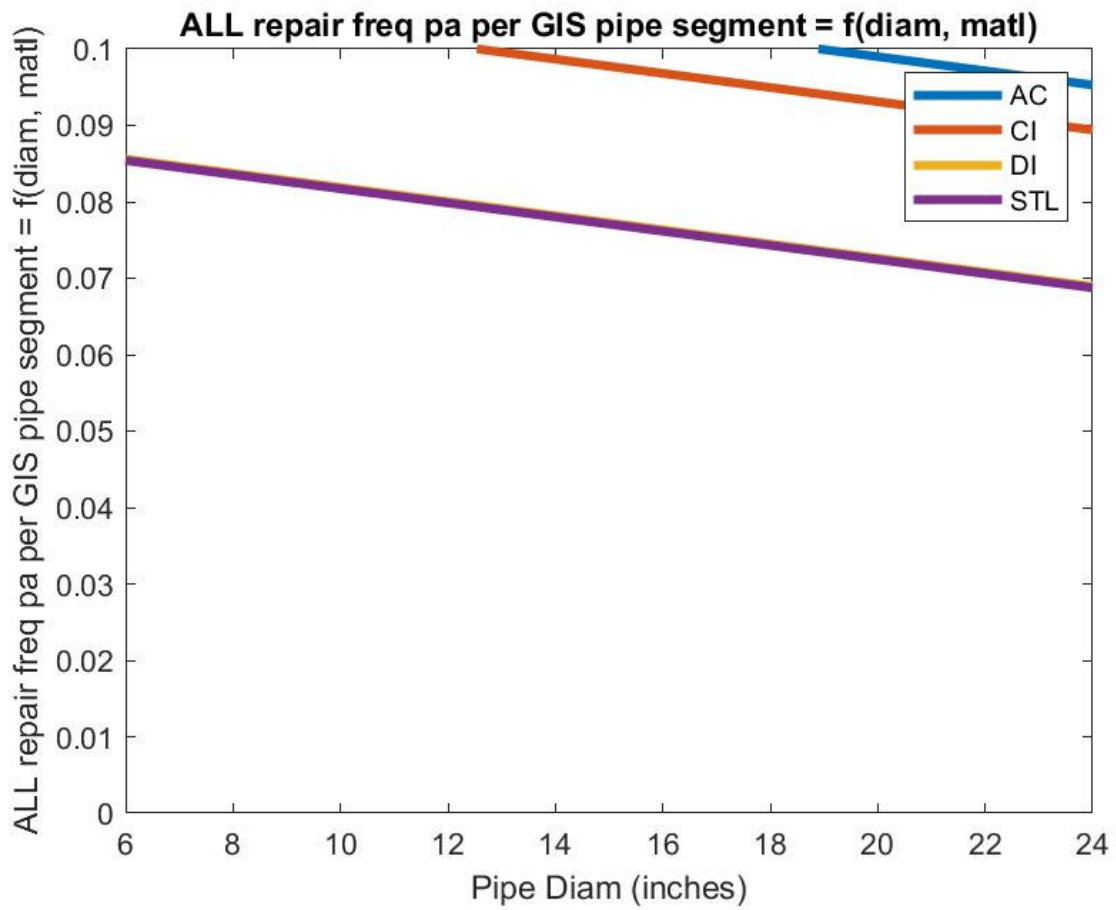


Figure 4-49. Raw Leak Frequency per GIS Pipe Segment, by Material and Diameter, Merged Data.

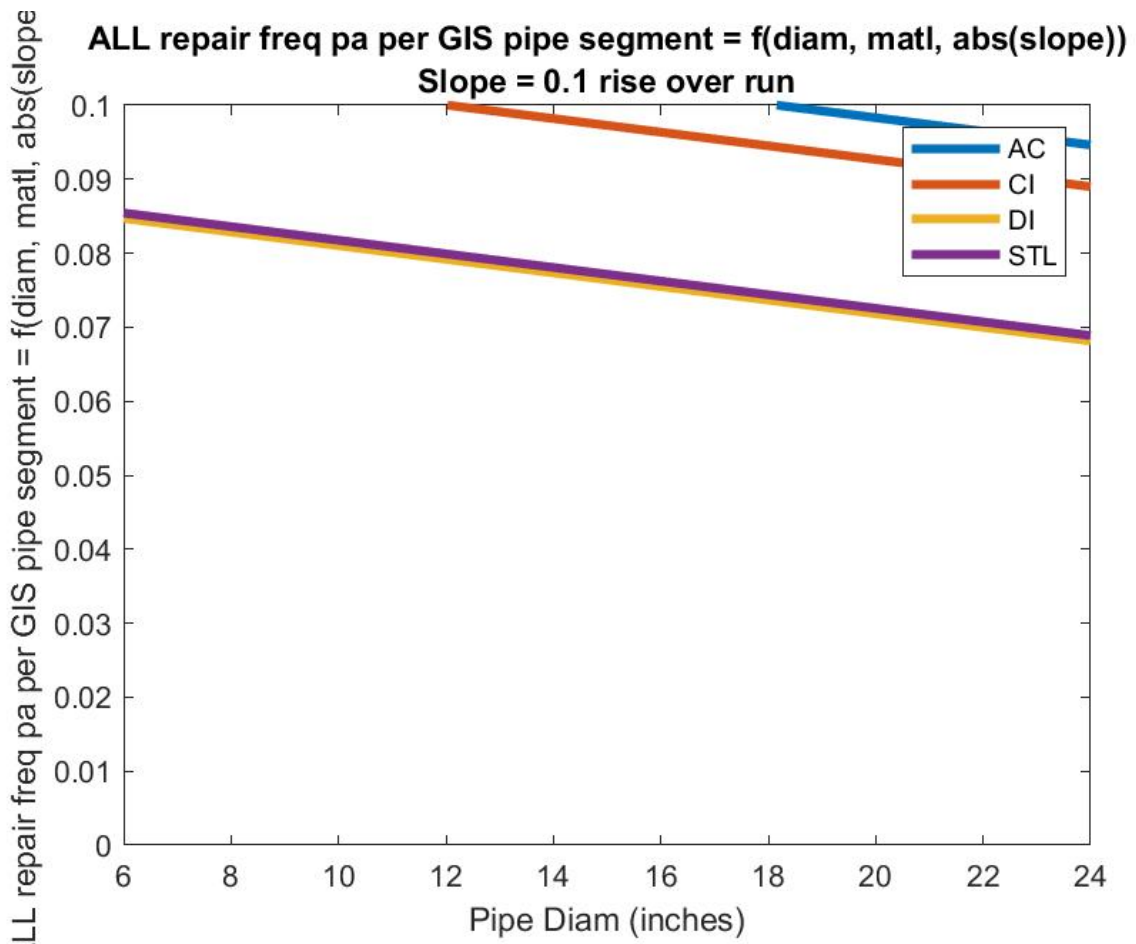


Figure 4-50. Leak Frequency per GIS Pipe Segment as a Function of Pipe Diameter, Material, and Slope, Merged Data.

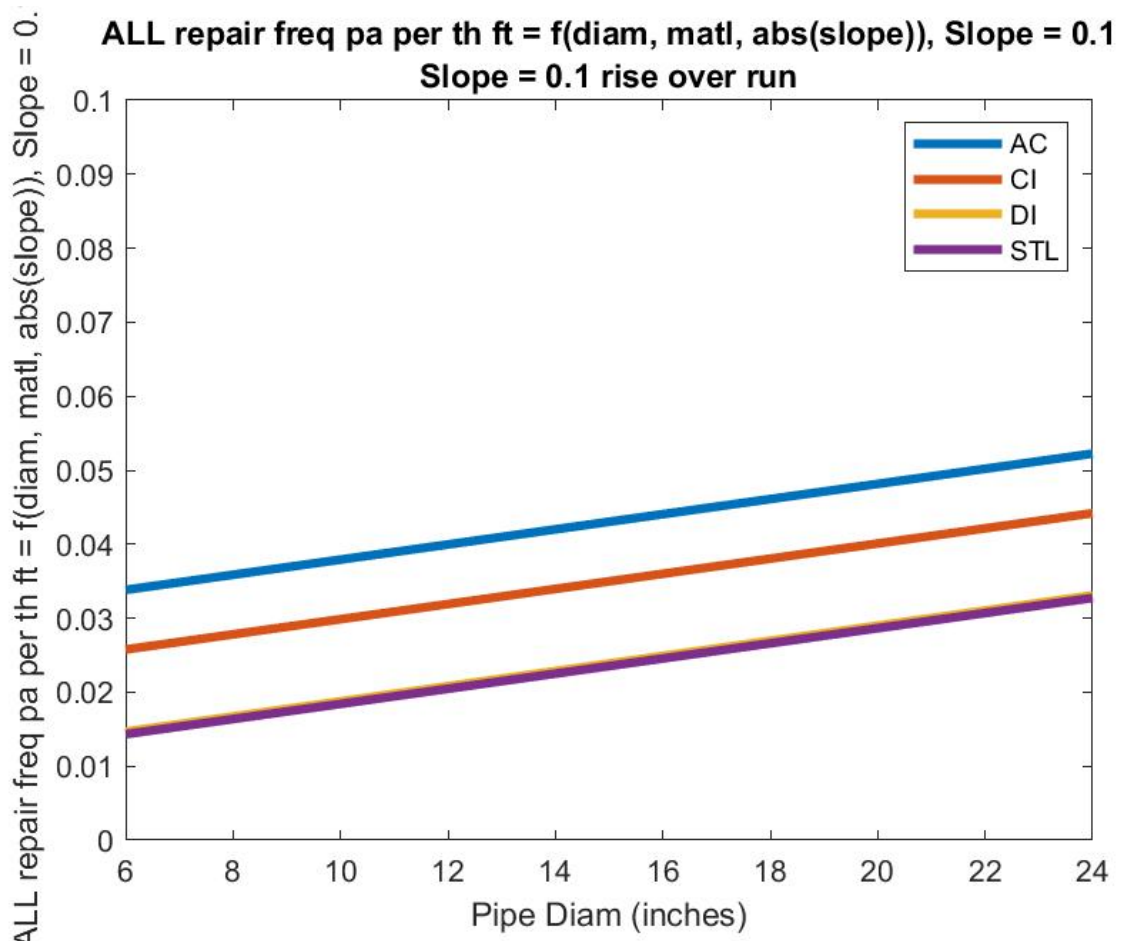


Figure 4-51. Leak Frequency per GIS Pipe Segment as a Function of Pipe Diameter, Material, and Slope, Merged Data.

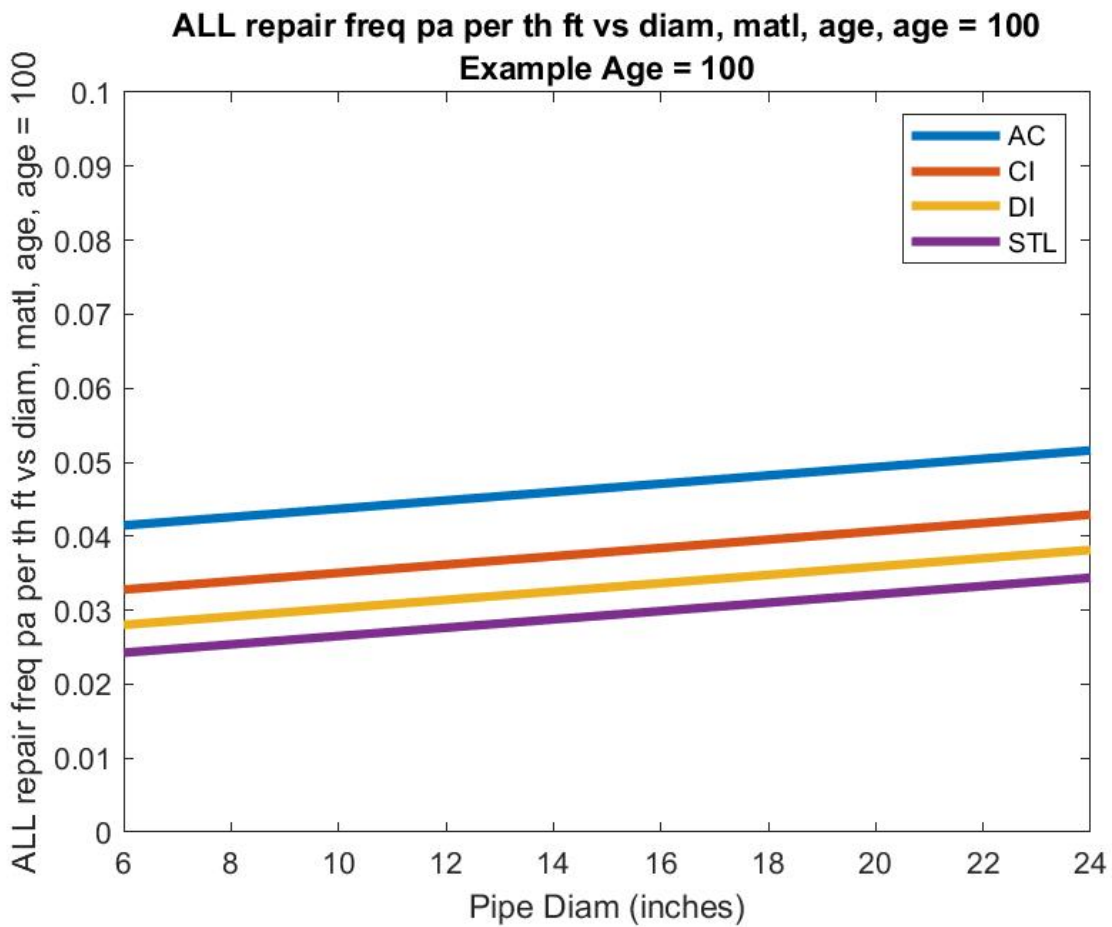


Figure 4-52. Repair Frequency per Thousand Feet of Pipe Considering Material, Age, and Diameter, Based on a Linear Model. Plot Is an Example for Pipe Age Equal to 100 Years, Merged Data.

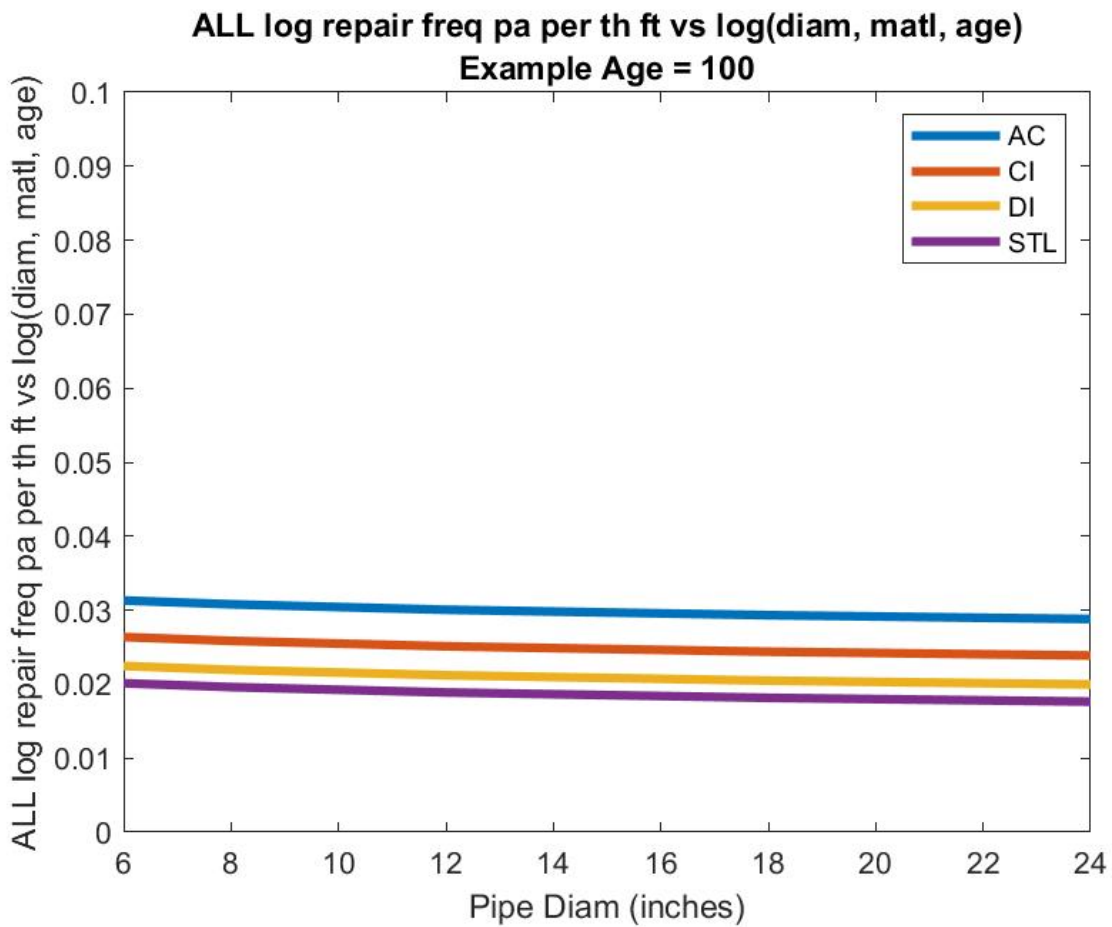


Figure 4-53. Repair Frequency per Thousand Feet of Pipe Considering Material, Age, and Diameter, Based on a Log-Log Model. Plot Is an Example for Pipe Age Equal to 100 Years, Merged Data.

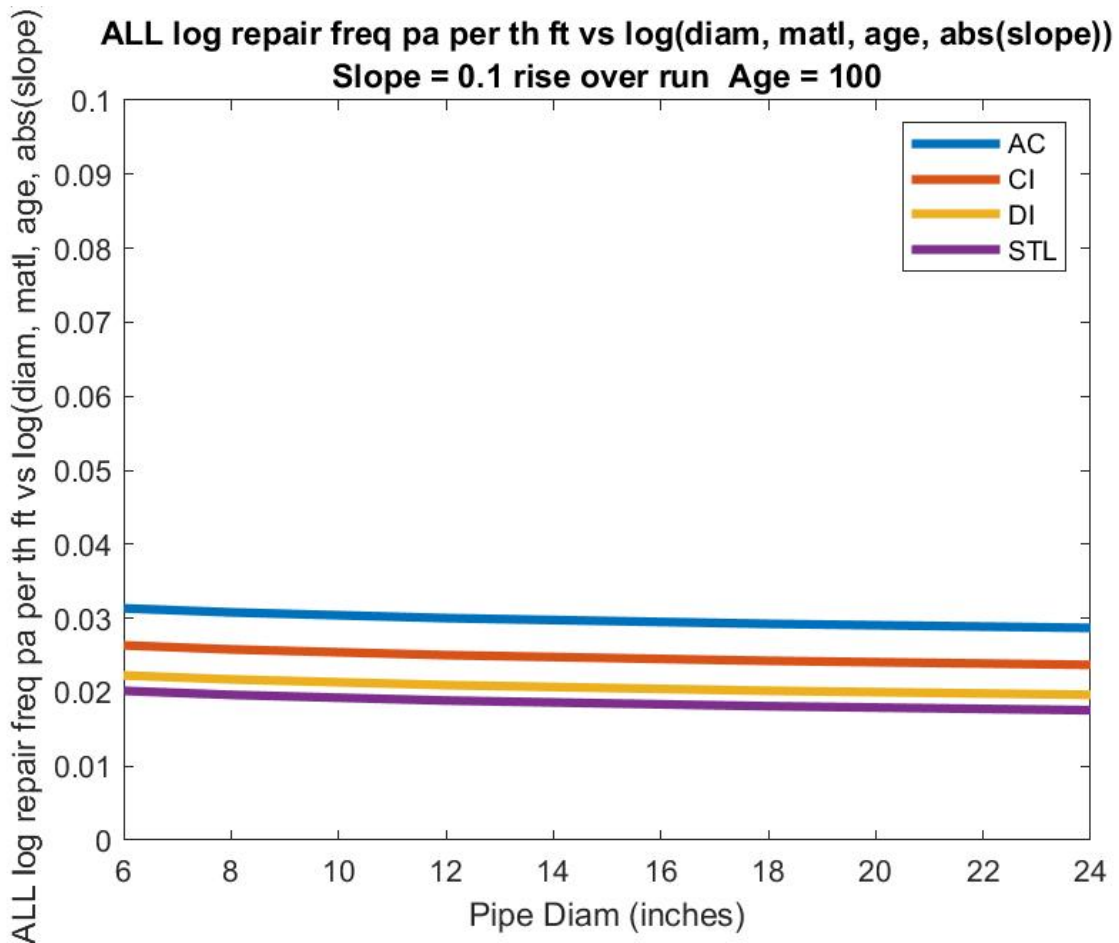


Figure 4-54. Repair Frequency per Thousand Feet of Pipe Considering Material, Age, Diameter and Slope Parallel and Perpendicular to the Pipe's Longitudinal Axis, Based on a Log-Log Model. Plot Is an Example for Pipe Age Equal to 100 Years, Merged Data.

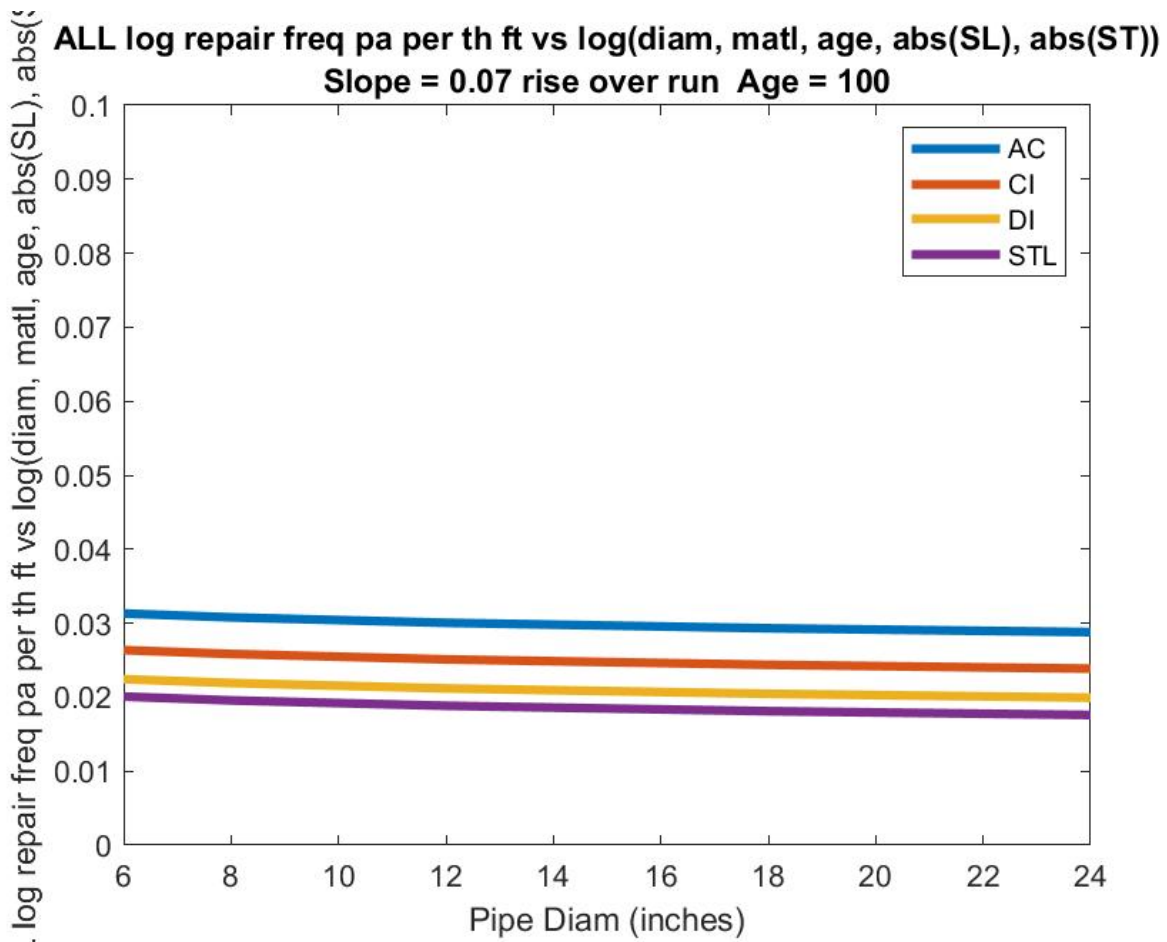


Figure 4-55. Repair Frequency per Thousand Feet of Pipe considering Material, Age, Diameter, and Slope Parallel and Perpendicular to the Pipe's Longitudinal Axis, Based on a Log-Log Model. Plot Is an Example for Pipe Age Equal to 100 Years, Merged Data.

4.4 Application

The previously developed relationships can be employed in a wide variety of ways. We provide one example: Figure 4-57 shows a plot of repair annual frequency per thousand ft. of 8" CI pipe as a function of age, showing that pipe has increasing repair rates as it gets older – 100 year old pipe has a repair frequency about 60% higher than 10 year old pipe.

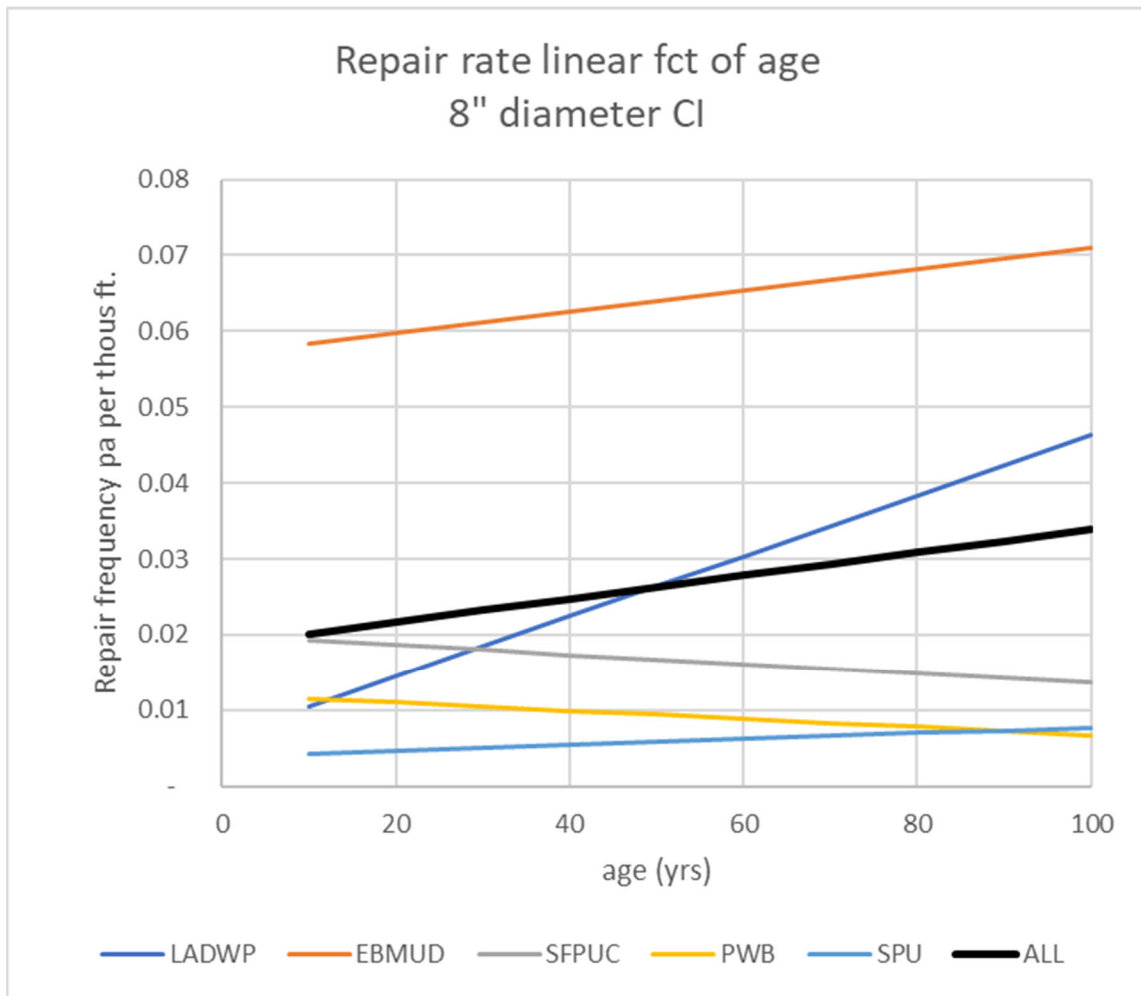


Figure 4-56. Repair Frequency Pa per Thousand Ft of 8" CI Pipe as a Function of Age, Showing That Pipe Has Increasing Repair Rates as It Gets Older.

4.5 Survival Analysis

In the context of this study, survival analysis is the analysis of time-to-failure or, for this study's data, time-to-repair. Survival analysis is a common technique in medicine, public health, engineering and in fact a part of reliability analysis. An important concept in survival analysis is censoring. In this study, some pipe segments may not yet have failed – they are still “surviving” – so that the dataset consists of two parts: those that have failed (which if complete would give us good knowledge of the expected life of the pipe), and those that have not yet failed. Data which do not yet reflect a failure are termed “right censored”, while “left censored” data is pipe for which we don't know the time of installation. That is, during a survival study either the individual pipe segment has been observed to fail at time T , or the observation on that segment cease at time c (which is 2017 for the LADWP data). Then the observation

is $\min(T, c)$ and an indicator variable I_c shows if the individual is censored or not. The calculations for hazard and survivor functions must be adjusted to account for censoring.

A common method employed in survival analysis is the Kaplan-Meier method or “KM” method (Bradley and Kohler 2007; Kaplan and Meier 1958) also known as the product limit estimator, which is a non-parametric statistic used to estimate the survival function from lifetime data. A plot of the Kaplan–Meier estimator is a series of declining horizontal steps which, with a large enough sample size, approaches the true survival function for that population. The value of the survival function between successive distinct sampled observations is assumed to be constant. An important advantage of the Kaplan–Meier curve is that the method can take into account some types of censored data, particularly *right-censoring*. When no truncation or censoring occurs, the Kaplan–Meier curve is the complement of the empirical cumulative distribution function.

The fundamental approach of this study is the comparison of KM curves for pipe segments subjected, and not subjected, to strong earthquake ground motions. If the survival curve for the earthquake-affected pipes is lower than that of not-affected pipes, then the KM curve reveals the reduced survivability or expected life of pipe caused by the strong ground motion, or earthquake-induced ‘aging’, all else being equal.

4.5.1 Basic Case

The first case will be a simple KM analysis of the entire data set, not considering earthquake effects. Two KM curves for the entire LADWP dataset are shown:

- The empirical cumulative distribution function (ECDF), Figure 4-58, which shows the probability of failure (in this case, leak repair) of a pipe segment, as a function of the time in years since the pipe’s installation
- The survival curve, Figure 4-59, which is the complement of the ECDF, and shows the probability of survival (ie, non-failure) of a pipe segment, as a function of the time in years since the pipe’s installation

As can be seen, the two figures are complementary – at 100 years, the probability of failure is 25%, equivalent to the Survival Function probability of survival (non-failure) of 75%.

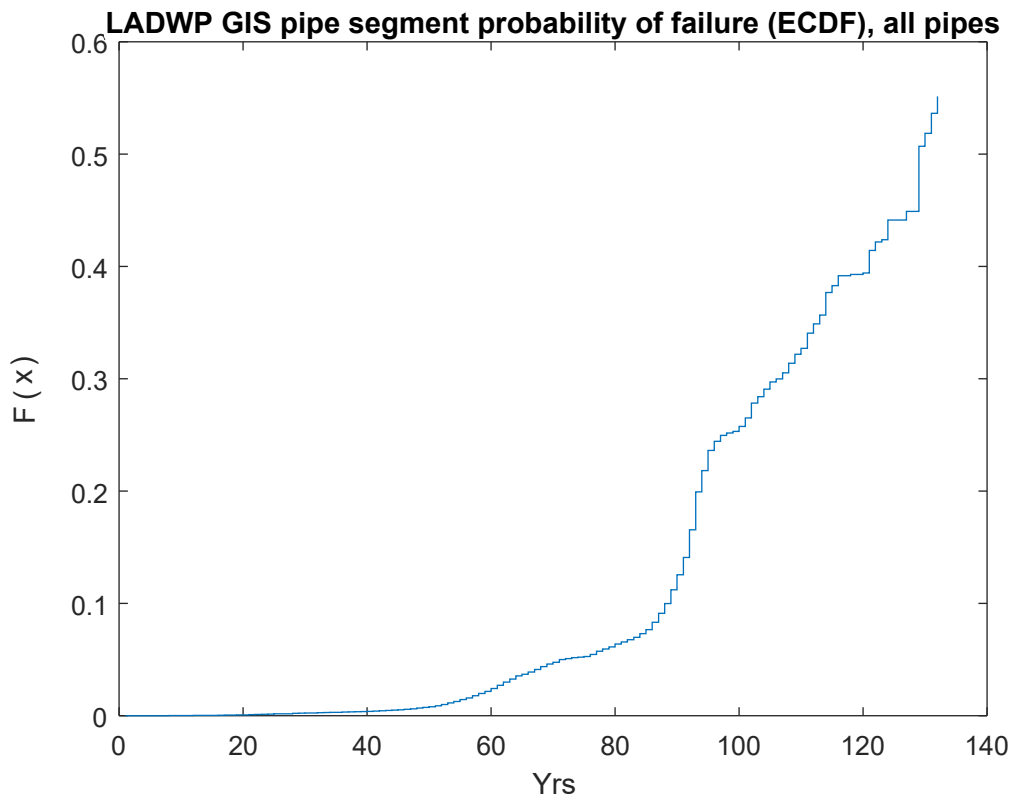


Figure 4-57. Empirical Cumulative Distribution Function (ECDF) for All GIS Pipe Segments, LADWP Data.

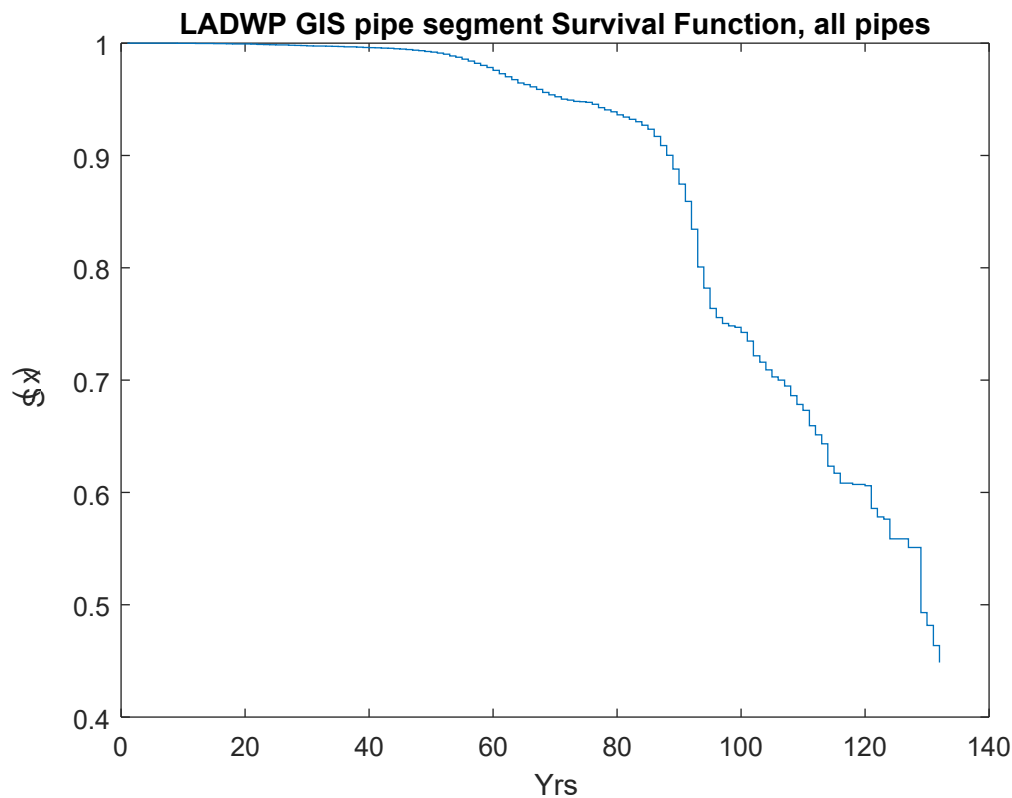


Figure 4-58. Survival Function for All GIS Pipe Segments, LADWP Data.

4.5.2 Effect of Earthquake

To examine the effect of earthquake on remaining pipe life, or survivability, this study partitioned the LADWP data set into two subsets, one affected by earthquake, the not affected. That is, recognize that the data set we have incorporates post-Northridge earthquake data and is geographically distributed, with a part of the LADWP system being subjected to strong ground motions in the Northridge earthquake, and a part (further away from the epicenter) not being subjected to strong ground motions. We select peak ground velocity (PGV, measured in kine or cm/sec) as a widely recognized measure of ground motion affecting buried pipes (ALA 2001; O'Rourke and Liu 2012; O'Rourke et al. 2014; Porter et al. 1991) and divide the dataset into two parts, those subjected to 20 kine⁴ or less in the 1994 Northridge earthquake (the gray area in the figure, total number of pipes in this portion is $n_{lo}=70,425$), and those subjected to more than 20 kine⁵ ($n_{hi} = 207,957$), where “hi” refers to those pipes experiencing PGV > 20 kine in the 1994 event, and “lo” have PGV ≤ 20 kine. Figure 4-60. A value of 20 kine is approximately Modified Mercalli Intensity VII and marks the beginning of significant damage, Figure 4-60. A map of the dataset overlaid on the 1994 earthquake pattern of PGV is shown in Figure 4-61, followed by the histogram of pipe install dates for the two data sets, Figure 4-62.

⁴ An initial value of 20 kine was employed, based on it being a reasonable boundary for initiation of damage. However, other values (10 kine, 30 kine...) were examined. In the end, 20 kine was selected as most appropriate.

⁵ That is, those areas colored green, yellow etc. Note that for illustrative purposes the PGV values were binned as shown, the actual USGS PGV data is more detailed.

PERCEIVED SHAKING	Not felt	Weak	Light	Moderate	Strong	Very strong	Severe	Violent	Extreme
POTENTIAL DAMAGE	none	none	none	Very light	Light	Moderate	Mod./Heavy	Heavy	Very Heavy
PEAK ACC.(%g)	<0.05	0.3	2.8	6.2	12	22	40	75	>139
PEAK VEL.(cm/s)	<0.02	0.1	1.4	4.7	9.6	20	41	86	>178
INSTRUMENTAL INTENSITY	I	II-III	IV	V	VI	VII	VIII	IX	X+

Scale based upon Worden et al. (2012)

Figure 4-59. Instrumental Intensity vs. Other Intensity Measures including PGV. Note That Instrumental Intensity is Essentially Synonymous with Modified Mercalli Intensity (MMI).

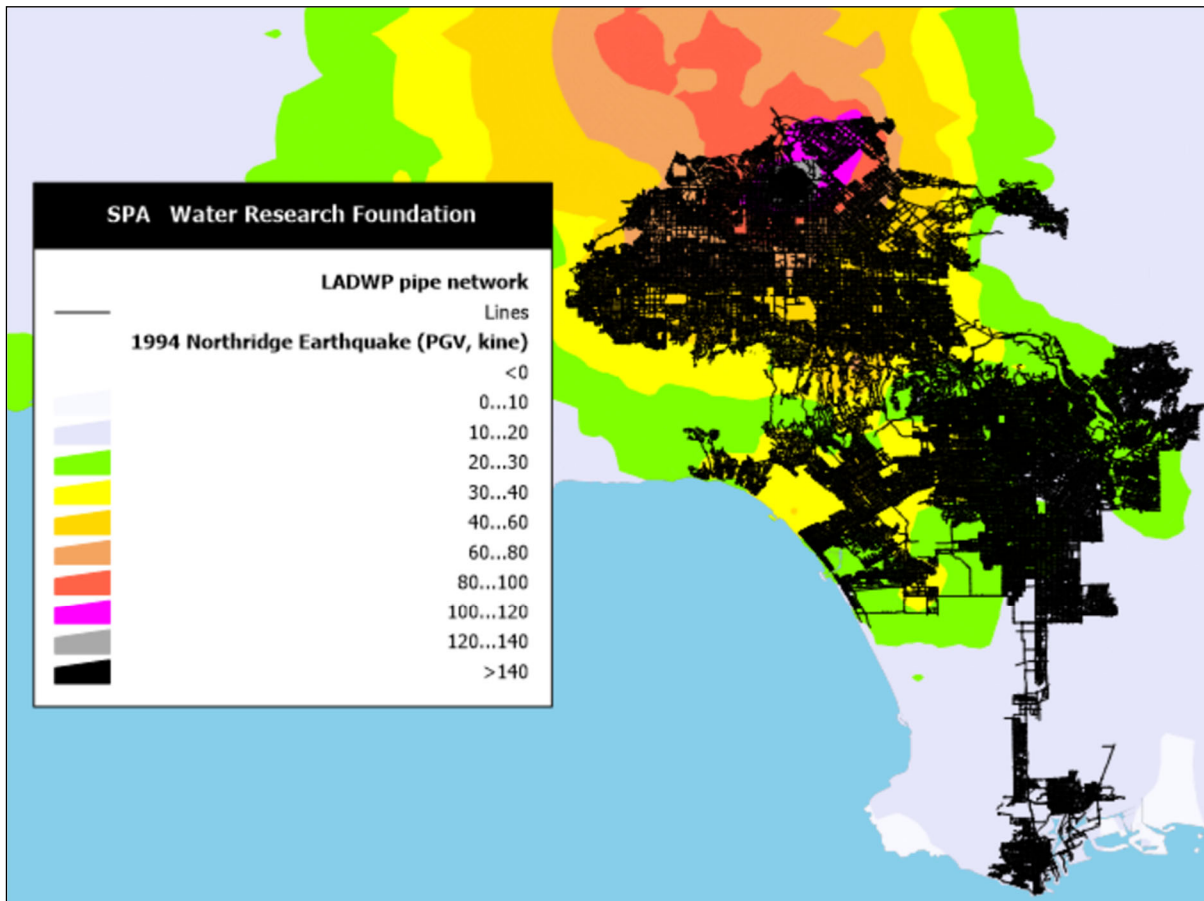


Figure 4-60. LADWP Pipe Network Overlaid on Northridge Earthquake ShakeMap PGV.

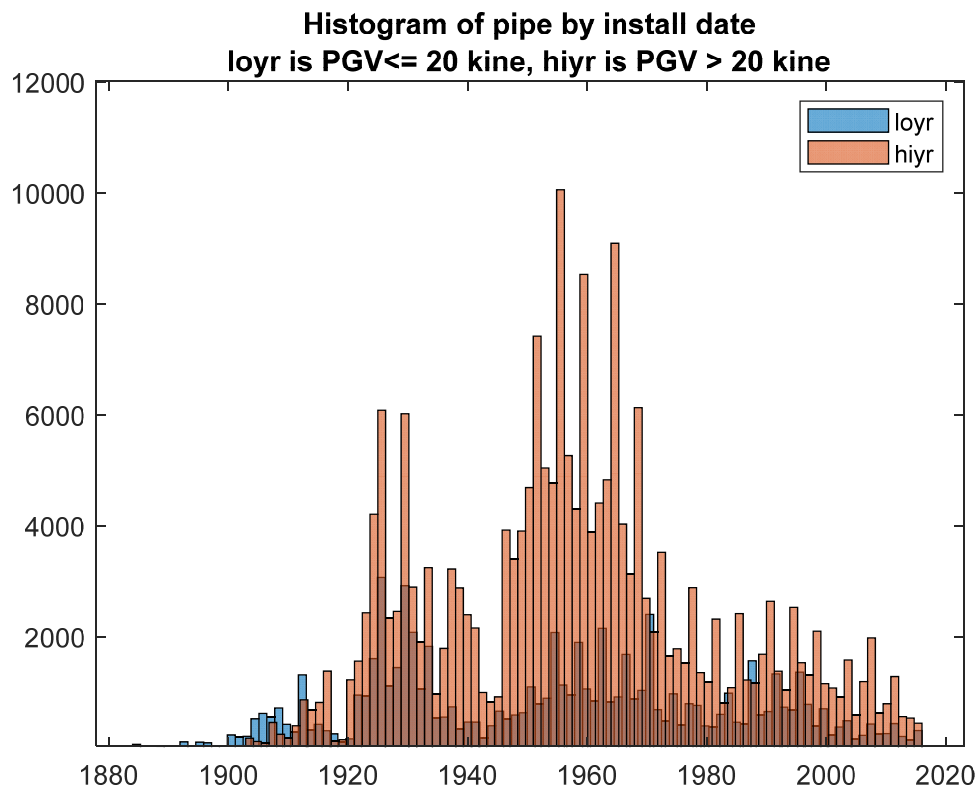


Figure 4-61. Histogram of Pipe by Installation Date, Where “Loyr” (Low Year) Is the Subset of the Dataset with PGV <= 20 Kine, While “Hiyr” Is the Subset with PGV > 20 Kine, LADWP Data.

From the histogram we can see that the two data sets have similar patterns of installation date – that is, one set is not substantially older or younger than the other data set.

Figure 4-62 below shows the KM probability of failure for the two data sets, from which it can be seen that the “hi” dataset has a significantly higher probability of failure – that is, the pipes subjected to higher PGV in the 1994 event have been failing on a greater rate than those not subjected to high PGV. For example, everything else being equal, a one hundred year old pipe (ie, installed in 1917) has about 25% probability of failure if it was subjected to PGV > 20 kine in the 1994 earthquake, while if it wasn’t subjected to this ground motion, it has about a 12% probability of failure (about half).

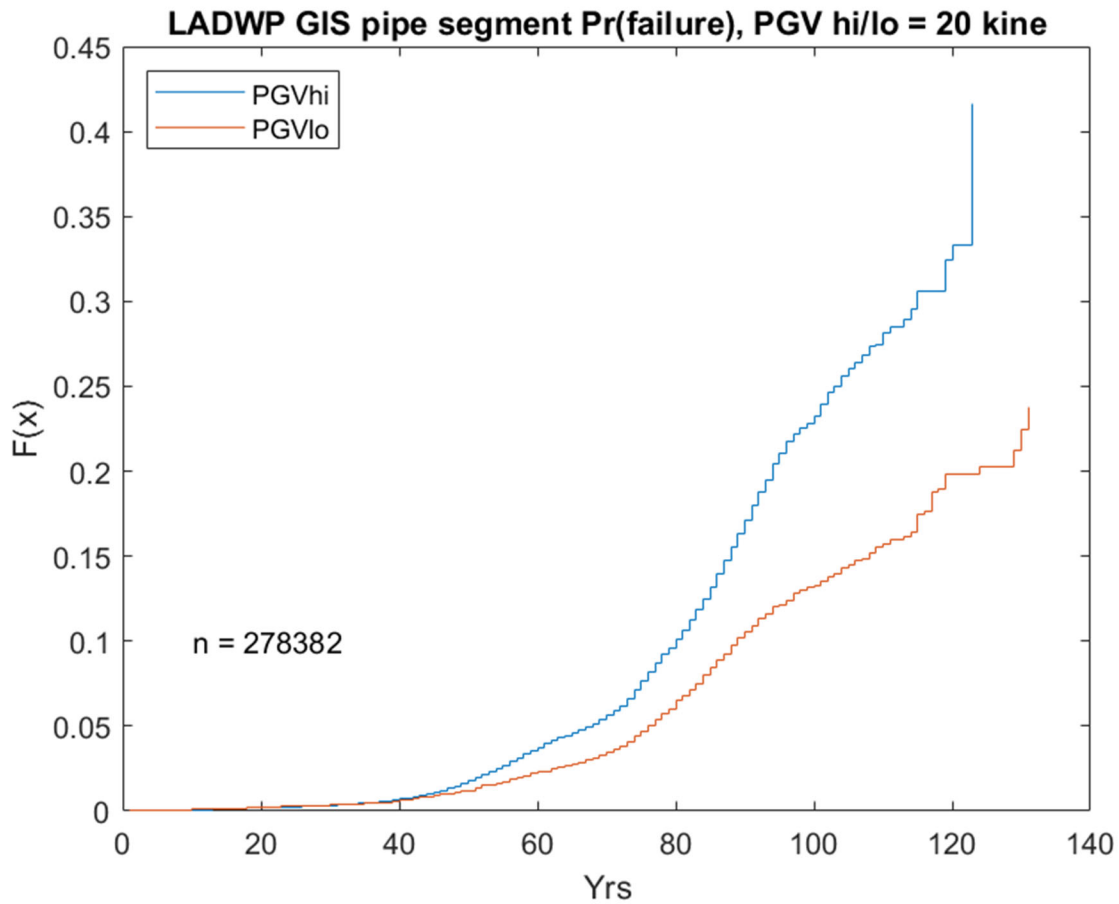


Figure 4-62. ECDF for LADWP Dataset Segmented by PGV Less than 20 Kine (PGVlo, Red Line) and More than 20 Kine (PGVhi, Blue Line).

This is a significant finding. If a utility determines 25% probability of failure is the criteria for replacement, the “hi” population has now reached the end of its useful life. **If the earthquake had not occurred, those pipes would have a useful life of about 40 years longer.** At a real interest rate of 3%, a \$1 of replacement expenditure postponed for 40 years will have a value at that time of \$3.26. Put another way, the earthquake has caused a loss **equivalent to 31% of the system’s replacement value.**

As of this writing, the 1994 Northridge earthquake was 26 years ago, so that the City of Los Angeles will in the next two decades be burdened with a much larger pipe replacement task, than if the earthquake had not occurred.

Survivability is affected by many factors, one of which is material. Figure 4-64 below show that this same trend is similar for cast iron pipe (CI), which accords with prior work, and not so pronounced for ductile iron (DI), Figure 4-65.

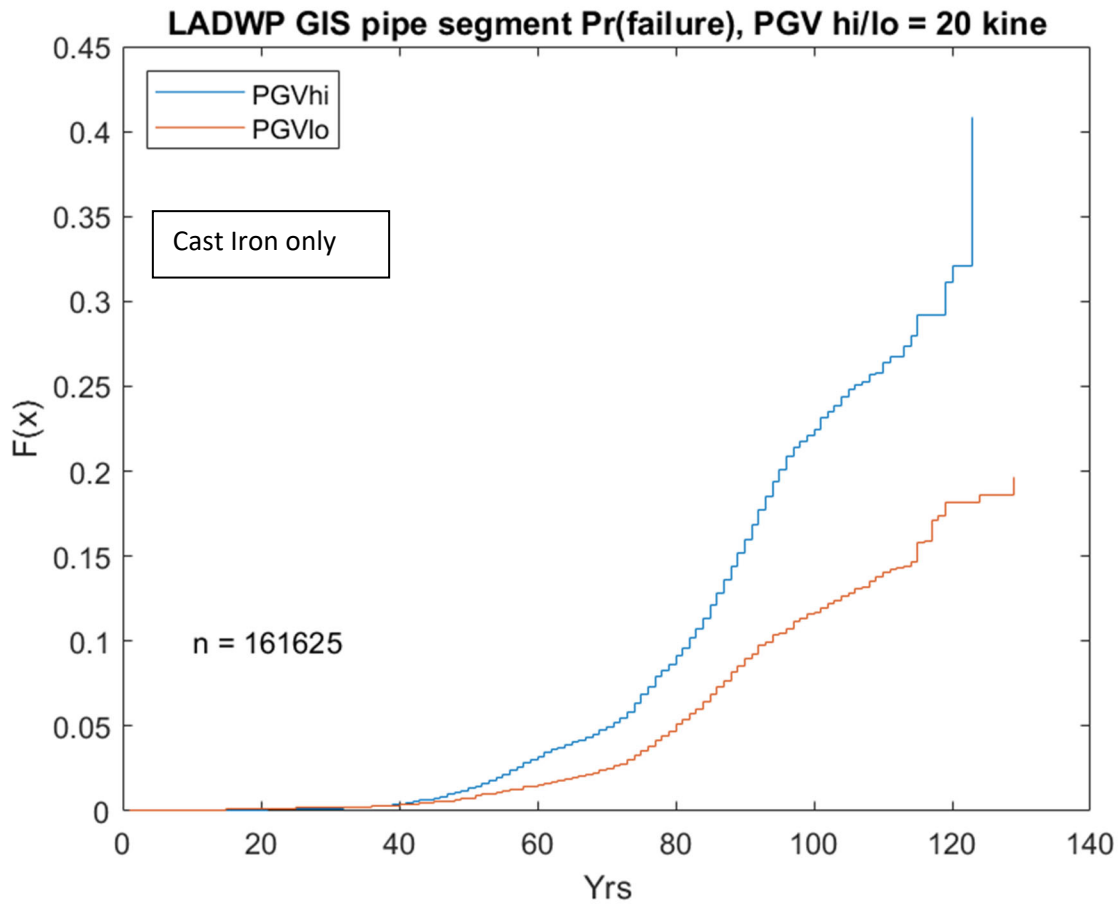


Figure 4-63. Similar to above except Only for CI, LADWP Data.

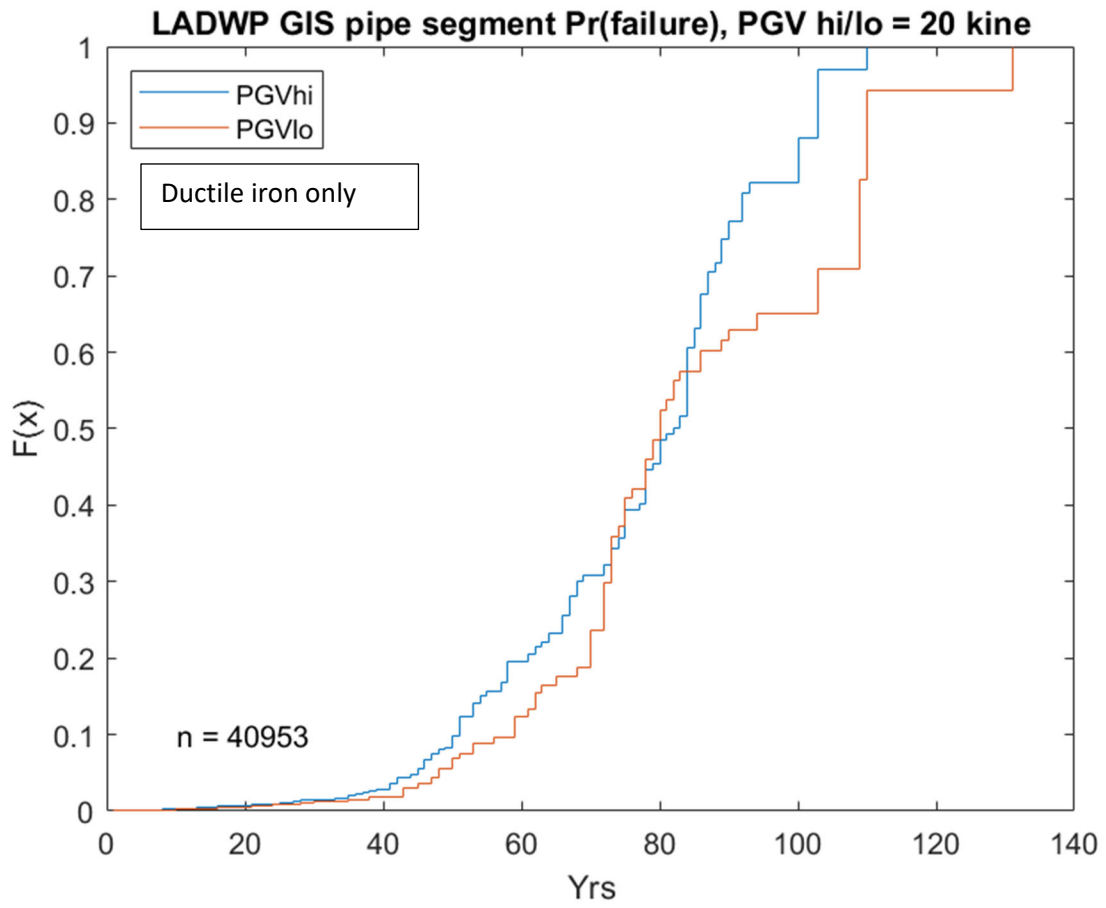


Figure 4-64. Similar to above except Only for DI, LADWP Data.

This finding is reinforced by comparison of the LADWP data with that from SPU (CI only, in both cases), Figure 4-66, which tends to corroborate this finding, in that the SPU ECDF curve tracks fairly closely with that of the LADWP < 20 kine data. That is, the SPU ECDF curve, not affected by earthquake, is closer in trend to the LADWP < 20 kine curve, than to the LADWP > 20 kine curve.

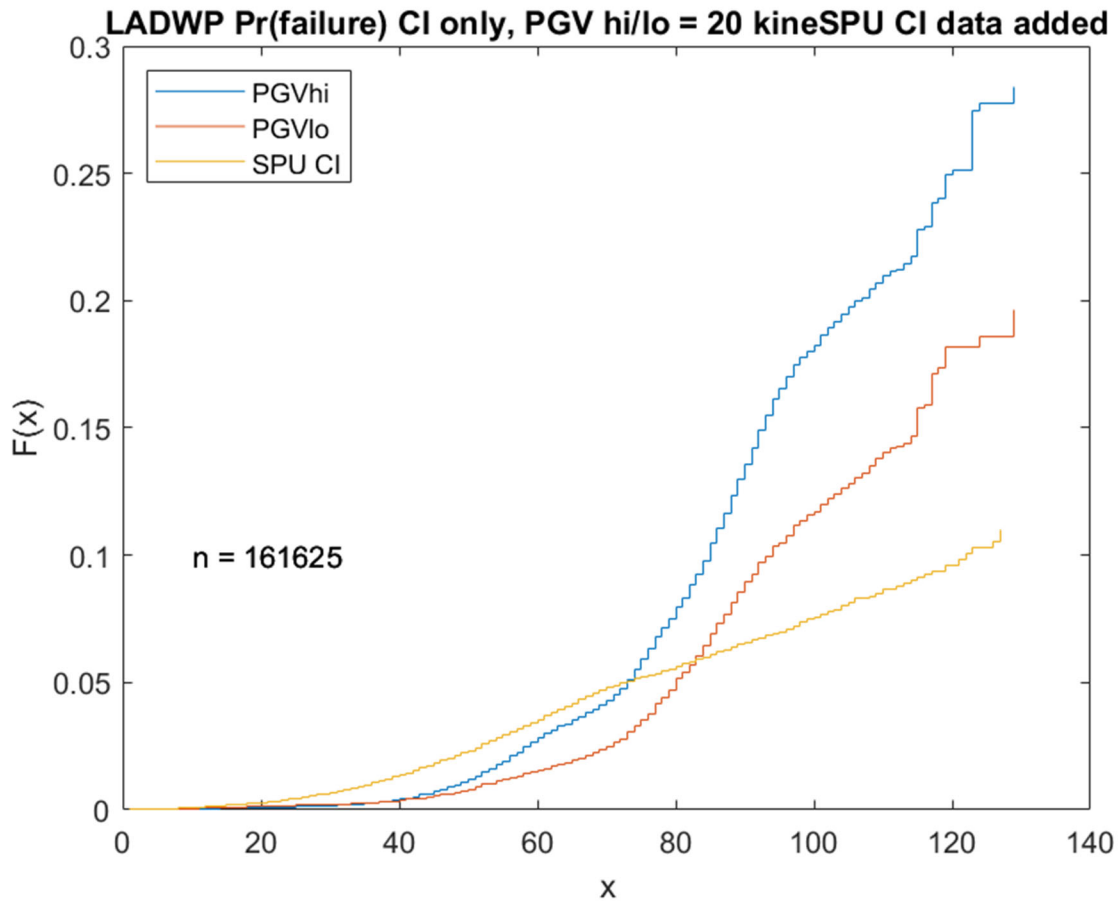


Figure 4-65. Similar to Figure 4-63 but Includes SPU (CI Only) as Well as LADWP (CI Only) Data.

CHAPTER 5

Findings and Concluding Remarks

5.1 Findings

This study's key finding is that earthquakes, beyond any prompt repairs, are found to reduce long-term service life of WDNs. In the case of LADWP, the portion of the LADWP pipe network that was strongly shaken in 1994 has had its useful life shortened by about 40 years, based on a comparison of portions of the system strongly shaken, and not strongly shaken, by the 1994 Northridge earthquake. Comparison of the LADWP data with that from SPU (CI only, in both cases) tends to corroborate this finding, in that the SPU ECDF curve tracks fairly closely with that of the LADWP < 20 kine data. That is, the SPU ECDF curve, not affected by earthquake, is closer in trend to the LADWP < 20 kine curve, than to the LADWP > 20 kine curve.

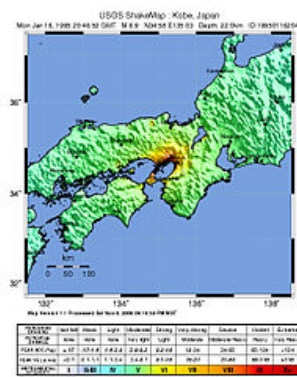
5.2 Implications

The main implication of this research findings is that **total costs of repair for earthquake damage are significantly underestimated by both water agencies and FEMA**, in that both parties only quantify the costs of repairs for a relatively short period (“prompt repairs”) following a major stress event. **The real losses due to an earthquake accrue over many decades and are significantly greater.** The stress event permanently reduces the service life of the pipe existing at the time of the earthquake vis-à-vis if the earthquake had not occurred. The reduction in service life results in pre-mature replacement of the pipe – in effect, the earthquake has “aged” the pipe. Disaster aid funding should be based on the recognition that system life for a significant portion of a water distribution network is shortened by the stress event.

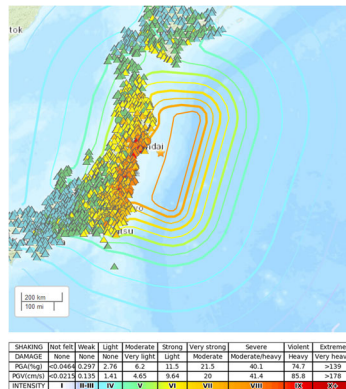
5.3 Future Research Recommendations

There are at least three areas for future work that suggest themselves to be of significant benefit:

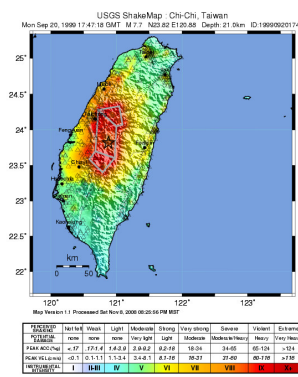
1. **Broaden the evidence:** While five datasets representing the largest cities on the west coast have been employed, the earthquakes were not of great magnitude and caused only relatively modest damage. This modest degree of damage is of course fortunate, but in fact is the result of the US not having had recent great earthquakes. It would further validate the results if data from regions with even stronger shaking could be employed. For this purpose, the regions would have to have comparable buried pipe technology to the US. Two such regions are Japan, and Taiwan. Japan has suffered a number of damaging earthquakes in the last few decades and at least two would provide rich datasets, being the 1995 Mw 6.9 Kobe and 2011 Ms 9.0 Tohoku earthquakes, Figure 5-1 (there are others, of course, that might also be considered). Data from these two events could be employed together with “control” regions such as Tokyo or Nagoya, for a similar analysis as presented here. Similarly, Taiwan suffered the 1999 Mw 7.7 Chichi earthquake, which affected several major cities but not Taipei, which Taipei could serve as a “not affected” control region.



1995 Mw 6.9 Hanshin



2011 Mw 9.0 Tohoku



1999 Mw 7.7 Chichi

Figure 5-1. Possible Events for Future Research.

Source: USGS n.d.b.

2. **Industry terminology:** The data from each of the five agencies employed in this study was found to vary in terminology. While Building Information Model (BIM) technology is now being increasingly employed in the water industry (Beesley 2018; Dodge 2018), most applications are still only for new construction and its penetration to asset management is lagging (Hackett 2019). Thus, cross-agency pooling of data for use in Big Data analysis is greatly hampered. An industry standardized taxonomy of water system assets, including standardized characterization of pipe and other component failure modes exists (Grigg and Ballantyne 2017a; Grigg and Ballantyne 2017b) and its application should be strongly encouraged for this purpose.
3. **Other stress events:** The major stress events studied in this project have been earthquakes which are clearly a significant natural hazard. Other major natural hazard stress events affecting large cities are floods, hurricanes, drought, freezes and wildfires. For example, New Orleans sustained major flooding in Hurricane Katrina in 2005, Houston in Harvey in 2007 and portions of New York in Sandy in 2012. Several investigators have commented that resulting saltwater saltwater has led to long-term degradation of buried pipe. Speaking of Hurricanes Katrina and Rita, Chisolm found:

“Another long-term impact to the underground infrastructure was accelerated degradation of the system and its components, resulting in failure before the full life of the various components was realized. Structural damage, loss of bedding support, and increased corrosion can all contribute to accelerated aging of underground pipelines, which must be addressed using pipe renewal techniques.” (Chisolm and Matthews 2012)

while (Allouche, Chisolm and Sterling 2008) found following the 1997 Grand Forks floods:

“In terms of long-term adverse impacts, the engineering staff felt that the over-pressurization of the pipe and the soil was likely to have a long-term impact on the service life of buried gravity systems.”

and (Wols and Van Thienen 2014) found:

“Failures in asbestos-cement (AC) and steel pipes increased during warm periods, which often simultaneously occurred when water consumptions were high. For cast iron pipes, failures increased at low temperatures. Drought parameters had a smaller effect on pipe failure than temperature, but still an increase in pipe failure was observed during dry periods for AC and steel pipes. No effect of weather conditions on pipe failure were observed for poly(vinyl chloride) and polyethylene pipes.”

More recently very large wildfires have extended into communities, with stress effects of a different nature (contamination of buried pipes) on the buried WDNs (Schulze and Fischer 2021).

A study comparable to that presented here, extending the analysis to several major flood or other stress events, could extend the applicability of this study's findings to regions not affected by seismic hazards, and even potentially globally.

4. **Tools:** Lastly, whether the findings of this study are ultimately confined to seismic hazards or extended more broadly, tools will be needed to enable utilities to quantify these findings following a major stress event. Such tools might be a GIS-based software package that could combine the effects of the stress event and network data to quickly estimate the long-term repairs and thus quantify in physical and financial terms the present value of long-term effects. Such tools could be combined with short-term effects to produce an overall claims estimation package to support utilities and FEMA in assessing the most truly appropriate disaster aid.

APPENDIX A

Literature Review

Over 50 papers were reviewed with a focus on identifying (a) key factors affecting buried pipe performance, (b) mechanistic models that can be adapted for project purposes, and (c) statistical methods than can be employed or adapted for project purposes. Key findings were:

- (Christodoulou et al. 2012) identifies key factors for pipe performance, projects hazard curves
- (Tefamariam et al. 2006) and (Sadiq et al. 2004) and several related papers provide a comprehensive mechanistic model than can be adapted for the project, perhaps including aspects from other’s work.
- (Carrión et al. 2010) provides a sampling scheme considering left truncation and right-censoring in the dataset, precisely problem we have – this is a high candidate to adapt this approach for our project.

A complete list of papers reviewed are listed at the end of this Appendix, with discussion of specific papers being provided in Table A-1.

Table A-1. Key Literature and Comments.

Reference	Comment
Aşchilean, Ioan, et al. "Determining priorities concerning water distribution network rehabilitation." <i>Energy Procedia</i> 112 (2017): 27-34.	Simple optimization exercise, not relevant
Bayesian belief network based data fusion model is developed for the failure prediction of water mains	Case study for Calgary using BBN, not specifically germane
Carrión, Andrés, et al. "Evaluation of the reliability of a water supply network from right-censored and left-truncated break data." <i>Water resources management</i> 24.12 (2010): 2917-2935.	sampling scheme considering left truncation and right-censoring in the dataset, precisely problem we have – high candidate to adapt this approach for our project
Christodoulou, Symeon E., and Agathoklis Agathokleous Anastasis Gagatsis, Savvas Xanthos, and Sofia Kranioti. 2012. "Urban Water Distribution Network Asset Management Using Spatio-Temporal Analysis of Pipe-Failure Data." Pp. 27–29. in Proc. International Conference for Computing in Civil and Building Engineering. Clearwater Beach FL.	The study is based on two datasets (one from New York City and the other from the city of Limassol, Cyprus), analytical and numerical methods, and artificial intelligence techniques (artificial neural networks and fuzzy logic) that capture the underlying knowledge and transform the patterns of the network’s behavior into a knowledge-repository and a DSS. The report also investigates the effects of intermittent water supply on the vulnerability of urban water distribution networks (UWDN) based on a three-year dataset from the cities of Limassol and Nicosia (Cyprus). Data stratification based on the pipes’ material type reveals that the hazard rate of the black-colour medium density polyethylene (MDPE) pipes is higher than galvanized (GI), asbestos cement (AC) and MDPE-blue pipes. The deviation in hazard rate between the various material types is about 0.0004 at the lower end of the pipes’ life expectancy (11,000 days, 30 years) and increases to about 0.0032 at the upper end of the pipes’ life expectancy (12,800 days, 35 years). Data stratification based on the type of incidents reveals that the hazard rate related to pipe

	deterioration greatly outpaces the hazard rate of the other incident types (corrosion, interference by others, tree roots, connection hose, other). NIREAS-IWRC/D5.14.2 59 The hazard rate related to corrosion accelerates in time and surpasses the rate of increase of interference-related, tree-roots and connectionhose incidents. Data stratification based on the pipe diameter reveals that medium and large diameter pipes have approximately the same hazard rate over time but small-diameter pipes have an increasing hazard rate. Relative importance, NYC and Limmasol data sets
Davis, Paul, et al. "A physical probabilistic model to predict failure rates in buried PVC pipelines." <i>Reliability Engineering & System Safety</i> 92.9 (2007): 1258-1266.	PVC pipe only, based on fracture mechanics
Duchesne, Sophie, Naoufel Chahid, Nabila Bouzida, and Babacar Toumbou. "Probabilistic Modeling of Cast Iron Water Distribution Pipe Corrosion." <i>Journal of Water Supply: Research and Technology—AQUA</i> 62, no. 5 (2013): 279–87.	Model of corrosion, based only on age of CI pipe, may be useful.
Folkman, Steven. "Water main break rates in the USA and Canada: A comprehensive study." (2018).	Useful study considering many factors on pipe break rates – will examine further.
García-Mora, Belén, et al. "Modelling the failure risk for water supply networks with interval-censored data." <i>Reliability Engineering & System Safety</i> 144 (2015): 311-318.	Treats interval censored data (ie, left or right truncated), good complement to (Carrión 2010)
Gehl, Pierre, Francesco Cavalieri, and Paolo Franchin. "Approximate Bayesian network formulation for the rapid loss assessment of real-world infrastructure systems." <i>Reliability Engineering & System Safety</i> 177 (2018): 80-93.	Bayesian updating methodology, useful but not specifically germane
Grigg, Neil S. "Water main breaks: Risk assessment and investment strategies." <i>Journal of Pipeline Systems Engineering and Practice</i> 4.4 (2013): 04013001.	explains the risk formulation of the decision process for pipeline replacement, the current rates of renewal, and the reasons why utilities renew pipes at low rates. Relevant but not specifically germane.
Habibian, Ahmad. "Effect of temperature changes on water-main breaks." <i>Journal of transportation engineering</i> 120.2 (1994): 312-321.	A strong correlation was found between water temperature and main break activity, mostly circular and occurred on grey cast-iron pipes. A failure mechanism is presented to explain the complex nature of temperature related main breaks. The mechanisms explains why break activity is not uniquely related to the temperature.
Hadzilacos, Thanassis, et al. "UtilNets: a water mains rehabilitation decision-support system." <i>Computers, environment and urban systems</i> 24.3 (2000): 215-232.	Provides a framework for considering various impacts on pipe – may be useful, to be examined further.
Hosseini, Mahmood, and Samira Jalili. "Assessment of the Nonlinear Behavior of Connections in Water Distribution Networks for Their Seismic Evaluation." <i>Procedia engineering</i> 14 (2011): 2878-2883.	FEM analysis of connections, not specifically germane
Ince, G. C., A. P. D. Reis, and G. Karakaisis. "The relationship between the performance of soil conditions and damage following an earthquake: a case study in Istanbul, Turkey." <i>Natural Hazards & Earth System Sciences</i> 11.6 (2011).	Examines soils but not specifically germane

Jiang, Chen, et al. "A general failure-pursuing sampling framework for surrogate-based reliability analysis." <i>Reliability Engineering & System Safety</i> 183 (2019): 47-59.	Machine learning exercise, not specifically germane
Kabir, Golam, et al. "Integrating failure prediction models for water mains: Bayesian belief network based data fusion." <i>Knowledge-Based Systems</i> 85 (2015): 159-169.	
Kleiner, Yehuda, and Balvant Rajani. "Prioritising individual water mains for renewal." <i>World Environmental and Water Resources Congress 2008: Ahupua'A</i> . 2008.	Overview of factors affecting pipe failure, may be useful.
Laucelli, D., et al. "Seismic reliability assessment of water distribution networks." <i>Procedia Engineering</i> 70 (2014): 998-1007.	Network analysis model, not specifically germane
Liu, Xing, Elisa Ferrario, and Enrico Zio. "Identifying resilient-important elements in interdependent critical infrastructures by sensitivity analysis." <i>Reliability Engineering & System Safety</i> 189 (2019): 423-434.	Network analysis model, not specifically germane
Manshoori, Mohammad Reza. "Evaluation of seismic vulnerability and failure modes for pipelines." <i>Procedia Engineering</i> 14 (2011): 3042-3049.	Jejune review of industrial pipes not specifically germane
Moglia, Magnus, Paul Davis, and Stewart Burn. "Strong exploration of a cast iron pipe failure model." <i>Reliability Engineering & System Safety</i> 93.6 (2008): 885-896.	A physical probabilistic failure model for buried cast iron pipes within a Monte-Carlo simulation framework to provide an estimated corrosion rate distribution, which agrees well with experimental results. A number of assumptions were chosen which improved the model to a stage where an acceptable fit was achieved. May be useful
Muhuri, Pranab K., and Rahul Nath. "A Novel Evolutionary Algorithmic Solution Approach for Bilevel Reliability-Redundancy Allocation Problem." <i>Reliability Engineering & System Safety</i> (2019): 106531.	Network reliability optimization model, not specifically germane
Park, Suwan, et al. "The proportional hazards modeling of water main failure data incorporating the time-dependent effects of covariates." <i>Water resources management</i> 25.1 (2011): 1-19.	Proportional hazards models (PHMs) for the times between consecutive pipe breaks were constructed using case study water main break data. The 150 mm individual cast iron pipes in the case study water distribution system were categorized into seven groups according to the past break history to construct a distinct PHM for each group. During the modeling process the assumption of the proportional hazards of covariates was examined to include the time-dependent effects of covariates on the failure hazard in the models. By analyzing the baseline hazard rates, the hazards of the third through the seventh break were found to follow a form similar to a bath-tub. The estimated regression coefficients and the hazard ratios of the selected covariates were used to analyze the variations in the factors and their effects, including the time-dependent effects on the pipe failures. The changes in the relative hazards of the covariates were also analyzed according to the number of breaks. May be useful
Park, Suwan. "Identifying the hazard characteristics of pipes in water distribution systems by using the proportional hazards model: 1. Theory." <i>KSCE Journal of Civil Engineering</i> 8.6 (2004): 663-668.	Not specifically germane

<p>Rajani, Balvant, and Yehuda Kleiner. "Comprehensive review of structural deterioration of water mains: physically based models." <i>Urban water</i> 3.3 (2001): 151-164.</p>	<p>Very good review of deterioration of water mains, The effects of temperature on pipe breakage rates have been observed and reported by many. (Walski and Pelliccia 1982) suggested that pipe breakage rates might be correlated to the maximum frost penetration in a given year. To account for the lack of frost penetration data, they correlated annual breakage rates with the air temperature of the coldest month, using a multiple regression analysis with age and air temperature as the covariates $N(t, T) = Ate^{BT} = (11)$ where t = pipe age; $N(t0)$ = breaks per km at year of installation; T = average air temperature in the coldest month; A, B = constants. The authors did not provide any information as to the quality of breakage predictions that were obtained by this model.</p>
<p>Rajani, Balvant, Yehuda Kleiner, and Jean-Eric Sink. "Exploration of the relationship between water main breaks and temperature covariates." <i>Urban Water Journal</i> 9.2 (2012): 67-84.</p>	<p>examines the impact of temperature changes on observed pipe breakage rate for three pipe materials, namely, cast iron, ductile iron and galvanised steel. Several water and air temperature-based were tested in conjunction with a non-homogeneous Poisson pipe break model to assess their impact on water main breaks, using data sets from three different water utilities in the USA and Canada. Temperature-based, such as average mean air temperature, maximum air temperature increase and decrease, and how fast the air temperature increase and decrease over a specific period of days, were found to be consistently significant. While the availability of water temperature data (which most utilities do not have) can enhanced the prediction of water main breaks, it appears that air temperature data alone (which most utilities can access) are usually sufficient. Useful.</p>
<p>Sadiq, Rehan, Balvant Rajani, and Yehuda Kleiner. "Probabilistic risk analysis of corrosion associated failures in cast iron water mains." <i>Reliability Engineering & System Safety</i> 86.1 (2004): 1-10.</p>	<p>method for corrosion associated failures in grey cast iron water mains using Monte Carlo (MC) to assess reduction in the factor of safety (FOS) of water mains over time. A sensitivity analysis revealed that the contribution of corrosion parameters to the variability of time to failure was more significant than the combined contributions of all other parameters – very useful will examine further</p>
<p>Safaei, Fatemeh, Jafar Ahmadi, and N. Balakrishnan. "A repair and replacement policy for repairable systems based on probability and mean of profits." <i>Reliability Engineering & System Safety</i> 183 (2019): 143-152.</p>	<p>not specifically germane</p>
<p>Shoji, G., and M. Tabata. "Evaluation of system reliability of lifeline networks in views of a seismic hazard." <i>Procedia engineering</i> 14 (2011): 590-597.</p>	<p>Network reliability analysis – not specifically germane</p>
<p>Sousa, V., N. Almeida, M. Luísa Sousa, A. Campos Costa, and J. Saldanha Matos. "A Methodology to Couple Vulnerability and Condition of Buried Pipes in Seismic Risk Assessment: Application to a Subsystem of the Lisbon Wastewater System." In the <i>15th World Conference on Earthquake Engineering</i>, Beijing, China (15WCEE), 2012.</p>	<p>Pipe damage COV = f(intensity) and condition added based on expert opinion factor</p>
<p>Tesfamariam, Solomon, Balvant Rajani, and Rehan Sadiq. "Possibilistic approach for consideration of uncertainties to estimate structural capacity of ageing cast iron water mains." <i>Canadian Journal of Civil Engineering</i> 33.8 (2006): 1050-1064.</p>	<p>analytical model based on Winklertype pipe–soil interaction (WPSI) is cast in a "possibilistic" framework to translate the remaining pipe wall thickness to current structural factor of safety. The WPSI model takes into consideration external (traffic, frost, etc.) and internal (operating and surge</p>

	pressures) loads, temperature changes, and loss of bedding support and the reduction of pipe structural capacity in the presence of corrosion pits. Uncertainties associated with the input data–parameters are handled using fuzzy arithmetic operations and interpreted through possibility theory. A Monte Carlo type random sampling method is carried out for performing sensitivity analyses to identify the critical data–parameters that merit further investigation. – very useful, will examine further
Tsitsifli, Stavroula, Vasilis Kanakoudis, and Ioannis Bakouros. "Pipe networks risk assessment based on survival analysis." <i>Water resources management</i> 25.14 (2011): 3729.	Application of the Discriminant Analysis and Classification (DAC) method to predict the future behaviour of network pipes. not specifically germane.
Yoo, Do, et al. "Rehabilitation priority determination of water pipes based on hydraulic importance." <i>Water</i> 6.12 (2014): 3864-3887.	Network aspects, not specifically germane
Zohra, Halfaya Fatma, Bensaibi Mahmouda, and Davenne Luc. "Vulnerability assessment of water supply network." <i>Energy Procedia</i> 18 (2012): 772-783.	Multi-factorial analysis of pipe break rate, may be useful.

List of Literature Reviewed

Adegbite, S., A. Fahimi, T. Evans, J. Farrow, D. Jesson, M. Mulheron, and P. Smith. "Trunk Mains Failures: The Effect of Corrosion on Residual Pipe Strength." In *4th International Conference on Integrity, Reliability and Failure*. Funchal, Portugal, 2013.

Bardet, Jean-Pierre, and Richard Little. "Epidemiology of Urban Water Distribution Systems." *Water Resources Research* 50, no. 8 (2014): 6447–65.

Cullin, Matthew J., Todd H. Petersen, and Anthony Paris. "Corrosion Fatigue Failure of a Gray Cast Iron Water Main." *Journal of Pipeline Systems Engineering and Practice* 6, no. 2 (2015): 05014003.

Folkman, Steven. "Water Main Break Rates in the USA and Canada: A Comprehensive Study," 2018.

———. "Water Main Break Rates in the USA and Canada: A Comprehensive Study, April 2012," 2012.

Giudicianni, Carlo, Armando Di Nardo, Michele Di Natale, Roberto Greco, Giovanni Francesco Santonastaso, and Antonio Scala. "Topological Taxonomy of Water Distribution Networks." *Water* 10, no. 4 (2018): 444.

Giustolisi, Orazio, Daniele Laucelli, and Dragan A. Savic. "Development of Rehabilitation Plans for Water Mains Replacement Considering Risk and Cost-Benefit Assessment." *Civil Engineering and Environmental Systems* 23, no. 3 (2006): 175–90.

Goulter, Ian C., and Ahad Kazemi. "Spatial and Temporal Groupings of Water Main Pipe Breakage in Winnipeg." *Canadian Journal of Civil Engineering* 15, no. 1 (1988): 91–97.

Grigg, Neil S. "Condition Assessment of Water Distribution Pipes." *Journal of Infrastructure Systems* 12, no. 3 (2006): 147–53.

Jesson, D. A., B. H. Le Page, M. J. Mulheron, P. A. Smith, A. Wallen, R. Cocks, J. Farrow, and J. T. Whiter. "Thermally Induced Strains and Stresses in Cast Iron Water Distribution Pipes: An Experimental Investigation." *Journal of Water Supply: Research and Technology—AQUA* 59, no. 4 (2010): 221–29.

Jesson, D. A., H. Mohebbi, J. Farrow, M. J. Mulheron, and P. A. Smith. "On the Condition Assessment of Cast Iron Trunk Main: The Effect of Microstructure and in-Service Graphitisation on Mechanical Properties in Flexure." *Materials Science and Engineering: A* 576 (2013): 192–201.

Kabir, Golam, Solomon Tesfamariam, Alex Francisque, and Rehan Sadiq. "Evaluating Risk of Water Mains Failure Using a Bayesian Belief Network Model." *European Journal of Operational Research* 240, no. 1 (2015): 220–34.

Kettler, A. J., and I. C. Goulter. "An Analysis of Pipe Breakage in Urban Water Distribution Networks." *Canadian Journal of Civil Engineering* 12, no. 2 (1985): 286–93.

Kleiner, Yehuda, and Balvant Rajani. "Comprehensive Review of Structural Deterioration of Water Mains: Statistical Models." *Urban Water* 3, no. 3 (2001): 131–50.

Korkmaz, Sinan. "A Methodology to Predict Fatigue Life of Cast Iron: Uniform Material Law for Cast Iron." *Journal of Iron and Steel Research, International* 18, no. 8 (2011): 42–45.

Le Gat, Yves, and Patrick Eisenbeis. "Using Maintenance Records to Forecast Failures in Water Networks." *Urban Water* 2, no. 3 (2000): 173–81.

Loganathan, Gobichettipalayam Vasudevan, S. Park, and H. D. Sherali. "Threshold Break Rate for Pipeline Replacement in Water Distribution Systems." *Journal of Water Resources Planning and Management* 128, no. 4 (2002): 271–79.

Malm, Annika, Olle Ljunggren, Olof Bergstedt, Thomas JR Pettersson, and Gregory M. Morrison. "Replacement Predictions for Drinking Water Networks through Historical Data." *Water Research* 46, no. 7 (2012): 2149–58.

Park, S., H. Jun, B. J. Kim, and G. C. Im. "Modeling of Water Main Failure Rates Using the Log-Linear ROCOF and the Power Law Process." *Water Resources Management* 22, no. 9 (2008): 1311–24.

Pietrucha-Urbanik, Katarzyna. "Failure Analysis and Assessment on the Exemplary Water Supply Network." *Engineering Failure Analysis* 57 (2015): 137–42.

Rajani, Balvant, and Yehuda Kleiner. "Comprehensive Review of Structural Deterioration of Water Mains: Physically Based Models." *Urban Water* 3, no. 3 (2001): 151–64.

Rajani, Balvant, John Lewandowski, and Alex Margevicius. "Failure Analysis of Cast Iron Trunk Main in Cleveland, Ohio." *Journal of Failure Analysis and Prevention* 12, no. 3 (2012): 217–36.

Rajani, Balvant, and Jon Makar. "A Methodology to Estimate Remaining Service Life of Grey Cast Iron Water Mains." *Canadian Journal of Civil Engineering* 27, no. 6 (2000): 1259–72.

Scheidegger, Andreas, Joao P. Leitao, and Lisa Scholten. "Statistical Failure Models for Water Distribution Pipes—A Review from a Unified Perspective." *Water Research* 83 (2015): 237–47.

Snider, Brett, and Edward A. McBean. "Watermain Breaks and Data: The Intricate Relationship between Data Availability and Accuracy of Predictions." *Urban Water Journal* 17, no. 2 (2020): 163–76.

Toprak, Selcuk, Engin Nacaroglu, Sjoerd van Ballegooy, Abdullah Cem Koc, Mike Jacka, Yasemin Manav, Eric Torvelainen, and Thomas Denis O'Rourke. "Segmented Pipeline Damage Predictions Using Liquefaction Vulnerability Parameters." *Soil Dynamics and Earthquake Engineering* 125 (2019): 105758.

Tsitsifli, S., and V. Kanakoudis. "Predicting the Behavior of a Pipe Network Using the 'Critical z-Score' as Its Performance Indicator." *Desalination* 250, no. 1 (2010): 258–65.

Xu, Qiang, Qiuwen Chen, Jinfeng Ma, and Koen Blanckaert. "Optimal Pipe Replacement Strategy Based on Break Rate Prediction through Genetic Programming for Water Distribution Network." *Journal of Hydro-Environment Research* 7, no. 2 (2013): 134–40.

Yamijala, Shridhar, Seth D. Guikema, and Kelly Brumbelow. "Statistical Models for the Analysis of Water Distribution System Pipe Break Data." *Reliability Engineering & System Safety* 94, no. 2 (2009): 282–93.

APPENDIX B

Glossary of Terms

AC	Asbestos cement (pipe)
Annual frequency	Mean probability of occurrence of a defined event
Backbone system	The network of key transmission and distribution components which serve a significant portion of the region – if all else is lost but the backbone system survives, much of the region will have partial water, even if it may have to be tankered short distances.
CI	Cast iron (pipe)
Compliant	Displacing in conformance with adjacent materials; for pipelines, moving with the surrounding soils
Continuous	Pipe that generally has the same cross-section and properties everywhere along its length. Continuous pipe is laid in relatively long lengths, and joined so as to be continuous, such as via welding.
Damage rate	Number of pipe damage occurrences, such as pipe breaks, normalized by the pipe length, so as to yield a damage rate of for example 1.5 breaks per kilometer
DI	Ductile iron (pipe)
GIS	Geographic Information Systems
Hazard (earthquake)	Depending on context, either (a) a general reference to damaging effects of earthquakes, such as shaking, landsliding, liquefaction, etc, or (b) more specifically, the probability of experiencing a specific measure of intensity at a specific location
HDPE	High density polyethylene (pipe)
Intensity	A metric of the effect, or the strength, of an earthquake hazard at a specific location, commonly measured on qualitative scales such as MMI
Kaplan Meier	Statistical estimator used to estimate the survival function from lifetime data.
Lifelines	Systems required for the function of modern cities, such as water, wastewater, electric power, transportation and other systems.
LSI	Liquefaction Severity Index. The amount of PGD, in inches, associated with lateral spreading on gently sloping ground and poor soil conditions (Youd and Perkins 1987).
PGD	Permanent ground deformation. Deformation hazard due to ground failure, such that the ground is permanently displaced relative to its pre-earthquake condition
PGD	Peak ground displacement
PGV	Peak ground velocity

PVC	Polyvinyl chloride (pipe)
RCC	Reinforced concrete cylinder (pipe)
Segmented	Pipe that is made up of relatively short sections or segments, such as bell and spigot pipe.
Survival analysis	Statistical analysis to determine the expected duration of time until one or more events happen, such as death in biological organisms and failure in mechanical systems.
Vs30	Shear wave velocity (mps) for the uppermost 30 m of soil
Wave propagation	Deformation hazard due to transient seismic waves

References

- ALA. 2001. *Seismic Fragility Formulations For Water Systems, Part 1 - Guidelines*. American Lifelines Alliance. 104.
- Allen, T.I., and D.J. Wald. 2007. *Topographic Slope as a Proxy for Global Seismic Site Conditions (Vs30) and Amplification Around the Globe*. U.S. Geological Survey. 69.
- Allouche, E.N., E. Chisolm, and R.L. Sterling. 2008. "Impact of Hurricanes on Buried Infrastructure Networks—A Case History." *Pipelines 2008: Pipeline Asset Management: Maximizing Performance of our Pipeline Infrastructure*. 1-13.
- Bardet, J.-P., and R. Little. 2014. "Epidemiology of Urban Water Distribution Systems." *Water Resources Research*. 50(8):6447-65.
- Bedrossian, T.L., P. Roffers, C.A. Hayhurst, J.T. Lancaster, W.R. Short, S. McCrea, B. Wanish, J. Thompson, A. Carney, and M.A. Myers. 2012. "Geologic Compilation of Quaternary Surficial Deposits in Southern California: California Geological Survey Special Report 217 (Revised), 21 p. 25 plates, scale 1: 100,000." Sacramento, CA: California Geological Survey, Department of Conservation.
- Beesley, C. 2018. "BIM Use in the Water Industry Soars as Local Governments Reap Benefits." *Government Design Hub*.
- Borcherdt, R. 2012. "Vs30 – A Site-Characterization Parameter for Use in Building Codes, Simplified Earthquake Resistant Design, Gmpes, and Shakemaps." *15th World Conference on Earthquake Engineering (15WCEE)*. Lisbon.
- Bradley, P.E., and N. Kohler. 2007. "Methodology for the Survival Analysis of Urban Building Stocks." *Building Research & Information*. 35(5):529-42.
- Carrión, A., H. Salano, M.L. Gamiz, and A. Debon. 2010. "Evaluation of the Reliability of a Water Supply Network from Right-Censored and Left-Truncated Break Data." *Water Resources Management*. 24(12):2917-35.
- Chisolm, E.I., and J.C. Matthews. 2012. "Impact of Hurricanes and Flooding on Buried Infrastructure." *Leadership and Management in Engineering*. 12(3):151-56.
- Christodoulou, S.E., and M. Fragiadakis. 2014. "Seismic Reliability Assessment of Lifeline Systems." *Computing in Civil and Building Engineering*. 1812-19.
- Christodoulou, S.E., A.A. Gagatsis, S. Xanthos, and S. Kranioti. 2012. "Urban Water Distribution Network Asset Management Using Spatio-Temporal Analysis of Pipe-Failure Data." *Proc. International Conference for Computing in Civil and Building Engineering*. Clearwater Beach FL. 27-29.
- Damodaran, N., J. Pratt, J. Cromwell, J. Lazo, E. David, R. Raucher, C. Herrick, E. Rambo, A. Deb, and J. Snyder. 2005. *Customer Acceptance of Water Main Structural Reliability*. Denver, CO: Prepared by Stratus Consulting Inc. PA Consulting Group and Weston Solutions for the Awwa Research Foundation and the US Environmental Protection Agency. 268.

- Davis, C.A., T.D. O'Rourke, M.L. Adams, and M.A. Rho. 2012. "Case Study: Los Angeles Water Services Restoration Following the 1994 Northridge Earthquake." *15th World Conference on Earthquake Engineering*. 24-28.
- Davis, C. 2018. *Assuring Seismic Resilience for the Los Angeles Water System*. 11th National Conference on Earthquake Engineering. Los Angeles, CA: Earthquake Engineering Research Institute.
- Deb, A.K., F.M. Grablutz, Y.J. Hasit, J.K. Snyder, G.V. Loganathan, and N. Agbenowski. 2002. *Prioritizing Water Main Replacement and Rehabilitation*. Denver, CO: Prepared by Roy F. Weston, Inc. and Virginia Polytechnic Institute and State University for the Awwa Research Foundation. 228.
- Dodge. 2018. *The Business Value of BIM for Water Projects*. Bedford, MA: Dodge Data & Analytics. 48.
- Fatemi, A., and L. Yang. 1998. "Cumulative Fatigue Damage and Life Prediction Theories: A Survey of the State of the Art for Homogeneous Materials." *International Journal of Fatigue*. 20(1):9-34.
- Folkman, S. 2018. *Water Main Break Rates in the USA and Canada: A Comprehensive Study*. Utah State University, Buried Structures Laboratory.
- Fragiadakis, M., and S.E. Christodoulou. 2014. "Seismic Reliability Assessment of Urban Water Networks." *Earthquake Engng Struct. Dyn.* 43:357-74.
- Grigg, N., and D. Ballantyne. 2017a. *Visual Guidance for Common Pipe Failures*. Denver, CO: Water Research Foundation. 66.
- . 2017b. *Visual Guidance for Common Pipe Failures - FIELD GUIDE*. Denver, CO: Water Research Foundation. 147.
- Grigg, N.S. 2004. *Assessment and Renewal of Water Distribution Systems*. Denver, CO: Awwa Research Foundation. 160.
- Hackett, Robert. 2019. *BIM's Asset Management Benefits Being Missed*. WWTonline. <https://wwtonline.co.uk/news/bim-s-asset-management-benefits-being-missed-bim4water-chair>. WWT - Water & Wastewater Treatment.
- Hancock, J., and J.J. Bommer. 2005. "The Effective Number of Cycles of Earthquake Ground Motion." *Earthquake Engineering & Structural Dynamics*. 34(6):637-64.
- Holzer, T.L., A.C. Padovani, M.J. Bennett, T.E. Noce, and J.C. Tinsley. 2005. "Mapping Nehrp Vs30 Site Classes." *Earthquake Spectra*. 21(2):353-70.
- Jeon, S.-S., and T.D. O'Rourke. 2005. "Northridge Earthquake Effects on Pipelines and Residential Buildings." *Bulletin of the Seismological Society of America*. 95(1):294-318.
- Kaplan, E.L., and P. Meier. 1958. "MP (1958) Non Parametric Astimations from Complete Observations." *J. Am. Stat. Assoc.* 53:163-79.
- Le Gat, Y., I. Kropp, and M. Poulton. 2013. "Is the Service Life of Water Distribution Pipelines Linked to Their Failure Rate?" *Water Science and Technology: Water Supply*. 13(2):386-93.
- Lund, L.V. 1996. "Lifeline Utilities Performance in the 17 January 1994 Northridge, California, Earthquake." *Bull. Seismol. Soc. Am.* 86(1b):S350-S61.

- Lund, L.V., and A.J. Schiff. 1992. *TCLÉE Pipeline Failure Database*. Technical Council on Lifeline Earthquake Engineering, American Society of Engineers.
- Mayoral Seismic Safety Task Force. 2014. *Resilience by Design*. 126. Los Angeles: Office of the Mayor, City of Los Angeles.
- Melchers, R.E., R.B. Petersen, and T. Wells. 2019. "Empirical Models for Long-Term Localised Corrosion of Cast Iron Pipes Buried in Soils." *Corrosion Engineering, Science and Technology*. 54(8):678-87.
- Nishiyama, M., and Y. Fillion. 2013. "Review of Statistical Water Main Break Prediction Models." *Canadian Journal of Civil Engineering*. 40(10):972-79.
- NOAA (National Oceanic and Atmospheric Administration). n.d. *Climate Data Online*. <https://www.ncdc.noaa.gov/cdo-web/>.
- NRC (National Research Council). 2007. *Drinking Water Distribution Systems: Assessing and Reducing Risks*. National Research Council, Washington: National Academies Press.
- O'Rourke, M., and X. Liu. 2012. *Seismic Design of Buried and Offshore Pipe*. Buffalo, NY: MCEER.
- O'Rourke, T.D., S.-S. Jeon, S. Toprak, M. Cubrinovski, M. Hughes, S. Ballegooy, and D. Bouziou. 2014. "Earthquake Response of Underground Pipeline Networks in Christchurch, NZ." *Earthquake Spectra*. 30(1).
- O'Rourke, T.D., S. Toprak, and Y. Sano. 1998. "Factors Affecting Water Supply Damage Caused by the Northridge Earthquake." *US-Japan Workshop on Earthquake Disaster Prevention For Lifeline Systems*. 57.
- Page, J. 1966. *Impact Tests on Pipes Buried Under Roads*. Road Research Laboratory.
- Park, S., J.W. Kim, A. Newland, B.J. Kim, and H.D. Jun. 2008. "Survival Analysis of Water Distribution Pipe Failure Data Using the Proportional Hazards Model." *World Environmental and Water Resources Congress 2008: Ahupua'A*. 1-10.
- Porter, K.A., C. Scawthorn, D.G. Honegger, T.D. O'Rourke, and F. Blackburn. 1991. *Performance of Water Supply Pipelines in Liquefied Soil*. 3-17. Los Angeles, CA, USA: Publ by Natl Inst of Standards & Technology, Gaithersburg, MD, USA.
- Rajani, B., and Y. Kleiner. 2001. *Comprehensive Review of Structural Deterioration of Water Mains: Physically Based Models*. 22. Ottawa: National Research Council of Canada.
- Rajani, B., Y. Kleiner, and J.-E. Sink. 2012. "Exploration of the Relationship between Water Main Breaks and Temperature Covariates." *Urban Water Journal*. 9(2):67-84.
- Rajani, B., and S. Tesfamariam. 2007. "Estimating Time to Failure of Cast-Iron Water Mains." *Proceedings of the Institution of Civil Engineers-Water Management*. 160:83-88.
- Randall-Smith, M., A. Russell, and R. Oliphant. 1992. *Guidance Manual for the Structural Condition Assessment of the Trunk Mains*. Swindon, UK: Water Research Centre.
- Sadiq, R., B. Rajani, and Y. Kleiner. 2004. "Probabilistic Risk Analysis of Corrosion Associated Failures in Cast Iron Water Mains." *Reliability Engineering & System Safety*. 86(10):1-10.

- Scawthorn, C. 2015. *Effects of 2015 Napa Earthquake on the City of Napa Water Distribution Piping*. 12: Pacific Earthquake Engineering Research Center, University of California, Berkeley.
- Schulze, S.S., and E.C. Fischer. 2021. "Prediction of Water Distribution System Contamination Based on Wildfire Burn Severity in Wildland Urban Interface Communities." *ACS EST Water*. 1:291–99.
- SPA Risk LLC. 2014. "24 August 2014 South Napa Mw 6 Earthquake Reconnaissance Report." Available: <http://www.sparisk.com/Pubs/Spa-2014-Napa-Report.Pdf>. 62.
- Stepp, J.C. 1972. "Analysis of Completeness of the Earthquake Sample in the Puget Sound Area and Its Effect on Statistical Estimates of Earthquake " 897-909. in *Proc. First Conf. Microzonation*. Seattle, WA.
- TCLEE (Technical Council for Lifeline Earthquake Engineering) (Ed.). 2005. *Fire Following Earthquake*. Reston: American Society of Civil Engineers, Technical Council for Lifeline Earthquake Engineering, Scawthorn et al (eds).
- Tesfamariam, S., B. Rajani, and R. Sadiq. 2006. "Possibilistic Approach for Consideration of Uncertainties to Estimate Structural Capacity of Ageing Cast Iron Water Mains." *Canadian Journal of Civil Engineering*. 33(8):1050-64.
- Toprak, S. 1998. "Earthquake Effects on Buried Lifeline Systems." 308. Ithaca: Cornell University.
- USGS (U.S. Geological Survey). 1994. *M 6.7 - 1km NNW of Reseda, CA*. <https://earthquake.usgs.gov/earthquakes/eventpage/ci3144585/shakemap/intensity>.
- USGS (U.S. Geological Survey). 2018. *USGS EROS Archive - Digital Elevation - Shuttle Radar Topography Mission (SRTM) Non-Void Filled*. https://www.usgs.gov/centers/eros/science/usgs-eros-archive-digital-elevation-shuttle-radar-topography-mission-srtm-non?qt-science_center_objects=0#qt-science_center_objects.
- USGS (U.S. Geological Survey). 2020. *1/3rd arc-second Digital Elevation Models (DEMs) - USGS National Map 3DEP Downloadable Data Collection*. <https://data.usgs.gov/datacatalog/data/USGS:3a81321b-c153-416f-98b7-cc8e5f0e17c3>.
- USGS (U.S. Geological Survey). n.d.a. *Vs30 Map Viewer*. <https://www.arcgis.com/apps/webappviewer/index.html?id=8ac19bc334f747e486550f32837578e1>.
- USGS (U.S. Geological Survey). n.d.b. *ShakeMap*. <https://earthquake.usgs.gov/data/shakemap/>.
- Walski, T.M., and A. Pelliccia. 1982. "Economic Analysis of Water Main Breaks." *Journal-American Water Works Association*. 74(3):140–47.
- Water World. 1999. *Aging Pipe Proves Expensive for Municipalities*. in Water World. <https://www.waterworld.com/drinking-water/infrastructure-funding/article/16193361/aging-pipe-proves-expensive-for-municipalities>. Accessed 23 July 2020.
- Wols, B.A., and P. Van Thienen. 2014. "Impact of Weather Conditions on Pipe Failure: A Statistical Analysis." *Journal of Water Supply: Research and Technology—AQUA*. 63(3):212-23.
- Youd, L.T., and D.M. Perkins. 1987. "Mapping of Liquefaction Severity Index." *Journal of Geotechnical Engineering*. 113(11):1374-92.

Zammit, A. 2018. *Shot Peening of Austempered Ductile Iron*. 10.5772/intechopen.79316.



advancing the science of water®



1199 North Fairfax Street, Suite 900
Alexandria, VA 22314-1445

6666 West Quincy Avenue
Denver, CO 80235-3098

www.waterrf.org | info@waterrf.org